EXPLORING ORODROMINE VARIATION IN THE TWO MEDICINE-JUDITH RIVER-BELLY RIVER CLASTIC WEDGE IN MONTANA AND ALBERTA.

by

Zakaria Joseph Dylan Hannebaum

A thesis submitted in partial fulfillment
of the requirements for the degree

of

Master of Science

in

Earth Sciences

MONTANA STATE UNIVERSITY
Bozeman, Montana

May 2025

©COPYRIGHT

by

Zakaria Joseph Dylan Hannebaum

2025

All Rights Reserved

ACKNOWLEDGEMENTS

One fictional hobbit famously provided some sagely advise to his younger protege “It's a dangerous business, Frodo, going out your door. You step onto the road, and if you don't keep your feet, there's no knowing where you might be swept off to.” Growing up in small town Indiana, my younger self frequently daydreamed about far off windswept badlands and the dinosaurian treasures they hoarded. Never in a million years did I perceive becoming a paleontologist was an attainable station in life, but once I fatefully made the decision to embark on this pursuit, not ever in my wildest dreams did I imagine the path I chose would bear dinosaurian fruit. I would not have been able to complete this project without the support of my dear wife, Stacey (and our two cats; Louie and Ollie). Stacey not only encouraged me to return to school but drove me to take risks and pursue my passions in paleontology. My family and friends have been a bastion of support that has carried me across the finish line. Special appreciation goes out to my grandmother, Patricia Gentry, whose investments surpassed her love and encompass providing some funds to procure a new computer for me which was integral to completing this thesis. The Museum of the Rockies has become a second home, and the staff there have in turn become like family. Montana State University staff Chris Organ, Devon Orme, and Giulio Panascì, helped train my scientific mind and they continue to challenge me through course work and the various projects we are partnered on. Many of the methods unleashed on this thesis were taught to me by these three. The friendships and partnerships I have made as an undergraduate and graduate student at Montana State University are unforgettable, and I will cherish them forever.

I want to extend my deepest thanks to my thesis advisor and chair, David Varrichio, for all the incredible opportunities he has given me at Montana State University. I am deeply humbled and appreciative of the trust he lent me in seeing this ambitious master's thesis to its end. My committee, John Scannella, Rodney Scheetz, and L.J. Krumenacker, provided invaluable support throughout this project and their critiques greatly improved this thesis. My chapter collaborators Haviv Avrahami, Caleb Brown, John Horner, and Ian Wolff were prized resources when puzzling out the more perplexing parts of the thesis. Special thanks to Haviv Avrahami for meeting almost weekly for the last five months of my thesis to tutor me in creating figures in Blender. Thanks to Eric Metz, John Scannella, Shino Sugimoto, David Evans, Brandon Strilisky, and Caleb Brown for collections access at their facilities. Special thanks also to John Horner for humoring my innumerable requests for field notes and pictures. His detailed and timely responses were greatly appreciated and significantly improved the quality of this research. Student workers also partnered with me on this thesis, often volunteering their time, which was deeply humbling and appreciated. These students were Brendan Clark, Saryna Smith, Brennon Valdez, and Seth Lopez. Lastly, I would like to thank Chis Organ and Emerald Bender for helping troubleshoot the script errors I generated as I wrote code for my phylogenetic analyses.

TABLE OF CONTENTS

1. INTRODUCTION TO THESIS 1

Orodromeus makelai 1
Orodromeus, past research. 2
Orodromeus research 2019-present. 2
Orodromine variation in the Two Medicine-
Judith River- Belly River clastic wedge. 3
An updated temporal framework for the
Two Medicine-Judith River clastic wedge. 4
Sexual dimorphism or systematic differences? 4
Literature Cited 8

2. THE EARLIEST ORODROMINE FROM THE UPPER CRETACEOUS JUDITH RIVER FORMATION ELUCIDATES A NEW SPECIES PREDATING *ORODROMEUS MAKELAI* IN THE CONTEMPORANEOUS TWO MEDICINE FORMATION. 12

Contribution of Authors and Co-Authors 12
Manuscript Information 13
Abstract 14
Introduction 14
Materials and methods 16
Phylogenetic Methods 17
Institutional abbreviations 18
SYSTEMATIC PALEONTOLOGY 18
Description 23
Jugal 23
Axial skeleton 26
Sternum 26
Appendicular Skeleton 26
Radius 26
Femur 27
Tibia 29
Fibula 30
Medial distal tarsal 31
Pes 32
Phylogenetic Analysis 37
Discussion 38
Conclusion 41
Acknowledgments 42
Literature Cited 57

TABLE OF CONTENTS CONTINUED

3. A NEW ORODROMINE (DINOSAURIA: ORNITHISCHIA) FROM THE UPPER CRETACEOUS TWO MEDICINE FORMATION OF NORTHCENTRAL MONTANA 71

Contribution of Authors and Co-Authors 71
Manuscript Information 72
Abstract 73
Introduction 73
Materials and methods 75
Phylogenetic Methods 76
Institutional Abbreviations 78
Systematic paleontology 78
Description 85
Cranium 86
Skull 86
Jugal 86
Cervical vertebrae 90
Atlas 90
Axis 91
Cervical vertebrae three to nine 92
Cervical ribs 94
Dorsal vertebrae 94
Dorsal ribs 95
Sacral vertebrae 96
Caudal vertebrae 96
Chevrons 97
Ossified tendons 98
Sternum 98
Appendicular skeleton 99
Scapula 99
Coracoid 101
Humerus 103
Ulna 104
Radius 105
Manus 105
Ilium 108
Pubis 109
Ischium 112
Femur 113
Tibia 116
Fibula 119
Astragalus 120

TABLE OF CONTENTS CONTINUED

Calcaneum 120
Distal tarsals 121
Pes 121
Phylogenetic results 126
Synapomorphies 127
Orodrominae 127
Thescelosaurinae 130
Thescelosauridae 130
Discussion 132
Orodromine paleobiogeography 133
Campanian small-bodied ornithischians coexistence 134
Conclusion 136
Acknowledgments 137
Literature Cited 182

4. THE OSTEOLOGY OF *ORODROMEUS MAKELAI* AND A REVIEW OF ORODROMINE SYSTEMATICS 202

Contribution of Authors and Co-Authors 202
Manuscript Information 203
Abstract 204
Introduction 205
Materials and methods 206
Institutional Abbreviations 207
Systematic Paleontology 208
Description 211
Cranium 211
Skull 211
Premaxilla 211
Maxilla 212
Nasal 213
Prefrontal 214
Supraorbital 215
Lacrimal 217
Jugal 218
Quadratojugal 220
Postorbital 221
Quadrate 222
Squamosal 223
Parietal 223
Frontal 224
Predentary 224

TABLE OF CONTENTS CONTINUED

Dentary 225
Surangular 226
Angular 227
Splenial 228
Prearticular 228
Articular 228
Axial skeleton 229
Cervical vertebrae 229
Atlas 229
Axis 230
Cervical vertebrae three to nine 231
Cervical ribs 232
Dorsal vertebrae 232
Dorsal ribs 233
Sacral vertebrae 233
Caudal vertebrae 235
Chevrons 235
Ossified tendons 236
Sternum 237
Appendicular skeleton 238
Scapula 238
Coracoid 239
Humerus 240
Ulna 241
Radius 242
Manus 242
Ilium 243
Pubis 246
Ischium 247
Femur 249
Tibia 253
Fibula 254
Astragalus 255
Calcaneum 256
Distal tarsals 256
Pes 257
Discussion 260
Orodromine systematics overview 263
Albertadromeus syntarsus 264
"*Laosaurus minimus*" 265
"BV Orodromine" 266
"Kaiparowits Orodromine" 268

TABLE OF CONTENTS CONTINUED

TMP 2008.045.0002 (Oldman Formation) 270
Conclusion 271
Acknowledgments 272
Literature Cited 303

5. CONCLUSION TO THESIS 316

CUMULATIVE REFERENCES CITED 318

LIST OF TABLES

Table Page

1. Table 1. Measurements of appendicular elements in cm. Underlined numbers = incomplete. 44
2. Table 1.1. Measurements for figured *Pikunidromeus* vertebrae (cm.). 141
3. Table 1.2. Forelimb measurements (cm.). 143
4. Table 1.3. Pelvic measurements (cm.). 145
5. Table 1.4. Hindlimb measurements (cm.). 146
6. Table 2.1. Informal thescelosaurid taxa. 150
7. Table 2.2. Indeterminate specimens of significance. 151
8. Table 1.1 Measurements for figured *Orodromeus* vertebrae (cm.) 274
9. Table 1.2: *Orodromeus* forelimb measurements (cm.) 276
10. Table 1.3: *Orodromeus* pelvic measurements (cm.) 277
11. Table 1.4: *Orodromeus* hindlimb measurements (cm.) 278

LIST OF FIGURES

Figure Page

1. Figure 1.1. Stratigraphic section of the Two Medicine-Judith River-Belly River clastic wedge and southern Utah, with orodromine occurrences denoted by genera. Of the five skulls discussed above, MOR 436 and 473 are assigned to *Pikunidromeus ancellae* above the lacustrine interval of the Flagg Butte Member of the Two Medicine Formation; MOR 294, 1136, and 1141 encapsulate the cranial morphology of *Orodromeus makelai* which is confined to the lacustrine interval. In the Lower Judith River Formation MOR 14147 and 14148 mark the temporal distribution of *Akanthodromeus judithi*. This figure was created using the figures and data referenced from Brown et al. (2013), Ramezani et al. (2022), and Rogers et al. (2024). 7

2. Figure 1. Geological map of Judith River Formation with *Akanthodromeus judithi* fossil localities denoted by red stars. Judith River Formation outcrops are shaded in gray with the following tribal lands outlined in black with cross-hatched interiors: (from left to right on map; Chippewa Cree Tribe, Fort Belknap Reservation, and Fort Peck Indian Reservation). Scale bar equals 30.0 miles. [Planned for page width]..... 45

3. Figure 2. Campanian stratigraphic section of northwestern Montana, southern Alberta, northcentral Montana, and southern Utah with orodromine occurrences denoted through time. This figure was created using data and figures from Brown et al. (2013), Ramezani et al. (2020), and Rogers et al. (2024). [Planned for page width]. 46

4. Figure 3. MOR 14147 right jugal rendered with and without texture in [from top to bottom in each row] (A) lateral; (B) anterior; (C) medial; and (D) posterior views. **Abbreviations: f**, nutrient foramen; **jh**, jugal horn; **jw**, jugal wing; **or**, orbital rim; **pr**, postorbital ramus; **s**, sulcus. [Planned for page width]..... 47

5. Figure 4. (A-B) MOR 14148 sternal plate in two views. (C-E) *Orodromeus* sternal plates: (C-D) "Frankies *Orodromeus*" F#8.5.95, (E.) MOR 623. (F.) *Haya* [IGM 100/2015]. (G.) *Parksosaurus* [ROM 804]. White shading denotes visible bone, while grey shading shows matrix. White dashed lines demarcate broken edges. Arrow denotes anterior. **Abbreviations: f**, facet; **f ?**, potential facet. Scale bar equals 5.0 centimeters (cm.). [Planned for page width] 48

LIST OF FIGURES CONTINUED

Figure Page

6. Figure 5. MOR 14148 partial radius rendered with and without texture in (A) Anterior?, lateral, medial, and posterior? views; (B) *Orodromeus makelai* radius [MOR 294] in lateral and anterior views; and (C) "Landslide Butte Orodromine" radius [MOR 473] in lateral and anterior views. **Abbreviations: rg**, ridge. [Planned for column width]. 49

7. Figure 6. MOR 14148 partial right femur rendered with and without texture in [from top to bottom in each row] (A.) anterior, proximal, and posterior; (B.) lateral, distal, and medial; (C.) anterior, proximal, and posterior; and (D.) lateral, distal, and medial views. **Abbreviations: f**, nutrient foramen; **ft**, fourth trochanter; **icl**, insertion pit for *M. caudofemoralis longus*; **lt**, lesser trochanter; **s**, sulcus. [Planned for page width]..... 50

8. Figure 7. MOR 14148 right tibia rendered with and without texture in (A) lateral, anterior, medial, and posterior views; and (B) proximal and distal views. **Abbreviations: cc**, cnemial crest; **fic**, inner condyle; **lm**, lateral malleolus; **mm**, medial malleolus. [Planned for page width]. 51

9. Figure 8. MOR 14148 right fibula rendered with and without texture in (A) anterior and posterior views; (B) proximal and distal views; and (C) MOR 14148 compared to *Orodromeus makelai* fibula [MOR 623]. MOR 14148 scaling is doubled. (C) Black silhouette is of MOR 623 with MOR 14148 overlaid. [Planned for page width]..... 52

10. Figure 9. Right medial distal tarsi in dorsal (=proximal) view; (A) MOR 14148; (B) *Orodromeus* [MOR 623]; (C) TM-088 Orodrominae indet.; (D) *Oryctodromeus* [MOR 1642]; (E) "Landslide Butte Orodromine" [MOR 473]; and (F) *Fona* [NCSM 36280]. **Abbreviations: mp**, medial process; **pr**, proximal ridge. Scale bar equals 2.0 centimeters (cm.). [Planned for page width. 53

11. Figure 10. MOR 14148 right pes rendered with and without texture in (A) anterior; (B) posterior; (C) proximal; (D) distal; (E) medial; and (F) lateral views. **Abbreviations: MDT**, medial distal tarsal. [Planned for page width]. 54

LIST OF FIGURES CONTINUED

Figure Page

12. Figure 11. Time-calibrated tree resulting from Bayesian phylogenetic analysis of early diverging ornithischian dinosaurs with the root, Dinosauria, and Ornithischia constrained using a condensed version of the character matrix from Avrahami et al. (2024) displaying only taxa exhibiting 50% or more of the characters in matrix. Numbered node labels represent posterior probability of those nodes, and the red bars represent the 95% credible interval for the estimated ages. Silhouettes are all downloaded from Phylopic.org. 55

13. Figure 11. Non-time calibrated phylogenetic Bayesian analysis of early diverging ornithischian dinosaurs using an updated version of the Avrahami et al. (2024). Numbers represent posterior probability of support for each node. 36 % of the taxa in the character matrix included in analysis. Taxa lacking 50% of the characters culled. Silhouettes are all downloaded from Phylopic.org. [Planned for page width] 56

14. Figure 1. Geographic map of *Pikunidromeus* ancellae localities. (A) Regional geological formations with fossil localities symbolized by stars. Blackfeet Reservation outlined with a dashed border. Geological formation abbreviations: **DFP**, Dinosaur Park Formation; **JRF**, Judith River Formation; **OF**, Oldman Formation; **TMF**, Two Medicine Formation. *Pikunidromeus* fossil locality abbreviations: **DPP**, Dinosaur Provincial Park; **LSB**, Landslide Butte Field Area; and **TMR**, Two Medicine River Field Area. (B) Photograph of Carrie Ancell and John Horner near TM-019 during the collection of referred specimen MOR 436. Quarry image provided by Museum of the Rockies. [Planned for column width] 138

LIST OF FIGURES CONTINUED

Figure Page

15. Figure 2. *Pikunidromeus* diagnostic features. Figure rendered without texture. (A) *Pikunidromeus* autapomorphies. (A1) lack of transvers dorsal groove on atlantal intercentrum; (2) small, triangular, posterolaterally deflected jugal horn core; (A3) hypapophysis on ventral keel of cervical vertebrae four; (A4) transition of dorsal ribs from vertical to near horizontal articulation occurs between dorsal vertebrae six and eight; (A5) medial condyle of femur inflated and partially invading the posterior intercondylar sulcus on distal femur; (A6) an angle <120° formed between the tibial and fibular facets on the calcaneum; (7) averaged length/width ratio PI-I is 4.15. (B) Orodromine synapomorphies. (B1) presence of a jugal horn core; (B2) bifurcated maxillary ramus of the jugal; (B3) two nutrient foramen on the medial wall of the jugal; (B4) anterior dorsal rib sub-oval in cross section distally; (B5) length of scapula blade to minimum width shows a ratio between 6.0 and 7.3; (B6) posterior scapular flange; (B7) metacarpal I shows obliquely inclined, asymmetric distal condyles; (B8) anteriorly the prepubic process dorsoventrally expands it a large pad; (B9) anteroposteriorly trending striations on anterior terminus of prepubic process; (B10) prepubic process lateral inflection medially placed; (B11) lack of twist in the ischial shaft; (B12) no intertrochanteric notch; (B13) “mailbox flag” shaped metatarsal V; (B14) deep pit on the ventromedial shaft of P1-1 just proximal to the distal articular condyles. (C) Thescelosaurid synapomorphies. (C1) orbital rim on anterior margin of postorbital ramus of jugal; (C2) ventral keel on cervical vertebrae; (C3) location of the first chevron is on the distal end of the second caudal vertebra rather than the first; (C4) sharp scapular spine; (C5) rounded dorsal margin of the ilium in lateral view; (C6) laterally inflection of the prepubic process; (C7) lateral inflection of the ischial shaft into thin blade-like protuberance in the distal third; (C8) cranial expansion of the greater trochanter; (C9) no anterior intercondylar groove on distal femur; (C10) fibular condyle is larger than accessory condyle on tibia; (C11) a flange projects from the fibular shaft along the distal half of the fibula. Gray represents matrix in figure. [Planned for column width]..... 140

LIST OF FIGURES CONTINUED

Figure Page

16. FIGURE 3: *Pikunidromeus* jugal rendered with and without texture. (A) Right jugal of MOR 473 and ROM 64600 in lateral view; (B) right jugal of MOR 473 and ROM 64600 in medial view; (C) left jugal of MOR 473 and right jugal of MOR 613 in lateral view; and (D) left jugal of MOR 473 and right jugal of MOR 613 in medial view. **Abbreviations: jh**, jugal horn; **jw**, jugal wing; **f**, foramen; **mr**, maxillary ramus; **or**, orbital rim; **pr**, postorbital ramus; **qj**, quadratojugal. [Planned for page width] 152

17. Figure 4. *Pikunidromeus* cervical series [MOR 473] rendered with and without texture. (A) Left lateral view, (B) dorsal view, (C) right lateral view, and (D) ventral view. Red arrow denotes potential hypapophysis-like structure. **Abbreviations: atc**, atlantal intercentrum; **axc**, axis intercentrum; **cr**, cervical rib; **dap**, diapophysis; **ns**, neural spine; **odp**, odontoid process; **pap**, parapophysis; **poz**, postzygapophysis; **prz**, prezygapophysis; **tp**, transverse process; **vk**, ventral keel. [Planned for page width] 153

18. Figure 5. *Pikunidromeus* dorsal series [MOR 473] rendered with and without texture. (A) Left lateral view, (B) dorsal view, (C) right lateral view, and (D) ventral view. **Abbreviations: dap**, diapophysis; **ns**, neural spine; **pap**, parapophysis; **poz**, postzygapophysis; **prz**, prezygapophysis; **tp**, transverse process. [Planned for page width] 154

19. Figure 6. *Pikunidromeus* pelvis and sacral vertebrae rendered with and without texture. (A-B) ROM 64600 right ischium, (C-D) ROM 64600 postacetabular process of ilium and MOR 473 sacral series and pelvic elements, (E-F, H-I) MOR 473 left and right prepubic processes, (G, K) ROM 64600 right prepubic process. Gray represents matrix. **Abbreviations: bs**, brevis shelf; **icc**, intercentrum cavities; **il**, ilium; **is**, ischium; **isp**, ischiac peduncle; **li**, lateral inflection; **of**, obturator foramen; **op**, obturator process; **p**, pubis; **pa**, postacetabular process; **st**, striations; **S#**, sacral vertebra number. [Planned for page width] 155

LIST OF FIGURES CONTINUED

Figure Page

20. Figure 7. *Pikunidromeus* caudal series rendered with and without texture. (A) ROM 64600 anterior and distal caudal vertebrae of uncertain axial placement, (B) MOR 473 caudal vertebrae 1 through 3, (C) ROM 64600 caudal series in dorsolateral view, series is broken up into two blocks with at least two vertebrae separating them. Gray represents matrix. **Abbreviations: ch**, chevron; **chf**, chevron facet; **ns**, neural spine; **poz**, postzygapophysis; **prz**, prezygapophysis; **tp**, transverse process; **vg**, ventral groove. [Planned for page width]..... 156

21. Figure 8. *Pikunidromeus* scapulae and coracoids rendered with and without texture. (A-D) MOR 473 left and right coracoids, (E-H) MOR 473 left and right scapulae, and (I-J) ROM 64600 left and right scapulae and coracoids. Red arrows denote posterior ventral flange of the scapula. **Abbreviations: ap**, acromion process; **cf**, coracoid foramen; **cr**, cervical rib; **cv**, cervical vertebra; **gl**, glenoid fossa; **sb**, supraglenoid boss; **sgb**, supraglenoidal buttress; **sgf**, supraglenoid fossa; **spr**, sternal process; **ss**, scapular spine; **vf**, ventral fossa. [Planned for page width] 157

22. Figure 9. *Pikunidromeus* humeri rendered with and without texture. (A-B) MOR 473 left and right humeri, (C-D) ROM 64600 left and right humeri, and (E) MOR 436 right humerus. **Abbreviations: bis,** bicipital sulcus**; dc**, deltopectoral crest; **hh**, humeral head olecranon process; **rc**, radial condyle; **uc**, ulnar condyle. [Planned for page width]..... 158

23. Figure 10. *Pikunidromeus* forearm. Specimens rendered with and without texture. (A-B) MOR 473 left and right radii and ulnae without texture, (C-D) MOR 473 left and right radii and ulnae with texture, (E) ROM 64600 left radii and ulnae, (F) MOR 436 left radii and ulnae texture, (G) ROM 64600 left radii without texture, and (H) MOR 436 left radii without texture. Gray represents matrix. **Abbreviations: op**, olecranon process; **r**, radius; **u**, ulna. [Planned for page width]..... 159

LIST OF FIGURES CONTINUED

Figure Page

24. Figure 11. *Pikunidromeus* manus. Skeletal elements rendered with and without texture. (A, E) MOR 473 metacarpals and manual phalanges, (B, D) MOR 473 manus figured with left forearm and lateral and medial views, (E) ROM 64600 metacarpal I, (F, J) MOR 473 metacarpals and manual phalanges, (G, I) MOR 473 manus figured with left forearm and lateral and medial views, and (H) ROM 64600 metacarpal I. Red arrows denote obliquely inclined, asymmetric articular condyles of metacarpal I. Phalanges denoted by roman numerals. Gray represents matrix. [Planned for page width] 160

25. Figure 12. *Pikunidromeus* femora rendered with texture. (A1) left femora (n=5) and (B1) right femora (n=9). Arrows denote swollen inflection of medial condyle (char. 359:1). **Abbreviations: df,** distal femur; **f**, foramen **fi,** fibula; **ft**, fourth trochanter; **gt**, greater trochanter; **ic,** posterior intercondylar groove; **lc**, lateral condyle; **lt**, lesser trochanter; **mc**, medial condyle; **s**, sulcus; **ti**, tibia. [Planned for page width] 161

26. Figure 13. *Pikunidromeus* femora rendered without texture. (A1) left femora (n=5) and (B1) right femora (n=9). Arrows denote swollen inflection of medial condyle (char. 359:1). **Abbreviations: df,** distal femur; **f**, foramen **fi,** fibula; **ft**, fourth trochanter; **gt**, greater trochanter; **ic,** posterior intercondylar groove; **lc**, lateral condyle; **lt**, lesser trochanter; **mc**, medial condyle; **s**, sulcus; **ti**, tibia. [Planned for page width] 162

27. Figure 14. *Pikunidromeus* tibiae rendered with and without texture. (A, B) left tibia (n=4) in (left to right) lateral and anterior views, then below in proximal and distal views; and (C, D) right tibia (n=3) in (left to right) lateral and anterior views, then below in proximal and distal views. **Abbreviations: ac,** accessory condyle; **as,** astragalus; **ca**, calcaneum; **cc**, cnemial crest; **fc**, fibular condyle; **fe,** femur; **fi,** fibula; **ic**, inner condyle; **im**, inner malleolus; **ldt**, lateral distal tarsal; **mdt**, medial distal tarsal; **mt**, metatarsal; **om**, outer malleolus. [Planned for page width] 163

LIST OF FIGURES CONTINUED

Figure Page

28. Figure 15. *Pikunidromeus* fibulae rendered with and without texture. (A) MOR 473 right tibia and fibula, (B) ROM 64600 right tibia and fibula, and (C) ROM 64600 left fibula. Gray represents matrix **Abbreviations: as,** astragalus**; ca**, **calcaneum; dr**, dorsal rib; **dv,** dorsal vertebra; **fi,** fibula; **fl,** medial flange; **mt**, metatarsal; **ti**, tibia. [Planned for page width] 164

29. Figure 16. MOR 473 tarsals rendered with and without texture. (A) MOR 473 right tibia, fibula, tarsals, and the proximal portions of metatarsal II-V, (B) in three views with texture; posterior, anterior, and distal, and (C) in three views without texture; posterior, anterior, and distal. Metatarsals denoted by roman numerals. Gray represents matrix. **Abbreviations: as,** astragalus**; ca,** calcaneum**; fi,** fibula; **ldt**, lateral distal tarsal; **mdt**, medial distal tarsal; **ti**, tibia. [Planned for page width] 165

30. Figure 17. *Pikunidromeus* pes rendered with texture. (A) MOR 473 right pes, (B) ROM 64600 right pes, (C) MOR 436 left pes, and (D) MOR 530 left pes. Metatarsals and phalanges denoted by roman numerals. [Planned for page width] 166

31. Figure 18. *Pikunidromeus* pes rendered without texture. (A) MOR 473 right pes, (B) ROM 64600 right pes, (C) MOR 436 left pes, and (D) MOR 530 left pes. Metatarsals and phalanges denoted by roman numerals. Gray represents matrix. [Planned for page width] 167

32. Figure 19. Time-calibrated consensus tree resulting from phylogenetic Bayesian analysis of early diverging ornithischian dinosaurs using an updated version of the Avrahami et al. (2024). Branch lengths are scaled by time in millions of years. Numbers represent posterior probability of support for each node. Red bars illustrate the 95% credible interval for the estimated node ages. 100% of the taxa in the character matrix included. Silhouettes are all downloaded from Phylopic.org. [Planned for page width] 168

LIST OF FIGURES CONTINUED

Figure Page

33. Figure 20. Time-calibrated consensus tree resulting from phylogenetic Bayesian analysis of early diverging ornithischian dinosaurs using an updated version of the Avrahami et al. (2024). Branch lengths are scaled by time in millions of years. Numbers represent posterior probability of support for each node. Red bars illustrate the 95% credible interval for the estimated node ages. 86 % of the taxa in the character matrix included in analysis. Taxa lacking 90% of the characters culled. Silhouettes are all downloaded from Phylopic.org. [Planned for page width]. 169

34. Figure 21. Time-calibrated consensus tree resulting from phylogenetic Bayesian analysis of early diverging ornithischian dinosaurs using an updated version of the Avrahami et al. (2024). Branch lengths are scaled by time in millions of years. Numbers represent posterior probability of support for each node. Red bars illustrate the 95% credible interval for the estimated node ages. 67 % of the taxa in the character matrix included in analysis. Taxa lacking 80% of the characters culled. Silhouettes are all downloaded from Phylopic.org. [Planned for page width]. 170

35. Figure 22. Time-calibrated consensus tree resulting from phylogenetic Bayesian analysis of early diverging ornithischian dinosaurs using an updated version of the Avrahami et al. (2024). Branch lengths are scaled by time in millions of years. Numbers represent posterior probability of support for each node. Red bars illustrate the 95% credible interval for the estimated node ages. 51 % of the taxa in the character matrix included in analysis. Taxa lacking 70% of the characters culled. Silhouettes are all downloaded from Phylopic.org. [Planned for page width]. 171

36. Figure 23. Time-calibrated consensus tree resulting from phylogenetic Bayesian analysis of early diverging ornithischian dinosaurs using an updated version of the Avrahami et al. (2024). Branch lengths are scaled by time in millions of years. Numbers represent posterior probability of support for each node. Red bars illustrate the 95% credible interval for the estimated node ages. 44 % of the taxa in the character matrix included in analysis. Taxa lacking 60% of the characters culled. Silhouettes are all downloaded from Phylopic.org. [Planned for page width]. 172

LIST OF FIGURES CONTINUED

Figure Page

37. Figure 24. Time-calibrated consensus tree resulting from phylogenetic Bayesian analysis of early diverging ornithischian dinosaurs using an updated version of the Avrahami et al. (2024). Branch lengths are scaled by time in millions of years. Numbers represent posterior probability of support for each node. Red bars illustrate the 95% credible interval for the estimated node ages. 36 % of the taxa in the character matrix included in analysis. Taxa lacking 50% of the characters culled. Silhouettes are all downloaded from Phylopic.org. [Planned for page width]. 173

38. Figure 25. Non-time calibrated phylogenetic Bayesian analysis of early diverging ornithischian dinosaurs using an updated version of the Avrahami et al. (2024). Numbers represent posterior probability of support for each node. 100 % of the taxa in the character matrix included in analysis. Silhouettes are all downloaded from Phylopic.org. [Planned for page width]. 174

39. Figure 26. Non-time calibrated phylogenetic Bayesian analysis of early diverging ornithischian dinosaurs using an updated version of the Avrahami et al. (2024). Numbers represent posterior probability of support for each node. 86 % of the taxa in the character matrix included in analysis. Taxa lacking 90% of the characters culled. Silhouettes are all downloaded from Phylopic.org. [Planned for page width] 175

40. Figure 27. Non-time calibrated phylogenetic Bayesian analysis of early diverging ornithischian dinosaurs using an updated version of the Avrahami et al. (2024). Numbers represent posterior probability of support for each node. 67 % of the taxa in the character matrix is included in analysis. Taxa lacking 80% of the characters culled. Silhouettes are all downloaded from Phylopic.org. [Planned for page width] 176

41. Figure 28. Non-time calibrated phylogenetic Bayesian analysis of early diverging ornithischian dinosaurs using an updated version of the Avrahami et al. (2024). Numbers represent posterior probability of support for each node. 51 % of the taxa in the character matrix included in analysis. Taxa lacking 70% of the characters culled. Silhouettes are all downloaded from Phylopic.org. [Planned for page width] 177

LIST OF FIGURES CONTINUED

Figure Page

42. Figure 29. Non-time calibrated phylogenetic Bayesian analysis of early diverging ornithischian dinosaurs using an updated version of the Avrahami et al. (2024). Numbers represent posterior probability of support for each node. 44 % of the taxa in the character matrix included in analysis. Taxa lacking 60% of the characters culled. Silhouettes are all downloaded from Phylopic.org. [Planned for page width] 178

43. Figure 30. Non-time calibrated phylogenetic Bayesian analysis of early diverging ornithischian dinosaurs using an updated version of the Avrahami et al. (2024). Numbers represent posterior probability of support for each node. 36 % of the taxa in the character matrix included in analysis. Taxa lacking 50% of the characters culled. Silhouettes are all downloaded from Phylopic.org. [Planned for page width] 179

LIST OF FIGURES CONTINUED

Figure Page

44. Figure 31. Stratigraphic section of Late Cretaceous northern Laramidia and southern Utah, with orodromine (red), thescelosaurine (purple), thescelosaurid (blue), *Parksosaurus* (dark orange), leptoceratopsid (light orange), and pachycephalosaurid (yellow) occurrences denoted. *Pikunidromeus ancellae* holotype symbolized by a star. Marginalized taxon/specimen occurrences straddle the column edge signify uncertain placement within respective formations. Positioning on the column border is not reflective of stratigraphic positioning in the formation. For indeterminate forms, specimen numbers are preferentially shown if known. Pachycephalosaurid #13 represents a handful of undescribed specimens informally designated *Stegoceras sp*. from the Judith River Formation reposited at the MOR. This chronostratigraphic framework synthesizes data provided in Jerzykiewicz and Norris (1995), Fowler (2017), Arbour et al. (2020), Ramezani et al. (2022), and Rogers et al. (2024). Orodromine taxon/specimen occurrences drawn from Brown et al. (2013), Druckenmiller et al. (2021), Hudgins (2021), Rogers et al. (2024), personal communications with C. Brown, and this study; *Thescelosaurus* taxa sourced from Morris (1976) and Brown et al. (2011); thescelosaurid #1 (="Wapiti Thescelosaurid") was described in Hudgins (2021); *Parksosaurus* temporal occurrences obtained from Brown and Druckenmiller (2011), Druckenmiller et al. (2021), Hudgins (2021), and Sues et al (2023); leptoceratopsid taxon/specimen occurrences compiled using data from Brown et al. (2012), Evans et al. (2013), Druckenmiller et al. (2021), Ryan et al. (2023), and Rogers et al. (2024); pachycephalosaurid taxon/specimen data informed from Sullivan (2006). Schott et al. (2009), Evans et al. (2015), Mallon et al. (2015); Schott and Evans (2017), Dyer et al. (2022), Horner et al. (2022), Woodruff (2022), Woodruff and Schott (2023), Rogers et al. (2024), and personal observations of undescribed Judith River pachycephalosaurid specimens at the MOR. Silhouettes sourced from Phylopic.org 181

45. FIGURE 1. Geographic map of Two Medicine Formation with orodromine taxa occurrences denoted by colored silhouettes. (A) North America; (B) Two Medicine Formation; and (C) the late Robert Makela, photo taken in front of his tipi at Egg Mountain in 1980. Photo of Robert Makela courtesy of John Horner. Blackfeet Reservation is outlined with a dashed border, and the Two Medicine Formation is shaded gray. [Planned for page width] 273

LIST OF FIGURES CONTINUED

Figure Page

46. FIGURE 2. *Orodromeus makelai* holotype [MOR 294] skull rendered with and without texture. (**A**) MOR 294 in left lateral and dorsal views; (B) anterior and posterior views; (**C)** right lateral and ventral views; (D) disarticulated right mandible and jugal; (E) MOR 294 in left lateral and dorsal views with colored element interpretation; (F) anterior and posterior views; and (G) right lateral and ventral views. [planned for page width] 281

47. FIGURE 3. *Orodromeus makelai* paratype [MOR 1141] skull rendered with and without texture. (**A**) Textured model in left lateral view and (B) Reconstruction of MOR 1141 in left lateral view. [planned for page width] 282

48. FIGURE 4. *Orodromeus makelai* juvenile skull [MOR 1136] skull rendered with and without texture. (**A**) Textured model with in-situ elements; (B) Untextured model with colored interpretation of skeletal elements in-situ; (C) MOR 1136 reconstructed in left and right lateral views; (D) dorsal and ventral views; and (E) anterior and posterior views. [planned for page width] 283

49. FIGURE 5. *Orodromeus makelai* cervical series rendered with and without texture. (A1 & A2) Holotype specimen [MOR 294] cervical series C2 through C9 in right and left lateral view; (B1 & B2) paratype specimen [MOR 1141] atlantal intercentrum in dorsal, ventral, and anterior views; (C1 & C2) MOR 1141 cervical vertebrae two and three in left lateral, dorsal, right lateral, and ventral views; (D1 & D2) MOR 1141 posterior cervical vertebra of uncertain placement in (left to right) left lateral, right lateral, dorsal, and ventral views; and (E1 & E2) . Abbreviations: atc, atlantal intercentrum; axc, axis intercentrum; cr, cervical rib; dap, diapophysis; gr, groove; ns, neural spine; odp, odontoid process; pap, parapophysis; poz, postzygapophysis; prz, prezygapophysis; tp, transvers process; vk, ventral keel. [planned for page width] 284

50. FIGURE 6. *Orodromeus makelai* dorsal series rendered with and without texture. (A) Holotype specimen [MOR 294] incomplete dorsal series in left lateral view, and (B) MOR 623 incomplete dorsal series in left lateral view. **Abbreviations**: **dap**, diapophysis; **f**, foramen; **ns**, neural spine; **pap**, parapophysis; **poz**, postzygapophysis; **prz**, prezygapophysis. [planned for page width]..... 285

LIST OF FIGURES CONTINUED

Figure Page

51. FIGURE 7. *Orodromeus makelai* sacral series [MOR 623 and PU 23409] rendered with and without texture. (A_1) MOR 623 in left lateral view; (A_2) MOR 623 in dorsal view; (A_3) MOR 623 in right lateral view; (A_4) MOR 623 in ventral view; (B_1) PU 23409 in left lateral view; (B_2) PU 23409 in dorsal view; (B_3) PU 23409 in right lateral view; and (B_4) PU 23409 in ventral view. **Abbreviations**: **f**, foramen; **icc**, intercentral cavity; **ics**, intercentral socket; **ns**, neural spine; **prz**, prezygapophysis; **poz**, postzygapophysis; **sr**, sacral rib. [planned for page width] 286

52. FIGURE 8. *Orodromeus makelai* caudal series 1-5 [MOR 623] rendered with and without texture. (A) MOR 623 left lateral view; (B) MOR 623 dorsal view; (C) MOR 623 right lateral view; and (D) MOR 623 ventral view. **Abbreviations**: **chf**, chevron facet; **f**, foramen; **ns**, neural spine; **prz**, prezygapophysis; **poz**, postzygapophysis; **tp**, transverse process; **vg**, ventral groove. [planned for column width] 287

53. FIGURE 9. *Orodromeus makelai* sternal plates rendered with and without texture. (A) Holotype specimen [MOR 294] sternal plates; (B) F# 08.05.95 ("Frankies *Orodromeus*") sternal plates; and (C) MOR 623 sternal plate. **Abbreviations**: **fa**, facet. [planned for column width] 288

54. FIGURE 10. *Orodromeus makelai* dorsal ribs rendered with and without texture. (A-C) MOR 623 dorsal ribs in lateral and anterior views. **Abbreviations**: **cp**, capitulum; and **tp**, tuberculum. [planned for page width] 289

55. FIGURE 11. *Orodromeus makelai* scapulocoracoid rendered with and without texture. (A) MOR 623 left scapula and coracoid in lateral and ventral view; (B) PU 23443 left scapula and coracoid in lateral and ventral views; (C) holotype specimen [MOR 294] left and right scapulocoracoid in lateral and ventral views; (D) PU 23246 right scapula in lateral view; and (D) PU 23443 lefft scapula in lateral view. **Abbreviations**: **ap**, acromion process; **cf**, coracoid foramen; **gl**, glenoid fossa; **sb**, supraglenoid boss; **sf**, scapular flange; **sgb**, supraglenoidal buttress; **sgf**, supraglenoid fossa; **spr**, sternal process; **ss**, scapular spine; **vf**, ventral fossa. [planned for page width] 290

LIST OF FIGURES CONTINUED

Figure Page

56. FIGURE 12. *Orodromeus makelai* humeri rendered with and without texture. (A) MOR 623 left humerus in anterior, and lateral views; (B) MOR 248 left humerus in anterior and lateral views; (C) both humeri holotype specimen [MOR 294] in anterior and lateral views; (D) MOR 404 right humerus in lateral and anterior views; (E_1) MOR 1136 right humerus in lateral and anterior views; and (E_2) MOR 1136 right humerus in-situ placement. **Abbreviations: bis,** bicipital sulcus**; dc**, deltopectoral crest; **hh**, humeral head olecranon process; **rc**, radial condyle; **uc**, ulnar condyle. [planned for page width] 291

57. FIGURE 13. *Orodromeus makelai* holotype specimens forearm rendered with texture and without. (A_1 & A_2) MOR 294 left radius and ulna in articulation; (B_1 & B_2) MOR 294 ulna in lateral, posterior, anterior, and medial views; and (C_1 & C_2) MOR 294 radius in lateral, posterior, anterior, and medial views. **Abbreviations**: **olp**, olecranon process. [planned for page width] 292

58. FIGURE 14. *Orodromeus makelai* manus rendered with and without texture. (A) PU 23442 in antipalmar and palmar views; (B) MOR 623 metacarpi in antipalmar and palmar views; (C) holotype specimen [MOR 294] metacarpi in two views. **Abbreviations**: **dc**, distal carpal; **i**, intermedium; **rd**, radiale; **ul**; ulnare. [planned for column width] 293

59. FIGURE 15. *Orodromeus makelai* ilia rendered with and without texture. (A) Holotype specimen [MOR 294] articulated ilia, ossified tendon, left femur, sacral vertebrae two through seven, and caudal vertebrae one through three in (left to right) dorsal, ventral, left lateral, and right lateral views; (B) MOR 623 left and right ilia in lateral, dorsal, and medial; (C) F#06.29.95 right ilia in lateral and dorsal views; (D) PU 23257 right partial ilia in lateral and dorsal views; and (E) MOR 331 left ilia in lateral view. **Abbreviations**: **bs**, brevis shelf; **ch**, chevron; **fe**, femur; **ics**, intercentrum socket; **il**, ilium; **isp**, ischiac peduncle; **ot**, ossified tendon; **pep**, preacetabular process; **pop**, postacetabular process; **pp**, pubic peduncle; [planned for page width] 294

60. FIGURE 16. *Orodromeus makelai* ischia rendered with and without texture. (A) PU 23431 and PU 23246 left and right ischia in dorsal view; and (B) PU 23431 and PU 23246 in ventral view. **Abbreviations**: **ip**, iliac peduncle; **obp**, obturator process; **pup**, pubic peduncle; **st**, sutural surface. [planned for page width] 295

LIST OF FIGURES CONTINUED

Figure Page

61. FIGURE 17. *Orodromeus makelai* pubis rendered with and without texture. (A) MOR 623 right pubis in dorsal and lateral views; (B) MOR 623 left pubis in dorsal and lateral views; (C) PU 23442 right pubis in posterior and lateral views; (D) holotype specimen MOR 294 left pubis in dorsal and lateral views. **Abbreviations**: **f**, foramen; **fos**, fossa; **obf**, obturator foramen; **pad**, prepubic pad; **ppp**, postpubic process; **prep**, prepubic process; **st**, striations. [planned for column width] 296

62. FIGURE 18. *Orodromeus makelai* femora in posterior and lateral views. (A) Nine femora rendered with texture. MOR 623 is the exception as the texture file was not retained in error when the mesh was created. Both left femora are currently undergoing histological sampling and are unavailable to rescan; (B) Nine femora rendered without texture. **Abbreviations**: **ic**, posterior intercondylar groove; **f**, foramen; **ft**, forth trochanter; **gt**, greater trochanter; **lc**, lateral condyle; **lt**, lesser trochanter; **mc**, medial condyle; **s**, sulcus. [planned for age width] 297

63. FIGURE 19. *Orodromeus makelai* tibiae rendered with and without texture. (A) MOR 623 left tibia in posterior and lateral views, no textured scan available and tibia is currently unavailable due to histological sampling; (B_1 & B_2) holotype specimen left tibia [MOR 294] in posterior and lateral views; (C_1 & C_2) MOR 1003 distal epiphysis and proximal head in articulation with the right femur, also distal half of left tibia with articulated astragalus; (D_1 & D_2) TM-006 proximal half of a right tibia in posterior and lateral views; and (E_1 & E_2) MOR 248 proximal half of the right tibia. **Abbreviations**: **as**, astragals; **cc**, cnemial crest; **df**, distal femur; **ic**, inner condyle; **im**, inner malleolus; **om**, outer malleolus. [planned for page width] 298

64. FIGURE 20. *Orodromeus makelai* fibula [MOR 623]. (A) MOR 623 right fibula rendered with texture, and (B) MOR 623 right fibula rendered without texture. **Abbreviations**: **fl**, flange. [planned for column width] 299

65. FIGURE 21. *Orodromeus makelai* tarsals rendered with and without texture. (A) Interpreted articulation of disarticulated tarsals of right hindlimb [MOR 623], and (B) tarsals in (descending order) anterior, dorsal, ventral, lateral, and medial views. **Abbreviations**: **as**; astragalus; **asp**: ascending process; **ca**, calcaneum; **f**, foramen; **ldt**, lateral distal tarsal; **mdt**, medial distal tarsal. [planned for column width] 300

LIST OF FIGURES CONTINUED

Figure Page

66. FIGURE 22. *Orodromeus makelai* juvenile pes [PU 23246] rendered with and without texture. (A) PU 23246 right pes with tarsals in anterior view; (B) PU 23246 left pes, tarsals, and tibia in anterior view; (C) PU 23246 right pes and tarsal in posterior view; and (D) PU 23246 left pes, tarsals, and tibia in posterior view. **Abbreviations**: **as**, astragalus; **ca**, calcaneum; **ldt**, lateral distal tarsal; **mdt**, medial distal tarsal; **ti**, tibia; **vp**, ventral pit. [planned for page width]..... 301

67. FIGURE 23. *Orodromeus makelai* subadult pes [MOR 623] rendered with and without texture. (A) MOR 623 right pes in anterior view; (B) MOR 623 left pes in anterior view; (C) MOR 623 right pes in posterior view; and (D) MOR 623 left pes in posterior view. **Abbreviations**: **vp**, ventral pit. [planned for page width]..... 302

ABSTRACT

Quantifying intraspecific variation within dinosaur assemblages is a quagmire that's vexed by limited samples and poor temporal constraints for many dinosaur taxa. This thesis attempts to explore variation within a large sample of early diverging ornithischian dinosaurs that spans across the Two Medicine-Judith River-Belly River clastic wedge in Montana, USA and Alberta, Canada. Orodromines were a group of small-bodied ornithischians that rapidly diversified in the Campanian of western North America and are disproportionally abundant within the Two Medicine Formation. Previous workers assigned all Two Medicine orodromine material to the monospecific genus *Orodromeus makelai*. This thesis reevaluates orodromine specimens within a newly updated chronostratigraphic framework. These new temporal constraints facilitate accurate comparisons with other orodromines elsewhere in the clastic wedge. Comparative morphological analyses reveal at least three previously unrecognized morphotypes within the Two Medicine-Judith River-Belly River clastic wedge with minimal temporal overlap. Data suggests these morphotypes are indicative of interspecific variation and do not support an intraspecific interpretation. This thesis proposes three new orodromine taxa and creates new systematic divisions between specimens previously considered to all be *Orodromeus makelai*.

Disclaimer: This thesis is not intended to meet the provision of the ICZN (1999) regarding the publication of nomenclatural acts [Art. 8.2]. No name or nomenclatural act proposed herein should be considered available as defined by the ICZN.

CHAPTER ONE

INTRODUCTION TO THESIS

Orodromeus makelai

Ornithischians are one of two major clades of dinosaurs with charismatic members of notoriety like *Triceratops*, *Stegosaurus*, *Edmontosaurus*, and *Ankylosaurus*. Thescelosauridae is an early diverging family within Ornithischia, and the subfamilies Thescelosaurinae and Orodrominae nested within it (Avrahami et al., 2024; Madzia et al., 2021). Orodromines are an enigmatic group of small-bodied ornithischians from the Cretaceous of North American thought to exhibit a burrowing habit, with burrowing potentially the thescelosaurid archetype condition (Avrahami et al., 2024; Boyd, 2012; Button et al., 2023; Huh et al., 2010). This burrowing habit is unique among dinosaurs and is proposed for *Orodromeus makelai* from the Upper Cretaceous Two Medicine Formation (Hannebaum et al., 2022; Martin, 2014) but only demonstrated in the Middle Cretaceous thescelosaurine *Oryctodromeus cubicularis* from the Blackleaf and Wayan Formations (Fearon et al., 2016; Krumenacker et al., 2019; Varricchio et al., 2007; Woodruff et al., 2011), with multiple individuals (juveniles and adults) from the latter occurring together within burrow traces (Krumenacker et al., 2019; Varricchio et al., 2007). This fossorial habit provides an unprecedented opportunity for direct anatomical comparisons of co-occurring individuals, while also facilitating exceptional preservation of specimens and an abundance of fossil material for these taxa in their respective formations. *Orodromeus makelai* is one of the quintessential “hypsilophodontid-grade” early diverging ornithischians long considered a stable

taxon with well resolved phylogenetic affinities thanks to a large sampling from the Two Medicine Formation.

Orodromeus, past research.

Orodromeus makelai has a long history of collection in the Campanian Two Medicine Formation. This has produced the largest sample for a thescelosaurid with hundreds of specimens held at the Museum of the Rockies (MOR) in Bozeman, MT (Scheetz, 1999). The first specimens were first discovered during John Horner's famous Princeton University expeditions of 1978 and 1979 to the Two Medicine Formation (Horner et al., 1988), which notably also produced the first dinosaur eggs and nests in North America (Horner et al., 1979). Subsequent *Orodromeus* studies encompassed thermoregulation (Barrick et al., 1996), an unpublished osteological description (Scheetz, 1999), and a comparative long bone histological analysis to infer growth rates (Horner et al., 2009). *Orodromeus makelai* also serves as a stable locus for many phylogenetic analyses (Avrahami et al., 2024; Dieudonné et al., 2021; Madzia et al., 2021; Poole, 2023). To date, all orodromine skeletal material collected in the Two Medicine and Judith River Formations are assigned to the monospecific genus *Orodromeus* (Scheetz, 1999; Wolfe and Horner, 2003).

Orodromeus research 2019-present.

I have conducted a preliminary taphonomic assessment of all the orodromine skeletal material held by the MOR, along with newly collected specimens from the Egg Mountain fossil locality (TM-006). This assessment established common taphonomic characteristics shared between *Orodromeus* and *Oryctodromeus* likely indicating similar taphonomic modes driving preservation [i.e., burrows] (Hannebaum et al., 2022). This survey also produced a large dataset

based on femora (n=150), charting the mortality profile of the Two Medicine orodromine assemblage which revealed most specimens are skeletally immature and mortality peaks in individuals approaching one year old (Hannebaum et al., 2023*)*.

Orodromine variation in the Two Medicine-
Judith River- Belly River clastic wedge.

Orodromines are unique amongst early diverging ornithischian lineages as they exhibit prominent laterally, or posterolaterally, deflecting jugal horn cores; potentially homologous to the jugal bosses of *Heterodontosaurus* (Norman et al., 2011). Five well preserved orodromine skulls exist from the Two Medicine Formation and consist of three juveniles (MOR 294, 436, 1136) and two adults (MOR 473, 1141). The two adult skulls are noteworthy because they represent two distinct morphs based on their differing jugal horns. In MOR 473, the jugal horn core is small, posterolaterally deflecting, and triangular in cross section. Meanwhile, the jugal horn core of MOR 1141 is large, posterolaterally projecting, and shows prominent ridges on the anterior, posterior, and ventral faces. Furthermore, isolated indent. orodromine jugal horn cores collected from elsewhere in the Two Medicine Formation, and the contemporaneous Judith River Formation, are inconsistent with either morph. For example, MOR 14147 was recovered near the base of the McClelland Ferry Member of the Judith River Formation and consists of an isolated large, robust, laterally deflecting jugal horn, distinct from any other known orodromine. This suggests orodromine jugal horn variation may be examples of intra-specifical variation, as many modern animals exhibit prominent sexually dimorphic cranial display features used, in large part, for sexual display. Therefore, perhaps the disparate jugal horn morphologies documented here are examples of sexual dimorphism in the cranial display features of *Orodromeus makelai*.

An updated temporal framework for the Two Medicine-Judith River clastic wedge.

Recent chronostratigraphic work has created a robust temporal framework facilitating accurate placement of most orodromine specimens in the Two Medicine and Judith River Formations (Ramezani et al., 2022; Rogers et al., 2016; Rogers et al., 2023; Rogers et al., 2024). This reveals orodromine occurrences are stretched across a significant time interval in the Two Medicine-Judith River clastic wedge. Two 'zones' of orodromine occurrences emerge in the Two Medicine assemblage. The youngest, exemplified best by MOR 473, is restricted temporally to strata above the lacustrine interval of the Flag Butte Member of the Two Medicine Formation. The second 'zone' comprises the entirety of the lacustrine interval of the Flag Butte Member and includes MOR 1141, and the juvenile *Orodromeus makelai* holotype, MOR 294 (Rogers et al., 2024). In the Judith River Formation, orodromine skeletal material previously assigned to *Orodromeus* (MOR 14148) or pachycephalosaurs (MOR 14147) are restricted to the bottom of the McClelland Ferry Member, preceding most orodromine occurrences in the Two Medicine Formation (Figure 1.1).

Sexual dimorphism or systematic differences?

Detecting sexual dimorphism in extinct organisms is a notoriously difficult endeavor (Hedrick and Dodson, 2013; Hone and Mallon, 2017; Mallon, 2017) even though it was likely widespread based on extensive modern examples in sexually reproducing animals (Kim et al., 2013; Shine et al., 2002; Tarnawski et al., 2014). Many non-avian dinosaurs are proposed to exhibit dimorphic characteristics based on physiological variation between specimens within species, such as *Stegosaurus*, *Coelophysis*, and *Heterodontosaurus* (Rinehart et al., 2009; Saitta, 2015; Thulborn, 1974). However, to date, proposed instances of sexual dimorphism lack large

robust samples which preclude statistical analyses, and many examples of dimorphism are now attributed to unrecognized ontogenetic change or intraspecific variation (Mallon, 2017). To counteract the uncertainty when assessing morphological variation, we suggest certain criteria must be known: (1) the ontogenetic age of the specimens, (2) the sex of an individual, and (3) the stratigraphic relationships of the specimens within a sample.

Histological sampling is a powerful tool to assess the developmental stage, age, and sex of an individual (Erickson and Tumanova, 2000; Schweitzer et al., 2016; Woodward et al., 2016). Histological sampling exceeds the bounds of much of this study and as no orodromine specimens have been recovered with eggs internally, sexing individuals remains elusive. However, as highlighted above, a revised chronostratigraphic framework for the Two Medicine-Judith River clastic wedge shows distinct 'zones' of orodromine occurrences with no discernable temporal or locality overlap. This is suggestive of multiple unrecognized orodromine taxa present within the sample.

The osteology of orodromine specimens in the Two Medicine-Judith River-Belly River clastic wedge is here explored, revealing at least two distinct orodromine species in the Two Medicine Formation (*Pikunidromeus ancellae*, gen. et sp. nov. and *Orodromeus makelai*), while a novel third species occupies the Lower Judith River Formation (*Akanthodromeus judithi*, gen. et sp. nov.). These taxonomic revelations show orodromines diversified rapidly during the Campanian in a specific regressive/transgressive phase of the Western Interior Cretaceous Seaway (WICS) and northern Laramidia hosted a wide range of these small ornithischians. It also highlights how unusual their rapid disappearance remains, as no orodromines are documented in strata younger than ca. 73.0 Ma. (Druckenmiller et al., 2021) and seemly are

replaced by their larger cousins *Parksosaurus* and *Thescelosaurus* (Brown et al., 2013). The subsequent chapters will explore the osteology of *Akanthodromeus judithi* (Chapter 2), *Pikunidromeus ancellae* (Chapter 3), and re-diagnose *Orodromeus makelai* (Chapter 4).

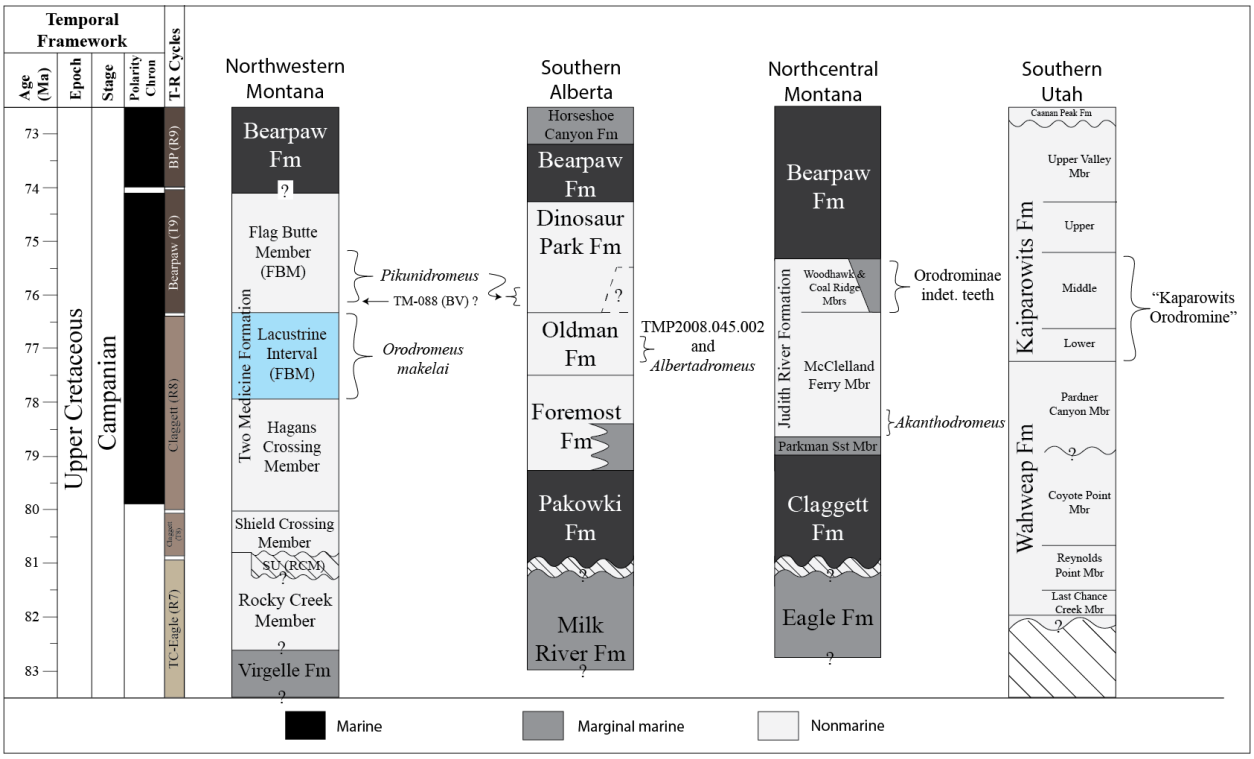


Figure 1.1. Stratigraphic section of the Two Medicine-Judith River-Belly River clastic wedge and southern Utah, with orodromine occurrences denoted by genera. Of the five skulls discussed above, MOR 436 and 473 are assigned to *Pikunidromeus ancellae* above the lacustrine interval of the Flagg Butte Member of the Two Medicine Formation; MOR 294, 1136, and 1141 encapsulate the cranial morphology of *Orodromeus makelai* which is confined to the lacustrine interval. In the Lower Judith River Formation MOR 14147 and 14148 mark the temporal distribution of *Akanthodromeus judithi*. This figure was created using the figures and data referenced from Brown et al. (2013), Ramezani et al. (2022), and Rogers et al. (2024).

Literature Cited

Avrahami, H. M., Makovicky, P. J., Tucker, R. T., & Zanno, L. E. (2024). A new semi-fossorial thescelosaurine dinosaur from the Cenomanian-age Mussentuchit Member of the Cedar Mountain Formation, Utah. *Anatomical record (Hoboken, N.J.: 2007)*. doi:10.1002/ar.25505

Brown, C. M., Evans, D. C., Ryan, M. J., & Russell, A. P. (2013). New data on the diversity and abundance of small-bodied ornithopods (Dinosauria, Ornithischia) from the Belly, River Group (Campanian) of Alberta. *Journal of vertebrate paleontology*, 33(3), 495-520. https://doi.org/10.1080/02724634.2013.746229.

Druckenmiller, P. S., Erickson, G. M., Brinkman, D., Brown, C. M., & Eberle, J. J. (2021). Nesting at extreme polar latitudes by non-avian dinosaurs. *Current Biology*, 31(16), 3469-3478.

Erickson, G. M., & Tumanova, T. A. (2000). Growth curve of *Psittacosaurus mongoliensis* Osborn (Ceratopsia: Psittacosauridae) inferred from long bone histology. *Zoological Journal of the Linnean Society*, *130*(4), 551-566.

Hone, D. W. E., & Mallon, J. C. (2017). Protracted growth impedes the detection of sexual dimorphism in non-avian dinosaurs. *Palaeontology, 60*(4), 535-545. doi:10.1111/pala.12298

Hedrick, B. P., & Dodson, P. (2013). Lujiatun Psittacosaurids: Understanding Individual and Taphonomic Variation Using 3D Geometric Morphometrics. *PloS one, 8*(8), e69265. doi:10.1371/journal.pone.0069265

Kim, Y. K., Koyabu, D., Lee, H., & Kimura, J. (2013). Sexual Dimorphism of Craniomandibular Size in the Korean Water Deer, Hydropotes inermis argyropus. *Journal of Veterinary Medical Science, 75*(9), 1153-1159. doi:10.1292/jvms.13-0125

Mallon, J. C. (2017). Recognizing sexual dimorphism in the fossil record; lessons from nonavian dinosaurs. *Paleobiology, 43*(3), 495-507. doi:10.1017/pab.2016.51

Norman, D. B., Crompton, A. W., Butler, R. J., Porro, L. B., & Charig, A. J. (2011). The Lower Jurassic ornithischian dinosaur *Heterodontosaurus tucki* Crompton & Charig, 1962: cranial anatomy, functional morphology, taxonomy, and relationships. *Zoological Journal of the Linnean Society*, 163(1), 182-276.

Ramezani, J., Beveridge, T. L., Rogers, R. R., Eberth, D. A., & Roberts, E. M. (2022). Calibrating the zenith of dinosaur diversity in the Campanian of the Western Interior Basin by CA-ID-TIMS U–Pb geochronology. *Scientific Reports*, *12*(1), 16026.

Rinehart, L. F., Lucas, S. G., Heckert, A. B., Spielmann, J. A., & Celesky, M. D. (2009). The Paleobiology of Coelophysis bauri (Cope) from the Upper Triassic (Apachean) Whitaker quarry, New Mexico, with detailed analysis of a single quarry block. *New Mexico Museum of Natural History and Science Bulletin* (45), 1-260.

Rogers, R. R., Kidwell, S. M., Deino, A. L., Mitchell, J. P., Nelson, K., & Thole, J. T. (2016). Age, correlation, and lithostratigraphic revision of the Upper Cretaceous (Campanian) Judith River Formation in its type area (north-central Montana), with a comparison of low-and high-accommodation alluvial records. *The Journal of Geology*, *124*(1), 99-135.

Rogers, R. R., Eberth, D. A., & Ramezani, J. (2024). The “Judith River–Belly River problem” revisited (Montana-Alberta-Saskatchewan): New perspectives on the correlation of

Campanian dinosaur-bearing strata based on a revised stratigraphic model updated with CA-ID-TIMS U-Pb geochronology. *Bulletin*, *136*(3-4), 1221-1237.

Rogers, R., Horner, J., Ramezani, J., Roberts, E., and Varricchio. D. (2024). Updating the Upper Cretaceous (Campanian) Two Medicine Formation of Montana: Lithostratigraphic revisions, new CA-ID-TIMS U-Pb ages, and a calibrated framework of dinosaur occurances. The Geologial Society of America Bulletin.

Saitta, E. T. (2015). Evidence for sexual dimorphism in the plated dinosaur Stegosaurus mjosi (Ornithischia, Stegosauria) from the Morrison Formation (Upper Jurassic) of western USA. *PloS one, 2015*(4), e0123503-e0123503. doi:10.1371/journal.pone.0123503

Schweitzer, M. H., Zheng, W., Zanno, L., Werning, S., & Sugiyama, T. (2016). Chemistry supports the identification of gender-specific reproductive tissue in *Tyrannosaurus rex*. *Scientific Reports, 6*(1), 23099-23099. doi:10.1038/srep23099

Shine, R., Reed, R., Shetty, S., & Cogger, H. (2002). Relationships between sexual dimorphism and niche partitioning within a clade of sea-snakes (Laticaudinae). *Oecologia, 133*(1), 45-53. doi:10.1007/s00442-002-1012-7

Tarnawski, B. A., Cassini, G. H., & Flores, D. A. (2014). Skull allometry and sexual dimorphism in the ontogeny of the southern elephant seal (Mirounga leonina). *Canadian journal of zoology, 92*(1), 19-31. doi:10.1139/cjz-2013-0106

Thulborn, R. A. (1974). A new heterodontosaurid dinosaur (Reptilia; Ornithischia) from the Upper Triassic red beds of Lesotho. *Zoological journal of the Linnean Society, 55*(2), 151-175. doi:10.1111/j.1096-3642.1974.tb01591.x

Wolff, E., & Horner, J. R. (2003). The first occurrence of *Orodromeus makelai* postcrania from the Late-Campanian Judith River Formation of eastern Montana. *Journal of Vertebrate Paleontology*, 23(3), 122.

Woodward, H. N., Fowler, E. A. F., Farlow, J. O., & Horner, J. R. (2015). *Maiasaura*, a model organism for extinct vertebrate population biology: a large sample statistical assessment of growth dynamics and survivorship. *Paleobiology*, 41(4), 503-527.

CHAPTER TWO

THE EARLIEST ORODROMINE FROM THE UPPER CRETACEOUS JUDITH RIVER FORMATION ELUCIDATES A NEW SPECIES PREDATING *ORODROMEUS MAKELAI* IN THE CONTEMPORANEOUS TWO MEDICINE FORMATION.

Contribution of Authors and Co-Authors

Manuscript in Chapter 2

Author: Zakaria J. Hannebaum

Contributions: Conceived the study, performed analyses, interpreted results, and wrote the manuscript.

Co-Author: David J. Varricchio

Contributions: Conceived the study, discussed results and implications, and edited manuscript drafts.

Co-Author: Ewan Wolffe

Contributions: Provided preliminary specimen description and edited manuscript drafts.

Co-Author: John R. Horner

Contributions: Excavated specimens, curated specimens, and edited manuscript drafts.

Manuscript Information

Zakaria Hannebaum, David J. Varricchio, Ewan Wolff, John R. Horner

Journal of Vertebrate Paleontology

☒ Prepared for submission to a peer-reviewed journal
☐ Officially submitted to a peer-reviewed journal
☐ Accepted by a peer-reviewed journal
☐ Published in a peer-reviewed journal

Abstract

Orodromines are noticeably uncommon in the Judith River Formation of northcentral Montana, with only isolated teeth documenting their presence in the uppermost strata of the formation. Historically, *Orodromeus makelai* stood as a monolith to which all orodromine taxonomic assignments in the Two Medicine and Judith River Formations gravitated. Here, we refer two specimens, MOR 14147 and MOR 14148, to a new species of orodromine erected as *Akanthodromeus judithi*, gen. et sp. nov. MOR 14148 fell previously under the taxonomic shadow of *Orodromeus makelai* but displays a distinct morphology. MOR 14147 is a right jugal horn which laterally deflects, unique amongst the posterolaterally deflecting jugal horns of other orodromines. Both specimens occur in the lowermost Judith River Formation and within the most recent chronostratigraphic framework, places *Akanthodromeus* as the oldest named orodromine in the Two Medicine-Judith River-Belly River clastic wedge predating *Orodromeus makelai* in the Two Medicine Formation.

Introduction

The Campanian-aged terrestrial Judith River Formation of northcentral Montana has been a nexus of paleontological research for well over a century, with the first vertebrate and dinosaur fossils collected and described over 160 years ago (Leidy, 1856). In contrast to the other formations comprising the Two Medicine-Judith River-Belly River clastic wedge, dinosaur fossils in the Judith River Formation are largely fragmentary with complete skulls or skeletons uncommon. Exceptional specimens do exist though, like the spectacularly preserved holotype specimen (ROM 75860) of the ankylosaurid *Zuul crurivastator* (Arbour and Evans, 2017), along

with large monospecific ceratopsian (Chiba et al., 2018) and hadrosaurid bonebeds (Freedman, 2015; LaRock, 2000). The *Daspletosaurus wilsoni* holotype (BDM 107) is one of the most complete theropods from the formation (Warshaw and Fowler, 2022), with the group otherwise represented by shed teeth (Fiorillo and Currie, 1994) and very fragmentary remains (Dalman and Lucas, 2015; Wilson and Fowler, 2021). Microfossil sites are plentiful in the formation and capture much of the faunal compositions through time (Sahni, 1972; Fiorillo and Currie, 1994).

Orodromines are one dinosaur group markedly rare in the Judith River Formation. Orodromines are a charismatic group of small-bodied early diverging ornithischians [SBEDOs] (Avrahami et al., 2024). Orodromines may have exhibited a burrowing habit (Avrahami et al., 2024; Boyd, 2012; Button and Zanno, 2023), are abundant in the neighboring Two Medicine Formation (Horner et al., 2001; Scheetz, 1999) and have noted occurrences in the Oldman and Dinosaur Park Formations (Brown et al., 2013; Hudgins, 2021). Until recently, 12 Galton, 1995; Sahni, 1972) and three teeth (Umeno and Tanoue, 2016), referred to *Orodromeus makelai*, represented the only documented occurrence of an orodromine in the Judith River Formation restricting these dinosaurs to the uppermost strata of the Judith River Formation. Here, we describe new cranial and postcranial material documenting a new orodromine in the Lower Judith River Formation. *Akanthodromeus judithi* gen. et sp. nov. becomes the second oldest occurrence of an orodromine in North America, reducing the ghost lineage between *Zephyrosaurus* and *Orodromeus* in North America (Avrahami et al., 2024), and highlights an unusual and unrecognized disparity in the cranial display features and hindlimb morphology of this group.

Materials and methods

SBEDOs (small-bodied early diverging ornithischians) is an acronym recently coined by Avrahami et al. (2024). SBEDOs acknowledges a "grade" of distantly related early diverging ornithischian lineages which exhibit similar body plans (i.e. bipedal, small-bodied, similar dentition, etc.) that previous researchers termed "Fabrosaurids" (Galton, 1978), "Hypsilophodontids" (Weishampel and Heinrich, 1992), and "basal ornithopods" (Norman et al., 2004). These previous terms were erected to group unrelated taxa within a phylogenetic context and ignored their gradational context.

We discuss anatomy using the Romerian anatomical and directional terms for fossil vertebrates (Wilson, 2006), in preference of veterinarian terms like rostral or caudal to limit misunderstandings as a rostral bone is a derived feature of ceratopsians, which thescelosaurids lack.

Specimens are defined here as any independent occurrence of an individual represented from a single non-toothed element to associated skeletal materials. The two specimens described below are curated at the Museum of the Rockies in Bozeman, Montana and accessed therein. MOR 14148 was excavated from within a *Brachylophosaurus* bonebed (MOR 1071, JR-224) on a Bureau of Land Management parcel near Malta, MT by MOR field crews sometime during the summer field seasons of 1998 and 1999 (LaRock, 2000). MOR 14147 was collected by David Varricchio in Kennedy Coulee northwest of Havre, MT on July 4th, 2010, while prospecting private ranchland with Yoshi Katsura and Jason Moore (field notes of D. J. Varricchio). Specimens in this study were digitally imaged using the photogrammetry application called Abound (v. 3.0.0) on an iPhone 13 mini and 16 pro max, using a macro-lens at times, following

the workflow outlined by Avrahami et al. (2023). The MOR's Creaform model Go!SCAN 20 supplemented Abound in digitally imaging some elements and meshes were processed in VXelements v.11. Digital models were assembled in Blender v.4.3. The geological map was created using QGIS (v. 3.34.1) with GIS data sourced from the Montana Bureau of Mines and Geology, Montana State Library, and geoBoundaries.org. Adobe Photoshop v.25.12 and Illustrator v.28.7.1 were employed to create some final versions of figures.

Phylogenetic Methods

The phylogenetic relationships of *Akanthodromeus judithi* were assessed using MrBayes v3.2.7a (Ronquist et al., 2012) performed on the Tempest High Performance Computing System, operated and supported by University Information Technology Research Cyberinfrastructure at Montana State University. Specimens were added to the character matrix of Avrahami et al. (2024). This matrix contains 91 taxa and 411 characters. The benefits of employing Bayesian analytical methods over parsimony are discussed in detail in Avrahami et al. (2024) and Krumenacker et al. (2024). *Akanthodromeus* is missing 95% of the 411 characters in this dataset and because of its fragmentary nature we conducted two analyses in MrBayes, one analysis constraining the tips and basal node ages, while the second lacked a time constraint. These analyses removed taxa missing 50% of the data to retain taxa with the strongest phylogenetic signals. We ran four Markov-chain Monte Carlo (MCMC) replicates for 20,000,000 generations, each with four chains, sampling every 1,000 with a burn-in of 25% for both analyses. Due to the poor representation of *Marasuchus* in this dataset *Silesaurus* was chosen as the outgroup in the 50% reduced dataset. Minimum last appearance dates were determined from a primary survey of the literature and pulled from the Paleobiology Database to fix the tip dates and basal node ages.

The full dataset tree, character matrix nexus file, excel spreadsheet of missing data percentages for each taxon, and MrBayes script are in the supplementary materials. Our MrBayes script is constructed with input from the MrBayes script provided in the supplementary materials of Krumenacker et al. (2024). R studio v.3.6.0 was employed to create the time tree using packages "ggtree", "treeio:, "deeptime", "ggplot2", and "ape". Our R script was built with input from R script examples provided in Christopher Organ's Phylogenetics class taught in the spring of 2024 at Montana State University.

Institutional abbreviations

BDM, Badlands Dinosaur Museum, Dickinson Museum Center, Dickinson, North Dakota, United States; **IGM**, Institute of Geology, Mongolia, Ulaanbaatar, Mongolia; **IMNH**, Idaho Museum of Natural History, Pocatello, Idaho, United States; **MCZ**, Museum of Comparative Zoology, Harvard University, Cambridge, Massachusetts, United States; **MOR**, Museum of the Rockies, Bozeman, Montana, United States; **NCSM**, North Carolina Science Museum, Raleigh, North Carolina, United States; **PMOL**, Paleontological Museum of Liaoning, Shenyang, China; **PRC**, Palaeontological Research and Education Centre, Mahasarakham University, Maha Sarakham, Thailand; **ROM**, Royal Ontario Museum, Toronto, Ontario, Canada; **UMNH**, Natural History Museum of Utah, Salt Lake City, Utah, United States.

SYSTEMATIC PALEONTOLOGY

DINOSAURIA Owen, 1842

ORNITHISCHIA Seeley, 1887

NEORNITHISCHIA Cooper, 1985 (sensu Madzia et al., 2021)

THESCELOSAURIDAE Sternberg, 1937 (sensu Madzia et al., 2021)

ORODROMINAE Brown et al., 2013 (sensu Madzia et al., 2021)

AKANTHODROMEUS gen. nov.

(Figs. 4-11)

Type Species—*Akanthodromeus judithi*, sp. nov.

Generic Etymology—Greek words *akantho* and *dromeus*, together meaning the 'thorn runner', name is in reference to the large laterally projecting jugal horn and spike-like medial projection of the medial distal tarsal, along with alluding to the animal's presumed cursorial habits.

Diagnosis—As for type.

AKANTHODROMEUS JUDITHI gen. et sp. nov.

Holotype—MOR 14148, partial postcranial skeleton.

Referred specimen—MOR 14147, isolated right jugal.

Specific etymology—*'judithi'* honors the Upper Cretaceous Judith River Formation where all specimens described here are collected.

Diagnosis—A SBEDO differentiated by the following combinations of morphological characters with autapomorphies denoted by an *: large laterally projecting jugal horn core*; paired nutrient foramina on medial wall of jugal; orbital rim on anteromedial border of postorbital ramus of jugal; fourth trochanter proximal to femoral head; tibia lateral malleolus extending distally lower than articular surface of medial malleolus; medial distal tarsal fused to metatarsal III*; medial distal tarsal blocky, thin, and squarish in proximal view with small medially projecting triangular process*; and ridge on dorsal face of metatarsal IV*.

Horizon—The Judith River Formation represents the coastal frontier of a large clastic wedge part of the Western Interior Basin (WIB), a retroarc foreland basin with sedimentation derived from the North American cordillera highlands of the subcontinent Laramidia (Fuentes et al., 2012; Kauffman, 1977). Deposition within the Judith River Formation largely tracks the Campanian regressive and transgressive cycles of the Western Interior Cretaceous Seaway (WICS). The Judith River Formation is bordered to the west by the Two Medicine Formation and the Belly River Group in the north (Rogers et al., 2016; Rogers et al., 2023). The Judith River Formation is subdivided into four members; the basal Parkman Sandstone, the McClelland Ferry, the Coal Ridge, and the Woodhawk Members (Rogers et al., 2016). Deposition began prior to ca. 78.594 ± 0.024 Ma. and largely concluded ca. 75.219 ± 0.031 Ma. (Ramezani et al., 2022).

The historical dearth of dinosaur fauna in the Judith River Formation stands in sharp contrast to neighboring formations within the Two Medicine-Judith River-Belly River clastic wedge, especially the Dinosaur Park Formation in Alberta, where over 45 dinosaur taxa are currently recognized (Arbour and Evans, 2017). Over the past 15 years, a surge of dinosaur discoveries has transformed our understanding of dinosaur communities in the Judith River Formation and revealed an interconnectedness with neighboring formations previously unrecognized (Loewen et al., 2024; Takasaki et al., 2022). These discoveries reveal a faunal composition dominated by ceratopsians like *Lokiceratops*, *Judiceratops*, *Medusaceratops*, *Avaceratops*, *Mercuriceratops*, *Spiclypeus*, and *Furcatoceratops* (Dodson, 1986; Ishikawa et al., 2023; Loewen et al., 2024; Longrich, 2013; Mallon et al., 2016; Ryan et al., 2010; Ryan et al., 2014). Hadrosaurs are present such as *Probrachylophosaurus*, *Brachylophosaurus*, *Gryposaurus*, and *Corythosaurus* (Freedman, 2015; Freedman and Horner, 2015; LaRock, 2000; Takasaki et

al., 2022), along with the ankylosaur *Zuul* (Arbour and Evans, 2017), with at least one pachycephalosaur, *Colepiocephale* (Schott et al., 2009). Theropods are represented by shed teeth (Dalman and Lucas, 2015), eggs (Jackson et al., 2010), and fragmentary specimens (Wilson and Fowler, 2020) but an exceptional skeleton of *Daspletosaurus* was recently described (Warshaw and Fowler, 2022).

Locality—The jugal (MOR 14147) is recovered from MOR locality JR-866 in the lowermost section of the McClelland Ferry Member of the Upper Cretaceous Judith River Formation. JR-866 is a microsite locality residing in Kennedy Coulee on private ranchland in northcentral Montana. Other fossil material collected from the JR-866 consists of shed tyrannosaurid teeth, fish scales and vertebrae, crocodilian osteoderms, and a coprolite. JR-866 lies above a prominent coal bed at the base of the coulee and below a notable monodominant *Gryposaurus sp.* bonebed (JR-429) (field notes of D. J. Varricchio; Freedman, 2015). Freedman (2015) surmises this coal bed correlates to the informal Taber Coal Zone coeval with the Upper Foremost Formation. The JR-866 microsite horizon sources from a thick sandstone bed above the Taber Coal Zone assigned to the Herronton Sandstone Zone by Freedman (2015). However, utilizing informal marker beds and units to make broad regional correlations between the Foremost, Judith River, and Oldman Formations may be problematic and only likely is applicable at a local scale (Rogers et al., 2023). The Herronton Sandstone Zone, as mentioned above, may prove useful for correlating faunal occurrences within Kennedy Coulee but its proposed chronostratigraphic expressions elsewhere in the Foremost and Oldman Formations are contested (Rogers et al., 2023), with some placing it at the top of the Foremost Formation (Eberth, 2005; 2015) and others the base of the Oldman Formation (Cullen et al., 2016; Eberth,

2024). Furthermore, there is no readily discernible pattern in thick fluvial sandstone bodies at surface sections or in well logs at the type-section of the McClelland Ferry Member of the Judith River Formation, as they are distributed throughout (Rogers et al., 2023). Recent work instead focuses on the potential chronostratigraphic significance of the Coal Marker A bed in the Taber Coal Zone. The Taber Coal Zone lies at the top of the Foremost Formation and is correlated with coal seams at the base of Kennedy Coulee (Eberth, 2024; Lowen et al., 2024). A bentonite within Coal Marker A at Kennedy Coulee recently produced U-Pb dates of 78.594 ± 0.024 Ma (Ramezani et al., 2022). Therefore, though JR-866 lacks exact placement in the basal thick sandstone bed figured in Freedman (2015) we know the MOR 14147 was recovered within 15.0 m. above the Taber Coal Zone.

MOR 14148 is the holotype specimen and is a partial post cranial skeleton discovered associated within a *Brachylophosaurus sp.* bonebed (JR-224) near Malta in northcentral Montana (LaRock, 2000). Like JR-866, JR-224 is recovered from the lowermost section of the McClelland Member of the Judith River Formation. All skeletal material from this site is catalogued under MOR 1071, which included this specimen; however, MOR 14148 was recently given this separate designation to distinguish it from the *Brachylophosarus* specimens. JR-224 sits approximately 16.0 meters above the marine Claggett Formation and 9.0 meters above the Parkman Sandstone (LaRock, 2000). The bonebed is confined to a fine-grained, well sorted, tan to brown, friable sublitharenite approximately 1.8 meters thick (LaRock 2000). The bonebed is dominated by at least six partially articulated *Brachylophosaurus sp.* individuals stacked against a tree trunk which runs perpendicular through the quarry. LaRock (2000) interprets the bonebed as fluvially deposited against a log jam.

Comments—MOR 14148 was presented previously as the first postcranial occurrence of *Orodromeus makelai* in the Judith River Formation at the 2003 Society of Vertebrate Paleontology annual meeting (Wolff and Horner, 2003).

Description

Akanthodromeus judithi is represented by a single right jugal (MOR 14147) and an associated partial postcranial skeleton consisting of a sternal plate, incomplete radius, and a partial right hindlimb (MOR 14148). Many of the anatomical comparisons that follow will be made against an orodromine taxon here denoted as the "Landslide Butte Orodromine" (Chapter 3). This taxon was previously presented on and referred to as such in Hannebaum et al. (2024) and will primarily reference specimens MOR 436 and 473. Another orodromine taxon from the Campanian of Utah is informally referred to as the "Kaiparowits Orodromine", the osteology of which was described in detail in a doctoral dissertation (Boyd, 2012) and also briefly in Gates et al. (2013). Lastly, comparisons will be made to a mysterious orodromine taxon represented only by jugals colloquially called the "BV Orodromine" from the fossil locality TM-088 (BV) in the Two Medicine Formation (Chapters 3 & 4).

Cranium

Jugal—Orodromine jugals are triradiate-shaped and frame the ventral and posteroventral margins of the orbit. The maxillary ramus projects anteriorly, the postorbital ramus extends dorsally, and the jugal wing extends posteriorly. The most distinguishing features of orodromine jugals are the jugal horn cores (=boss) which project from the lateral face of the jugal, with two nutrient foramina on the medial face, opposing the jugal horn core. A sharp orbital rim marks the

anteromedial edge of the postorbital ramus in orodromines, just below a sulcus which receives the ventral ramus of the postorbital.

MOR 14147 is partially complete, and a broken edge defaces the anterior margin of the jugal horn core indicating where the maxillary ramus once projected. It is common for isolated orodromine jugals to be found missing the maxillary ramus, with examples in the "Kaiparowits Orodromine" [UMNH VP 1947], *Pikunidromeus* [MOR 613 and ROM 64600] *Orodromeus* [F#7.7.99.28 and MOR 647], and *Zephyrosaurus* [YPM 56695 and OMNH V1048]. MOR 14147 displays a large pyramidal horn core which projects from the lateral face of the element. The horn core is triangular in cross-section, with anterior, dorsal, and posteroventrally flattened faces. In MOR 14147, rugosity is restricted to those surfaces with pronounced vascular canals running mediolaterally, which likely fed a keratinous sheath in life. The ridge separating the dorsal and ventral faces is "pinched" at the base of the horn core. The horn core of MOR 14147 terminates in a rounded tip. The medial wall of MOR 14147 is concave with two nutrient foramina. These foramina are exposed along a broken edge on the anterior margin of the jugal. The most conspicuous of the two nutrient foramina opens into a vascular canal on the anterior face of the horn core. The jugal wing process projects posteriorly and terminates ventrally in a triangular-shaped point. Just dorsal to this triangular-shaped process is a broken surface indicating the jugal wing was potentially bifurcated, which is a common condition across Thescelosauridae (Avrahami et al., 2024; Barrett and Han, 2009; Jin et al., 2010; Makovicky et al., 2011). The triangular process is very similar to the morphology of the ventral process of the bifurcated jugal wing of the "Landslide Butte Orodromine" [MOR 473]. A D-shaped robust postorbital process extends dorsally with a notable sulcus demarcating the anterodorsal margin. The posterodorsal

margin exhibits a broken edge partially along its length. The medial wall of the postorbital process is gently concave with a sharp ridge (=orbital rim) marking the anteromedial edge.

The morphology described above is most consistent with that of the jugals of orodromines. Three diagnostic features of MOR 14147 point to this assignment. The first is the large laterally projecting jugal horn core. Jugal horns are a synapomorphy of Orodrominae (Boyd, 2012; Scheetz, 1999; Sues, 1980) and convergent with the jugal bosses of Heterodontosaurs (Sereno, 2012). The second diagnostic feature of MOR 14147 is the two nutrient foramina observed medial to the horn core. Scheetz (1999) first posited these nutrient foramina could be diagnostic. We confirm this to be the case as paired nutrient foramina are only observed in the "Landslide Butte Orodromine" [MOR 473 and MOR 613], the "BV Orodromine", the "Kaiparowits Orodromine" [UMNH VP 19470], and *Zephyrosaurus* [MCZ 4392]. The thescelosaurines *Fona* [NCSM 33548] and the neoceratopsian *Prenoceratops* (Fig. 5, Chinnery, 2004) exhibit a singular nutrient foramen along the medial wall of the jugal. *Cerasinops* shows at least two nutrient foramina [MOR 300]. *Thescelosaurus neglectus* novelly shows three nutrient foramina on the medial wall of the jugal (NCSM 15728] which may also be shared in *Minimocursor* [PRC 150] based on Figure 5 in Manitkoon et al. (2023), as Avrahami et al. (2024) noted the jugal figured is exposed medially. The third diagnostic jugal feature of MOR 14147 is the protruding anteromedial ridge (=orbital rim) of the postorbital ramus. This pronounced orbital rim on the postorbital ramus of MOR 14147 is shared only with orodromines like *Orodromeus* [MOR 613 and 1141], the "Landslide Butte Orodromine" [MOR 473], the "BV Orodromine", the "Kaiparowits Orodromine" [UMNH VP 19470], and *Zephyrosaurus* [MCZ 4392].

Axial skeleton

Sternum—MOR 14148 preserves a single sternal plate, and some uncertainty surrounds if it's a left or right. Though we do not know its anatomical positioning, when discussing anatomical directions its important to note lateral, medial, anterior, and posterior edges are the same regardless if it's the left or right plate, only the dorsal and ventral surface is unable to be determined. The sternal plate is flat with a weakly crescentic lateral margin like *Orodromeus* specimens MOR 294 and 623 (Scheetz, 1999). Posteriorly, the sternal plate terminates in a rounded tip, while anteriorly the lateral corner exhibits a small facet likely for articulation with the coracoid. This facet is also observed in *Orodromeus* [MOR 623, F#8.5.95] and the "Landslide Butte Orodromine" [MOR 473]. The sternal plate is very thin (at midpoint of plate) and its thickness falls within the range of sternal plates for *Orodromeus* [0.22-0.29 cm.] and the "Landslide Butte Orodromine" [0.25 cm.]. On one side of the sternal plate the outer surface of MOR 14148 is heavily eroded but along the medial portion much of the outer bone surface is retained.

Appendicular Skeleton

Radius—A partial radial shaft is recovered for MOR 14148, lacking both articular ends. We identified this element as the radius because a ridge runs lengthwise on the lateral edge as observed in the "Landslide Butte Orodromine" [MOR 436], *Orodromeus* [MOR 294], *Haya* (Barta and Norell, 2021), and *Fona* (Avrahami et al., 2024;). In MOR 14148, this shaft also expands as it approaches both broken edges. The sub-oval cross-section of this fragment may is consistent alternatively with the cross-section of the postpubic shaft of the pubis; however,

orodromines exhibit a straight pubic shaft, which is much more rod-like and straight in comparison to this element in MOR 14148 which is slightly curved. As MOR 14148 also comes from a *Brachylophosaurus* bonebed it is also reasonable to suggest this fragment could be a piece of ossified tendon. It is unlikely to be a fragment of *Brachylophosarus* ossified tendon as again the curvature of the shaft is dissimilar to the relatively straight ossified tendons of hadrosaurids; furthermore, the inner cortex of ossified tendons is rather dense in cross-sections where MOR 14148 offers instead a hollow shaft. The expanded shaft approaching both ends is also inconsistent with an ossified tendon designation. All in all, the sub-oval cross-section of MOR 14148, slight medial bowing, and the expanded broken epiphyses support this incomplete element is a partial radius, and closely matches the morphology seen in the "Landslide Butte Orodromine" [MOR 436, 473, and ROM 64600] and *Orodromeus* [MOR 294]. Notably the radius of MOR 14148 demonstrates a similar thickness to the radius of a juvenile specimen [MOR 436] of the "Landslide Butte Orodromine", though MOR 14148 was a larger animal, comparable in size to the subadult *Orodromeus* specimen MOR 623.

Femur—A partial proximal section of a right femur is recovered for MOR 14148. The femur morphology is degraded by modern weathering processes that obliterated the greater trochanter, while post-burial compression collapsed portions of the diaphysis. Nevertheless, certain features are still observable. The femoral head exhibits a neck-like constriction, a feature common in SBEDOs but absent in some early lineages like *Heterodontosaurus*, *Lesothosaurus*, and the theropod *Herrerasaurus* (Baron et al., 2017; Novas, 1994; Santa Luca, 1980). In MOR 14148, the neck of the femoral head is angled away from the diaphysis at 125 degrees. Amongst SBEDOs this angle varies, but most thescelosaurids exhibit a femoral head-diaphysis angled

greater than 100 degrees like *Oryctodromeus*, *Nevadadromeus*, *Fona*, *Zephyrosaurus*, and *Haya* (Avrahami et al., 2024; Bonde et al., 2022; Krumenacker et al., 2024; Barta and Norrell, 2021). In *Orodromeus*, it's worth noting there is an observed irregularity in this angle between specimens attributable to taphonomic distortion from post-burial compression but also likely due to some degree of individual variation (pers. observ.) which casts some doubt on the credibility of this character [char. 345] in the matrix of Avrahami et al. (2024). In MOR 14148, the posterior face of the femoral head is marked by a deep, prominent, obliquely angled U-shaped sulcus which serves as the insertion site and route of the *m. iliotrochantericus* (Maidment and Barrett, 2011). This sulcus is common amongst thescelosaurids but is also observed in *Gideonmantellia*, *Hypsilophodon*, *Minimocursor*, *Convolosaurus* (Andrzejewski et al., 2019; Galton, 1975; Manitkoon et al., 2023; Ruiz-Omeñaca et al., 2012) and elasmarians like *Notohypsilophodon* and *Anabisetia* (Coria and Calvo, 2002; Ibiricu et al., 2014). This U-shaped sulcus is deeply penetrating in MOR 14148 like the "Landslide Butte Orodromine" [MOR 436 and 473], *Fona* (Avrahami et al., 2024), and *Oryctodromeus* (Krumenacker et al., 2024). This condition is dissimilar to the shallowly depressed sulcus observed in *Notohypsilophodon* (Ibiricu et al., 2014). The lesser trochanter of MOR 14148 is narrow in lateral profile and its dorsal margin is positioned even with the femoral head, a condition similarly observed in *Orodromeus* (Scheetz, 1999), the "Landslide Butte Orodromine" [MOR 436 and 473], and *Oryctodromeus* (Krumenacker et al., 2024). The fourth trochanter of MOR 14148 arises from the posteromedial surface of the diaphysis proximal to the head. The fourth trochanter is broken near its base. A shallow rugose elliptical fossa lies medial to the fourth trochanter marking the insertion site for the *M. caudofemoralis longus* and potentially the *M. puboischiofemoralis internus* (Maidment

and Barrett, 2011). This single shallow rugose fossa, confined to the medial margin of the diaphysis, is the also observed broadly in SBEDOs (Andrzejewski et al., 2019; Barta and Norrell, 2021; Galton, 1975; Scheetz, 1999). A small nutrient foramen is observed near the dorsal base of the fourth trochanter on the posterior surface. The femur is triangular in cross section at the fourth trochanter like *Fona* and *Oryctodromeus* (Avrahami et al., 2024; Krumenacker et al., 2024).

Tibia—A right tibia is recovered with MOR 14148, but like the femur, both epiphyses of the tibia are partially deteriorated, and the shaft is collapsed in parts due to post-burial compression. The complete tibia length of MOR 14148 is 17.19 cm. which is comparable to the tibia length of the probable subadult *Orodromeus* specimen MOR 623 [16.57 cm.]. The distal epiphysis is transversely expanded in MOR 14148. In many ornithischians like *Zalmoxes*, *Talenkauen*, *Oryctodromeus*, and *Thescelosaurus* the tibial shaft is twisted on its axis (Brown et al., 2011; Krumenacker et al., 2024; Rozadilla et al., 2019; Weishampel et al., 2003). The shaft of MOR 14148 is not twisted on its axis, but as noted above, post-burial compression has given the tibia a flattened profile which likely tempered the original degree of axial torsion.

The proximal articular epiphysis of MOR 14148 is poorly preserved and moderately anteroposteriorly expanded like the “Landslide Butte Orodromine” [MOR 473], and *Albertadromeus* (Brown et al., 2013). The cnemial crest is mostly intact. It is rounded with a narrow fossa, the *insisura tibialis* (Butler et al., 2011), separating it from the fibular condyle, which is represented only by its distal base. The inner (=posterior) condyle is similarly intact and is rather broad, triangular in lateral view, before arcing posteriorly to a rounded point like A*lbertadromeus* (Brown et al., 2013) and the “Landslide Butte Orodromine” [MOR 473]. The

inner condyle does not demonstrate the hooked morphology observed in some *Oryctodromeus* specimens [MOR 1636, 1642, 8660; IMNH 44604, 44939]. The tibial shaft is triangular in cross-section at midshaft.

The medial and lateral malleoli, otherwise referred to as the inner and outer malleoli by Galton (1975), are largely intact in MOR 14148 only lacking some of the articular surface. The lateral malleolus extends distally lower than the articular surface of the medial malleolus, a condition observed in many SBEDOs like *Fona*, *Jeholosaurus*, *Hypsilophodon*, and *Convolosaurus* (Andrzejewski et al., 2019; Avrahami et al., 2024; Galton 1975; Han et al., 2012;). This differs from *Parksosaurus* where the distal margins of the malleoli are subequal (Sues et al., 2023). The posterior edge of the lateral malleolus exhibits a sharp flange along the approximately distal third of the tibia. This differs from the reduced flange exhibited in the "Landslide Butte Orodromine" and *Oryctodromeus* (Krumenacker et al., 2024). The lateral malleolus is separated from the medial malleolus posteriorly by a partially preserved ridge which is a prominent feature observed in many SBEDOs (Avrahami et al., 2024; Coria and Salgado, 1996; Galton, 1975; Han et al., 2012; Ibiricu et al., 2014; Krumenacker et al., 2023; Manitkoon et al., 2023; Ruiz-Omeñaca et al., 2012; Sheetz, 1999; Sues et al., 2023). The medial malleolus is not as robust in comparison to *Orodromeus* (Scheetz, 1999) or the "Landslide Butte Orodromine" [MOR 473].

Fibula—A portion of the proximal neck of the right fibular shaft is preserved in MOR 14148. As in the "Landslide Butte Orodromine", the fibular neck is proximately expanded before tapering into the shaft. The medial surface is concave as observed in *Fona* and *Orodromeus* (Avrahami et al., 2024; Sheetz, 1999), but note the shaft is also collapsed in MOR 14148.

Medial distal tarsal—The right medial distal tarsal remains in articulation and appears to be coossified, or fused, with metatarsal III, as the suture separating the two is partially closed in MOR 14148. This ankylose condition is relatively uncommon in SBEDOs and likely arose convergently in ankles of heterodontosaurids (Sereno, 2012), thescelosaurids like *Changmiania* (Yang et al., 2020), *Albertadromeus* (Brown et al., 2013), and *Koreanosaurus* (Haviv Avrahami, pers. comm.), the elasmarian *Anabisetia* (Coria and Calvo, 2002), and neoceratopsians (Arbour and Evans, 2019; Lee et al., 2011; Makovicky, 2010). The medial distal tarsal is thin with a squarish proximal profile in MOR 14148 which is a morphology shared with *Orodromeus*, *Hypsilophodon*, *Fona*, *Nanosaurus*, and the "Landslide Butte Orodromine" [MOR 473] (Avrahami et al., 2024; Galton, 1975; Galton and Jensen, 1973; Scheetz, 1999). *Lesothosaurus* exhibits a medial distal tarsal that is disc-shaped with concave surfaces dorsally and ventrally (Baron et al., 2017), like the semi-circular dorsal profile of *Gasparinisaura* (Salgado et al., 1997). In *Diluvicursor,* the medial distal tarsal is thin, wavy, and quadrangular in shape (Herne et al., 2018).

Notably, MOR 14148 presents a small medially projecting sub-triangular process extending from the main body of the medial tarsal. MOR 14148 observed condition is most like the reduced triangular medial process of *Fona* and *Nanosaurus* (Avrahami et al., 2024; Galton and Jenson, 1973). This process, though similar, is strikingly reduced and distinct from *Orodromeus* [MOR 623] and the "Landslide Butte Orodromine" [MOR 473] which exhibits a much broader, sub-rectangular and robust medial process. This same process is elongated in *Oryctodromeus* with a sharp proximal ridge running medial-laterally (Krumenacker et al., 2024). Han et al. (2012) surmises the medial distal tarsal consists of two fused tarsals. The medial

process discussed above could be interpreted as one of these fused tarsals with the main body the second; however, no visible suture is identified here but a prominent ridge demarks the dorsal face.

Pes—Four metatarsi are preserved in MOR 14148, only lacking metatarsal V. Though the tibia of MOR 14148 is comparable in size to probable subadult specimens of *Orodromeus* [MOR 623] the foot is proportionally larger. The metatarsal III/tibia length ratio of MOR 14148 is 0.55, which is more like 0.54 in *Minimocursor* [PRC 150], compared to a ratio of 0.49 for *Orodromeus* [MOR 623]. Other thescelosaurids exhibit similar metatarsal III/tibia length ratios to *Orodromeus* like *Changmiania* 0.48 [PMOL AD00114], and *Nanosaurus* 0.47 (Galton and Jensen, 1973). *Haya* [0.42-0.50], *Jeholosaurus* [0.47-0.55] and *Hypsilophodon* [0.45-0.53] all show a range in their metatarsal III/tibia length ratios. This is because there is a change in this ratio through ontogeny as the largest specimens display the lowest values in these taxa. Thescelosaurines like *Fona* 0.42 [NCSM 33548] *Thescelosaurus neglectus* 0.40 [MOR 1185] but also *Convolosaurus* 0.41 [SMU70534] all show proportionally low metatarsal III/tibia ratios.

The proximal portion of metatarsal I is broken and missing, making the nature of its articulation with the distal tarsals uncertain in MOR 14148, but the tapering profile of metatarsal I hints at a proximately thinning splintlike morphology common in SBEDOs (Boyd, 2012; Butler et al., 2011; Han et al., 2012; Ruiz-Omeñaca et al., 2012; Scheetz, 1999). In MOR 14148, metatarsal I is mediolaterally compressed at the break before expanding anteroposteriorly and transversely distally into a robust articular face. This translates to a triangular cross-section which is shared with other SBEDOs like *Jeholosaurus*, *Hypsilophodon*, *Minimocursor*, *Parksosaurus*, and *Convolosaurus* (Andrzejewski et al., 2019; Butler et al., 2011; Galton, 1975;

Manitkoon et al., 2023; Sues et al., 2023). This triangular cross-section differs from *Orodromeus* [MOR 623], the "Landslide Butte Orodromine" [MOR 436, 530, and 473] and *Oryctodromeus* [MOR 1642] which exhibit oval to sub-oval cross-sections; further, divergent from the D-shaped cross-section of metatarsal I in *Fona* (Avrahami et al., 2024). The lateral face of metatarsal I [MOR 14148] is flattened, and slightly concave proximately, with a sharp ridge running its length dorsoventrally, a feature shared with *Convolosaurus* (Andrzejewski et al., 2019). In MOR 14148, the dorsal surface of the shaft of metatarsal I is convex, sloping ventrolaterally. The distal articular face is subdivided into condyles, which we designate as the medial and lateral condyles. These condyles are separated posteriorly by a shallow U-shaped intercondylar groove. In *Oryctodromeus* this groove is V-shaped [MOR 1642]. In MOR 14148, a pronounced ligament pit marks the lateral surface of the lateral condyle like in many SBEDOs (Butler et al., 2011; Han et al., 2012; Krumenacker et al., 2024; Scheetz, 1999), but notably, another smaller ligament pit marks the medial face of the medial condyle as observed in *Oryctodromeus* [MOR 1642] and *Orodromeus* [MOR 623].

Metatarsal II is one of the three main weight-bearing metatarsi in MOR 14148, the other two being metatarsi III and IV. As with metatarsal I, metatarsal II is broken and lacks the proximal half. Below the midshaft break of metatarsal II, the shaft is straight and mediolaterally compressed, but the lateral face is slightly concave where it appressed against the medial face of metatarsal III. This results in a D-shaped cross-section of the shaft in MOR 14148. The contact between these metatarsi is quite extensive when compared to *Oryctodromeus* where metatarsal II diverges from III in the distal third of metatarsal III (Krumenacker et al., 2024). This contact entails most of the length of the lateral face of metatarsal II, stopping just dorsal to the lateral

ligament pit of the lateral condyle as in *Jeholosaurus*, *Fona*, and *Orodromeus* (Avrahami et al., 2024; Han et al., 2012; Scheetz, 1999). In MOR 14148, the shaft expands transversely and anteroposteriorly distally as it approaches the articular face of metatarsal II, which is also subdivided into a medial and lateral condyle. Of the two, the lateral condyle is larger, whereas the medial condyle is very reduced and deflects posteromedially. Prominent collateral ligament pits mark the medial and lateral condyles as in metatarsal I. These ligament pits are deep, especially the medial pit which shallowly marks the second metatarsi of *Orodromeus* [MOR 623] and the "Landslide Butte Orodromine" [MOR 436 and 473]. A U-shaped intercondylar groove separates the medial and lateral condyles in MOR 14148 as in *Orodromeus* [MOR 623, PU 23246] and the "Landslide Butte Orodromine" [MOR 436 and 473] differing from the steep walled V-shaped intercondylar groove on metatarsal II of *Oryctodromeus* [MOR 1642] and *Fona* (Avrahami et al., 2024). Well preserved, branching, vascular canals radiate towards the center of the articular surface of metatarsal II in MOR 14148.

Metatarsal III is largely complete, only lacking a small portion of the proximal epiphysis and shaft in MOR 14148. In *Orodromeus* [MOR 623], the "Landslide Butte Orodromine" [MOR 436, 473], and the "Kaiparowits Orodromine" (Boyd, 2012) the proximal epiphysis of metatarsal III is transversely compressed and anteroposteriorly expanded creating a thin rectangular cross-section, proximately, this differs from the proximal epiphysis of MOR 14148 which not as narrow and is transversely expanded to a much greater. In MOR 14148, metatarsal III is parallelogram-shaped in cross-section at mid-shaft before becoming sub-rectangular distally. The shaft is straight through proximal length before veering laterally just below the midshaft. The posterior face of the shaft collapses in parts but a pronounced ridge is observed to be running

dorsoventrally. This ridge forms the posterior margin of the medial articular fossa where metatarsal II would closely press medially. Beginning above the distal third portion of the shaft, another concavity marks the anterolateral contact for metatarsal IV. The distal shaft of MOR 14148 is transversely and anteroposteriorly expanded into a broad articular face subdivided into two condyles, medial and lateral. The lateral condyle is larger than the medial condyle like the "Landslide Butte Orodromine" [MOR 436 and 473]. Both condyles exhibit collateral ligament pits, with the lateral-most ligament pit the deeper of the two as in *Jeholosaurus* (Han et al., 2012). The condyles of metatarsal III in MOR 14148 are separated posteriorly by a shallow U-shaped intercondylar groove like *Fona* (Avrahami et al., 2024) and the "Landslide Butte Orodromine" [MOR 436 and 473], whereas the intercondylar groove on the third metatarsi of *Orodromeus* [MOR 623] and *Oryctodromeus* (Krumenacker et al., 2024) is much deeper and V-shaped. A conspicuous semicircular fossa marks the anterior surface of metatarsal III just above the distal condyles in MOR 14148. This fossa is documented in *Orodromeus*, *Jeholosaurus*, and *Changchunsaurus* (Butler et al., 2011; Han et al., 2012; Scheetz, 1999) and is distinct from the shallowly depressed fossa seen in *Oryctodromeus*, *Fona*, and *Haya* (Avrahami et al., 2024; Barta and Norrell, 2021; Krumenacker et al., 2024).

MOR 14148 retains a mostly complete metatarsal IV, which lacks only the most proximal articular face. The proximal most portion of the shaft is crushed anteroposteriorly in a similar fashion to the posterior face of metatarsal III. Metatarsal IV is slightly sinusoidal through its length but remains closely appressed to metatarsal III for the proximal half of its length. The shaft of MOR 14148 is flattened to slightly concave medially, in this proximal half of metatarsal IV, denoting its close contact with metatarsal III. A ridge diagonally crosses the posterior face of

metatarsal IV in MOR 14148 before curving into its termination at the lateral condyle. This ridge is common in SBEDOs, and is specifically denoted in *Fona*, *Changchunsaurus*, *Jeholosaurus*, *Parksosaurus*, *Hypsilophodon*, *Orodromeus*, and *Oryctodromeus* (Avrahami et al., 2024; Butler et al., 2011; Galton 1975; Han et al., 2012; Krumenacker et al., 2023; Scheetz, 1999; Sues et al., 2023). Another ridge diagonally crosses the anterior face of the shaft [MOR 14148], following the same trajectory and placement as the posterior ridge before also terminating at the lateral condyle. Distally, metatarsal IV becomes anteroposteriorly expanded into an articular face which is parallelogram-shaped in ventral view. This expanded distal articular surface is dwarfs *Orodromeus* [MOR 623] and is much more robust in comparison. Metatarsal IV is subdivided into two articular condyles. The medial condyle of MOR 14148 is large and rounded, whereas the laterally projecting lateral condyle is flange-like and reduced. The flange-like lateral condyle is much more developed than *Orodromeus* [MOR 623] and the "Landslide Butte Orodromine" [MOR 436 and 473]. A deep intercondylar groove is absent, with only a shallow depression separating the condyles. Ligament pits mark both condyles.

Six non-ungual phalanges are recovered with MOR 14148, all from the right foot. The first two non-ungual phalanges are recovered for each pedal digit in MOR 14148. Their articular faces are ginglymoid and distally subdivide into robust condyles exhibiting prominent collateral ligament pits. Subtriangular fossae (=dorsal pit) mark most of the phalanges just dorsal to the condyles. All the phalanges show abnormal rugosity which congregates near the articular faces which some phalanges even display protruding bone calluses as demonstrated with phalanges II-I, III-1, IV-I, and III-II. This rugosity may be attributable to osteoarthritis. Though osteoarthritis is more common in older individuals and thus indicates MOR 14148 was likely a non-juvenile, it

cannot be used as a definitive indicator for the ontogenetic stage of MOR 14148. This osteoarthritic bone surface is a uniting feature of the phalanges of MOR 14148 and allows for confident assignment of phalange III-I to MOR 14148 even though this bone was stored separate from the rest of the MOR 1071 bonebed in a small box labeled “Blob 4” which may indicate it was found separate from the rest of MOR 14148 in the MOR 1071 bonebed. Phalange III-I appears unusual as its proximoventral articular face is lipped, which is the condition normally demonstrated in phalanges distal to the first phalange in each digit. This is confirmed when compared to thescelosaurids like *Fona*, *Oryctodromeus*, the “Kaiparowits Orodromine”, and *Haya* (Avrahami et al., 2024; Barta and Norell, 2021; Boyd, 2012; Krumenacker et al., 2024). However, *Jeholosaurus* specimen IVPP V15939 exhibits a proximoventral lipped phalange III-I (Han et al., 2012) just like MOR 14148.

Phylogenetic Analysis

The phylogenetic affinities of *Akanthodromeus judithi* were explored through Bayesian analytics applied to an updated version of the Avrahami et al. (2024) character matrix. *Akanthodromeus* lacks 95% of the characters in this dataset, because of this, we reduced the updated Avrahami et al., (2024) character matrix to only include taxa that exhibit 50% of the characters within the matrix. This resolved matrix retained 36% of the taxa which exhibited the strongest phylogenetic signals. Two analyses were conducted, one with the taxa constrained by time and the other with taxa non-time constrained. This produced two trees which similarly recovered *Akanthodromeus* as an orodromine closely aligned with the “Landslide Butte Orodromine” and *Orodromeus* (Figure 11 and 12).

To note, we edited or clarified select characters and states in the Avrahami et al. (2024) character matrix. We added a character state to character 60; presence of a tall, non-ornamented, laterally projecting boss on the lateral surface of the jugal (4). Another state was added to character 67, jugal, morphology of portion of maxillary process that overlaps maxilla is bifurcated (2). Character 352 was changed in *Orodromeus* from (1) to (0&1) because all specimens of *Orodromeus makelai* preserving this character lack an intertrochanteric notch besides MOR 623. We updated the coding for *Oryctodromeus* (242:2) with the release of Krumenacker et al. (2024).

Discussion

There is a sustained orodromine presence throughout the later period of the Claggett regressive phase (R8) and much of the Bearpaw transgressive phase (T9) of the Western Interior Cretaceous Seaway (WICS) in the Two Medicine-Judith River-Belly River clastic wedge (Brown et al., 2013; Rogers et al., 2024; Scheetz, 1999). Previous work documented orodromine teeth only in the uppermost strata of the Judith River Formation (Galton, 1995; Sahni, 1972). These teeth overlap temporally with the “Landslide Butte Orodromine” in the Two Medicine Formation. Analyses of the two specimens describe herein document the first occurrences of orodromine skeletal material in the Lower Judith River Formation and support erecting a new species, *Akanthodromeus judithi* gen. et sp. nov., predating the earliest occurrences of *Orodromeus makelai* in the Two Medicine Formation (Scheetz, 1999).

The morphology of *Akanthodromeus* is consistent with that of orodromines and not with other small-bodied ornithischian groups present in North America during the Campanian like

pachycephalosaurs and leptoceratopsids. The laterally projecting pyramidal jugal horn core of *Akanthodromeus* [MOR 14147] is unique among orodromines but may be convergent with the laterally projecting, pyramidal jugal horns of the early diverging ceratopsid *Psittacosaurus sinensis* (Averianov et al., 2006). The jugal horns of the "Kaiparowits Orodromine" [UMNH VP 19470] and the "Landslide Butte Orodromine" [MOR 473] are like *Akanthodromeus* as they all exhibit flattened faces with distinct ridging and, in the case of "Kaiparowits Orodromine", pronounced rugosity and vascular canals (Boyd, 2012). Furthermore, the "Kaiparowits Orodromine" shares the blunted terminus of *Akanthodromeus*. The "Landslide Butte Orodromine" [MOR 473 and 613] exhibits a triangular cross-section like *Akanthodromeus* but differs in its smaller size and posterolateral deflection. The jugal horn of *Akanthodromeus* is further differentiated from *Orodromeus* [MOR 1141] which exhibits a large posterolaterally deflected horn with prominent anterior, ventral and posterior ridges. The "BV Orodromine" in the Two Medicine Formation is like *Orodromeus* as it projects posterolaterally with a cylindrical cross-section but differs as it lacks ridging before terminating to a sharp point. *Zephyrosaurus* uniquely exhibits a rectangular, flange-like jugal horn, which again projects posterolaterally (Sues, 1980). The jugal horn core of MOR 14147 does not resemble those of leptoceratopsids which form a ventrally deflected flange (Ryan et al., 2012), nor does it match the morphology of the cranial horn cores of pachycephalosaurs which tend to occur not in isolation and exhibit extremely rugose bone surface texture away from the cranial horn cores (Horner and Goodwin, 2009) or alternatively exhibit the low, elongate, anteroventrally inclined ridge of *Wannanosaurus* (Butler and Zhao, 2009). MOR 14147 presents two nutrient foramina on the medial face of the jugal opposite the horn core. These paired foramina are a synapomorphy of Orodrominae and

inconsistent with Pachycephalosaurus like *Wannanosaurus* which lack these medially placed foramina (Butler and Zhao, 2009), or leptoceratopsids like *Prenoceratops* where only one nutrient foramen is documented (Chinnery, 2004). Another feature of MOR 14147 distinct from Pachycephalosaurs is the presence of the protruding orbital rim on the postorbital ramus of the jugal (Fig. 6, Butler and Zhao, 2009).

The hindlimb morphology of *Akanthodromeus* [MOR 14148] is inconsistent with the hindlimb morphology of the other two documented non-orodromine groups of small-bodied ornithischians present in the Two Medicine-Judith River-Belly River clastic wedge: pachycephalosaurs and leptoceratopsids (Rogers et al., 2024; Ryan et al., 2012; Schott et al., 2009). In the hindlimbs of pachycephalosaurs like *Stegoceras* and *Homalocephale*, the femoral head lacks the prominent sulcus for the *ligamentum capitis femoris*, the fourth trochanter of the femur is located midshaft along the femur, and the tibia distal malleoli are subequal (Maryanska and Osmólska, 1974; Moore, 2021). This is inconsistent with the morphology of *Akanthodromeus* where the femoral head is marked by a prominent sulcus, the fourth trochanter begins proximate to the femur head, and the lateral malleolus extends distally lower than the medial malleolus on the tibia. Similar to thescelosaurids, leptoceratopsids exhibit a femoral head with a slight incising depression on the femur head for the *ligamentum capitis femoris* (Chinnery and Weishampel, 1998) but follow pachycephalosaurs and present tibia with subequal distal malleoli (Arbour and Evans, 2019; Brown, 1914). Leptoceratopsid femora further deviate from orodromines and exhibit a fourth trochanter at the midshaft (He et al., 2015) which probably correlates to their quadrupedal locomotion and larger body size.

Furthermore, the fusion of the medial distal tarsal to metatarsal three is relatively novel amongst SBEDOs, and in conjunction with the fused distal fibula and tibia of *Albertadromeus* (Brown et al., 2024) and *Koreanosaurus* (Avrahami, pers. comm.) hints at a coalescence of thescelosaurid hindlimb fusion patterns convergent with some lineages of non-avian and avian therapods. Perhaps this ankylose hindlimb serves as another adaptation for the proposed burrowing habit of orodromines (Button and Zanno, 2023; Boyd, 2012, Huh et al., 2010).

MOR 14147 and 14148 both occur in the lowermost Judith River Formation. They are separated by a significant geographic distance and do not exhibit any overlapping material. It's reasonable to suggest these two specimens could be representative of two different orodromine taxa; however, this possibility is unlikely when compared to orodromine occurrences in the nearby Two Medicine Formation. *Orodromeus* and the "Landslide Butte Orodromine" both occur in distinct "zones" with no documented overlap between the two taxa thus far. If this pattern holds true in neighboring formations, then it's unlikely for two orodromine taxa to occupy the same time intervals in the Lower Judith River Formation and warrants the assignment of both MOR 14147 and 14148 to *Akanthodromeus*.

Conclusion

Here we provide the first osteological description of an orodromine, *Akanthodromeus judithi* gen. et sp. nov., from the Lower Judith River Formation which showcases a unique laterally projecting jugal horn and distinct distal tarsal morphology. Reassessing orodromine skeletal material in the Two Medicine and Judith River Formations is revealing taxonomic divisions between specimens long considered *Orodromeus makelai*. Three distinct forms are now recognized here as the "Landslide Butte Orodromine", the "BV Orodromine", and

Akanthodromeus. These newly recognized taxonomic divisions demonstrate orodromine diversity exploded during the Campanian Stage of the Cretaceous, especially in northern Laramidia, and mark *Akanthodromeus* as the second oldest named orodromine in the Two Medicine-Judith River-Belly River clastic wedge. The multi-formational occurrences of the "Landslide Butte Orodromine" (Chapter 3) illustrates that further exploration of not only the Lower Judith River Formation but also contemporary strata in the Two Medicine Formation and Belly River Group have the potential to reveal more *Akanthodromeus* specimens. *Akanthodromeus* also reaffirms a documented lack of temporally overlapping occurrences between orodromines and their sister group the thescelosaurines in much of North America during the Cretaceous (Avrahami et al., 2024; Brown et al., 2013). A perplexing enigma, considering the documented co-occurrences of these groups in the high latitude Campanian Prince Creek Formation of Alaska (Druckenmiller et al., 2021) which implies the possibility of ecological coexistence and suggests that orodromines were likely not replaced by thescelosaurines through ecological competition.

Acknowledgments

This research was conducted by Z. J. H. as part of the fulfillment of a Master's degree at Montana State University in Bozeman, MT. D. J. V. collected MOR 14147 on July 4th, 2010, while prospecting Kennedy Coulee in northcentral Montana with Y. Katsura and J. Moore. Special thanks to Dan and Lila Redding for allowing D. J. V., Y. Katsura, and J. Moore to prospect on their property and for donating MOR 14147 to the MOR. Also, MOR 14148 was collected from Bureau of Land Management lands and special thanks to the BLM for granting collection permits to the MOR. Specimen access was granted by J. Scannella and E. Metz at the

MOR. E. Metz first recognized the potential taxonomic affinity and significance of MOR 14147 and brought it to the author's attention. Special thanks to C. Organ and E. Bender for their assistance in trouble shooting issues with time-tree scripts as they arose. Research was supported by the generous funding of the Jurassic Foundation and by the Geological Society of America through a Graduate Student Geoscience Grant. C. Brown, D. Evans, and R. Rogers graciously provided their anatomical insights into MOR 14147, and discussions with H. Avrahami, C. Brown, L. J. Krumenacker, R. Scheetz, and J. Scannella greatly enhanced the quality of this paper. S. Smith surfaced scanned and processed imaging of much of MOR 14148. B. Valdez expertly created the skeletal silhouette used in this manuscript. Special thanks to the editors.

Table 1. Measurements of appendicular elements in cm. Underlined numbers = incomplete.

Specimen	Element	Le	Width(prox.)	Width(dist.)	Thickness	
MOR 14148	Sternal Plate					
	Radius	**4.16**	0.73	0.89	0.65	

Specimen	Element	Le(D/V)	Wp(M/L)	Wp(A/P)	Wd(M/L)	Wd(A/P)
MOR 14148	Femur	**8.08**	3.95	-	-	-
	Tibia	17.19	-	3.99	-	3.04
	Fibula	**2.14**	-	-	-	-

Specimen	Element	Le(D/V)	W(M/L)	W(A/P)
MOR 14148	Distal tarsal	0.99	2.44	1.85

Specimen	Element	Le(D/V)	Wp(M/L)	Wp(A/P)	Wd(M/L)	Wd(A/P)
MOR 14148	Metatarsal I	**2.68**	-	-	1.03	0.88
	Metatarsal II	**5.5**	-	-	1.36	1.21
	Phalange 1	2.83	1.39	1.35	1.2	1.08
	Phalange 2	2.12	1.19	1.24	1.12	0.85
	Metatarsal III	9.49	-	-	1.71	1.28
	Phalange 2	1.84	1.28	1.1	1.17	0.76
	Metatarsal IV	**8.04**	-	-	1.42	1.35
	Phalange 1	2.22	1.47	1.29	1.13	1.05
	Phalange 2	1.72	1.14	1.24	1.1	0.95

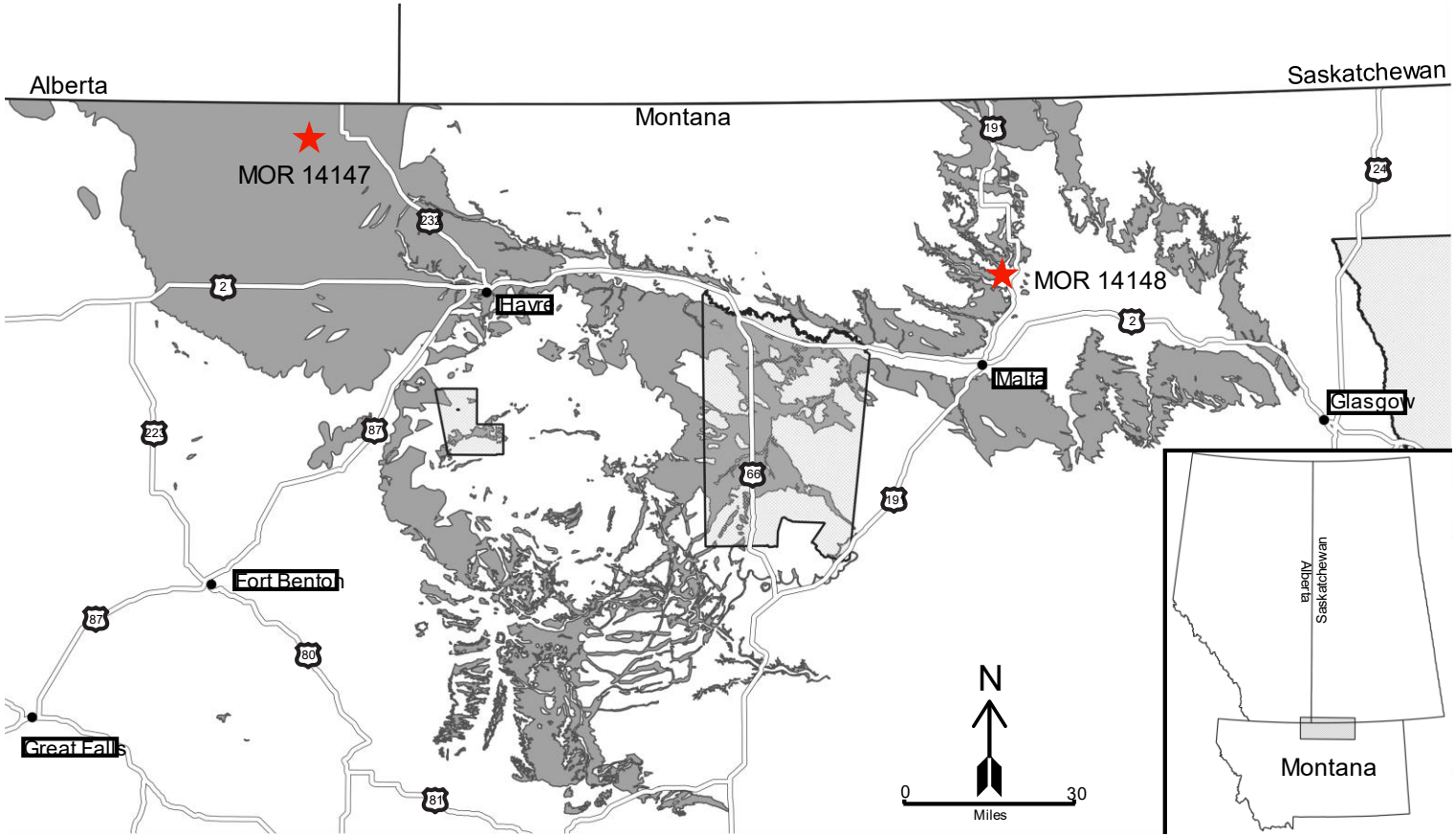


Figure 1. Geological map of Judith River Formation with *Akanthodromeus judithi* fossil localities denoted by red stars. Judith River Formation outcrops are shaded in gray with the following tribal lands outlined in black with cross-hatched interiors: (from left to right on map; Chippewa Cree Tribe, Fort Belknap Reservation, and Fort Peck Indian Reservation). Scale bar equals 30.0 miles. [Planned for page width].

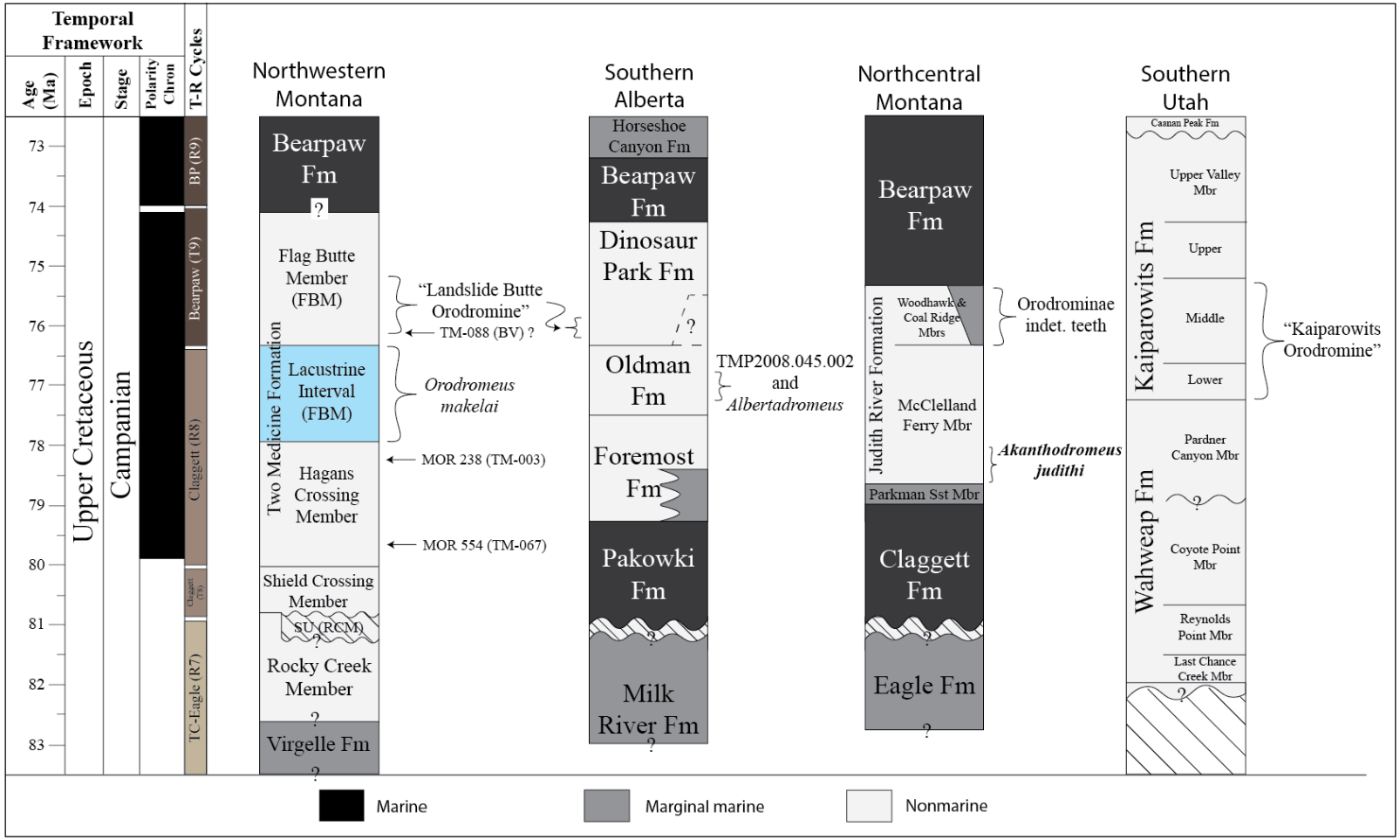


Figure 2. Campanian stratigraphic section of northwestern Montana, southern Alberta, northcentral Montana, and southern Utah with orodromine occurrences denoted through time. This figure was created using data and figures from Brown et al. (2013), Ramezani et al. (2020), and Rogers et al. (2024). [Planned for page width].

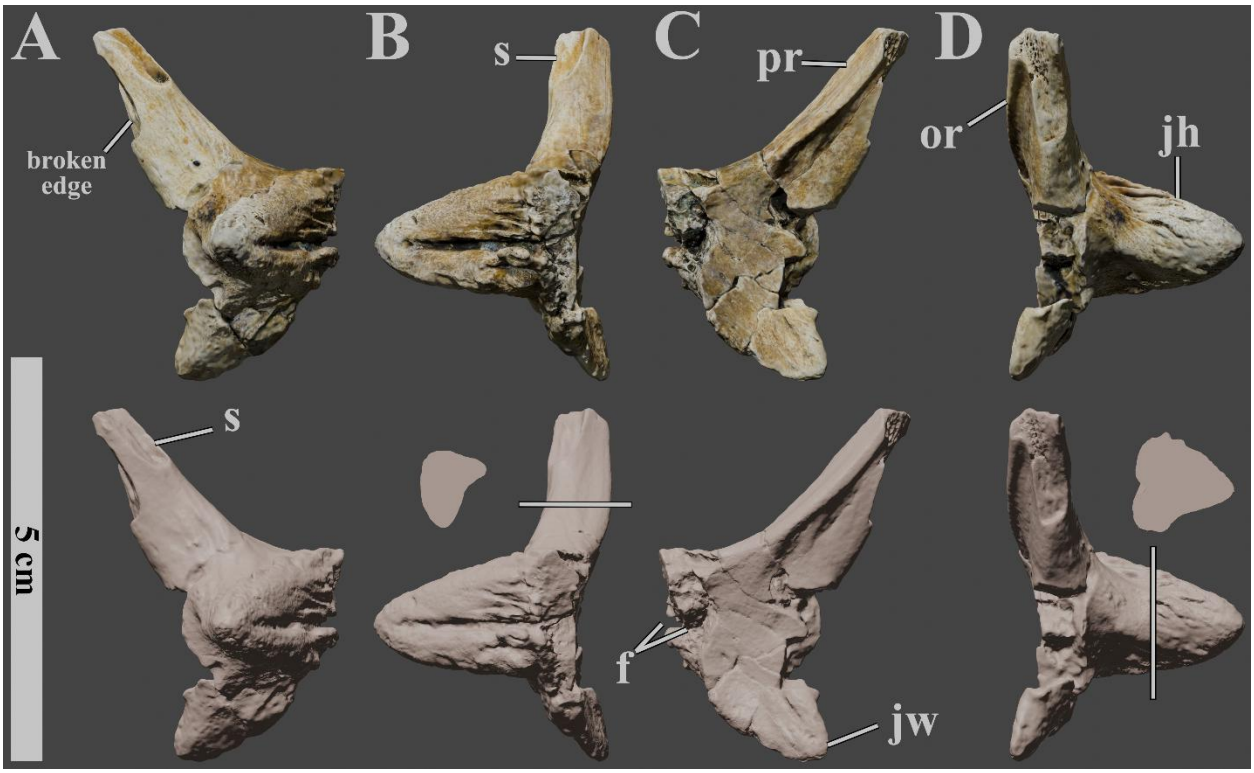


Figure 3. MOR 14147 right jugal rendered with and without texture in [from top to bottom in each row] (A) lateral; (B) anterior; (C) medial; and (D) posterior views. **Abbreviations: f**, nutrient foramen; **jh**, jugal horn; **jw**, jugal wing; **or**, orbital rim; **pr**, postorbital ramus; **s**, sulcus. [Planned for page width].

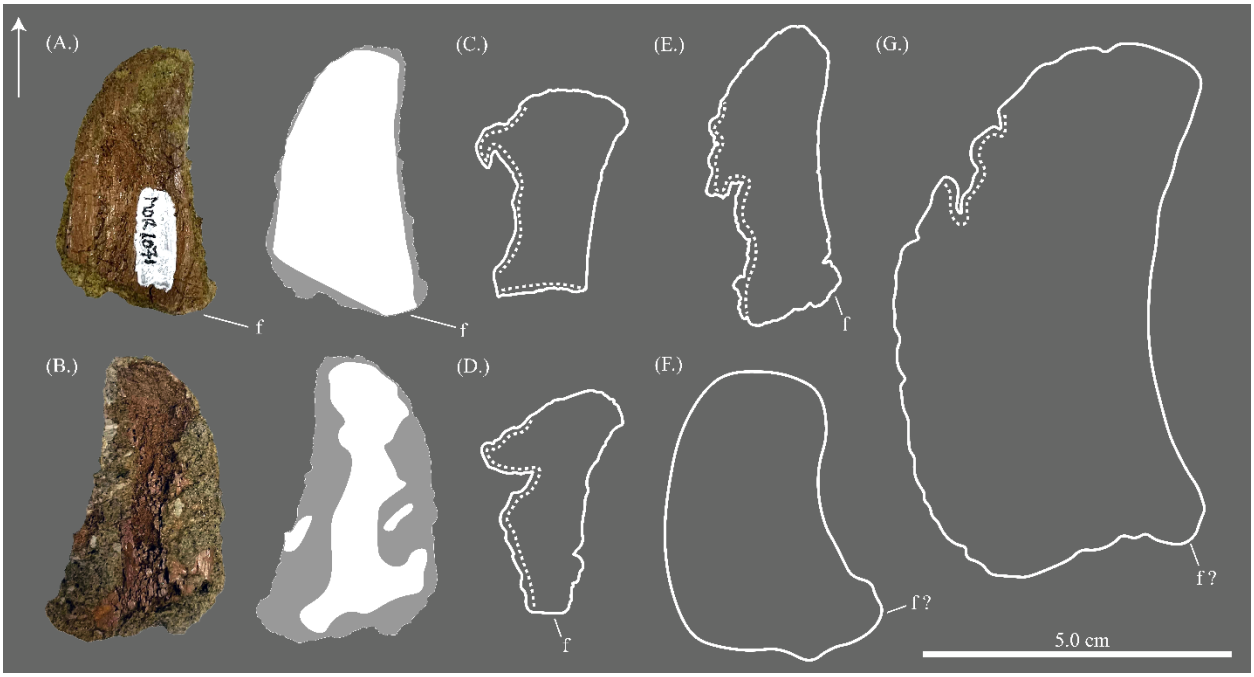


Figure 4. (A-B) MOR 14148 sternal plate in two views. (C-E) *Orodromeus* sternal plates: (C-D) "Frankies *Orodromeus*" F#8.5.95, (E.) MOR 623. (F.) *Haya* [IGM 100/2015]. (G.) *Parksosaurus* [ROM 804]. White shading denotes visible bone, while grey shading shows matrix. White dashed lines demarcate broken edges. Arrow denotes anterior. **Abbreviations: f**, facet; **f ?**, potential facet. Scale bar equals 5.0 centimeters (cm.). [Planned for page width]

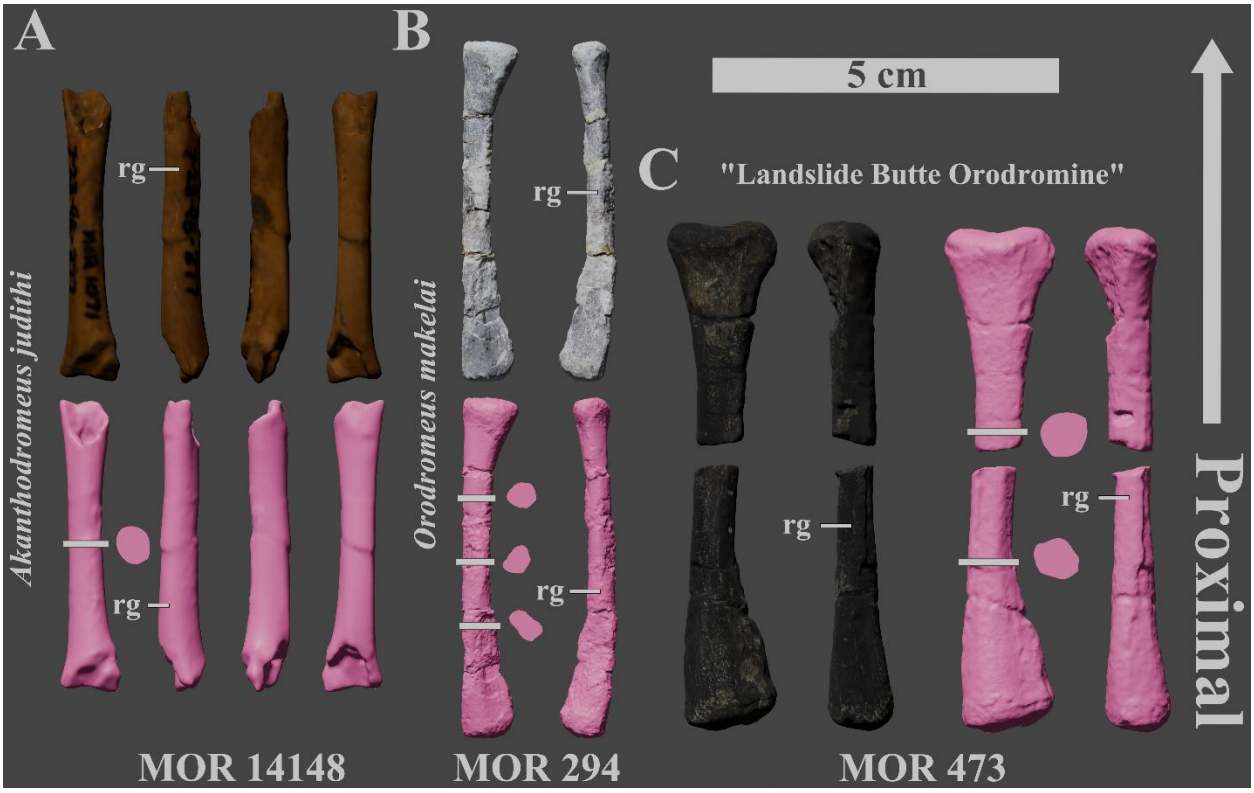


Figure 5. MOR 14148 partial radius rendered with and without texture in (A) Anterior?, lateral, medial, and posterior? views; (B) *Orodromeus makelai* radius [MOR 294] in lateral and anterior views; and (C) "Landslide Butte Orodromine" radius [MOR 473] in lateral and anterior views. **Abbreviations: rg**, ridge. [Planned for column width].

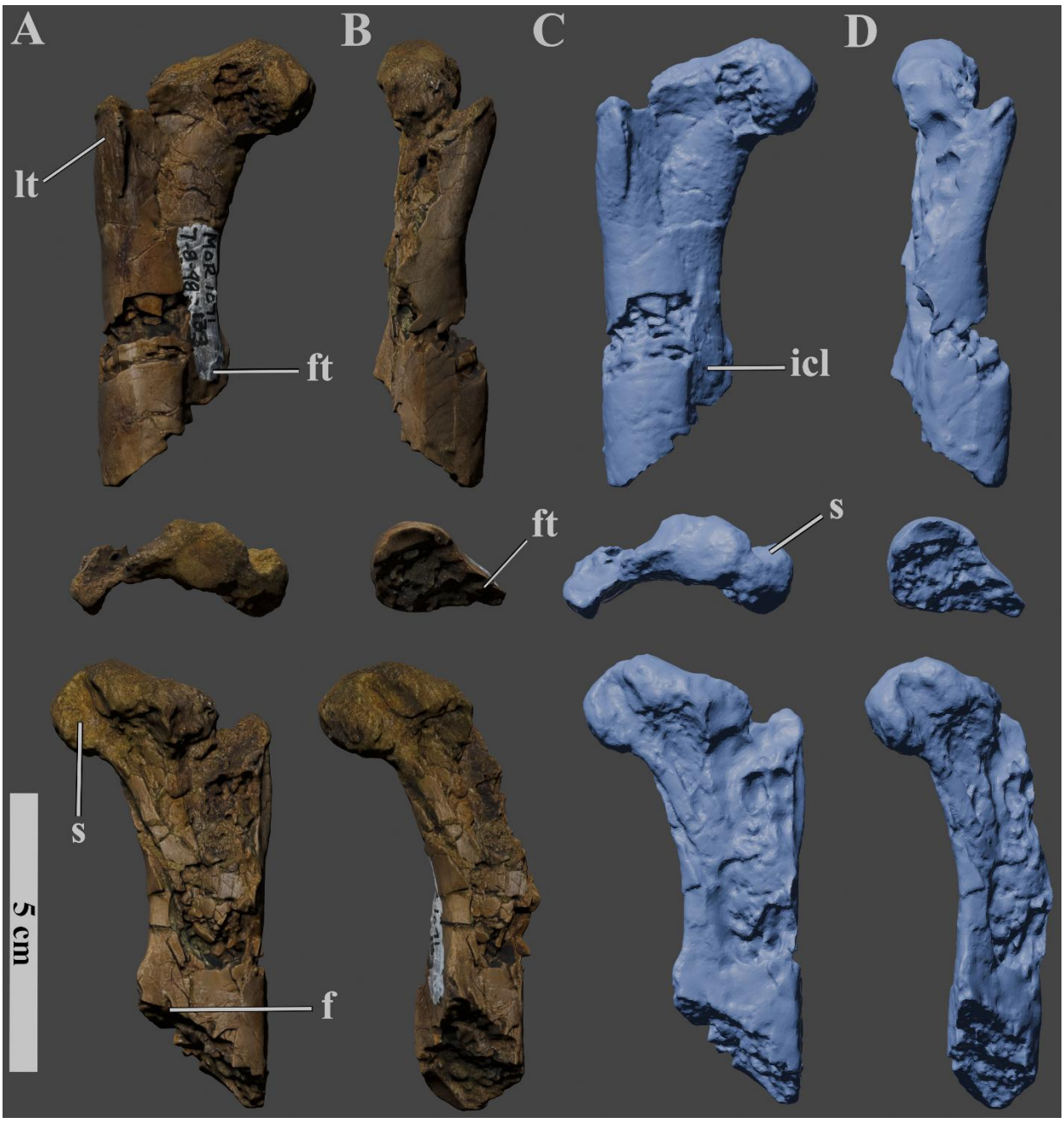


Figure 6. MOR 14148 partial right femur rendered with and without texture in [from top to bottom in each row] (A.) anterior, proximal, and posterior; (B.) lateral, distal, and medial; (C.) anterior, proximal, and posterior; and (D.) lateral, distal, and medial views. **Abbreviations: f**, nutrient foramen; **ft**, fourth trochanter; **icl**, insertion pit for *M. caudofemoralis longus*; **lt**, lesser trochanter; **s**, sulcus. [Planned for page width]



Figure 7. MOR 14148 right tibia rendered with and without texture in (A) lateral, anterior, medial, and posterior views; and (B) proximal and distal views. **Abbreviations: cc**, cnemial crest; **fic**, inner condyle; **lm**, lateral malleolus; **mm**, medial malleolus. [Planned for page width].

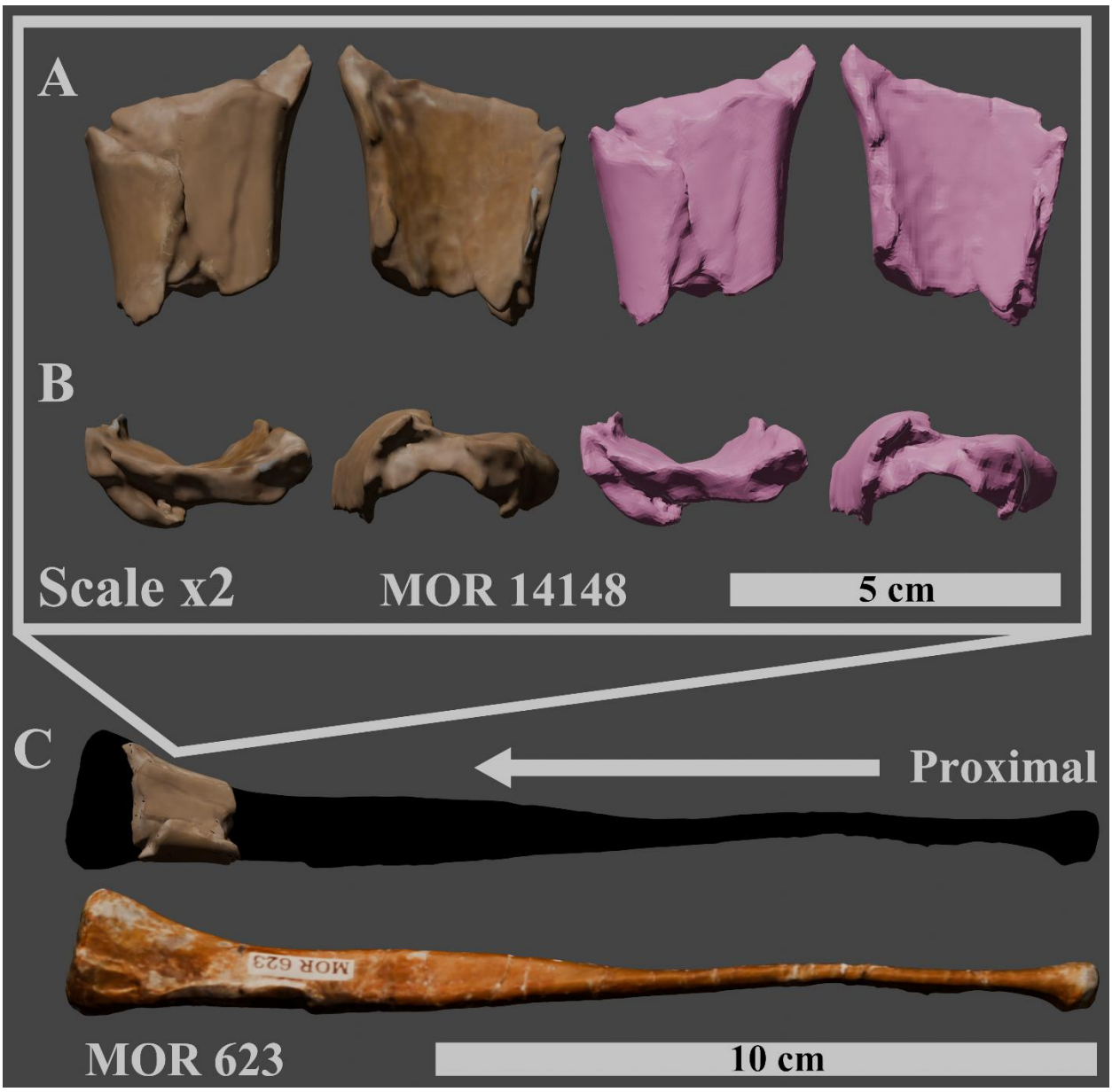


Figure 8. MOR 14148 right fibula rendered with and without texture in (A) anterior and posterior views; (B) proximal and distal views; and (C) MOR 14148 compared to *Orodromeus makelai* fibula [MOR 623]. MOR 14148 scaling is doubled. (C) Black silhouette is of MOR 623 with MOR 14148 overlaid. [Planned for page width].

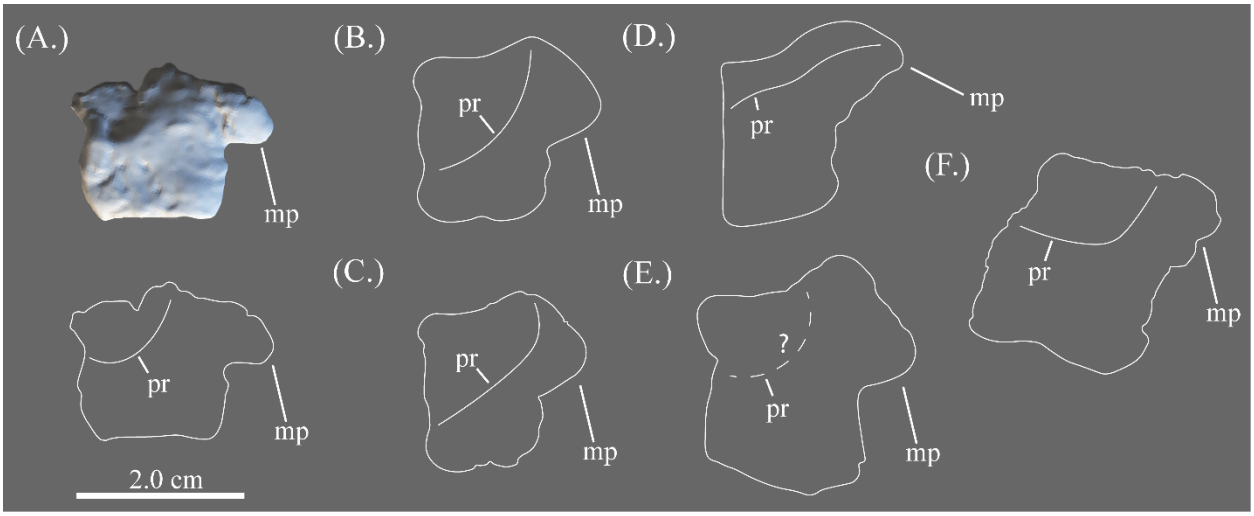


Figure 9. Right medial distal tarsi in dorsal (=proximal) view; (A) MOR 14148; (B) *Orodromeus* [MOR 623]; (C) TM-088 Orodrominae indet.; (D) *Oryctodromeus* [MOR 1642]; (E) "Landslide Butte Orodromine" [MOR 473]; and (F) *Fona* [NCSM 36280]. **Abbreviations: mp**, medial process; **pr**, proximal ridge. Scale bar equals 2.0 centimeters (cm.). [Planned for page width.



Figure 10. MOR 14148 right pes rendered with and without texture in (A) anterior; (B) posterior; (C) proximal; (D) distal; (E) medial; and (F) lateral views. **Abbreviations: MDT**, medial distal tarsal. [Planned for page width].

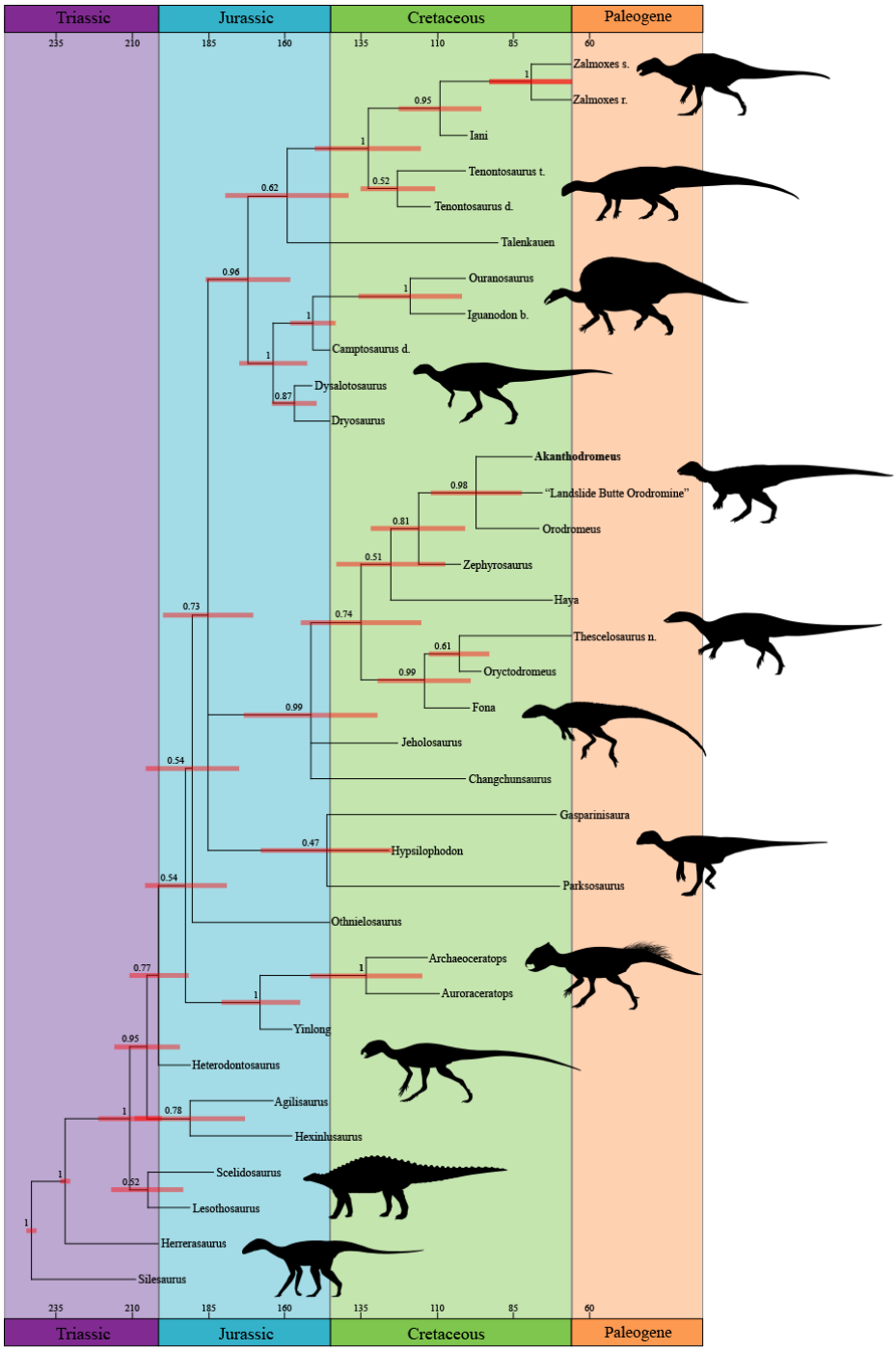


Figure 11. Time-calibrated tree resulting from Bayesian phylogenetic analysis of early diverging ornithischian dinosaurs with the root, Dinosauria, and Ornithischia constrained using a condensed version of the character matrix from Avrahami et al. (2024) displaying only taxa exhibiting 50% or more of the characters in matrix. Numbered node labels represent posterior probability of those nodes, and the red bars represent the 95% credible interval for the estimated ages. Silhouettes are all downloaded from Phylopic.org.

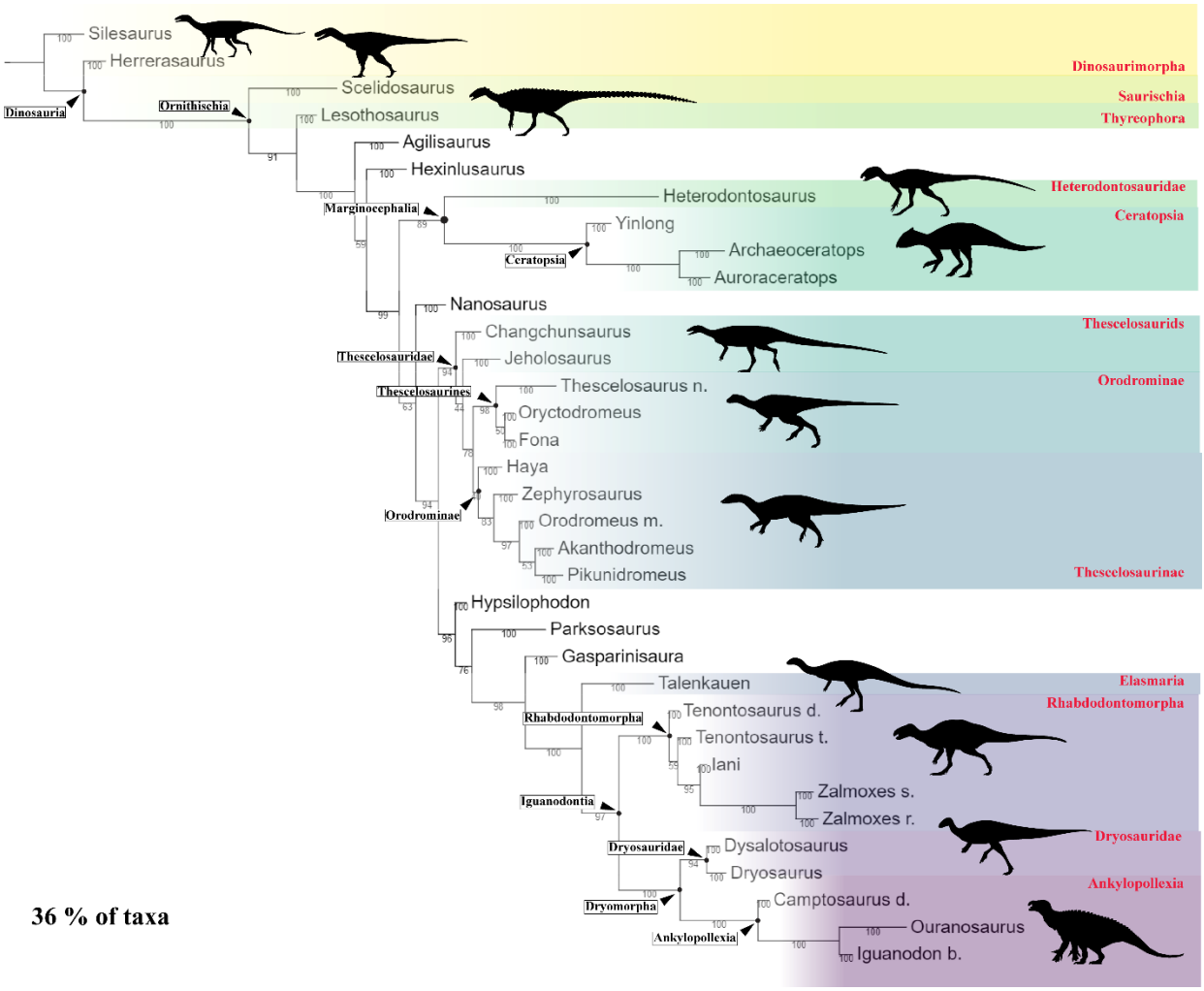


Figure 11. Non-time calibrated phylogenetic Bayesian analysis of early diverging ornithischian dinosaurs using an updated version of the Avrahami et al. (2024). Numbers represent posterior probability of support for each node. 36 % of the taxa in the character matrix included in analysis. Taxa lacking 50% of the characters culled. Silhouettes are all downloaded from Phylopic.org. [Planned for page width]

Literature Cited

Andrzejewski, K. A., Winkler, D. A., & Jacobs, L. L. (2019). A new basal ornithopod (Dinosauria: Ornithischia) from the Early Cretaceous of Texas. *PloS one*, 14(3), e0207935.

Arbour, V. M., & Evans, D. C. (2017). A new ankylosaurine dinosaur from the Judith River Formation of Montana, USA, based on an exceptional skeleton with soft tissue preservation. *Royal Society Open Science*, 4(5), 161086–161086.

Arbour, V. M., & Evans, D. C. (2019). A new leptoceratopsid dinosaur from Maastrichtian-aged deposits of the Sustut Basin, northern British Columbia, Canada. *PeerJ*, *7*, e7926.

Avrahami, H. M., Lindsey, K. P., & Herzog, L. (2023). Advances in 3D surface scanning: Mobile device applications set a new standard for digitization of fossils and museum artifacts. *Journal of Vertebrate Paleontology* Program Abstract 83:77.

Avrahami, H. M., Makovicky, P. J., Tucker, R. T., & Zanno, L. E. (2024). A new semi-fossorial thescelosaurine dinosaur from the Cenomanian-age Mussentuchit Member of the Cedar Mountain Formation, Utah. *The Anatomical Record*.

Averianov, A. O., Voronkevich, A. V., Leshchinskiy, S. V., & Fayngertz, A. V. (2006). A ceratopsian dinosaur *Psittacosaurus sibiricus* from the Early Cretaceous of West Siberia, Russia and its phylogenetic relationships. *Journal of Systematic Palaeontology*, 4(4), 359-395.

Baron, M. G., Norman, D. B., & Barrett, P. M. (2017). Postcranial anatomy of *Lesothosaurus diagnosticus* (Dinosauria: Ornithischia) from the Lower Jurassic of southern Africa:

implications for basal ornithischian taxonomy and systematics. *Zoological Journal of the Linnean Society*, 179(1), 125-168.

Barrett, P. M. & Han, F. -L. (2009) Cranial anatomy of *Jeholosaurus shangyuanensis* (Dinosauria: Ornithischia) from the Early Cretaceous of China. Zootaxa, 2072, 31-55.

Barta, D. E., & Norell, M. A. (2021). The osteology of *Haya griva* (Dinosauria, Ornithischia) from the Late Cretaceous of Mongolia. Bulletin of the American Museum of Natural History, 445 (1), 1-112.

Bonde, J. W., Hall, R. L., Krumenacker, L. J., & Varricchio, D. J. (2022). *Nevadadromeus schmitti* (gen. et sp. nov.), a New Basal Neornithischian with Affinities to the Thescelosaurinae, from the Upper Cretaceous (Cenomanian) Willow Tank Formation of Southern Nevada. *Journal of the Arizona-Nevada Academy of Science*, 50(1), 1-8.

Boyd, C. A. (2012). *Taxonomic revision of latest Cretaceous North american basal neonithischian taxa and a phylogenetic analysis of basal ornithischian relationships* University of Texas - Austin.

Brown, B. (1914). *Leptoceratops*, a new genus of Ceratopsia from the Edmonton Cretaceous of Alberta. Bulletin of the AMNH; v. 33, article 36.

Brown, C. M., Boyd, C. A., & Russell, A. P. (2011). A new basal ornithopod dinosaur (Frenchman Formation, Saskatchewan, Canada), and implications for late Maastrichtian ornithischian diversity in North America. *Zoological Journal of the Linnean Society*, 163(4), 1157-1198.

Brown, C. M., Evans, D. C., Ryan, M. J., & Russell, A. P. (2013). New data on the diversity and abundance of small-bodied ornithopods (Dinosauria, Ornithischia) from the Belly, River Group (Campanian) of Alberta. Journal of vertebrate paleontology, 33(3), 495-520.

Butler, R. J., & Zhao, Q. (2009). The small-bodied ornithischian dinosaurs *Micropachycephalosaurus hongtuyanensis* and *Wannanosaurus yansiensis* from the Late Cretaceous of China. *Cretaceous Research*, 30(1), 63-77.

Button, D. J. & Zanno, L. E. (2023). Neuroanatomy of the late Cretaceous *Thescelosaurus neglectus* (Neornithischia: Thescelosauridae) reveals novel ecological specialisations within Dinosauria. Scientific Reports, 13(1), 19224-19224.

Chiba, K., Ryan, M. J., Fanti, F., Loewen, M. A., & Evans, D. C. (2018). New material and systematic re-evaluation of *Medusaceratops lokii* (Dinosauria, Ceratopsidae) from the Judith River Formation (Campanian, Montana). *Journal of Paleontology*, 92(2), 272–288.

Chinnery, B. (2004). Description of *Prenoceratops pieganensis* gen. et sp. nov. (Dinosauria: Neoceratopsia) from the Two Medicine Formation of Montana. *Journal of Vertebrate Paleontology*, 24(3), 572-590.

Chinnery, B. J., & Weishampel, D. B. (1998). *Montanoceratops cerorhynchus* (Dinosauria: Ceratopsia) and relationships among basal neoceratopsians. *Journal of Vertebrate Paleontology*, 18(3), 569-585.

Cooper, M. R. (1985). A revisoin of the ornithischian dinosaur *Kangnasaurus coetzeei* Haughton, with classification of the Ornithischia. *Annals of the South African Museum*. 95, 281-317.

Coria, R. A., & Salgado, L. (1996). A basal iguanodontian (Ornithischia: Ornithopoda) from the Late Cretaceous of south America. *Journal of Vertebrate Paleontology*, 16(3), 445-457.

Coria, R. A., & Calvo, J. O. (2002). A new iguanodontian ornithopod from Neuquén Basin, Patagonia, Argentina. *Journal of Vertebrate Paleontology*, *22*(3), 503-509.

Cullen, T. M., Fanti, F., Capobianco, C., Ryan, M. J., & Evans, D. C. (2016). A vertebrate microsite from a marine-terrestrial transition in the Foremost Formation (Campanian) of Alberta, Canada, and the use of faunal assemblage data as a paleoenvironmental indicator. *Palaeogeography, Palaeoclimatology, Palaeoecology*, 444, 101-114.

Dalman, S. G., & Lucas, S. G. (2015). New data on the tyrannosaurid theropods from the middle Campanian lower Judith River Formation of north-central Montana. *New Mexico Museum of Natural History and Science*, 67, 77-89.

Dodson, P. (1986). *Avaceratops lammersi*: a new ceratopsid from the Judith River Formation of Montana. *Proceedings of the Academy of Natural Sciences of Philadelphia*, 305-317.

Druckenmiller, P. S., Erickson, G. M., Brinkman, D., Brown, C. M., & Eberle, J. J. (2021). Nesting at extreme polar latitudes by non-avian dinosaurs. *Current Biology*, 31(16), 3469-3478.

Eberth, D. A., Currie, P. J., & Koppelhus, E. B. (2005). The geology. *Dinosaur Provincial Park: a spectacular ancient ecosystem revealed*, Indiana University Press, Bloomington, 54-82.

Eberth, D. A. (2015). Origins of dinosaur bonebeds in the Cretaceous of Alberta, Canada. *Canadian Journal of Earth Sciences*, 52(8), 655-681.

Eberth, D. A. (2024). Stratigraphic architecture of the Belly River Group (Campanian, Cretaceous) in the plains of southern Alberta: Revisions and updates to an existing model and implications for correlating dinosaur-rich strata. *Plos one*, 19(1), e0292318.

Fiorillo, A. R., & Currie, P. J. (1994). Theropod teeth from the Judith River Formation (Upper Cretaceous) of south-central Montana. *Journal of Vertebrate Paleontology*, 14(1), 74–80.

Freedman, E. A. (2015). *Evolution and ontogeny of Hadrosaurs (Dinosauria: Ornithischia) in the Judith River Formation (late Cretaceous: Campanian) of northcentral Montana*. Montana State University – Bozeman, College of Letters & Science.

Freedman Fowler, E. A., & Horner, J. R. (2015). A new brachylophosaurin hadrosaur (Dinosauria: Ornithischia) with an intermediate nasal crest from the Campanian Judith River Formation of northcentral Montana. *PloS one*, *10*(11), e0141304.

Fuentes, F., DeCelles, P. G., & Constenius, K. N. (2012). Regional structure and kinematic history of the Cordilleran fold-thrust belt in northwestern Montana, USA. *Geosphere*, 8(5), 1104-1128.

Galton, P. M. (1975). The ornithischian dinosaur *Hypsilophodon* from the Wealden of th Isle of Wight. Bulletin of the British Museum (Natural History) Geology, 25(1), 1-152.

Galton, P. M., & Jensen, J. A. (1973). Skeleton of a hypsilophodontid dinosaur (*Nanosaurus* (?) *rex*) from the Upper Jurassic of Utah. *Brigham Young University Geology Studies*, 20(4), 137-157.

Galton, P. M. (1978). Fabrosauridae, the basal family of ornithischian dinosaurs (Reptilia: Ornithopoda). *Paläontologische Zeitschrift*, 52(1), 138-159.

Galton, P. M. (1995). The species of the basal hypsilophodontid dinosaur *Thescelosaurus* Gilmore (Ornithischia: Ornithopoda) from the Late Cretaceous of North America. *Neues Jahrbuch für Geologie und Paläontologie-Abhandlungen*, 198(3), 297-311.

Gates, T. A., Lund, E. A., Boyd, C. A., DeBlieux, D. D., Titus, A. L., Evans, D. C., Getty, M. A., Kirkland, J. I., & Eaton, J. G. (2013). Ornithopod Dinosaurs from the Grand Staircase-Escalante National Monument Region, Utah, and Their Role in Paleobiogeographic and Macroevolutionary Studies. In (pp. 463). Indiana University Press.

Han, F. L., Barrett, P. M., Butler, R. J., & Xu, X. (2012). Postcranial anatomy of *Jeholosaurus shangyuanensis* (Dinosauria, Ornithischia) from the Lower Cretaceous Yixian Formation of China. *Journal of Vertebrate Paleontology*, 32(6), 1370-1395.

Hannebaum, Z. J., Varricchio, D. J., Scheetz, R., Brown, C. M., and Avrahami, H. (2024). The three species problem: a revised look at the systematics and phylogenetic relationships of neornthischian dinosaurs in the Upper Cretaceous Two Medicine Formation of northcentral Montana. *Journal of Vertebrate Paleontology Program Abstracts*, (2024).

He, Y., Makovicky, P. J., Wang, K., Chen, S., Sullivan, C., Han, F., & Xu, X. (2015). A new leptoceratopsid (Ornithischia, Ceratopsia) with a unique ischium from the Upper Cretaceous of Shandong Province, China. *PLoS One*, *10*(12), e0144148.

Herne, M. C., Tait, A. M., Weisbecker, V., Hall, M., Nair, J. P., Cleeland, M., & Salisbury, S. W. (2018). A new small-bodied ornithopod (Dinosauria, Ornithischia) from a deep, high-energy Early Cretaceous river of the Australian–Antarctic rift system. *PeerJ*, *5*, e4113.

Horner, J. R., Schmitt, J. G., Jackson, F., & Hanna, R. (2001). Bones and rocks of the Upper Cretaceous Two Medicine-Judith River clastic wedge complex, Montana. In *Society of Vertebrate Pa− leontology 61th Annual Meeting: Mesozoic and Cenozoic Paleontol− ogy in the Western Plains and Rocky Mountains. Museum of the Rockies Occasional Paper* (Vol. 3, pp. 1-14).

Horner, J. R., & Goodwin, M. B. (2009). Extreme cranial ontogeny in the Upper Cretaceous dinosaur Pachycephalosaurus. *PLoS One*, *4*(10), e7626.

Hudgins, M. N. (2021). *The Paleobiology, Paleoecology, and Evolution of Thescelosauridae (Ornithischia) from Alberta, Canada*. Univeristy of Alberta.

Huh, M., Lee, D.-G., Kim, J.-K., Gwangju, Lim, J.-D., Daejeon, & Godefroit, P. (2010). A new basal ornithopod dinosaur from the Upper Cretaceous of South Korea. *Neues Jahrbuch für Geologie und Paläontologie. Abhandlungen, 259(1), 1-24.*, *259*, 1-24.

Ibiricu, L. M., Martínez, R. D., Luna, M., & Casal, G. A. (2014). A reappraisal of *Notohypshilophodon comodorensis* (Ornithischia: Ornithopoda) from the Late Cretaceous of Patagonia, Argentina. *Zootaxa*, 3786 (4), 401-422.

Ishikawa, H., Tsuihiji, T., & Manabe, M. (2023). *Furcatoceratops elucidans*, a new centrosaurine (Ornithischia: Ceratopsidae) from the upper Campanian Judith River Formation, Montana, USA. *Cretaceous Research*, *151*, 105660.

Jackson, F. D., Horner, J. R., & Varricchio, D. J. (2010). A study of a *Troodon* egg containing embryonic remains using epifluorescence microscopy and other techniques. *Cretaceous Research*, 31(2), 255-262.

Jin, L., Jun, C., Zan, S., Butler, R. J., & Godefroit, P. (2010). Cranial anatomy of the small ornithischian dinosaur *Changchunsaurus parvus* from the Quantou Formation (Cretaceous, Aptian-Cenomanian) of Jilin Province, northeastern China. Journal of vertebrate paleontology, 30(1), 196-214.

Kauffman, E. G. (1977). Geological and biological overview: Western Interior Cretaceous basin. *The Mountain Geologist*.

Krumenacker, L. J., Varricchio, D. J., Organ, C., Gardner, J. D., Britt, B. B., & Boyd, C. (2024). Osteology and phylogenetic relationships of the mid-Cretaceous neornithischian dinosaur *Oryctodromeus cubicularis* Varricchio, 2007. *Journal of Vertebrate Paleontology*, 43(5), e2330581.

LaRock, J. W. (2000). *Sedimentology and taphonomy of a dinosaur bonebed from the Upper Cretaceous (Campanian) Judith River Formation of north central Montana*. Montana State University – Bozeman, College of Letters & Science.

Lee, Y. N., Ryan, M. J., & Kobayashi, Y. (2011). The first ceratopsian dinosaur from South Korea. *Naturwissenschaften*, *98*, 39-49.

Leidy, J. (1856). Notices of remains of extinct reptiles and fishes, discovered by Dr. F. V. Hayden in the badlands of the Judith River, Nebraska Terr. *Proceedings of the Academy of Natural Sciences of Philadelphia*, 72–73.

Loewen, M. A., Sertich, J. J. W., Sampson, S., O'Connor, J. K., Carpenter, S., Sisson, B., Øhlenschlaeger, A., Farke, A. A., Makovicky, P. J., Longrich, N., and Evans, D. C. (2024). *Lokiceratops rangiformis* gen. et sp. nov. (Ceratopsidae: Centrosaurinae) from the Campanian Judith River Formation of Montana reveals rapid regional radiations and extreme endemism within centrosaurine dinosaurs. *PeerJ*, 12:e17224.

Longrich, N. R. (2013). *Judiceratops tigris*, a new horned dinosaur from the middle Campanian Judith River Formation of Montana. *Bulletin of the Peabody Museum of Natural History*, 54(1), 51-65.

Madzia, D., Arbour, V. M., Boyd, C. A., Farke, A. A., Cruzado-Caballero, P., & Evans. D. C. (2021). The phylogenetic nomenclature of ornithischian dinosaurs. *PeerJ* (San Francisco, CA), 9, e122362-e12362.

Maidment, S. C., & Barrett, P. M. (2011). The locomotor musculature of basal ornithischian dinosaurs. *Journal of Vertebrate Paleontology*, 31(6), 1265-1291.

Makovicky, P. J. (2010). A redescription of the *Montanoceratops cerorhynchus* holotype, with a review of referred material. *New perspectives on horned dinosaurs*, 68-82.

Makovicky, P. J., Kilbourne, B. M., Sadleir, R. W., & Norell, M. A. (2011). A new basal ornithopod (Dinosauria, Ornithischia) from the Late Cretaceous of Mongolia. *Journal of Vertebrate Paleontology*, 31(3), 626-640.

Mallon, J. C., Ott, C. J., Larson, P. L., Iuliano, E. M., & Evans, D. C. (2016). *Spiclypeus shipporum* gen. et sp. nov., a boldly audacious new chasmosaurine ceratopsid (Dinosauria: Ornithischia) from the Judith River Formation (Upper Cretaceous: Campanian) of Montana, USA. *PloS one*, *11*(5), e0154218.

Manitkoon, S., Deesri, U., Khalloufi, B., Nonsrirach, T., Suteethorn, V., Chanthasit, P., Boonla, W. & Buffetaut, E. (2023). A New Basal Neornithischian Dinosaur from the Phu Kradung Formation (Upper Jurassic) of Northeastern Thailand. *Diversity*, 15(7), 851.

Maryanska, T. E. R. E. S. A., & Osmólska, H. (1974). Pachycephalosauria, a new suborder of ornithischian dinosaurs. *Palaeontologia Polonica*, 30, 45-102.

Moore, B. R. S. (2021). *The postcranial anatomy of pachycephalosaurs (Ornithischia: Pachycephalosauria) and its phylogenetic and myological implications* (Doctoral dissertation, Carleton University).

Norman, D. B., Sues, H. -D., Witmer, L. M., & Coria, R. A. (2004). Basal Ornithopoda. In D. B. Weishampel, P. Dodson, and H. Osmólska (editors), The Dinosauria: 413-437. Berkeley: Unversity of California Press.

Novas, F. E. (1994). New information on the systematics and postcranial skeleton of *Herrerasaurus ischigualastensis* (Theropoda: Herrerasauridae) from the Ischigualasto Formation (Upper Triassic) of Argentina. *Journal of Vertebrate Paleontology*, 13(4), 400-423.

QGIS.org (2023). QGIS Geographic Information System. Open Source Geospatial Foundation Project. http://qgis.org

Osmólska, H. (1981). Coossified tarsometatarsi in theropod dinosaurs and their bearing on the problem of bird origins. *Palaeontologia Polonica*, 42, 79-95.

Owens, R. 1842. Report on British fossil reptiles. Part II. *Report for the British Association for the Advancement of Science*, 11, 60-204.

Ramezani, J., Beveridge, T. L., Rogers, R. R., Eberth, D. A., & Roberts, E. M. (2022). Calibrating the zenith of dinosaur diversity in the Campanian of the Western Interior Basin by CA-ID-TIMS U–Pb geochronology. *Scientific Reports*, 12(1), 16026.

Rogers, R. R., Kidwell, S. M., Deino, A. L., Mitchell, J. P., Nelson, K., & Thole, J. T. (2016). Age, correlation, and lithostratigraphic revision of the Upper Cretaceous (Campanian) Judith River Formation in its type area (north-central Montana), with a comparison of low-and high-accommodation alluvial records. *The Journal of Geology*, 124(1), 99-135.

Rogers, R. R., Eberth, D. A., & Ramezani, J. (2023). The “Judith River-Belly River problem” revisited (Montana-Alberta-Saskatchewan); new perspectives on the correlation of

Campanian dinosaur-bearing strata based on revised stratigraphic model updated with CA-ID-TIMS U-Pb geochronology. Geological Society of America bulletin, 136(3/4), 1221.

Rogers, R., Horner, J., Ramezani, J., Roberts, E., and Varricchio. D. (2024). Updating the Upper Cretaceous (Campanian) Two Medicine Formation of Montana: Lithostratigraphic revisions, new CA-ID-TIMS U-Pb ages, and a calibrated framework of dinosaur occurances. *The Geologial Society of America Bulletin*.

Ronquist, F., Teslenko, M., van der Mark, P., Ayres, D., Darling, A., Höhna, S., Larget, B., Liu, L., Suchard, M. A., & Huelsenbeck, J. P. (2012). MrBayes 3.2: Efficient Bayesian phylogenetic inference and model choice across a large model space. Systematic Biology, 61(3), 539–542.

Rozadilla, S., Agnolín, F. L., & Novas, F. E. (2019). Osteology of the Patagonian ornithopod *Talenkauen santacrucensis* (Dinosauria, Ornithischia). *Journal of Systematic Palaeontology*, 17(24), 2043-2089.

Ruiz-Omeñaca, J. I., Canudo, J. I., Cuenca-Bescós, G., Cruzado-Caballero, P., Gasca, J. M., & Moreno-Azanza, M. (2012). A new basal ornithopod dinosaur from the Barremian of Galve, Spain. *Comptes Rendus Palevol*, 11(6), 435-444.

Ryan, M. J., Russell, A. P., & Hartman, S. (2010). A new chasmosaurine ceratopsid from the Judith River Formation, Montana. *New perspectives on horned dinosaurs*, 181-188.

Ryan, M. J., Evans, D. C., Currie, P. J., Brown, C. M., & Brinkman, D. (2012). New leptoceratopsids from the upper Cretaceous of Alberta, Canada. *Cretaceous Research*, *35*, 69-80.

Ryan, M. J., Evans, D. C., Currie, P. J., & Loewen, M. A. (2014). A new chasmosaurine from northern Laramidia expands frill disparity in ceratopsid dinosaurs. *Naturwissenschaften*, *101*, 505-512.

Sahni, A. (1972). The vertebrate fauna of the Judith River Formation, Montana. Bulletin of the AMNH; v. 147, article 6.

Salgado, L., Coria, R. A., & Heredia, S. E. (1997). New materials of *Gasparinisaura cincosaltensis* (Ornithischia, Ornithopoda) from the Upper Cretaceous of Argentina. *Journal of Paleontology*, 71(5), 933-940.

Scheetz, R. D. (1999). *Osteology of Orodromeus makelai and the phylogeny of basal ornithopod dinosaurs*. Montana State University-Bozeman.

Schott, R. K., Evans, D. C., Williamson, T. E., Carr, T. D., & Goodwin, M. B. (2009). The anatomy and systematics of *Colepiocephale lambei* (Dinosauria: Pachycephalosauridae). *Journal of Vertebrate Paleontology*, 29(3), 771-786.

Seeley H. G. 1887. On the classification of the fossil animals commonly named Dinosauria. *Proceedings of the Royal Society of London*, 43, 481-494.

Sereno, P. C. (2012). Taxonomy, morphology, masticatory function and phylogeny of heterodontosaurid dinosaurs. *ZooKeys*, (226), 1.

Sternberg, C. M. 1937. A classification of *Thescelosaurus*, with a description of a new species. *Geological Society of America, Proceedings and Abstracts*, 1936-375.

Sues, H.-D. (1980). Anatomy and relationships of a new hypsilophodontid dinosaur from the Lower Cretaceous of North America. *Palaeontographica. Abt. A., Palaeozoologie-Stratigraphie*, 169, 51-72.

Sues, H. D., Evans, D. C., Galton, P. M., & Brown, C. M. (2023). Anatomy of the neornithischian dinosaur *Parksosaurus warreni* (Parks, 1926) from the Upper Cretaceous (lower Maastrichtian) Horseshoe Canyon Formation of Alberta, Canada. *Cretaceous Research*, 141, 105369.

Takasaki, R., Chiba, K., Fiorillo, A. R., Brink, K. S., Evans, D. C., Fanti, F., Saneyoshi. M., Maltese, A. & Ishigaki, S. (2023). Description of the first definitive *Corythosaurus* (Dinosauria, Hadrosauridae) specimens from the Judith River Formation in Montana, USA and their paleobiogeographical significance. *The Anatomical Record*, 306(7), 1918-1938.

Umeno, A., & Tanoue, K. (2016). Description of Dinosaur Teeth from the Upper Cretaceous Judith River Formation in Montana, USA. *福岡大学理学集報*, 46(2), 77-84.

Warshaw, E. A., & Fowler, D. W. (2022). A transitional species of *Daspletosaurus* Russell, 1970 from the Judith River Formation of eastern Montana. *PeerJ* (San Francisco, CA), 10, e14461–e14461.

Weishampel, D. B., & Heinrich, R. E. (1992). Systematics of hypsilophodontidae and basal Iguanodontia (Dinosauria: Ornithopoda). *Historical Biology*, 6(3), 159-184.

Weishampel, D. B., Jianu, C. M., Csiki, Z., & Norman, D. B. (2003). Osteology and phylogeny of *Zalmoxes* (ng), an unusual euornithopod dinosaur from the latest Cretaceous of Romania. *Journal of Systematic Palaeontology*, 1(2), 65-123.

Wilson, J. A. (2006). Anatomical nomenclature of fossil vertebrates: standardized terms or 'lingua franca'?. *Journal of Vertebrate Paleontology*, *26*(3), 511-518.

Wilson, J. P., & Fowler, D. W. (2021). The easternmost occurrence of *Saurornitholestes* from the

Judith River Formation, Montana, indicates broad biogeographic distribution of *Saurornitholestes* in the Western Interior of North America. *Historical Biology*, 33(12), 3302–3306.

Wolff, E., & Horner, J. R. (2003). The first occurrence of *Orodromeus makelai* postcrania from the Late-Campanian Judith River Formation of eastern Montana. *Journal of Vertebrate Paleontology*, 23(3), 122.

Yang, Y., Wu, W., Dieudonné P.-E., & Godefroit, P. (2020). A new basal ornithopod dinosaur from the Lower Cretaceous of China. PeerJ (San Francisco, CA), 8, e9832-e9832.

CHAPTER THREE

A NEW ORODROMINE (DINOSAURIA: ORNITHISCHIA) FROM THE UPPER CRETACEOUS TWO MEDICINE FORMATION OF NORTHCENTRAL MONTANA.

Contribution of Authors and Co-Authors

Manuscript in Chapter 3

Author: Zakaria Hannebaum

Conceived the study, performed analyses, interpreted results, and wrote the manuscript.

Co-Author: David J. Varricchio

Contributions: Conceived the study, discussed results and implications, and edited manuscript drafts.

Co-Author: Brendan Clark

Contributions: Performed segmentation of CT imagery

Co-Author: Rodney Scheetz

Contributions: Provided preliminary descriptions of specimens, edited manuscript drafts.

Manuscript Information

Zakaria J. Hannebaum, David J. Varricchio, Brendan Clark, Rodney Scheetz

Journal of Vertebrate Paleontology

☒ Prepared for submission to a peer-reviewed journal
☐ Officially submitted to a peer-reviewed journal
☐ Accepted by a peer-reviewed journal
☐ Published in a peer-reviewed journal

Abstract

Orodromines are a consistent constituent of the Two Medicine Formation dinosaur fauna, especially in the Flag Butte Member. Since the erection of the species *Orodromeus makelai* in 1988, all orodromine skeletal material in the Two Medicine Formation subsequently fell under the purview of this monospecific genus. However, these skeletal occurrences span a significant temporal expanse (~ 5.0 Ma) and variation previously observed in this sample warrants a thorough re-analysis. *Pikunidromeus ancellae* gen. et. sp. nov. is the first new taxon to emerge from the orodromine Two Medicine assemblage and becomes the youngest in the Two Medicine-Judith River-Belly River clastic wedge. *Pikunidromeus* exhibits a jugal horn morphology distinct from other orodromines and illuminates important aspects of the orodromine body plane previously poorly understood (i.e., manus and tail). Furthermore, *Pikunidromeus* raises important questions about the subsequent disappearance of the clade from Laramidia after the Campanian, and how orodromines were able to coexist with other small-bodied ornithischians. *Pikunidromeus* specimens from Alberta also reveal a faunal interconnectedness between the Upper Two Medicine and the Dinosaur Park Formation in small-bodied taxa previously unrecognized.

Introduction

Orodromines are small-bodied early diverging ornithischian dinosaurs thought to exhibit a burrowing habit (Avrahami et al., 2024; Boyd, 2012; Button and Zanno, 2023). They were widespread on the subcontinent of Laramidia, from Utah to Alaska (Brown et al., 2013; Druckenmiller et al., 2021; Gates et al., 2013; Scheetz, 1999; Sues, 1980), with group diversity

peaking in the Campanian during the Claggett regressive phase (R8) and most of the Bearpaw transgressive phase (T9) of the Western Interior Cretaceous Seaway (WICS) (Chapter 2; Brown et al., 2013). Still, the actual biodiversity of this group is likely understated and impaired by general taphonomic size biases favoring large-bodied dinosaur taxa in many Cretaceous formations (Brown et al., 2013), but also by worker biases as they figuratively, and quite literally, are overshadowed by their larger and more popular ornithischian relatives.

The Two Medicine Formation is extremely fossiliferous throughout most of its deposition which spans much of the Campanian (Rogers et al., 2025). Historically, all small-bodied early diverging ornithischian fossils, hereafter SBEDOs (Avrahami et al., 2024), in the Two Medicine Formation were assigned to the monospecific genus *Orodromeus makelai* (Sheetz, 1999). *Orodromeus makelai* is by far the best sampled orodromine, and thescelosaurid more broadly, with hundreds of specimens documented from the Two Medicine Formation (Scheetz, 1999). A newly availably chronostratigraphic framework for the Two Medicine Formation has recalibrated dinosaur faunal occurrences in the Formation (Rogers et al., 2025) and allows for precise placement of orodromine specimens in the formation.

Promptly, three morphotypes emerge in the Two Medicine orodromine assemblage. The first morphotype, presented as the “Landslide Butte Orodromine” previously (Hannebaum et al., 2024), is temporally restricted to localities above the lacustrine interval of the Flagg Butte Member, while the second, representing *Orodromeus makelai*, becomes restricted to the lacustrine interval of the Flagg Butte Member of the Two Medicine Formation. The third morphotype we refer colloquially to as the “BV Orodromine” and is represented by only isolated jugals from the fossil locality TM-088 (Bob’s Vacation Site [BV]). The “Landslide Butte

Orodromine" specimens span an ontogenetic spectrum and exhibit morphological characters distinct from other orodromines. Here, we formally designate the "Landslide Butte Orodromine" as a new species, *Pikunidromeus ancellae* gen. et. sp. nov. Notably, one apomorphic character of *Pikunidromeus ancellae* gen. et. sp. nov. links Two Medicine Formation specimens with two femora collected from time equivalent strata in the Lower Dinosaur Park Formation (TMP1997.80.03 and TMP1998.93.14) suggesting an unrecognized faunal interconnectedness between the Two Medicine and Dinosaur Park Formations in small-bodied dinosaur taxa. *Pikunidromeus ancellae* increases the diversity of Late Cretaceous orodromines in North America, restricts *Orodromeus makelai* occurrences temporally, and validates that northern Laramidia was a hotbed of orodromine diversity in the Late Campanian.

Materials and methods

SBEDOs is an acronym which stands for small-bodied early diverging ornithischians. It was recently coined by Avrahami et al. (2024) and references a "grade" of distantly related early diverging ornithischian lineages exhibiting similar body plans (i.e. bipedal, small-bodied, similar dentition, etc.), this "grade" does not include marginocephalians or thyreophorans. Over the years, other researchers have used different terms to describe such dinosaurs calling them "Fabrosaurids" (Galton, 1978), "Hypsilophodontids" (Weishampel and Heinrich, 1992), or "basal ornithopods" (Norman et al., 2004). Unlike the SBEDOs acronym, these earlier terms tried to group unrelated taxa within a phylogenetic context. We follow the naming schemes denoted in Brochu (1996) for vertebral ossification when describing vertebral fusion. Anatomy is discussed using the Romerian anatomical and directional terms for fossil vertebrates, in preference of veterinarian terms like rostral or caudal to limit misunderstandings (Wilson, 2006)

as rostral bones are a derived feature of ceratopsians, which thescelosaurids lack. Specimens are defined here as any independent occurrence of an individual represented from a single non-toothed element to associated skeletal materials.

The specimens discussed here are curated, and accessed, at the Museum of the Rockies in Bozeman, Montana, United States; the Royal Tyrell Museum of Paleontology, Drumheller, Alberta, Canda; and the Royal Ontario Museum, Toronto, Ontario, Canada. Almost all *Pikundromeus ancellae* specimens documented herein were collected under permit from tribal lands within the Blackfeet Reservation in northcentral Montana by Museum of the Rockies staff, TMP specimens were collected in Dinosaur Provincial Park in Alberta while the ROM specimen was purchased from a private collector. Specimens in this study were digitally imaged using the photogrammetry application called Abound (v. 3.0.0) on an iPhone 13 mini and 16 pro max, using a macro-lens at times, following the workflow outlined by Avrahami et al. (2023). The MOR's Creaform model Go!SCAN 20 supplemented Abound in digitally imaging some elements and meshes were processed in VXelements v.11. Digital models were assembled in Blender v.4.3. The geological map was created using QGIS (v. 3.34.1) with GIS data sourced from the Montana Bureau of Mines and Geology, Montana State Library, and geoBoundaries.org. Adobe Photoshop v.25.12 and Illustrator v.28.7.1 were employed to create final versions of some figures.

Phylogenetic Methods

The phylogenetic relationships of *Pikunidromeus ancellae* were assessed Bayesian analytical methods using MrBayes v3.2.7a (Ronquist et al., 2012) performed on the Tempest High Performance Computing System, operated and supported by University Information Technology

Research Cyberinfrastructure at Montana State University. Specimens and new characters were added to the SBEDO character matrix provided in the supplementary materials of Avrahami et al. (2024) and coded in Mesquite v.3.81. This updated matrix contains 94 taxa and 425 characters. The benefits of employing Bayesian analytical methods over parsimony are discussed in detail in Avrahami et al. (2024) and Krumenacker et al. (2024); however, the effects missing data have on the posterior node support and topology of phylogenies are unexplored. *Pikunidromeus ancellae* gen. et. sp. nov. is missing only 35% of the 425 characters in this dataset, while 64% of the 94 taxa in the tree lack over 50% of the characters. To assess the effect of missing data on node support and tree topology, we conducted six time-calibrated and six non-time-calibrated Bayesian analyses using MrBayes. The first analysis for both types was conducted with all the taxa in the matrix included. The five subsequent analyses culled fragmentary taxa by their percentage of missing characters, starting with taxa lacking 90% of the data. The following four runs ran in 10% decreasing increments (i.e., 80%, 70%, 60%, and 50%). Each analysis ran four Markov-chain Monte Carlo (MCMC) replicates for 20,000,000 generations, each with four chains, sampling every 1,000 with a burn-in of 25% for both analyses. *Marasuchus* is considered the oldest known dinosauriform and was used as an outgroup in the analyses of the full dataset, 90%, and the 80% reduced datasets. *Asilisaurus* became the outgroup for the 70% and 60% reduced datasets as *Marasuchus* is missing 80% of the characters, and *Silesaurus* was the outgroup in the 50% reduced dataset as *Asilisaurus* lacks 55% of the characters. Minimum last appearance dates were determined from a primary survey of the literature and pulled from the Paleobiology Database to fix the tip dates and basal node ages. Our MrBayes script was constructed with input from the MrBayes script provided in the supplementary materials of

Krumenacker et al. (2024). R studio v.3.6.0 was employed to create time-trees using the packages “ggtree”, “treeio:, “deeptime”, “ggplot2”, and “ape”. Our R script was built with input from R script examples provide in Christopher Organ’s Phylogenetics class taught in the spring of 2024 at Montana State University.

Institutional Abbreviations

BYU, Brigham Young University, Provo, Utah, United States; **IGM**, Institute of Geology, Mongolian Academy of Sciences, Ulaan Baatar, Mongolia; **IMNH**, Idaho Museum of Natural History, Pocatello, Idaho, United States; **IVPP**, Institute of Vertebrate Paleontology and Paleoanthropology, Beijing, China; **MOR**, Museum of the Rockies, Bozeman, Montana, United States; **NCSM**, North Carolina Science Museum, Raleigh, North Carolina, United States; **NMV**, Museums Victoria (formerly, National Museum of Victoria), Melbourne, Victoria, Australia; **PMOL**, Paleontological Museum of Liaoning, Shenyang, China; **PRC**, Palaeontological Research and Education Centre, Mahasarakham University, Maha Sarakham, Thailand; **PU**, Princeton University, Princeton, New Jersey, United States; **RSM**, Royal Saskatchewan Museum, Regina, Saskatchewan, Canada; **ROM**, Royal Ontario Museum, Toronto, Canada; **TMP**, Royal Tyrrell Museum of Paleontology, Drumheller, Alberta, Canada; **UMNH**, Natural History Museum of Utah, Salt Lake City, Utah, United States; **USNM**, United States National Museum, Washington, D. C., United States.

Systematic paleontology

DINOSAURIA Owen, 1842

ORNITHISCHIA Seeley, 1887

NEORNITHISCHIA Cooper, 1985 (sensu Madzia et al., 2021)

THESCELOSAURIDAE Sternberg, 1937 (sensu Madzia et al., 2021)

ORODROMINAE Brown et al., 2013 (sensu Madzia et al., 2021)

PIKUNIDROMEUS gen. nov.

(Figs. 3-19)

Type Species—*Pikunidromeus ancellae, sp. nov.*

Generic Etymology—Algonquian word *Pikuni* for the Blackfeet Nation and the Greek word *dromeus* meaning 'runner', together 'Blackfeet runner', honors the Blackfeet Nation whose tribal lands are where most of the specimens described here were recovered, while also alluding to a probable cursorial habit.

Diagnosis—As for type and only species.

PIKUNIDROMEUS ANCELLAE gen. et sp. nov.

Holotype—MOR 473, a partial skull and postcranial skeleton of a skeletally mature individual.

Paratype—ROM 64600, a fragmentary skull and postcranial skeleton of a skeletally mature individual.

Referred specimens— MOR 436, partial skeleton of at least one skeletally immature individual; MOR 350, partial skeleton; MOR 411, misc. skeletal fragments; MOR 412, partial ischial shaft; MOR 528, partial skeleton; MOR 530, partial skeleton of a skeletally immature individual; MOR 533, partial tibia and metatarsal; MOR 995, left and right paired frontals; MOR 10925; TMP1998.093.0014, right femur; TMP1997.080.0003, distal epiphysis of a right femur; ROM 64601, at least one partial skeleton of a late stage juvenile or subadult individual.

Specific etymology—*ancellae* honors retired Museum of the Rockies field paleontologist and fossil preparator Carrie Ancell in recognition of her decades spent expertly preparing fossils of an impressive portfolio of thescelosaurid material encompassing multiple taxa such as *Zephyrosaurus*, *Akanthodromeus*, *Orodromeus*, *Pikunidromeus*, *Oryctodromeus*, and *Thescelosaurus neglectus*, while also acknowledging her field contributions as co-discoverer and preparator of MOR 436 and 473.

Diagnosis—A SBEDO differentiated by the following combinations of morphological characters with autapomorphies denoted by *: presence of a small posterolaterally deflected jugal horn core on the lateral face of the jugal*; two nutrient foramen on medial surface of the jugal; bifurcated maxillary jugal ramus*; no transverse dorsal groove on intercentrum*; sharp ventral keel on cervical vertebrae; hypapophysis on ventral keel of cervical vertebrae four*; fourteen dorsal vertebrae; tuberculum and capitulum transition of dorsal ribs from vertical to near horizontal occurs between dorsal vertebrae six and eight*; anterior dorsal ribs are sub-oval in cross-section distally; sharp scapular spine across lateral surface of acromion process; posterior scapular flange; scapula length to width ratio of 6.0 to 7.3; metacarpal I with obliquely inclined, asymmetric articular condyles *; seven sacral vertebrae; rounded dorsal margin of the ilium in lateral view; anterior terminus of the prepubic process is heavily striated; prepubic process dorsoventrally enlarges into a large pad anteriorly; prepubic process swells laterally and is medially placed along the length of the process; first chevron articulates on the distal end of the second caudal vertebrae; lack of ischial shaft rotation/twist about axis; no intertrochanteric cleft (=notch) along dorsal margin of the trochanteric region of femur; lateral inflection of the ischial shaft into thin blade-like protuberance in the distal third; no anterior intercondylar sulcus on

distal femur; medial condyle of femur inflated and partially invading the posterior intercondylar sulcus on distal femur*; fibular condyle larger than the accessory condyle on tibia; flange on distal fibula, and the angle between the articular facets of the tibia and fibula on the calcaneum is less than 120 degrees*; “mail-box flag-like” profile of metatarsal V; averaged length/width ratio PI-I is 4.15*; deep pit on the ventromedial shaft of P1-1 proximal to the distal articular condyles.

Horizons—The Upper Cretaceous nonmarine Two Medicine Formation represents proximal deposition within a retroarc foreland basin called the Western Interior Basin (WIB), locally part of an eastward thinning clastic wedge which included the Belly River Group and Judith River Formation (Fuentes et al., 2012; Kauffman, 1977). The formation is subdivided into four members: the Rocky Creek, Shields Crossing, Hagans Crossing, and Flag Butte Members (Rogers et al., 2024). Deposition was heavily influenced throughout by western transgressive and regressive cycles of the Western Cretaceous Interior Seaway (WICS) which bisected North America north to south (Rogers et al., 2024). Temporally, deposition encompasses much of the Campanian at a paleolatitude of 56ºN occurring between ca. 82.4 Ma. to 74.4 Ma. (Lorenz and Gavin, 1984; Fricke et al., 2010; Rogers et al., 2024). Siliciclastic detritus derived from the North American Cordillera dominates, deposited primarily in eastward flowing fluvial and lacustrine systems, with periodic influxes of effusive volcaniclastics sourced from the Elkhorn Mountain Volcanic Field (Lorenz and Gavin, 1984; Rogers et al., 1993; Lageson et al., 2001; Horner et al., 2001). Paleoclimatic conditions were semi-arid and influenced greatly by monsoonal regimes as evidenced by abundant caliche nodules, growth interruptions in conifer wood, herbivorous dinosaur coprolites, invertebrate traces, and taphonomic data supporting

episodic drought (Freimuth et al., 2019; Freimuth et al., 2021; Lorenz and Gavin, 1984; Rogers, 1990; Chin, 2007; Fricke et al., 2010).

The Dinosaur Park Formation is part of the Belly River Group which comprises the northernly portion of a much larger, eastwardly thinning clastic wedge including the Two Medicine and Judith River Formations. The Belly River Group is subdivided into the Foremost, Oldman, and Dinosaur Park Formations (here listed in temporally ascending order). Dinosaur Park Formation deposition occurred ca. 76.470 +0.14/-0.084 Ma. to 74.44 +0.30/-0.11 Ma. (Ramezani et al., 2022) at a paleolatitude of 57ºN (Fricke et al., 2010) which corresponds to the initial phases of the last major transgressive phase of the WICS, and much of the Flagg Butte Member of the Two Medicine Formation above the lacustrine interval (Rogers et al., 2024). The lower stratum of the Dinosaur Park Formation is dominated by sandy alluvial paleochannel deposits which transition into muddy overbank deposits in the upper part capped by the Lethbridge Coal Zone (Ramezani et al., 2022; Mayo et al., 2023). Paleolandscape inferences suggest that well-drained habits dominated the lower portions of the formation before transitioning into a seasonally wetland/dry floodplain mosaic of habitats which experienced frequent overbank flooding and ponding prior to the onset of the Lethbridge Coal Zone, a period of deposition heavily tidally influenced from the encroaching Bearpaw Sea (Matson, 2010). Growth interruptions seen in tree rings, paired with macroflora fossils, suggest a paleoclimate that was seasonally warm to temperate, to sub-humid, and experienced no frost (Matson, 2010). Traveling south this climatic picture contrasts with the sub-arid coeval Two Medicine Formation. The Dinosaur Park Formation would have experienced periods of significant rainfall in comparison, creating an extensive meandering stream system across a broad floodplain perhaps

akin to the modern seasonal wetlands of Bangladesh (Matson, 2010).

Localities—MOR 436 and 473 are recovered within the Flag Butte Member of the Upper Two Medicine Formation at sites TM-019 and TM-036 in the Landslide Butte Field Area within the Blackfeet Reservation (Rogers et al., 2025). The Landslide Butte Field Area borders the United States/Canada international border and lies 40 km northwest of the nearby town of Cut Bank, MT. Site TM-019 sits ~10 meters below the datum ash bed LSB-1-14 (dated 75.243 ± 0.023 Ma.) and is dated to 75.34 +0.36/-0.06 Ma (Rogers et al., 2025). TM-019 is a notable *Hypacrosaurus blackfeetensis* bonebed and MOR 436 was found just to the east-southeast of the bonebed. This locality lacks a lithological description; however, some bone material remains confined in small grey calcareous mudstone nodules. A photograph documenting the collection of MOR 436 shows the specimen being extracted from a mudstone horizon within a hillside in a large nodule. Site TM-036 sits just above the datum ash bed LSB-1-14 and is a lambeosaurid nesting locality withing a siltstone horizon (Rogers et al., 2025). TM-036 also lacks a lithological description but photographs documenting the collection of MOR 473 corroborated the specimen lied within a siltstone horizon. Matrix still adhered to the anterior cervical vertebrate of MOR 436 is fine grained grey siltstone with sparse coarse angular black volcanic grains. The dinosaur fauna at the Landslide Butte Field Area is remarkably distinct from the rest of the Two Medicine Formation (Rogers et al., 2025). Saurolophines like *Maiasaura*, *Gryposaurus*, and *Acristavus* dominate the Hagans Crossing Member (Rogers et al., 2025), while the Landslide Butte Field Area in the upper Flagg Butte Member showcases a diverse dinosaur assemblage dominated by Ceratopsians like *Styracosaurus*, *Stellasaurus*, *Brachyceratops*, *Prenoceratops*, *Einiosaurus*, and *Achelousaurus* (Rogers et al., 2025).

TM-018 is a fossil locality on a privately leased land parcel along the Two Medicine River on the Blackfeet Reservation. TM-018 lacks a lithological description, but some specimens retain matrix. The matrix consists of a gray siltstone with sparse coarse angular black volcanic lithics. TM-018 lies above bentonite 90TMT-590-U60 which is dated to 75.252. ± 0.024 Ma, which is statistically indistinguishable from the bentonite LSB-1-14 (discussed above) and likely represent the same ash-fall event (Rogers et al., 2025). Multiple fragmentary *Pikunidromeus* specimens (MNI=11) were recovered from the site, as well as a partial *Pikunidromeus* skeleton [MOR 528] and shed teeth of *Daspletosaurus sp*.

TM-088 or "Bob's Vacation Site" is located on tribal lands along the Two Medicine River on the Blackfeet Reservation. It lies just above the bentonite L2R061517-1 (76.252 ± 0.087 Ma.) and has been dated to 75.96 +0.20/-0.41 Ma. This locality is unique, as it was deposited just above the lacustrine interval of the Flagg Butte Member near the maximum transgression of the WICS, nearly 350 km. inland from the paleo coastline (Cobban et al., 1994). The site produced an exceptional vertebrate assemblage preserved within silty claystones in what has been interpreted as a small floodplain depression which held only ephemeral bodies of water (Varricchio, 2002). The site has produced an abundance of not only orodromine material but also the small pterosaur *Piksi barbarulna* (Agnolin and Varricchio, 2012), a dromaeosaurid skeleton, an in situ *Troodon* egg clutch, small therapod teeth, tyrannosaurid and hadrosaurid teeth, exception lizard and frog skeletons, marsupial and multituberculate mammal teeth, and terrestrial planispiral gastropods (Varricchio, 2002).

TMP1997.080.0003 and TMP1998.093.0014 were recovered from separate channel lag deposits within the Lower Dinosaur Park Formation. TMP1998.093.0014 was discovered in

isolation but baenid turtle peripherals were found in conjunction with TMP1997.080.0003.

Comments—referred specimens were presented previously as the "Landslide Butte Orodromine" at the 2024 Society of Vertebrate Paleontology annual meeting (Hannebaum et al., 2024). ROM 64600 and 64601 were purchased by the ROM from a private landowner withing the Blackfeet Reservation. The final sale brokered by Pangaea Fossil in the early 2010s. Information relating to the purchase and sale can be found with the ROM.

Description

Pikunidromeus ancellae gen. et. sp. nov. is best exemplified by MOR 473 which is a skeletally mature individual represented by a mostly complete skull and postcranial skeleton. Other *Pikunidromeus* specimens contributing to this description are ROM 64600, 64601, MOR 436 and multiple fragmentary specimens from two fossil localities situated on tribal lands along the Two Medicine River [TM-018 and TM-088]. TMP1998.93.14 and TMP1997.80.03 are two femora which share an autapomorphic character of *Pikunidromeus* and are recovered from the Lower Dinosaur Park Formation in Alberta, Canada in strata temporally equivalent to the *Pikunidromeus* specimens in the Flag Butte Member of the Two Medicine Formation. When discussing osteology, we will refer to another orodromine taxon from the Campanian of Utah informally as the "Kaiparowits Orodromine", the osteology of which is explored in detail in a doctoral dissertation (Boyd, 2012) and briefly in Gates et al. (2013). Lastly, comparisons are made to a mysterious orodromine taxon represented only by jugals colloquially categorized as the "BV Orodromine" from the fossil locality TM-088 (BV) in the Two Medicine Formation (Chapter 4).

Cranium

Skull—What follows is a detailed description of the jugals only. The rest of the cranial material in MOR 436 and 473 is difficult to interpret as is and was CT imaged. This imaging is still being processed and without it a more detailed cranial osteology is impossible.

Jugal—Several jugals are recovered for *Pikunidromeus* and span an ontogenetic spectrum from small juveniles [MOR 436, MOR 613] to adults [MOR 473 and ROM 64600]. This series shows the morphology of the jugal in *Pikunidromeus* is established early in ontogeny. The jugal is a triradiate-shaped bone with long slender maxillary and postorbital rami projecting anterior and dorsally, respectively, a bifurcated jugal wing process extending posteriorly, and a horn (=boss) projecting from the lateral surface of the jugal. This slender jugal profile provides a sharp contrast to the robust jugals of *Heterodontosaurus* (Norman et al., 2011), *Akanthodromeus* [MOR 14147], *Orodromeus* [MOR 1141], the "Kaiparowits Orodromine" [UMNH VP 19470], and the "BV Orodromine". The jugal of *Pikunidromeus* forms the posteroventral floor of the orbit and contributes slightly to the anteroventral corner of the infratemporal fenestra. The latter is a condition noted to unite thescelosaurines like *Haya*, *Thescelosaurus neglectus*, *Jeholosaurus*, and *Changchunsaurus* (Avrahami et al., 2024) but is similarly manifest in *Pikunidromeus* and *Orodromeus* [MOR 294].

The mediolaterally compressed maxillary ramus thickens posteriorly as it nears a posterolaterally deflected jugal horn core and the ramus is only preserved fully in MOR 473. The maxillary ramus is straight in lateral view like *Thescelosaurus neglectus* (Boyd, 2014). Anteriorly the terminus of the maxillary ramus is bifurcated into a dorsal and ventral prong, a condition only shared with the thescelosaurids *Orodromeus* [MOR 294] and *Haya* (Barta and Norell, 2021), but also convergently *Heterodontosaurus* (Norman et al., 2011). The lacrimal

contact is uncertain but likely contacted the dorsal prong of the maxillary ramus based on *Orodromeus* [MOR 294]. The ventral prong of the maxillary process inserts solely with the maxilla. In *Heterodontosaurus*, a channel-like extension of the antorbital fossa divides the dorsal and ventral prongs of the maxillary process of the jugal (Norman et al., 2011). This channel is absent in *Pikunidromeus* [MOR 473], *Orodromeus* [MOR 294], and *Haya* (Barta and Norell, 2021); furthermore, the jugal does not contribute to the border of the antorbital fenestra as in *Heterodontosaurus* (Norman et al., 2011), *Agilisaurus* (Barrett et al., 2005), or the early therapod *Herrerasaurus* (Sereno and Novas, 1994). No small foramina are visually observed on the anterior termini or the lateral face of the anterior portion of the maxillary ramus, though they are observed in *Haya* (Barta and Norell, 2021)

In *Pikunidromeus*, a modestly sized jugal horn core arises from the lateral face of the jugal and deflects posterolaterally. Jugal horns are a derived feature of orodromines and may be convergent with the rounded jugal bosses seen in some heterodontosaurids (Sereno, 2012). Orodromine jugal horn cores either project laterally (Chapter 2) or posterolaterally (Boyd, 2012; Scheetz, 1999; Sues, 1980). Thescelosaurines are the sister group to orodromines and conspicuously lack jugal horns. Instead thescelosaurines exhibit a variety of smooth, rugose, ridged, knobby, or swollen lateral jugal faces (Avrahami et al., 2024; Boyd, 2014; Krumenacker et al., 2024). Other early thescelosaurids showcase a jugal with a rugose lateral surface like *Nanosaurus* (Carpenter and Galton, 2018), rugose and swollen lateral faces in *Jeholosaurus* (Barrett and Han, 2009), or a low node-like boss like *Changchunsaurus* (Jin et al., 2010). *Minimocursor* (Manitkoon et al., 2023) is noted to have a similar node-like boss, but Avrahami et al., (2024) recently contested this interpretation as they believe the jugal is figured in medial

view and not lateral. The jugal horn core of *Pikunidromeus* is triangular in cross-section with a triad of flattened faces; two oriented anterodorsally and anteroventrally, and a singular posteriorly slightly rounded face. The two anteriorly oriented faces are separated by a sharp ridge which originates from the lateral surface of the maxillary ramus before continuing posterolaterally and terminating at the distal tip of the horn core. Similarly, two ridges arise from the lateral face of the jugal on the dorsal and ventral margins of the horn core, before ascending to meet the anterior ridge at the distal horn core terminus. The triangular cross-section of the jugal horn is a shared trait with *Akanthodromeus* (Chapter 2), which diverges from the cross-sections of other orodromine jugal horns. *Orodromeus makelai* exhibits a posterolaterally deflected jugal horn framed by multiple prominent ridges with a large distinctive concavity anteroventrally separating the anterior and ventral ridges of the horn [F#.7.7.99.28, MOR 294, 647, 1136, and 1141]. This concavity is present variably in some *Pikunidromeus* specimens [MOR 473 and ROM 64600], even between left and right jugals [MOR 473]. This may be due to taphonomic distortion or just intraspecific horn variation. The main jugal horn differences to emphasize between *Orodromeus* and *Pikunidromeus* are the flattened faces of the latter taxon, especially the anterodorsally inclined face, the rugosity and extensive ridging of *Orodromeus* [MOR 647 and 1141], and the pronounced horn size disparity between adult specimens of both taxa. Another key point is that like *Pikunidromeus*, multiple jugals are available for *Orodromeus* spanning an ontogenetic spectrum and showing this morphology is established early in ontogeny. This theme is similarly expressed in the enigmatic “BV Orodromine”. This taxon displays a sub-oval jugal horn in cross-section, with prominent rugosity, anteroposteriorly flattened faces, and a sharp terminus which is established in a small juvenile individual. The “Kaiparowits

Orodromine" exhibits a jugal horn with anteroposteriorly flattened faces, prominent rugosity, a sub-oval cross-section, but differs from other orodromines as it exhibits a ventral ridge and a rounded terminus (Boyd, 2012). Similarly, *Zephyrosaurus* exhibits a jugal horn core morphology to the "BV Orodromine" and the "Kaiparowits Orodromine" but diverges in its squarish terminus (Sues, 1980). Scheetz (1999) proposed orodromine jugals may be typified by the presence of two nutrient foramina piercing the jugal medial wall in opposition to the jugal horn. Chapter 2 finds these paired nutrient foramina are an orodromine synapomorphy shared by *Akanthodromeus* [MOR 14147], the "BV Orodromine", the "Kaiparowits Orodromine" [UMNH VP 19470], and *Zephyrosaurus* [OMNH 34832, YPM 56695, and MCZ 4394]. Paired nutrient foramina are not visually observed in the *Pikunidromeus* holotype, MOR 473, but are readily observed along the medial wall of other *Pikunidromeus* jugals [MOR 613 and ROM 64600]. The lack of nutrient foramina in MOR 473 may just be an artifact of taphonomy as the medial surface of those jugals are poorly preserved. Future CT imaging may illuminate the presence, or lack thereof, of these foramina in that specimen.

The postorbital ramus of the jugal of is subequal to the length of the maxillary ramus [MOR 473]. It is D-shaped in cross-section and is flattened to slightly concave medially, traits shared with the "Kaiparowits Orodromine" (Boyd, 2012) and *Orodromeus makelai* [MOR 1141]. A sulcus on the lateral tip of the dorsal ramus of the jugal marks the insertion point for the ventral ramus of the postorbital as in *Orodromeus* [MOR 1141], *Haya* (Barta and Norell, 2021), and *Zephyrosaurus* (Sues 1980). This lateral contact of the postorbital and jugal is shared with *Changmiania* where the ventral ramus of the postorbital overlaps the dorsal ramus of the jugal laterally and broadly (Yang et al., 2020). In *Pikunidromeus* and *Orodromeus* [MOR 294], a

distinctive ridge protrudes along the anteromedial margin of the postorbital ramus of the jugal. The jugal wing, or posterior ramus, in *Pikunidromeus* is incomplete in all specimens.

Axial skeleton

Cervical vertebrae— The cervical vertebrae count for most early-diverging neornithischians is nine, except for *Changmiania* which shows six (Yang et al., 2020). MOR 473 exhibits a complete cervical series and shows a count of nine. MOR 436 and ROM 64600 both retain partial cervical series. The morphology of cervical vertebrae three through nine is slightly distorted from post-burial compression in MOR 473, with some of the neural processes skewed off their long axis towards the right dorsolaterally. No foramina are apparent on the lateral faces of any of the cervical centra in MOR 436, 473, or ROM 64600, a shared condition with the thescelosaurids *Fona*, *Koreanosaurus*, and *Changchunsaurus* (Avrahami et al., 2024; Butler et al., 2011; Huh et al., 2010). In contrast with *Fona* (Avrahami et al., 2024), paired foramina deeply incise the floor of the neural canal in some of the cervical vertebrae preserved in ROM 64600. In MOR 436 and ROM 64600, the neurocentral sutures are fully open in all the retained cervical vertebrae, but in MOR 473 cervical vertebrae two through four are closed and gradually open moving posteriorly through the series (sensu Brochu, 1996).

Atlas—Little is recovered of the atlas for *Pikunidromeus* and only the type specimen (MOR 473) preserves the atlantal intercentrum. The atlantal intercentrum is sub-crescentic in anterior view with a smoothly rounded dorsal facet for articulation with the odontoid process of the axis but also shows a sharp ventral margin for acceptance of the occipital condyle. Shallow facets mark the dorsolateral corners of the intercentrum where the atlas neural arches would articulate. The posterolateral corners of intercentrum exhibit knob-like bosses (=parapophyses)

for attachment of the atlantal ribs. The robust atlantal intercentrum is more rectangular in anterior view when compared to the atlantal intercentrum of a similarly sized *Orodromeus* adult (MOR 1141). Sheetz (1999) reported two proatlas in MOR 473, described as short wing-shaped bones which articulate with the occiput. The proatlas unfortunately is not figured in Sheetz (1999) and presently are missing (as of this publication).

Axis—The axis consists of an unfused centrum, neural arch, odontoid process, and axial intercentrum. The neural spine of the axis is incomplete, missing much of the dorsal margin. The neurocentral suture is fully open. The prezygapophyses lack the anterior tips, with only the posterior body of both remaining. A distinct lateral notch occurs just ventral to the prezygapophyses. The odontoid process is a narrowing tongue-shaped bone, dorsally concave which flattens slightly anteriorly. The odontoid process lacks a well-developed ventral anteroventral ridge for articulation with the atlantal intercentrum as seen in *Orodromeus* [MOR 1141]. The axis intercentrum is half-moon shaped in ventral view and inserts into the anteroventral border of the axis centrum, projecting past the anterior centrum face. The larger atlantal intercentrum articulates with the axis intercentrum via tongue-and-grove articulation as noted for *Haya* (Barta and Norrell, 2021). The odontoid process and axis intercentrum are not fused to the axis, a condition also observed in *Changchunsaurus*, *Haya*, *Orodromeus*, and *Hypsilophodon* (Barta and Norrell, 2021; Butler et al., 2011; Galton, 1975; Sheetz, 1999). The axis exhibits an amphiplatyan condition like *Orodromeus* [MOR 294] and *Jeholosaurus* (Han et al., 2012). Matrix obscures most of the left lateral face of the axis centrum in MOR 473, thus hindering recognition of a ventral keel on the axial centrum, but the lateral faces of centrum show slight incurvatures hinting a ventral keel is likely present. The axial centrum is the longest

of the cervical series with every subsequent posterior cervical centrum decreasing slightly in length.

Cervical vertebrae three to nine—The centra of these cervical vertebrae are amphiplatyan to slightly amphicoelous in MOR 436 and 473. Centra faces are D-shaped, the body is ventrolaterally concave, and each vertebrae is sharply keeled ventrally as seen in many SBEDOs like *Convolosaurus*, *Albertadromeus*, *Changchunsaurus*, Fona, *Jeholosaurus*, *Koreanosaurus*, *Oryctodromeus*, *Sanxiasaurus*, *Orodromeus* [MOR 294, 623, and 1141], and *Zephyrosaurus* (Andrzejewski et al., 2019; Avrahami et al., 2024; Brown et al., 2013; Butler et al., 2011; Han et al., 2012; Huh et al., 2010; Krumenacker et al., 2024; Li et al., 2021; Sues, 1980). Cervical three mirrors the longer profile of the axis, with a centrum body length 1.6 times its height. The neural spine of cervical three is reduced to a small dorsal ridge arising centrally over the centrum body as in *Orodromeus* [MOR 294 and 1141]. The prezygapophyses project anteriorly past the anterior face of the centrum. The prezygapophyses are elongate and narrow, with an obliquely angled facet for reception of the corresponding postzygapophyses of the atlas. The short transverse diapophyses arise dorsal to the central point of the lateral face of the centrum, above the neurocentral suture, and mark where the dorsal facet of cervical rib three articulated. The ventral facet of the cervical rib would meet the robust lateral boss-like parapophyses projecting from the centrum body just ventral to the neurocentral suture. Cervical three's centra faces are narrow dorsoventrally. The postzygapophyses are roughly parallel to the dorsal surface of the centrum body and extend just past the posterior face of the centrum. The postzygapophyses are elongated with ventrally flattened facets for reception of the prezygapophyses of cervical four.

Cervical four marks a transitional locus in the morphology of the cervical series in MOR

473. The morphology of this vertebrae showcases features typical of the anterior and posterior vertebrae in this series. Cervical four retains the elongated prezygapophyses of cervical three but at an inclination slightly more dorsal. The neural spine is likewise a thin ridge but differs from cervical three as it projects more anterodorsally. The postzygapophyses are slightly reduced and mirror the stouter form of posterior cervical vertebrae in this series. The postzygapophyses are ventrally flattened in cervical vertebrae four. The anterior centrum face of four is dorsoventrally narrow like three, while the posterior face is laterally expanded yielding a more rounded morphology like the posterior cervical vertebrae. Most notably, the ventral keel of cervical four exhibits an anteriorly placed bulge akin to the hypapophyses observed in the dorsal vertebrae of theropod dinosaurs like *Troodon formosus* [MOR 553]. Hypapophyses or hypapophysis-like structure are not explicitly documented in the cervical vertebrae of SBEDO's; however, in the holotype *Jeholosaurus* specimen [IVPP V12529], cervical four may exhibit a hypapophysis-like structure bulging medially from the ventral keel (Fig. 1, Han et al., 2012) but it is difficult to determine with certainty as figured. Similarly, a potential hypapophysis-like structure is medially placed on the ventral keel on a cervical vertebra with unknown placement in *Fona* [NCSM 36200] (Fig. 9, Avrahami et al., 2024). The posterior cervical vertebrae, five through nine, mirror each other in the consistency of their morphology. The prezygapophyses are short and robust, angled dorsally, and marginally project past the anterior face of each centra. In cervical vertebrae five and six, the neural spine arises over the center of the centra and projects anterodorsally. The neural processes of cervical eight are broken just above the neurocentral suture, but vertebra nine shows an anterodorsally inclined and lengthened neural spine as in *Orodromeus* [MOR 294 and 623]. Small nutrient foramina mark the collateral faces of the centra in the juvenile

Pikunidromeus specimen MOR 436, but not in the presumed adult specimen MOR 473.

Cervical ribs— A handful of cervical ribs are preserved in ROM 64600. They are tightly bundled on the medial face of the right scapula and partially obscured by a partially articulated string of three cervical vertebrae. Not much can be said about their morphology beside they bow along their short lengths, and bifurcate anteriorly for articulation with the axial column.

Dorsal vertebrae—A complete series of fourteen dorsal vertebrae are recovered for MOR 473. MOR 436, ROM 64600, and 64601 preserve incomplete series. The elasmarian *Macrogryphosaurus* also presents fourteen total dorsal vertebrae in its series (Rozadilla et al., 2020). Unfortunately, no other orodromine perseveres a complete dorsal series for comparison. Thescelosaurids like *Oryctodromeus*, *Haya*, *Changchunsaurus*, and *Jeholosaurus* exhibit vertebral counts of fifteen dorsal vertebrae (Barta and Norell, 2021; Butler et al., 2011; Han et al., 2012; Krumenacker et al., 2024), while *Thescelosaurus garbanii* may show a count of 20 dorsal vertebrae (Morris, 1976) and *Thescelosaurus assiniboiensis* has an incomplete series of sixteen (Brown et al., 2011). The dorsal centra of MOR 436 and 473 are slightly amphicoelous. The neurocentral sutures of MOR 473 are fully open until dorsal vertebra eleven, partially closed in vertebra twelve, and fully close in thirteen and fourteen. In the posterior dorsals while anteriorly they are fully open. At least one dorsal from ROM 64600 is partially closed but it is of uncertain placement in the axial column. In MOR 436 and ROM 64601 all neurocentral sutures are fully open. The anterior most vertebrae are slightly ventrally keeled, but not as sharply as the cervical vertebrae. Some dorsal vertebrae from ROM 64600 and ROM 64601 show medially placed small foramina which pierced the body of the centrum ventrally. Small foramina dot the lateral aspects of some dorsal vertebra in the adult specimen of ROM 64600. Like the cervical

vertebrae, the centra shorten in length traveling posteriorly in the series. The neural processes are short and rectangular, arising anteriorly on each centrum. Like *Fona* (Avrahami et al., 2024), the transverse dia- and parapophyses are separate from each other in the anterior vertebrae of the dorsal series [MOR 473]; however, dorsal vertebra three is the only anterior dorsal retaining an intact neural process in MOR 473. Dorsal vertebrae six [MOR 473] shows the dia- and parapophyses have migrated towards each other to form a stair-step configuration on the transverse process high on the vertebra. By dorsal vertebrae eight, this stair-step configuration journeys ventrally to the neural centrum suture and stays orientated at the suture through the rest of the posterior dorsal series. This transverse stair-step configuration of the dia- and parapophyses does not broaden anteroposteriorly like in the posterior dorsal vertebrae of *Fona* [NCSM 33548].

Dorsal ribs—Few dorsal ribs are recovered in MOR 473. Fragments of rib shafts show a sub-oval cross-section, which has been suggested as a potential synapomorphy of orodromines (Avrahami et al., 2024). As noted above, the transverse dia- and parapophyses migrate in their positioning along the axial column in the dorsal series. This translates to a change in the orientation of the tuberculum and capitulum of the dorsal ribs from a near vertical articulation with the axial column to one more horizontal. This transition begins at dorsal vertebrae six and concludes by dorsal vertebrae eight. This transition occurs further posteriorly than in *Orodromeus* [MOR 294] which occurs between vertebra five and six. In this regard, *Pikunidromeus* converges with thescelosaurines like *Oryctodromeus* (supplemental materials, Krumenacker et al., 2024) and *Thescelosaurus assiniboiensis* (Brown et al., 2011) where this transition also begins between dorsal vertebrae six and eight.

Sacral vertebrae—The sacrum of *Pikunidromeus* comprises of seven vertebrae [MOR 473]. None of the sacral vertebrae centra are fused together in MOR 436 or 473, but the visible neurocentral sutures are closed in MOR 473. Sacral vertebral count was decided by examining the centra faces where a vertebra was considered a sacral if it demonstrated at least one centrum face with a sutural or scalloped texture (Avrahami et al., 2024). Seven sacral vertebra is a condition limited to orodromines, thescelosaurines, and *Zalmoxes* amongst SBEDOs.

Much of the dorsal processes and lateral surfaces of the centra of the sacral vertebrae are obscured by other bones and matrix in MOR 473 which limit their interpretation; further compounded by MOR 436, where all the sacral vertebrae display fully open neurocentral sutures and do not retain the neural processes. The sacral centra are slightly amphicoelous like in the dorsal series. The ventral surfaces of the sacral vertebrae are flat except for sacral vertebrae seven, which is slightly concave or grooved. This differs from the elongated grooves present extensively in the sacral of *Fona* (Avrahami et al., 2024), *Oryctodromeus* (Krumenacker et al., 2024), and *Orodromeus* [MOR 294 and 623]. Sacral vertebrae two and three are the most robust of the series, due in part to the lateral expansion of their articular faces at their connection. This expansion marks part of the sacropubal articulation point. In *Orodromeus* [MOR 294, 623, and PU 23409] and *Oryctodromeus* this lateral expansion is a solid facet, or socket, but in at least one specimen of *Fona* [NCSM 36218] this is expressed in massive, laterally symmetrical, intercentral cavities just ventral to the sacropubal articulation. Notably, MOR 473 also possesses intercentral cavities like *Fona* (Avrahami et al., 2024).

Caudal vertebrae—The caudal series for *Pikunidromeus* is incomplete making the total tail length uncertain, as is the case for orodromines broadly. Before this study, only one specimen

[TMP 2008.045.0002] provided any significant snapshot of an orodromine tail, retaining fifteen articulated caudal vertebrae. For *Pikunidromeus*, two specimens retain caudal vertebrae. The first three caudal vertebrae are retained with MOR 473, along with five more vertebrae of uncertain placements. ROM 64600 preserves a beautifully articulated tail section split between two blocks, coupled with three proximal, and one distal, disarticulated caudal vertebrae. With this accounting, ROM 64600 preserves at least 25 caudal vertebrae, as the isolated distal we surmise connects the two articulated caudal series in this specimen. In ROM 64600 and MOR 473 all neurocentral sutures are closed in the caudal series (sensu Brochu, 1996). The caudal centra are slightly amphicoelous. Anterior caudals display very square centra in lateral profile which progressively narrow in dorsoventral height in posterior succession through the caudal series. The neural spines extend posteriorly beyond the centrum face. One isolated anterior caudal [ROM 64600] exhibits very lengthy transverse processes which project posterolaterally. The most diagnostic feature of the caudal vertebrae is a ventral groove, which deeply incise the centra. This ventral groove is a feature shared with *Orodromeus* [MOR 294 and 623], *Zephyrosaurus* [YPM 56695], *Oryctodromeus* (Krumenacker et al., 2024), *Parksosaurus* [ROM 804], *Fona* (Avrahami et al., 2024), and some specimens of *Jeholosaurus* (Han et al., 2012). An anteroposteriorly trending ridge projects from the lateral faces of each caudal centra distal in the series [ROM 64600].

Chevrons—A handful of chevrons are recovered with MOR 436 and 473, but twelve are retained in articulation in ROM 64600. Chevrons are more elongated proximally but shorten distally through the series. The distal terminus of each chevron is rounded, but as one travels distally in the series the shortened chevrons widen anteroposteriorly distally. They articulate with

the axial column at the ventral junction of each caudal vertebrae via anterior and posterior facets on the ventral centrum faces beginning at the junction of caudal vertebrae two and three. Each chevron bifurcates proximally and exhibits a distinct anteroposterior oriented canal.

Ossified tendons—Isolated bundles of ossified tendons are recovered with ROM 64600. These tendons are sub-oval in cross section, rod-like, and run in parallel to each other. This arrangement is most consistent with the epaxial ossified tendons bundles observed running parallel to the long axis of the dorsal and sacral series in *Orodromeus* [MOR 294] and *Oryctodromeus* [IMNH 44591]. No ossified tendons are preserved, or perhaps exist, along the articulated tail sections nor the available prepared dorsal and sacral vertebrae of ROM 64600. Orodromines differ from thescelosaurines, as they only exhibit ossified epaxial tendons running parallel to the long axis of the spinal column in the dorsal and sacral regions (Brown et al., 2013; Scheetz, 1999). Thescelosaurines like *Oryctodromeus* (Krumenacker et al., 2024) and *Thescelosaurus neglectus* (Gilmore, 1915) instead demonstrate both epaxial and hypaxial ossified tendons. It's worth noting; however, that ossified tendon preservation can be variable between specimens within a species (pers. observ.).

Sternum—MOR 473 preserves what we surmise is a single partial sternal plate. The plate is flat and lacks much of the marginal edges. Prominently, a facet is prominent on a corner of this sternal plate. This facet is like the distinctive facet observed in *Akanthodromeus* [MOR 14148], *Orodromeus* [MOR 623], and *Nanosaurus* [BYU ESM-163R] (Hannebaum et al., 2024). The orientation of the plate based on this facet is uncertain. In *Nanosaurus*, the facet is distinct on the posterolateral corner of the plate (Galton and Jensen, 1973) but in *Orodromeus* and *Akanthodromeus* this facet is located at its articulation with the coracoid.

Appendicular skeleton

Scapula—*Pikunidromeus* is represented by five scapulae [MOR 473, ROM 64600, and an unnumbered specimen from TM-018]. For description, we follow Avrahami et al. (2024) and Rozadilla et al. (2019), placing the scapula with the long axis dorsoventrally oriented. The scapula is slightly longer than the humerus in MOR 473. In MOR 473, both scapulae lack the distal dorsal margins, but still, the scapulae appear rather anteroposteriorly narrowed in comparison to *Orodromeus* [MOR 294 and 623], especially when contrasted with the distally anteroposteriorly expanded and ventrally downturned scapulae of *Oryctodromeus* (Krumenacker et al., 2024), *Thescelosaurus neglectus* [MOR 979 and 1183], and *Fona* (Avrahami et al., 2024). The scapulae are medially concave, following the outline of the rib cage. The scapula shows a well-developed acromion process. The angle formed between the acromion process and the craniodorsal margin of the scapular blade is ~ 156° in both MOR 473 and ROM 64600. This is matched closely by *Orodromeus* specimens MOR 623 (157°) and PU 23442 (160°). Thescelosaurines may manifest a steeper angled division (~130°) exemplified by *Fona*, *Oryctodromeus*, and *Thescelosaurus neglectus* [MOR 1183], but note there is some variability in the expression of this angle in these taxa (Avrahami et al., 2024). A sharply ridged scapular process projects from the acromion process through its length. The scapular spine does not fold over ventrally like *Oryctodromeus* (Avrahami et al., 2024) and *Thescelosaurus neglectus* [MOR 1183 and 1185]. *Orodromeus* has previously been noted to exhibit this ventrally folded scapular spine based on specimen MOR 623 (Avrahami et al., 2024); however, many elements within this specimen show extensive post-burial compressive deformation, including the right scapula. Markedly, the proximal surface of the scapula [MOR 623] shows extensive crushing, including the scapular spine, which is offset distally, giving the false impression of ventral deflection (pers.

observ.). No medial tuberosity is observed in *Pikunidromeus*, in opposition to *Fona* and *Oryctodromeus* (Avrahami et al., 2024), and the rhabdodontomorphs *Iani* and *Rhabdodon* (Chanthasit, 2010; Zanno et al., 2023).

Only ROM 64600 presents a fused scapulocoracoid in *Pikunidromeus*. The sutural margin between the scapula and coracoid swells mediolaterally into a robust supraglenoid boss that spans this sutural margin [MOR 473 and ROM 64600]. Its placement and size are similar in its expression to *Orodromeus* specimens MOR 623 and PU 23442, which are very developed, more so than some specimens of *Oryctodromeus* and *Fona*; furthermore, some specimens of the latter taxa lack this boss which hints at potential variability in its manifestation in *Oryctodromeus* and *Fona* (Avrahami et al., 2024). A supraglenoid fossa is apparent in MOR 473 and ROM 6460 like in *Yueosaurus* and some specimens of *Fona* (Avrahami et al., 2024). The supraglenoid fossa is framed posteriorly by a large and raised supraglenoidal buttress (=boss) as seen in *Yueosaurus* (Zheng et al., 2012). No foramen is observed in this fossa in contrast to at least one *Fona* specimen [NCSM 36272) (Avrahami et al., 2024). A sharp flange projects posteriorly from the posterior edge of the scapulae [MOR 473 and ROM 64600] but is not present in the unnumbered probable juvenile scapula from TM-018. This interspecific variation is mirrored amongst *Orodromeus* specimens where ontogenetically advanced specimens present a scapular flange [MOR 623, PU 23442, and 23443], while juveniles lack it [MOR 294 and PU 23246]. At least one adult specimen of *Oryctodromeus* offers a posterior scapular flange [MOR 1642] but notably the adult holotype does not [MOR 1636a], which highlights variability in adult specimens not observed at present in *Orodromeus* and *Pikunidromeus*. *Fona* lacks a sharp posterior flange but does display a rounded swelling of similar placement to the posterior scapular flange [FMNH PR

4581]. *Yueosaurus* exhibits a posterior groove instead of the posterior scapular flange (Zheng et al., 2012). The distal marginations of both scapulae are rugose but there is no evidence of a suprascapula.

Coracoid—The coracoids of *Pikunidromeus* reflect the conservative orodromine morphology demonstrated well by *Orodromeus* specimens [MOR 623 and PU 23442], *Zephyrosaurus* (Kutter, 2004), and an indeterminate orodromine right coracoid from locality TM-088 [MOR 994]. Generally, orodromine coracoids are sub-oval in lateral view with a sternal process perpendicular to the glenoid. The coracoids of *Pikunidromeus* are incomplete, but as a composite fit this profile. This perpendicular deflection of the sternal process away from the glenoid is a morphology shared with orodromines like *Orodromeus* (MOR 294, 623, 1141 and PU 23442), *Zephyrosaurus* (Kutter, 2003), and the "Kaiparowits Orodromine" (Boyd, 2012), but also *Changchunsaurus* (Butler et al., 2011), *Changmiania* (Yang et al., 2020), and *Convolosaurus* (Andrzejewski et al., 2019). This morphology is different from the so called hatchet-shaped sternal processes exhibited by thescelosaurines like *Fona*, *Oryctodromeus*, and *Thescelosaurus neglectus* [MOR 979, 1183] (Avrahami et al., 2024; Krumenacker et al., 2024), thescelosaurids like *Nanosaurus*, *Koreanosaurus*, and *Haya* (Barta and Norell, 2021; Galton and Jensen, 1973; Huh et al., 2010), other SBEDOs such as *Hypsilophodon* (Galton, 1975), and *Gasparinisaura* (Coria and Salgado, 1996), but also the rhabdodontomorphs *Zalmoxes shqiperorum* (Weishampel et al., 2003), *Rhabdodon* (Chanthasit, 2010), and *Tenontosaurus tilletti* [MOR 682 and 2571], and lastly the neoceratopsians *Auroraceratops* (Morschhauser et al., 2018) *Leptoceratops* (Brown, 1914), and likely *Cerasinops* [MOR 300]. What hatchet-shaped means, regarding sternal processes, is poorly defined in the literature and is applied largely to

thescelosaurines (Avrahami et al., 2024; Huh et al., 2020; Krumenacker et al., 2024) and neoceratopsians (Morschhauser et al., 2018). In the broad context of SBEDOs and neoceratopsians, we define hatchet-shaped as a sternal process which sharply deflects away from the glenoid, thus presenting a sternal process in parallel to the articular face of the glenoid process of the coracoid.

The glenoid process of the coracoid is robust (mediolaterally thickened) in *Pikunidromeus* [MOR 473] and *Orodromeus* [MOR 1141, PU 23442] but less developed in the earliest member, *Zephyrosaurus* (Kutter, 2004). Medial to the glenoid process is the ovoid coracoid foramen, which is completely enclosed within the coracoid like all thescelosaurids (Avrahami et al., 2024; Boyd, 2012; Butler et al., 2011; Gilmore, 1915; Huh et al., 2010; Krumenacker et al., 2024; Scheetz, 1999).

The coracoid and scapula are not fused into a scapulocoracoid in MOR 473, but ROM 64600 does demonstrate a right fused scapulocoracoid. Many thescelosaurids develop a fused scapulocoracoid such as *Oryctodromeus* [MOR 1642], *Fona* [NCSM 33548], *Haya* [IGM 100/2015], *Changmiania* [PMOL AD00114], *Thescelosaurus neglectus* [MOR 979, 1183, and NCSM 15728], *Koreanosaurus* (Huh et al., 2010), and potentially *Nanosaurus* [YPM VP 1882], but so do Heterodontosaurids like *Tianyulong* and *Heterodontosaurus* (Santa Luca, 1980; Sereno, 2012), the elasmarian *Trinisaura* (Coria et al., 2013), neoceratopsians like *Montanaoceratops* [MOR 542], and some specimens of *Auroraceratops* (Morschhauser et al., 2018), and the dinosauriform *Silesaurus* (Dzik, 2003). In *Camptosaurus dispar*, some specimens are partially coossified scapulocoracoid [USNM V 4282] (Carpenter and Wilson, 2008). A single continuous fossa is present on both the right and left coracoids of MOR 473 and ROM 64600. This fossa

originates just ventral to the glenoid process and incises the ventral margin of the coracoid. This fossa is present also in *Orodromeus* [MOR 623 and 1141], an indeterminate orodromine coracoid from TM-088 [MOR 944], and convergently in the neoceratopsian *Cerasinops* [MOR 300]. In *Oryctodromeus* and *Fona*, this continuous fossa is subdivided into two separate pockets, the ventral fossa and lateral fossa. The fact that this fossa is not subdivided in any *Pikunidromeus* specimens supports the assertion made in Avrahami et al. (2024) that these fossae represent out pockets of a single individual complex.

Humerus—Three *Pikunidromeus* specimens retain humeri [MOR 436, 473, and ROM 64600]. The humerus is sigmoidal in lateral profile, but straight in anterior view. The proximal head deflects from the humeral shaft at an angle ranging from 115° [right humerus, MOR 473] to 144° [ROM 64600] (measured along the posterior border of the humerus). This inclination is steeper and outside the range presented in *Orodromeus*, 147° to 158° [MOR 248, 294, 404, and 1136], and *Fona*, 165° to 180° (Avrahami et al., 2024). In *Pikunidromeus*, the humeral head twists away from the deltopectoral crest, deflecting posteriorly as seen in *Hypsilophodon*, *Orodromeus*, *Haya*, *Oryctodromeus*, and *Convolosaurus* (Andrzejewski et al., 2019; Barta and Norell, 2021; Galton, 1975; Krumenacker, 2017; Scheetz, 1999). In *Pikunidromeus*, the humeral head is robust and flanked by a weakly defined lateral tuberosity but also by a moderately swollen medial tuberosity. Descending from the lateral tuberosity, the lateral edge narrows sharply but expands slightly as it nears the deltopectoral crest. The deltopectoral crest arises prominently from the lateral edge of the anterior humeral shaft and showcases a sharply angled outline in lateral view, akin to the condition observed in *Fona*, *Orodromeus*, *Zalmoxes shqiperorum*, and the “Kaiparowits Orodromine” (Avrahami et al., 2024; Boyd, 2012; Scheetz,

1999; Weishampel et al., 2003). In the larger-bodied thescelosaurine *Thescelosaurus neglectus* [MOR 979], the deltopectoral crest is poorly developed which is convergently shared with elasmarians like *Talenkauen*, *Notohypsilophodon*, *Anabisetia*, *Trinisaura*, and *Mahuidacursor* (Coria and Calvo, 2010; Coria et al., 2013; Cruzado-Caballero et al., 2019; Ibiricu et al., 2014; Rozadilla et al., 2019). Medial to the deltopectoral crest, the humeral shaft becomes deeply concave demarcating the bicipital sulcus (Barta and Norell, 2021). There is no small foramen in opposition to the deltopectoral crest on the posterior face of the humeral shaft in contrast to *Fona* (Avrahami et al., 2024). Distally the humeral shaft expands into two condyles, separated by steep walled V-shaped anterior intercondylar groove, and a shallow U-shaped posterior intercondylar groove. Medially, the ulnar condyle is larger than the radial condyle and extends past the distal margin of the radial condyle.

Ulna—*Pikunidromeus* exhibits a relatively elongate and moderately robust ulna, quantified by an ulna length to humerus length ratio of 0.77 [MOR 473]. This elongate ulna is a shared morphology reflected in some SBEDOs like *Orodromeus* [0.81, MOR 294], *Hypsilophodon* [0.85, R196 and R192], *Convolosaurus* [0.82, SMU 72834], *Mahuidacursor* [0.75, MAU-Pv-CO-596]. Other SBEDOs present proportionally short ulnae like *Changmiania* [0.70, PMOL AD 00114], *Fona* [0.71, NCSM 33548], *Thescelosaurus neglectus* [0.70, MOR 979], and *Parksosaurus* [0.67, ROM 804]. The lateral profile of the ulnae in *Pikunidromeus* is straight. Proximately the olecranon process is well developed and rises substantially above the coronary process. The trochlear notch exhibits weak curvature marginally which is the condition observed in *Rhabdodon*, *Notohypsilophodon*, *Convolosaurus*, *Haya*, *Parksosaurus*, *Hypsilophodon*, and the “Kaiparowits Orodromine” (Andrzejewski et al., 2019; Barta and Norell,

2021; Boyd, 2012; Galton, 1975; Ibiricu et al., 2014; Sues et al., 2023), while other SBEDOs contrast by showing strongly concave trochlear notches (Avrahami et al., 2024; Chanthasit, 2010; Coria and Calvo, 2002; Cruzado-Caballero et al., 2019; Huh et al., 2010; Santa Luca, 1980). The ulnae are D-shaped in cross-section at mid shaft. No foramina are observed on the dorsolateral surface of the ulnae as observed on *Thescelosaurus neglectus* specimen NCSM 15728 (Avrahami et al., 2024). Moving distally, the shaft constricts before expanding into the distal articular surface which is rounded.

Radius—A complete left radius is recovered in articulation with the left ulna in the juvenile *Pikunidromeus* specimen MOR 436, while one and two partial radii are preserved in the MOR 473 and ROM 64600 respectively. In anterior view, the radii bow slightly medially. Proximately, the radial head presents a flat, to slightly concave, articular face for reception of the radial condyle of the humerus (MOR 436 and 473). A ridge runs the long axis of the radius along the lateral surface as seen in *Akanthodromeus*, *Haya*, and *Fona* (Chapter 2, Avrahami et al., 2024; Barta and Norell, 2021). At midshaft the radius presents a sub-oval cross-section. The shaft expands slightly distally into a rounded articular face [MOR 473 and ROM 64600].

Manus—A partial manus recovered in ROM 64600 and a well-represented left manus in MOR 473 illustrate a manus morphology distinct from most SPEDOs. When discussing the manus, we follow Galton (1975), Barta and Norell (2021), and Avrahami et al. (2024) where dorsal (=antipalmar) and ventral (=palmar). In Figure 23 of Scheetz (1999), the left manus of *Orodromeus* specimen PU 23442 is figured and described as almost complete; however, PU 23442 only preserves articulated carpals and metacarpals. The phalanges figured in Figure 23 (Scheetz, 1999) belong instead to the partial left manus of MOR 473 (Scheetz, 1999). This is

important to note, as the reconstruction of PU 23442 in Scheetz (1999) has limited its applicability for comparative analyses of SBEDO manus morphology, no physical specimen existed matching Figure 23 leading many researchers to disregard, and rarely reference, this proposed orodromine manus template. Instead, an almost complete articulated left manus of a large individual of the "Kaiparowits Orodromine" exists [UMNH VP 12677] and clarifies the orodromine manus (Boyd, 2012; Gates et al., 2013). Scheetz (1999) assumes a small, reduced digit 1 was missing and reconstructed PU 23442 as preserving digits II–V. This assessment is more reflective of the species available at the time for comparison like *Heterodontosaurus* and *Hypsilophodon* (Galton, 1975; Santa Luca, 1980), as they both exhibit a digit I significantly shorter than digits II and III, coupled with an almost vestigial digit V (Galton, 1975; Santa Luca, 1980). SBEDO discoveries since 1999 have reinforced that this manus blueprint was widespread (Andrzejewski et al., 2019; Coria and Calvo, 2002; Manitkoon et al., 2023). The "Kaiparowits Orodromine" [UMNH VP 12677] instead demonstrates that the digit Scheetz (1999) postulated as digit II is really digit I in PU 23442, and orodromines deviate from the SBEDO norm and exhibit more proportionally uniform digit lengths, with digits I and IV being only slightly shorter than digits II and III (Boyd, 2012; Gates et al., 2013). For orodromines, this creates a manus much more squarely shaped, a trait shared with *Thescelosaurus neglectus* [MOR 979, USNM 7757, and ROM cast 80129] (Gilmore, 1915).

In MOR 473, four carpals are recovered and here tentatively interpreted as the radiale, an intermedium, ulnare, and a distal carpal based on their similarity to corresponding carpals in *Orodromeus* [PU 23442], the "Kaiparowits Orodromine" [UMNH VP 12677], and the *Thescelosaurus neglectus* hand cast ROM 80129. The radiale is trapezoidal in shape in lateral

view, with the proximal articular face reduced in comparison to the distal articular face. In proximal view, the radiale is cubic and depressed to accommodate the distal epiphysis of the radius. In distal view, a U-shaped depression receives the elongated and narrow proximal epiphysis of metacarpal I. The intermedium is mostly complete in MOR 473 but lack some of the outer bone surface on the posterior and anterior surfaces. The intermedium is cubic in lateral and proximal views and distinctly faceted proximally for articulation with the distal epiphyses of the radius and ulna. The carpal we identify as the ulnare matches closely in shape and positioning to the ulnare in the "Kaiparowits Orodromine" (Boyd, 2012). However, our interpretation of MOR 473 shows that the ulnare of UMNH VP 12677 is slightly displaced from life position and is rotated posteriorly away from the intermedium (Boyd, 2012). The distal carpal is elongate but thickens dorsoventrally anteriorly.

In MOR 473, metacarpals I and II are noticeably more robust than in *Orodromeus* [PU 23442 and MOR 623]. Metacarpal I is slightly shorter than metacarpal II in length. Both metacarpals I and II are hourglass shaped in palmer view as seen in *Orodromeus makelai* [MOR 294, MOR 623, and PU 23442]. The proximal epiphysis of metacarpal I in *Pikunidromeus* is significantly anteroposteriorly broadened in comparison to their counterpart specimens in *Orodromeus* and *Thescelosaurus*. Remarkably, the distal condyles of metacarpal I are asymmetric with an obliquely inclined articular face [MOR 473 and ROM 64600]. This suggests PI-I articulated with metacarpal I at an angle. This condition is observed convergently in *Psittacosaurus sibiricus* (Averianov et al., 2006) and Heterodontosaurus (Sereno, 2012). Metatarsal IV is broken at the midshaft and lacks a small portion of the shaft in MOR 473. A small bone, with a morphology consistent with ROM cast 80129, is likely ungual of digit V in

MOR 473. The phalangeal count for the manus *Pikunidromeus* is 2-?-?-3-?, but is likely 2-3-4-2-1 based on the "Kaiparowits Orodromine" [UMNH VP 12677] and *Thescelosaurus neglectus* [ROM cast 80129].

Ilium—No complete ilia are known for *Pikunidromeus* and are only represented by the fragmentary ilia of specimens MOR 436, 473, and ROM 64600. A potential portion of the preacetabular process is recovered for MOR 473 but not much can be said about the full preacetabular process, besides that this preacetabular fragment notably displays a ridge along the medial surface. The location of this ridge is consistent with those documented in other Thescelosaurids and *Hypsilophodon* (Avrahami et al., 2024; Galton, 1975; Han et al., 2012; Krumenacker et al., 2024).

The lateral surface of the ilium is concave, but also slightly crushed, which may affect this curvature [MOR 473]. The dorsal margin of the ilium appears slightly rounded, most similar to the condition observed *Changmiania*, *Haya*, *Jeholosaurus*, *Parksosaurus*, *Hypsilophodon*, and the indeterminate orodromine TMP2008.045.002 (Barta and Norell, 2021; Brown et al., 2013; Galton, 1975; Han et al., 2012; Sues et al., 2024; Yang et al., 2020), the postacetabular process of ROM 64600 is rather straight backed which suggests the degree of dorsal curvature would have been not been expressed as significantly as seen in heterodontosaurids like *Abrictosaurus* and *Heterodontosaurus* (Santa Luca, 1980; Sereno, 2012). The mid-ilia dorsal curvature preserved in MOR 473 differs from the flat dorsal profile observed in *Hexinlusaurus*, *Gideonmantellia, Oryctodromeus*, *Zephyrosaurus*, and *Minimocursor* (He and Cai, 1984; Krumenacker et al., 2024; Kutter, 2004; Manitkoon et al., 2023; Ruiz-Omeñaca et al., 2012) nor is it like the sigmoidal dorsal border of *Anabisetia*, *Talenkauen*, *Fona*, *Convolosaurus*, *Rhabdodon*,

Valdosaurus, *Dryosaurus*, *Macrogryphosaurus*, *Thescelosaurus* assiniboiensis, and *T. neglectus* [MOR 979; 1125; 1185] (Andrzejewski et al., 2019; Agnolín et al., 2024; Avrahami et al., 2024; Brown et al., 2011; Chanthasit, 2010; Coria and Calvo, 2002; Galton, 1981; Galton and Taquet, 1982; Rozadilla et al., 2020).

The ilia of MOR 473 and ROM 64600 show, in lateral view, that the postacetabular process narrows distally till it ends in a bluntly rounded margin. The brevis fossa is partially visible in lateral view in MOR 436 and 473, but it is fully visible in ROM 64600. The brevis shelf projects medially perpendicular to the dorsoventral axis of the postacetabular process like *Orodromeus* [MOR 294 and 623]. This differs from some SBEDOs where the brevis shelf deflects more ventrally (Avrahami et al., 2024; Makovicky et al., 2011; Manitkoon et al., 2023). The pubic peduncle is not recovered for *Pikunidromeus*.

The ischial peduncle frames the posterodorsal corner of the acetabulum. It is rather large and swollen in *Pikunidromeus*, dissimilar to the strap-like ischial peduncle noted in *Orodromeus* (Scheetz, 1999). This robust ischial peduncle is a trait shared with many Thescelosaurids like *Koreanosaurus*, *Changchunsaurus*, *Jeholosaurus*, *Haya*, *Thescelosaurus assiniboiensis*, *Thescelosaurus neglectus* [MOR 979], the indeterminate orodromine TMP2008.045.0002, but also the elasmarian *Talenkauen* (Agnolín et al., 2024; Barta and Norell, 2021; Brown et al., 2011; Brown et al., 2013; Butler et al., 2011; Han et al., 2012; Huh et al., 2010). *Pikunidromeus* also exhibits the same triangular-shaped cross-sections documented in ischial peduncles of *Fona* and *Oryctodromeus* (Avrahami et al., 2024; Krumenacker et al., 2024). It is unclear if dorsal rim of the acetabulum exhibited a shelf.

Pubis—The pubes of MOR 473 have never been described in detail (Scheetz, 1999),

likely because only portions of the postpubic processes appeared to be preserved in articulation with both ischia. Here, we note the left prepubic process was incorrectly identified as the distal portion of the right postpubic process by past workers and mistakenly glued into this position. The right prepubic process is well preserved but previously was misidentified as a rib fragment. We also recognized the main body of the left pubis from a box of indeterminate bone fragments. With these additions, MOR 473 now exhibits an almost complete left pubis (lacking only the posterior terminus of the pubic shaft) and most of the posterior shaft of the right pubis.

Descriptions of many orodromine prepubic processes often characterized them as long, slender, and mediolaterally compressed (Avrahami et al., 2024; Brown et al., 2013, Scheetz, 1999), as authors rely mostly on *Orodromeus* specimen MOR 623 for comparison. Though MOR 623 is rather skeletally complete, with both left and right pubes recovered, various elements exhibit significant taphonomic distortion, especially post-burial crushing. This is markedly true for the prepubic processes which are totally mediolaterally crushed generating the illusion of the narrow slender profile documented first by Scheetz (1999). The well preserved prepubic processes of MOR 473 instead demonstrate a robust profile, triangular in cross-section. Only the distal terminus is mediolaterally compressed with very prominent anteroposteriorly trending striations defacing the smooth lateral surface of the prepubic process. These striations are shared with orodromines like *Orodromeus* [MOR 623] and the indeterminate orodromine TMP2008.045.002 (Brown et al., 2013) but also are convergently seen in *Minimocursor* (Manitkoon et al., 2023). Posterior to the prepubic terminus the prepubic shaft swells laterally [MOR 473 and ROM 64600]. The apex of this lateral inflection is centrally placed along the long axis of the prepubic process. This lateral inflection is thin and forms a sharp ridge, in lateral

view, that trends ventrally to meet the ventral margin of the postpubic shaft. This ridge is still observed in like positioning on *Orodromeus* specimen MOR 623 though it is mostly flattened, while the ridge + inflection is evident on the left pubis of the indeterminate orodromine TMP2008.045.002 (pers. observ.). Avrahami et al. (2024) documented a similar lateral inflection of the prepubic process in *Fona* and we note it is present in the juvenile *Oryctodromeus* specimen MOR 1636b. The inflections in these thescelosaurines differ from orodromines as they emerge proximally to the main body of the pubis and are bulbous in *Fona* (Avrahami et al., 2024).

The main body of the pubis bulges from the shaft of the pubis anteriorly to frame the anteroventral corner of the acetabulum. Three large facets mark the body of the pubis and denote sites for a triple junction articulation between the pubis, pubic peduncle of the ilium, and sacrum. The dorsolaterally inclined facet accommodates the pubic peduncle, a dorsomedially inclined faced meets the ventral edge of the fused sacral ribs of sacral vertebrae two and three, and the broad medially flattened facet presses against the intercentral cavity in MOR 473. This tri-faceted pubic body in *Pikunidromeus* is a morphology shared with *Orodromeus* [MOR 623 and PU 23442] and *Fona* (Fig. 25, Avrahami et al., 2024) which both demonstrate a triple junction style articulation previously considered unique to *Thescelosaurus neglectus*.

The obturator foramen is anteromedial to the postpubic shaft [MOR 473 and ROM 64600]. Whether the obturator foramen was enclosed by bone, or open posteriorly forming a notch instead, is uncertain in both MOR 473 and ROM 64600 as this region of the pubic body is incomplete in both specimens. In many SBEDOs, the presence of either an obturator foramen or notch can vary between specimens within species (Avrahami et al., 2024; Galton 1975). Posterior

to the pubic body, the postpubic process is rod-like and slightly mediolaterally compressed, exhibiting a sub-oval cross-section [MOR 473]. Both pubes in MOR 473 lack the distal-most portions. One *Fona* specimen [NCSM 33548] exhibits partially fused and tightly appressed pubes (Avrahami et al., 2024). The pubes of *Pikunidromeus* are not fused.

Ischium—Two ischia are recovered in MOR 473 and one in ROM 64600. The ischium is an elongated bone which bifurcates anteriorly into two processes framing the posteroventral corner of the acetabulum. Anteriorly the ischium is robust with broad rugose articular faces on the dorsally inclined iliac peduncle and ventrally inclined pubic peduncle. In other thescelosaurids like *Fona*, *Jeholosaurus*, and *Orodromeus* the ischium is much narrower in anterior profile (Avrahami et al., 2024; Han et al., 2012; Scheetz, 1999). Instead, in *Pikunidromeus* these broad articular faces create a robust anterior profile more comparable to the conditions observed in other SBEDOs like *Macrogryphosaurus*, *Hypsilophodon* and *Parksosaurus* (Galton 1975; Rozadilla et al., 2020; Sues et al., 2023). The iliac and pubic peduncles are of subequal length in *Pikunidromeus*. Notably a small protrusion projects medially from the dorsomedial corner of the articular surface on the pubic peduncle in MOR 473 but not in ROM 64600. This protrusion is also documented in *Jeholosaurus*, *Hypsilophodon*, *Fona*, and *Oryctodromeus* (Avrahami et al., 2024; Galton 1975; Han et al., 2012; Krumenacker et al., 2024). The angle formed between the peduncles and the long axis of the ischial shaft is approximately 80°, which falls within an averaged range of between 87° and 65° for many other SBEDOs (Avrahami et al., 2024). The ischial shaft is straight in lateral view which is typical of thescelosaurids (Avrahami et al., 2024; Krumenacker et al., 2024; Scheetz 1999) but also *Heterodontosaurus* (Santa Luca, 1980), the elasmarian *Anabisetia* (Coria and Calvo, 2002), and

dryosaurids like *Iyuku* and *Valdosaurus* (Barrett, 2016; Forster et al., 2023). The obturator process is obscured ventrally by matrix and partially by the left ilium in MOR 473 and is incompletely represented in ROM 64600 but occurs in the proximal third of the ischium. In the distal third of the shaft, the shaft twists slightly dorsally but not to the extent documented in thescelosaurines like *Fona*, *Thescelosaurus neglectus* [NCSM 15728], and *Haya* (Avrahami et al., 2024; Barta and Norell, 2021). The medial and lateral margins of this distal portion of the ischial shaft also taper forming a blade like profile like *Changmiania* (Yang et al., 2020). The distal most termini of the ischial shafts are missing in both ischia of MOR 473 and in ROM 64600. No grooves are present along the proximal dorsal margin or lateral surface of the ischia shaft in MOR 473, but ROM 64600 does exhibit a shallow groove running the lateral margin of the shaft posterior to the obturator process.

Femur—Eleven femora are recovered for *Pikunidromeus* ranging in size and ontogenetic stages. In *Pikunidromeus*, the femoral shaft bows anteriorly. This degree of bowing is variable between specimens, likely influenced in part by post-burial deformation, and does not appear to trend with ontogeny. The femoral head projects medially on a constricted neck at an angle of 108° to 110° from the diaphysis, much shallower than the 125° exhibited by *Akanthodromeus* (Chapter 2). In *Fona* (Avrahami et al., 2024) and *Orodromeus* (pers. observ.), this angled projection of the femoral head can occur over quite a range amongst specimens, and at least in *Orodromeus*, this variability is attributable to taphonomic distortion from post-burial compression, but also likely due to some degree of intraspecific variability. In *Pikunidromeus*, an obliquely inclined U-shaped sulcus deeply incises the femoral head and marks the route and insertion site of the *m. iliotrochantericus* (Maidment and Barrett, 2011) along the posterior face

of the femoral head. This U-shaped sulcus is a shared trait with many SBEDOs like *Fona*, *Minimocursor*, and *Gideonmantellia* (Avrahami et al., 2024; Manitkoon et al., 2023; Ruiz-Omeñaca et al., 2012), but its depth of incision is notably variable amongst taxa and can be extremely shallow like the observed condition in *Notohypsilophodon* and *Sanxiasaurus* (Ibiricu et al., 2024; Li et al., 2021).

The dorsal margination of the trochanteric region is roughly subequal to the femoral head in *Pikunidromeus*, with the dorsal crests of the greater and lesser trochanters fused and continuous in the skeletal mature specimens, MOR 473 and ROM 64600. In juvenile specimens, like MOR 350, 436, and 10925, the lesser trochanter terminates just ventral to the dorsal border of the greater trochanter likely indicating some change in the length of the lesser trochanter through ontogeny in *Pikunidromeus*. This ontogenetic pattern is shared *Orodromeus* (pers. observ.) where the lesser trochanter migrates through ontogeny until it is subequal or equal to the greater trochanter. In contrast, *Fona* specimens show some intraspecific variability regardless of ontogeny in the extent of the dorsal margination of the lesser trochanter in relation to the greater trochanter (Avrahami et al., 2024). Dorsally, the trochanteric region is flat and squarish in lateral profile like *Orodromeus* [MOR 623] and *Gasparinisaura* (Coria and Salgado, 1996). The greater trochanter is anteroposteriorly expanded with a slightly convex lateral surface which flattens as it approaches the lesser trochanter. This flattened region of the greater trochanter is V-shaped in lateral view and tapers distally. The lesser trochanter is less developed in comparison to the greater trochanter. The lesser trochanter is mediolaterally flattened in MOR 473 and ROM 64600 but is rounded in the juvenile specimens MOR 350, 436, 10925, and 10927. The trochanteric region remains fully coossified through ontogeny lacking any dorsal separation, or

intertrochanter cleft, which is a morphological trajectory shared with *Gasparinisaura* specimens (Coria and Salgado, 1996; Salgado et al., 1997). Intertrochanter notches (=clefts) are observed in many SBEDOs along the dorsal rim of the trochanteric region and mark the division of the greater and lesser trochanters. We interpret this feature within its original context (Coria and Salgado, 1996) and define it as any structural dorsal division of the trochanteric region which sharply separates the greater and lesser trochanters. In SBEDOs like *Minimocursor*, *Convolosaurus*, *Nanosaurus*, *Dryosaurus*, and *Iyuku*, the observation of this intertrochanter cleft can be obvious as it deeply incises the trochanteric region (Andrzejewski et al., 2019; Forster et al., 2023; Galton, 1981; Galton and Jensen, 1973), but in some taxa this incision is subtle or variable between specimens as in *Kangnasaurus* and *Jeholosaurus* (Avrahami et al., 2024; Cooper, 1985; Han et al., 2012). Orodromines like the "Kaiparowits orodromine" (Boyd, 2012) and *Orodromeus* (pers. observ.) lack an intertrochanteric notch. One specimen of *Orodromeus* [MOR 623] appears to potentially have a slight cleft, but as every *Orodromeus* femur lacks a cleft we surmise it's likely not authentic morphology and is instead a taphonomic artifact.

The fourth trochanter arises in the approximate first 43% of the femur from the posteromedial border of the diaphysis and projects posteroventrally in juvenile and adult *Pikunidromeus* specimens. The fourth trochanter is lateromedially compressed and pendent-shaped, with a concave medial surface which tapers terminally. A single rugose shallow elliptical fossa marks the medial surface of the diaphysis below the fourth trochanter in many SBEDOs but is bisected by a sharp ridge in juvenile *Pikunidromeus* [MOR 436, 10925, 10927]. This bisected fossa likely marks the two insertion sites for the *M. caudofemoralis longus* and *M. puboischiofemoralis internus* muscles (Maidment and Barrett, 2011). A small circular nutrient

foramen marks the posterior face of the diaphysis near the base of the fourth trochanter as in *Orodromeus* (pers. observ), *Fona*, *Akanthodromeus*, *Jeholosaurus*, *Sanxiasaurus* and *Talenkauen* (Chapter 2, Avrahami et al., 2024; Han et al., 2012) but is absent in other SBEDOs such as *Haya*, *Nanosaurus*, *Hypsilophodon*, and Dryosaurids like *Kangnasaurus* or *Iyuku* (Barta and Norell, 2021; Cooper, 1985; Galton and Jensen, 1973; Galton, 1975; Forester et al., 2022). The shaft is D-shaped in cross-section just ventral to the fourth trochanter.

Distally the femur expands into large articular condyles separated posteriorly by a deeply incising intercondylar sulcus (=groove). There is no anterior intercondylar sulcus. Anterior intercondylar sulci are observed in many SBEDO groups like the thescelosaurines, elasmarians, dryosaurids, rhabdodontids, and iguanodontians (Avrahami et al., 2024; Galton 1981; Rozadilla et al., 2016; Verdú eta l., 2016; Weishampel et al., 2010) but are notably absent in small-bodied SBEDOs like the orodromines, *Jeholosaurus*, *Yandusaurus, Minimocursor* and many others (He and Cai 1984; Han et al., 2012; Huh et al., 2010; Manitkoon et al., 2023). The medial condyle (=tibial) is larger than the lateral condyle (=fibular). The medial condyle is laterally inflated which partially obscures the posterior intercondylar groove. This feature is observed in the thescelosaurids *Jeholosaurus*, *Haya,* and *Thescelosaurus assiniboiensis* (Barta and Norell, 2021; Brown et al., 2013; Han et al., 2012), but also *Parksosaurus* (Sues et al., 203) and *Leptoceratops* (Brown, 1914). Koreanosaurus, the "Kaiparowits Orodromine" (Boyd, 2012), and *Orodromeus* (pers. observ.) lack a lateral inflection of the medial condyle.

Tibia—*Pikunidromeus* is represented by five tibiae [MOR 436, 473, 530, 533, and ROM 64600]. The tibia is elongated with a shaft laterally bowed and twisted along its length, exhibiting a triangular cross-section mid-shaft. In *Pikunidromeus*, the tibia is longer than the

femur, exhibiting a tibia to femur length ratio of 1.20. This ratio is an averaged value calculated from the ratios of the left and right hindlimbs of both MOR 473 and ROM 64600. This tibia to femur ratio is consistent with many SBEDOs like *Minimocursor* [1.22], *Jeholosaurus* [averaged:1.22], *Hypsilophodon* [1.18], *Orodromeus* [averaged: 1.18], *Parksosaurus* [1.18], *Changmiania* [1.21], *Oryctodromeus* [1.18], and *Haya* [averaged: 1.21]. *Fona* [1.12], *Convolosaurus* [averaged:1.12] and *Koreanosaurus* [1.07] exhibit smaller tibia to femur length ratios.

The proximal epiphysis of the tibia in *Pikunidromeus* is moderately anteroposteriorly expanded like *Albertadromeus* (Brown et al., 2013), in comparison to the substantially expanded proximal tibia epiphyses of *Thescelosaurus assiniboiensis* (Brown et al., 2011), *Fona* (Avrahami et al., 2024), and some specimens of *Oryctodromeus* (pers. observ.). The proximal articular surface is crescent shaped in proximal view and arches medially like *Haya* and *Hypsilophodon* (Barta and Norell, 2021; Galton, 1975) but also ventrally akin to *Albertadromeus*, *Jeholosaurus*, and *Orodromeus* (Brown et al., 2013; Han et al., 2012, Scheetz, 1999). The proximal epiphysis is subdivided into three condyles: the cnemial crest, lateral condyle (=outer), and inner condyle (=medial). The cnemial crest is robust with a laterally deflected and rounded apex. The medial surface of the cnemial crest lacks the deep fossa with the raised anterior rim and striated floor observed in *Haya* (Barta and Norrell, 2021). The right tibia of MOR 473 exhibits an anterior rim on the medial face of the cnemial crest, but this is instead attributable to taphonomic alteration from post-burial crushing. A sulcus, the *incisura tibialis*, incises the proximal epiphysis separating the cnemial crest from the lateral condyle. The lateral condyle is bifurcated into a larger fibular and a smaller accessory condyle which is the condition observed in SBEDOs like

Fona, *Orodromeus*, *Changchunsaurus*, *Gideonmantellia*, *Haya*, and *Hypsilophodon* (Avrahami et al., 2024; Barta and Norrell 2021; Butler et al., 2011; Galton, 1975; Ruiz-Omeñaca et al., 2012; Scheetz, 1999). This accessory condyle is absent in *Lesothosaurus*, *Gasparinisaura*, *Jeholosaurus*, *Sanxiasaurus*, and *Notohypsilophodon* (Baron et al., 2017; Coria and Salgado, 2010; Han et al., 2012; Ibiricu et al., 2014; Li et al., 2021). Continuing anteriorly, the lateral condyle is separated from the inner condyle by a deep sulcus. The inner condyle tapers to a subtriangular, slightly rounded, downturned apex which is a shared condition with *Albertadromeus* (Brown et al., 2013) and *Nannosaurus* [BYU 163]. This downturned inner condyle is also shared with some specimens of *Oryctodromeus* but in this taxon the inner condyle is more strongly hooked [MOR 1636a, 1642, 8660; IMNH 44604, 44939].

In thescelosaurids like *Fona*, *Jeholosaurus*, *Albertadromeus* and *Haya*, the shaft bulges below mid length in a structure denoted as the fibular eminence, which articulates with the medial surface of the fibula (Avrahami et al., 2024; Barta and Norell, 2021; Brown et al., 2013; Han et al., 2012). *Pikunidromeus* presents a sharply edged fibular eminence below the midshaft of the tibia in MOR 436 and ROM 64600 but is poorly preserved in both tibiae of MOR 473. In *Oryctodromeus* the fibular eminence is only manifested in some tibiae (pers. observ.). Distally the tibia expands mediolaterally into the medial (=inner) and lateral (=outer) malleoli in *Pikunidromeus*. The lateral malleolus is larger and extends distally past the articular face of the medial malleolus. This uneven margination of the distal malleoli is a common SBEDO condition (Andrzejewski et al., 2019; Baron et al., 2017; Herne et al., 2018; Krumenacker et al., 2024). *Parksosaurus* is a notable exception which exhibits subequal malleoli (Fig. 16, Sues et al., 2024), a shared condition with pachycephalosaurids like *Stegoceras*, *Homalocephale*, and ROM 73555

(Maryanska and Osmólska, 1974; Moore, 2021; Woodruff, 2022). In *Pikunidromeus*, the lateral malleolus displays a sharp flange along the lateral edge where the fibula is tightly appressed. A pronounced ridge marks the posterior face of the distal epiphysis which separates the two malleoli. The media malleolus is more developed in contrast to *Akanthodromeus* (Chapter 2).

Fibula—The fibula is elongate in *Pikunidromeus* with an anteroposteriorly expanded proximal epiphysis which tapers distally into a bulbous distal epiphysis. The proximally expanded epiphysis angles posteriorly, which facilitates an inclined dorsal margin like *Oryctodromeus* and *Fona* (Avrahami et al., 2024; Krumenacker et al., 2024). This differs from *Hypsilophodon*, *Gasparinisaura*, and *Heterodontosaurus*, which though slightly uneven, shows a relatively horizontal dorsal apex with the slightest posterior inclination (Coria and Salgado, 1996; Galton, 1975; Santa Luca, 1980). In *Pikunidromeus*, the medial face of the proximal epiphysis is concave for articulation with the bifid lateral condyle of the tibia. Immediately distal, the shaft constricts anteroposteriorly and maintains this thickness till midshaft before narrowing distally. In *Orodromeus* and *Albertadromeus*, a significantly sized sharp flange projects medially from the shaft in the distal half of the fibula (Brown et al., 2013; Fig. 29, Scheetz, 1999). *Pikunidromeus* also showcases a sharply raised flange. The expression of the fibular flange appears to be under some ontogenetic control in *Orodromeus*. This ontogenetic trend appears present in *Pikunidromeus* also. In *Orodromeus* juveniles, this flange is reduced to a thin ridge [PU 23246] in comparison to the more skeletally mature specimens [MOR 623] which exhibit a distinctively large, thin, and rectangular flange. *Pikunidromeus* juveniles [MOR 436] appear to also demonstrate a reduced fibular flange in contrast to adult specimens [MOR 473 and ROM 64600]. Fibular flanges are seen broadly amongst thescelosaurids but also in

neoceratopsians like *Auroraceratops* (Fig. 27, Morschhauser et al., 2018) and *Cerasinops* [MOR 300]. Distally the fibula becomes anteroposteriorly expanded into a bulbous epiphysis which closely appressed against the anterior face of the lateral malleolus of the tibia, while also articulating with the fibular facet of the calcaneum. The fibula is not fused distally to the tibia as in *Albertadromeus* and *Heterodontosaurus* (Brown et al., 2013; Santa Luca, 1980), nor to the calcaneum and astragalus in a structural tibiotarsus like *Heterodontosaurus* (Santa Luca, 1980). In *Haya*, a triangular projection protrudes from the articular face of the distal fibular epiphysis which is not observed in any *Pikunidromeus* specimens (Barta and Norrell, 2021).

Astragalus—The astragalus is not fused to the calcaneum in MOR 473 or ROM 64600 but is tightly appressed like *Orodromeus* (Scheetz, 1999). In *Changmiania*, the astragalus and calcaneum are fused to the tibia in a tibiotarsus (Yang et al., 2020). The astragalus outline is crescentic in lateral view. Anteriorly, a sharp forked "spike-like" ascending process which cups the medial malleolus anteriorly as in *Fona*, *Orodromeus*, *Oryctodromeus*, and *Jeholosaurus* (Avrahami et al., 2024; Han et al., 2012; Krumenacker et al., 2024; Scheetz, 1999). In distal view, the astragalus is blocky but narrows laterally. Small globular protrusions emanate from the lateral face of the astragalus as in *Fona*, *Oryctodromeus* (Avrahami et al., 2024; Krumenacker et al., 2024), and *Orodromeus* [MOR 623] in contrast to *Jeholosaurus* which exhibits a concave lateral face (Han et al., 2012). It's unclear if a foramen marks the posterior surface of the astragalus just ventral to the ascending process as in *Fona* and *Jeholosaurus* (Avrahami et al., 2024; Han et al., 2012) and *Orodromeus* [MOR 623], as this surface is obscured in MOR 473, 530, and ROM 64600.

Calcaneum—The calcaneum is tightly appressed against the astragalus in MOR 473 and

ROM 64600 displaying a crescentic profile in lateral view. The calcaneum manifests two prominent facets; anterodorsally lies the fibular facet which articulates with the distal epiphysis of the fibula, while posterodorsally the tibia facet cups the medial malleolus of the tibia. The angle separating these articular facets is 106° in MOR 473, less than the more obtusely angled (> 120°) conditions observed in *Fona* and *Oryctodromeus* (Avrahami et al., 2024). There is no foramen observed at the contact with the astragalus as in *Fona* (Avrahami et al., 2024) and *Oryctodromeus* [MOR 1642].

Distal tarsals—In most SBEDOs, two distal tarsals are present (Andrzejewski et al., 2019; Avrahami et al., 2024; Galton, 1975) excluding *Heterodontosaurus* which exhibits three distal tarsals fused together (Santa Luca, 1980). For *Pikunidromeus*, both distal tarsals are seen in MOR 473 and partially in MOR 530. The medial distal tarsal is preserved fully in MOR 473 in proximal view and is still in articulation with the metatarsal three. The main body of the medial distal tarsal is thin with a squarish proximal profile like *Orodromeus* [MOR 623], *Fona*, *Oryctodromeus*, and *Akanthodromeus* (Chapter 2, Avrahami et al., 2024; Krumenacker et al., 2024). A large triangular process projects laterally as in *Orodromeus* (Fig. 30, Sheetz, 1999) in contrast to the reduced process in *Akanthodromeus* (Chapter 2). These all are distinct from the disc-shaped medial distal tarsals of *Lesothosaurus* (Baron et al., 2017) and the semi-circular proximal profile observed in *Gasparinisaura* (Salgado et al., 1997). Not much can be said about the lateral distal tarsal in MOR 473 besides it is cuboid in shape as it is mostly obscured by matrix.

Pes—The complete pes morphology is accounted for *Pikunidromeus* [MOR 436, 473, 530 and ROM 64600]. Before continuing, it is worth noting here that MOR 530 is portrayed as a

complete left pes with an articulated medial distal tarsal in Figure 31 of Scheetz (1999). In truth, the pes reconstruction portrayed is *Orodromeus* specimen MOR 623, which notably (until recently) was incorrectly reconstructed with two metatarsal II's and mismatched phalanges. Furthermore, digits I and II of the left pes of MOR 623 may be pathologic (pers. observ.). All these confounding factors likely have colored anatomical references and understanding of *Orodromeus* pes morphology, with Figure 31 (Scheetz, 1999) referenced as recently as 2024 (Avrahami et al., 2024). MOR 530 does preserve an articulated block of metatarsals, and phalange PI-I and partially PIV-1.

Metatarsal I is proximately mediolaterally thin and splint-like in medial profile for *Pikunidromeus* [MOR 530 and ROM 64600] just like *Diluvicursor*, *Fona*, *Jeholosaurus*, *Changchunsaurus*, and likely *Akanthodromeus* (Chapter 2; Avrahami et al., 2024; Butler et al., 2011; Han et al., 2012; Herne et al., 2018; Scheetz, 1999). At midshaft, the cross-section of metatarsal I is sub-oval in *Pikunidromeus* shared with *Orodromeus* [MOR 623] and differing from the D-shaped midshaft cross-section of *Fona* (Avrahami et al., 2024), and the triangular cross-sections documented in *Akanthodromeus*, *Jeholosaurus*, *Hypsilophodon*, *Minimocursor*, *Parksosaurus*, and *Convolosaurus* (Chapter 2; Andrzejewski et al., 2019; Butler et al., 2011; Galton, 1975; Manitkoon et al., 2023; Sues et al., 2023). In lateral view, metatarsal I arcs anteriorly. Distally, the shaft expands into a mediolaterally expanded articular surface for phalanx I. This epiphysis is subdivided into two poorly developed condyles posteriorly separated by a shallow U-shaped intercondylar groove.

Metatarsi II, III, IV serve as the main weight bearing pedal elements. Like metatarsal I, metatarsal II is mediolaterally compressed, as it closely appressed against metatarsal III along an

extensive contact. In anterior view, metatarsal II is relatively straight throughout its length. The distal epiphysis of metatarsal II is transversely and anteroposteriorly expanded forming a rounded articular face, subdivided into a medial and lateral condyle. Shallow collateral ligament pits demark the lateral and medial surfaces of both condyles like in *Orodromeus* (pers. observ.). Both condyles are separated by a U-shaped intercondylar groove like other orodromines such as *Akanthodromeus* and *Orodromeus*, but dissimilar to thescelosaurines like *Oryctodromeus* and *Fona* (Chapter 2; Avrahami et al., 2024.). The prominent vascular canals observed across the distal epiphysis of *Akanthodromeus* are not observed in any specimens (Chapter 2).

Metatarsal III is longer than II or IV, sigmoidal in anterior profile, deviating laterally along its distal length. The terminal epiphysis is similarly subdivided into a large medial and lateral condyle, with the lateral the larger of the two like *Akanthodromeus* (Chapter 2). As in metatarsal II, a shallow U-shaped intercondylar groove separates both condyles on metatarsal III like *Fona* and *Akanthodromeus* (Chapter 2; Avrahami et al., 2024), which differs from the deep V-shaped posterior intercondylar grooves observed in *Oryctodromeus* (Krumenacker et al., 2024) and *Orodromeus* (pers. observ.). Both condyles showcase shallowly developed collateral ligament pits on the lateral and medial faces of metatarsal III like *Diluvicursor* (Herne et al., 2018). A shallow semicircular fossa incises the anterior surface of the distal epiphysis just above and between the two condyles shared with the metatarsi of *Diluvicursor*, *Oryctodromeus*, *Fona*, and *Haya* (Avrahami et al., 2024; Barta and Norell 2021; Herne et al., 2018; Krumenacker et al., 2024), and unlike the deep fossa (=pit) noted in heterodontosaurids *Heterodontosaurus*, *Abrictosaurus*, and *Tianyulong* (Santa Luca, 1980; Sereno, 2012).

Metatarsal IV is complete in MOR 530 but is obscured by matrix through its entire

contact with metatarsal III, MOR 436, 473, and ROM 64600 retain fragmentary metatarsal IVs. In thescelosaurids like *Akanthodromeus* (Chapter 2), *Orodromeus* (pers. observ.), *Oryctodromeus* [MOR 1642], and *Jeholosaurus* (Han et al., 2012), the diaphysis of metatarsal IV is straight proximally but deflects laterally at midshaft before straightening slightly to contact metatarsal III again just above the lateral condyle. The lateral face of metatarsal IV in MOR 530 shows a similar trajectory. The distal epiphysis is anteroposteriorly expanded, and the articular face is sub-parallelogram-shaped in distal view [MOR 436, 473, 530, and ROM 64600]. The distal epiphysis is subdivided into two articular condyles. The medial condyle is large and rounded, whereas the later condyle tapers, displaying a flange-like morphology. This flange-like lateral condyle is not as exaggerated as metatarsal IV in *Akanthodromeus* (Chapter 2). The condyles are not separated by an intercondylar groove posteriorly and shallow collateral ligament pits mark the medial and lateral condyles.

Metatarsal V is identified here for the first time in specimen MOR 473 and illuminates a morphology consistent with orodromines like *Orodromeus* [MOR 623] and the "Kaiparowits Orodromine" (Boyd, 2012). The body of metatarsal V is positioned against the posterior face of the diaphysis of metatarsal III, while the rounded articular surface of metatarsal V lies near the proximal epiphysis of the disarticulated metatarsal IV. This placement likely is close to life position, which is corroborated by other thescelosaurids (Avrahami et al., 2024; Boyd, 2012; Brown et al., 2011; Galton and Jesen, 1973; Gilmore, 1915) and other SBEDOs (Galton, 1975; Herne et al., 2018; Sereno, 2012) that demonstrate articulation with the posterior epiphysis of metatarsal IV, before pressing against the posterior diaphysis of metatarsi IV and III. Metatarsal V in MOR 473 exhibits what we designate as a "mailbox flag" morphology only shared with

orodromines like *Orodromeus* [MOR 623] and the "Kaiparowits Orodromine" [UMNH VP 16281] (Boyd, 2012). The metatarsal V of MOR 473 is small, anteroposteriorly compressed, hinged ventrally, and exhibits a rounded proximal articular face. The metatarsal V of MOR 473 is more an intermediate between *Orodromeus* [MOR 623] and "Kaiparowits Orodromine" [UMNH VP 16281]. In *Orodromeus*, metatarsal V is short [MOR 623]. "Kaiparowits Orodromine" specimen UMNH VP 16281 is sharply hinged but more elongated than MOR 473 and *Orodromeus* [MOR 623]. Some thescelosaurids like *Fona* [NCSM 36276], *Oryctodromeus* [MOR 1642], and *Diluvicursor* [NMV P221080] display an elongate anteroposteriorly flattened metatarsal V (Avrahami et al., 2024; Krumenacker et al., 2024; Herne et al., 2024), others exhibit a small splint-like metatarsal V like *Jeholosaurus* [IVPP V12529], *Nanosaurus* [BYU ESM-163R], *Haya* [IGM 100/2013]; furthermore, *Thescelosaurus assiniboiensis* [RSM P 1225.1] and *Thescelosaurus neglectus* [USNM 7757] display a metatarsal V with an hourglass profile (Brown et al., 2011; Gilmore, 1915). Non-thescelosaurid SBEDOs maintain a rod-like or splint-like metatarsal V (Andrzejewski et al., 2019; Galton, 1975) but notably metatarsal V of *Parksosaurus* [ROM 804] is unique with a broad proximal epiphysis, tapering distally, creating a spike-like profile (Sues et al., 2023).

Between specimens MOR 436, 473, and ROM 64600 a full account of the pedal phalange arrangement for *Pikunidromeus*. The phalangeal count for *Pikunidromeus* is 2-3-4-5-0 which is shared broadly across SBEDOs. PI-I is more elongate other SBEDOS and *Pikunidromeus* demonstrates a PI-I length/midshaft width ratio of 4.02 [MOR 473], 4.15 [MOR 436], 4.11 [MOR 530], and 4.32 [ROM 64600]; averaged ratio of 4.15. Avrahami et al. (2024) notes most SBEDOs, including *Fona*, exhibit PI-I length/ratios between ~ 3.0 and 4.0. A deep depression

penetrates the ventromedial shaft of the PI-I just proximal to the distal articular condyles. In all three specimens, PIII-I is proximodorsally lipped. This differs from *Fona*, *Haya*, and *Jeholosaurus* (Avrahami et al., 2024; Barta and Norell, 2021; Han et al., 2012) where this lipped condition is variable in its expression between specimens. *Orodromeus* specimen MOR 623 also displays a lipped PIII-I. PIV-1 exhibits an obliquely angled proximal articular face to accommodate the parallelogram-shaped distal epiphysis of metatarsal IV. This oblique proximal inclination is observed also in *Akanthodromeus* [MOR 14148], *Orodromeus* [MOR 623, PU 23246], *Fona* (Fig. 31, Avrahami et al., 2024), and *Oryctodromeus* [MOR 1642]. The pedal unguals are very spade shaped, and ROM 64600 illustrates their arrangement. Each ungual is very spade shaped with pronounced medial and lateral grooves. Notably, the unguals of digits I and II deflect medially and are asymmetrical, as the ventral floor of the ungual broadens medially in an elongate sill. The ungual of digit III also deflects medially, does not exhibit asymmetric ungual sills, and is the largest pedal ungual. The digit IV ungual deflects laterally and is smaller than the PI ungual.

Phylogenetic results

Bayesian analytics were employed to explore the phylogenetic inclination of *Pikunidromeus ancellae* using the Avrahami et al. (2024) SBEDO character matrix. *Pikunidromeus* is well represented in the dataset and lacks only 35% of the characters. However, many taxa in this dataset are poorly represented, and lack much of the data. To investigate how missing data affects posterior node support and tree topology, six time- and non-time constrained trees were created. Every analysis recovers *Pikunidromeus* as an orodromine closely aligned with other orodromines in the Two Medicine-Judith River-Belly River clastic wedge of northern

Laramidia and the “Kaiparowits Orodromine” of southern Laramidia (Gates et al., 2013).

Synapomorphies

Orodrominae—Brown et al. (2013) established the clade Orodrominae and defined it as containing thescelosaurids more closely related to *Orodromeus makelai* (Horner and Weishampel, 1988) than to *Thescelosaurus neglectus* (Gilmore, 1913). They used the following characters to support this clade: foramen magnum between 20% and 30% of the width of the occipital condyle; a sharp and pronounced scapular spine; pubis articulating with a sacral rib; and a fibular shaft D-Shaped in cross-section. Madzia et al. (2021) further defined Orodrominae as the largest clade within Hypsilophodontidae v Thescelosauridae containing *Orodromeus makelai*, and defined Hypsilophodontidae as the largest clade containing *Hypsilophodon foxii* (Huxley, 1870) but not *Iguanodon bernissartensis* (Boulenger in Beneden, 1881) and *Rhabdodon priscus* (Matheron, 1869). We follow the Madzia et al. (2021) definition for Orodrominae as it closely conforms to the topologies recovered here.

First, we assessed the validity of the synapomorphies proposed in Brown et al. (2013) as this character matrix was directly incorporated into the character matrix of Boyd (2015), and thus the Avrahami et al. (2024) character matrix. Avrahami et al. (2024) character 169:1 corresponds to the first proposed synapomorphy of Brown et al. (2013) assessing the size of the foramen magnum. State 1 is only observed n *Thescelosaurus neglectus* and *Nanosaurus*, therefore not a valid orodromine synapomorphy. Character 255:1 is the second proposed synapomorphy of Brown et al. (2013). We verify the assertion made in Avrahami et al. (2024) that the sharp scapular spine is instead a synapomorphy of Thescelosauridae shared with the elasmarian *Trinisaura*. The third proposed Orodrominae synapomorphy is character 242:1. We correct the

Brown et al. (2013) assessment, and note the pubis articulates directly to the centrum of sacral vertebrae two and three in a deep ventrolateral socket (242:2). This state change unites orodromines like *Orodromeus*, and the "Kaiparowits Orodromine", other thescelosaurids like *Haya*, *Nanosaurus*, *Oryctodromeus*, but also convergently in *Rhabdodon*. This shows character 242:2 is likely a thescelosaurid synapomorphy, but two alternative articulation morphologies are also manifest in thescelosaurids. *Jeholosaurus* exhibits a pubis which does not articulate with the sacrum, while *Pikunidromeus, Fona,* and *Thescelosaurus neglectus* show pubes which articulate with a sacral rib. Lastly, character 375:1 was proposed in Brown et al. (2013) to unite Orodrominae, but we find it is instead expressed broadly across unrelated SBEDO taxa and is not a valid synapomorphy of Orodrominae.

We confirm the six synapomorphies proposed by Avrahami et al. (2024) uniting Orodrominae: (1) presence of a tall, non-ornamented, caudally projecting boss (horn) on the lateral surface of the jugal (char. 60:3), except for *Akanthodromeus* which exhibits a laterally projecting boss (char. 60:4); (2) jugal with sub-rectangular parallel dorsal and ventral margins (char. 67:1) as shared by *Orodromeus* and *Zephyrosaurus*, but *Pikunidromeus* exhibits a bifurcated anterior maxillary process a morphology shared with *Haya* and convergently with *Heterodontosaurus*; (3) ventral orientation of the basipterygoid process (char. 172:1) a shared trait between *Orodromeus* and *Zephyrosaurus*; (4) cranial dorsal ribs with non-laterally compressed, circular to oval cross-sections along their distal shafts (char. 228:0), uniting *Orodromeus*, *Pikunidromeus*, *Zephyrosaurus*, and convergently *Changmiania*; (5) lack of ischial shaft rotation/twist about its axis (char. 340:0), exhibited by *Orodromeus*, *Pikunidromeus*, and *Zephyrosaurus*; and (6) an angle >120° formed between the tibial and fibular facets on the

calcaneum (char. 383:0), shared between *Orodromeus*, *Albertadromeus*, *Zephyrosaurus*, and the "Kaiparowits Orodromine" but not *Pikunidromeus*.

We propose twelve new Orodrominae synapomorphies: (1) medial surface of jugal exhibits two nutrient foramina for jugal horn (=boss) (char. 413:1), ties *Pikunidromeus*, *Orodromeus*, *Zephyrosaurus*, *Akanthodromeus*, and the "Kaiparowits Orodromine"; (2) bifurcated maxillary jugal ramus, a shared morphology between *Pikunidromeus* [MOR 473], *Orodromeus* [MOR 294], the thescelosaurid *Haya*, and convergently in Heterodontosaurus; (3) foramen pierces the pterygoid wing of the quadrate (char: 423:1), manifested in *Orodromeus* and *Zephyrosaurus*; (4) scapula length to width ratio of 6.0 to 7.3 [MOR 473: 6.12] (char. 257:1), unites *Orodromeus*, *Pikunidromeus*, *Zephyrosaurus*, and the "Kaiparowits Orodromine", but also *Haya*; (5) posterior scapular flange, a shared feature of mature specimens of *Pikunidromeus* [MOR 473 and ROM 64600] and *Orodromeus* [PU 23442 and 23443] but also is scene in one specimen of *Oryctodromeus* [MOR 1642] and convergently in *Hypsilophodon* (Galton, 1975); (6) metacarpal I with obliquely inclined, asymmetric articular condyles is a shared trait between *Orodromeus* and *Pikunidromeus* [MOR 473 and ROM 64600]; (7) terminus of prepubic process striated on its lateral face (char. 414:1) seen in *Orodromeus*, *Pikunidromeus*, an indeterminate orodromine [TMP2008.045.0002], and convergently expressed in *Minimocursor*; (8) terminus of prepubic process enlarged dorsoventrally into large pad (char. 415:1), unites *Orodromeus*, *Pikunidromeus*, and an indeterminate orodromine TMP 2008.045.0002; (9) lateral inflection of the prepubic process occurs medially along the prepubic process's length (char. 417:0), verses *Fona* and *Oryctodromeus* where this process occurs more distally (char. 417:1), (char. 417:0) unites *Pikunidromeus*, and an indeterminate orodromine [TMP2008.045.0002]; (10)

intertrochanteric notch between the lesser and greater trochanters on the femur absent (char. 352:0), this state is shared between *Pikunidromeus*, the "Kaiparowits Orodromine", and *Orodromeus* but arose convergently in *Parksosaurus* and *Gasparinisaura*; (11) fifth metatarsal is "mailbox flag" shaped (char. 419: 2), uniting *Orodromeus*, *Pikunidromeus*, and the "Kaiparowits Orodromine"; (12) deep pit on the ventromedial shaft of P1-1 just proximal to the distal articular condyles (char: 420:1), a shared state between *Orodromeus*, the "Kaiparowits Orodromine", "*Laosaurus minimus*", and *Pikunidromeus*, but also *Jeholosaurus*.

Thescelosaurinae—Avrahami et al. (2024) erected 14 characters as synapomorphies that unite Thescelosaurinae. We confirm these characters with a minor addition. The lateral inflection of the prepubic process denoted as a potential autapomorphy of *Fona* is shared with some specimens of *Oryctodromeus*. In these taxa, the lateral inflection occurs proximate to the pubic body. This lateral inflection is also shared with orodromines, namely *Orodromeus*, *Pikunidromeus*, and an indeterminate orodromine from the Oldman Formation TMP2008.045.002. This lateral inflection in orodromines differs from thescelosaurines in being more medially placed along the length of the prepubic process. As of now, it appears a posteriorly lateral inflection of the prepubic process may be a synapomorphy of early thescelosaurines (char. 417:1), uniting *Fona* and *Oryctodromeus* but is lost in the derived *Thescelosaurus* genus.

Thescelosauridae—Avrahami et al. (2024) proposed thirteen synapomorphies of Thescelosauridae which we confirm. In conjunction with these, we present nine more thescelosaurid synapomorphies: (1) pronounced orbital ridge on anteromedial edge of postorbital ramus of jugal (char: 421:1), shared by *Fona*, *Oryctodromeus*, *Orodromeus*, *Pikunidromeus*,

Akanthodromeus, *Zephyrosaurus*, and the "Kaiparowits Orodromine"; (2) orbital edge of postorbital possesses an anteriorly directed inflation into orbit (char: 94:1), shared between *Fona*, *Oryctodromeus*, *Thescelosaurus neglectus*, *Thescelosaurus assiniboiensis*, *Orodromeus*, *Pikunidromeus*, *Zephyrosaurus*, *Haya*, and *Jeholosaurus*, but not *Changchunsaurus*, also convergently manifested in a handful of unrelated SBEDOs and *Herrerasaurus*; (3) pronounced medial process on the dentary symphysis (char. 424:2), seen in *Thescelosaurus neglectus*, *Thescelosaurus garbanii*, *Haya*, *Orodromeus*, and *Pikunidromeus*; (4) rounded dorsal margin of the ilium in lateral view (char. 308:2), uniting *Haya*, *Orodromeus*, *Pikunidromeus*, *Zephyrosaurus*, *Jeholosaurus*, *Micropachycephalosaurus*, *Changmiania*, and an indeterminate orodromine specimen [TMP 2008.045.0002], but is lost in thescelosaurines which demonstrate flat to sigmoidal dorsal margins; (5) lateral inflection of the prepubic process (char. 416:1), unites *Pikunidromeus*, indeterminate orodromine TMP2008.045.0002, *Fona*, and *Oryctodromeus*; (6) lateral inflection of the ischial shaft into thin blade-like protuberance in the distal third (422:1), unites *Fona*, *Oryctodromeus*, *Thescelosaurus neglectus*, *Haya* *Pikunidromeus*, *Zephyrosaurus*, *Nanosaurus*, *Jeholosaurus* but not *Orodromeus*. This feature is also manifest in a handful of other SBEDOs; (7) lack of an anterior intercondylar groove on distal femur (char. 357: 0), unites non-thescelosaurine thescelosaurids like *Nanosaurus*, *Haya*, *Changchunsaurus*, *Jeholosaurus*, *Koreanosaurus*, *Orodromeus*, *Pikunidromeus*, and the "Kaiparowits Orodromine"; (8) of the lateral proximal condyles of the tibia, the fibular condyle larger than the accessory condyle (char. 368:3), as in *Pikunidromeus*, *Albertadromeus*, *Haya*, *Oryctodromeus*, *Fona*, *Koreanosaurus*, *Changchunsaurus*, and *Jeholosaurus*, but also convergently in *Hypsilophodon* and *Micropachycephalosaurus*; (9) a flange projects from the

fibular shaft along the distal half of the fibular shaft (char. 418: 1), as in *Orodromeus*, *Pikunidromeus*, and *Albertadromeus*, *Fona*, *Oryctodromeus*, *Jeholosaurus*, *Haya*, and *Diluvicursor*.

Discussion

Pikunidromeus ancellae gen. et sp. nov. is an orodromine based on multiple features outlined as synapomorphies of Orodrominae above. *Pikunidromeus* displays a posterolaterally deflected jugal horn (char. 60:3); two nutrient foramina medial to the jugal horn (char. 413:1); cranial dorsal ribs with oval cross-sections along their distal shafts (char. 228:0); striations on the terminus of the prepubic process (char. 414:1); terminus prepubic process enlarged into pad (char. 415:1); lateral inflection of the prepubic process medially placed (char. 417:0); lack of ischial shaft rotation/twist about their axis (char. 340:0); intertrochanteric notch between the lesser and greater trochanters on the femur absent (char. 352:0); fifth metatarsal is “mailbox flag” shaped (char. 419: 2); and a deep pit on the ventromedial shaft of P1-1 just proximal to the distal articular condyles (char: 420:1). *Pikunidromeus* is distinguished from other orodromines by a plethora of autapomorphies. The jugal horns of orodromines are very distinctive and show a wide breadth of variation between taxa. *Pikunidromeus* differs by displaying a small, triangular, posterolaterally deflected jugal horn core on the lateral face of the jugal. The maxillary process of the jugal is bifurcated anteriorly. There is a potential hypapophysis on the ventral keel of cervical vertebrae four. The tuberculum and capitulum of the dorsal ribs transition from a vertical to near horizontal angled articulation between dorsal vertebrae six and eight. *Pikunidromeus* demonstrates a posterior scapular flange on the scapula. The manus shows a metacarpal I with asymmetric distal articular condyles. The femora of *Pikunidromeus* notably exhibits a medial

condyle inflated and partially invading the posterior intercondylar sulcus. The angle between the articular facets of the tibia and fibula on the calcaneum is less than 120 degrees.

Orodromine paleobiogeography

Pikunidromeus adds to a growing list of orodromine occurrences clustered in northern Laramidia. In addition to taxa like *Orodromeus* (Scheetz, 1999), *Albertadromeus* (Brown et al., 2013), *Akanthodromeus* (Chapter 2), coupled with informal taxa [the "Kaiparowits Orodromine" and the "BV Orodromine"] indeterminate specimens in the Oldman, Dinosaur Park, and Prince Creek Formations (Brown et al., 2013; Druckenmiller et al., 2021), and the potentially dubious *Laosaurus minimus* (Gilmore, 1924), all demonstrate orodromine diversity peaked during a specific transgressive/regressive phase of the WICS during the Campanian. Northern Laramidia appears to be the nexus for this pulse of orodromine diversity with only one southern orodromine taxon, the "Kaiparowits Orodromine". Whether this northern distribution is real, or a product of collection or researcher sampling biases is uncertain. For now, we assume that this northern concentration of taxa is true, along with the temporal constraints of the group. *Pikunidromeus* is the youngest orodromine in the Two Medicine-Judith River-Belly River clastic wedge, occurs in multiple formations, and reinforces orodromines as a group did not survive the Bearpaw Sea transgression/regression (B9) outside of a lingering population in Alaska (Druckenmiller et al., 2021). Furthermore, their replacement by thescelosaurines may have occurred rapidly. The cryptic "Wapiti Thescelosaurid" comes from the Wapiti Formation (Unit 3) roughly correlating to the maximum transgression of the Bearpaw Sea (Hudgins, 2021). Though this thescelosaurid is poorly represented skeletally, the significant size of the largest fibula would be exceptionally large for an orodromine. Its presence at this important interval may hint at rapid replacement of

orodromines by thescelosaurines.

Campanian small-bodied ornithischians coexistence

Small-bodied taxa are often the least represented constituents of Upper Cretaceous formations within the Western Interior Basin of Laramidia (Brown et al., 2013; Horner et al., 2011) which makes any assessments of their diversity and evolutionary history challenging. An overlooked exception to this rule is the considerably large orodromine sample from the Upper Cretaceous Two Medicine Formation, where hundreds of non-tooth specimens are reposited at the Museum of the Rockies. This profusion of orodromine specimens is unprecedented and when these specimens are included in an updated chronostratigraphic framework for the Two Medicine Formation, distinct zones of orodromine morphotypes are revealed. *Pikunidromeus ancellae* only occurs above the lacustrine interval of the Flagg Butte Member in the Upper Two Medicine, while *Orodromeus makelai* is restricted to only the lacustrine interval. The only apparent overlap in orodromine species is confined to a single fossil locality TM-088 (Bob's Vacation Site) between *Pikunidromeus* and the "BV Orodromine". The mysterious orodromine informally designated the "BV Orodromine" is represent only by jugal horns which are distinct from *Orodromeus* and *Pikunidromeus*. An alternative explanation for this overlap is that the BV taxon could represent a dimorphic jugal morph of *Pikunidromeus*; however, this hypothesis is poorly supported. Both taxa see their respective jugal horn morphologies establish early on in ontogeny and not in mature individuals, indicating sexual selection is likely not the driving force facilitating their development. This is further supported by the fact *Pikunidromeus,* and the "BV Orodromine", do not overlap again at any other fossil locality which demonstrates that these taxa are in fact distinct from each other.

Zooming out, a perplexing conundrum is the repeated coexistence of other small-bodied ornithischian groups (neoceratopsians and pachycephalosaurids) with orodromines in the Two Medicine-Judith River-Belly River clastic wedge during the height of orodromine diversity. Orodromines are documented in cooccurrence with neoceratopsians and pachycephalosaurids at fossil sites in specific settings within the Two Medicine Formation: namely coastal floodplain deposits. The neoceratopsian *Cerasinops* and indeterminate orodromine specimen MOR 554 are recovered at the bottom of the Hagans Crossing Member from the fossil locality TM-067, while *Pikunidromeus* specimens from the upper Flag Butte Member in an interval which it shares with two neoceratopsians *Brachyceratops*, *Prenoceratops*, and an indeterminate pachycephalosaurid (Rogers et al., 2025). The coastal cohabitation of these small-bodied ornithischians is corroborated in coastal intervals of neighboring formations within the clastic wedge. In the Judith River Formation, *Akanthodromeus* is coeval with *Colepiocephale* in the lower McClelland Ferry Member. In the Dinosaur Park Formation, *Pikunidromeus* and other indeterminate orodromine specimens (Brown et al., 2013; Hudgins, 2021) overlap with the neoceratopsian *Unescoceratops* and the pachycephalosaurids *Stegoceras validum*, *Sphaerotholus lyonsi*, and *Foraminacephale*.

Niche differentiation is a potential explanation for the coexistence of so many small-bodied ornithischians, but few studies have attempted to tackle this problem. A single assessment of the dentition of pachycephalosaurid *Stegoceras validum* and the thescelosaurine *Thescelosaurus neglectus* endeavored to investigate how pachycephalosaurids and thescelosaurids avoided mutual competition. This comparative analysis shows *Thescelosaurus neglectus* was likely a selective browser while *Stegoceras validum* was a more indiscriminate

forager (Hudgins et al., 2022). Whether these results are applicable more broadly to orodromines is uncertain, not to mention a full accounting of leptoceratopsian dietary preferences has never been undertaken. Further examinations of the strategies employed by these small-bodied ornithischian groups to coexist in these Late Cretaceous environments need to be further explored and may shed light on the disappearance of orodromines after the Bearpaw transgression and the persistence of neoceratopsians and pachycephalosaurids into the Latest Cretaceous.

Conclusion

All orodromine specimens collected in the Two Medicine and Judith River Formations over the past forty years had been assigned to the monospecific genus *Orodromeus makelai* (Scheetz, 1999; Wolfe and Horner, 2003). A review of this skeletal assemblage reveals distinct taxonomic divisions, first in *Akanthodromeus judithi* (Chapter 2), and now in *Pikunidromeus ancellae* gen. et sp. nov. Within an updated chronostratigraphic framework (Rogers et al., 2025), these divisions limit *Orodromeus makelai* to only the "lacustrine interval" of the Two Medicine Formation. Furthermore, indeterminate orodromine specimens in the Hagens Crossing Member, the "BV Orodromine", and the potentially dubius *Laosaurus minimus* (Gilmore, 1924) show an unrealized rapid increase in diversity which raises questions about why the Bearpaw (T9) transgressive and (R9) regressive phase was so conducive to the rapid diversification of this clade, and how so many small-bodied ornithischians cohabitated in the Two Medicine-Judith River-Belly River clastic wedge.

Acknowledgments

This research was conducted as partial fulfillment of Z. J. H.'s Masters degree at Montana State University in Bozeman, MT. We are eternally grateful to the Blackfeet Nation for permission to the MOR to collect fossil specimens from tribal lands, and thanks to the Bureau of Indian Affairs for granting collection permits. Specimen access was granted by J. Scannella and E. Metz at the MOR, C. Brown and B. Strilisky at the TMP, and D. Evans, S. Sugimoto, and I. Morrison at the ROM. Thanks to J. Horner his patience and willingness to answer the never-ending emails sent by Z. J. H. Special thanks to C. Organ and E. Bender for their assistance in trouble shooting errors with time-tree scripts as they arose. Research was supported by the generous funding of the Jurassic Foundation and by the Geological Society of America through a Graduate Student Geoscience Grant. Discussions with H. Avrahami, C. Brown, L. J. Krumenacker, R. Scheetz, and J. Scannella greatly enhanced the quality of this paper. Thanks to S. Hannebaum for reviewing drafts of this manuscript. Special thanks to the editors for their feedback and corrections which greatly improved the scholarship of this research.

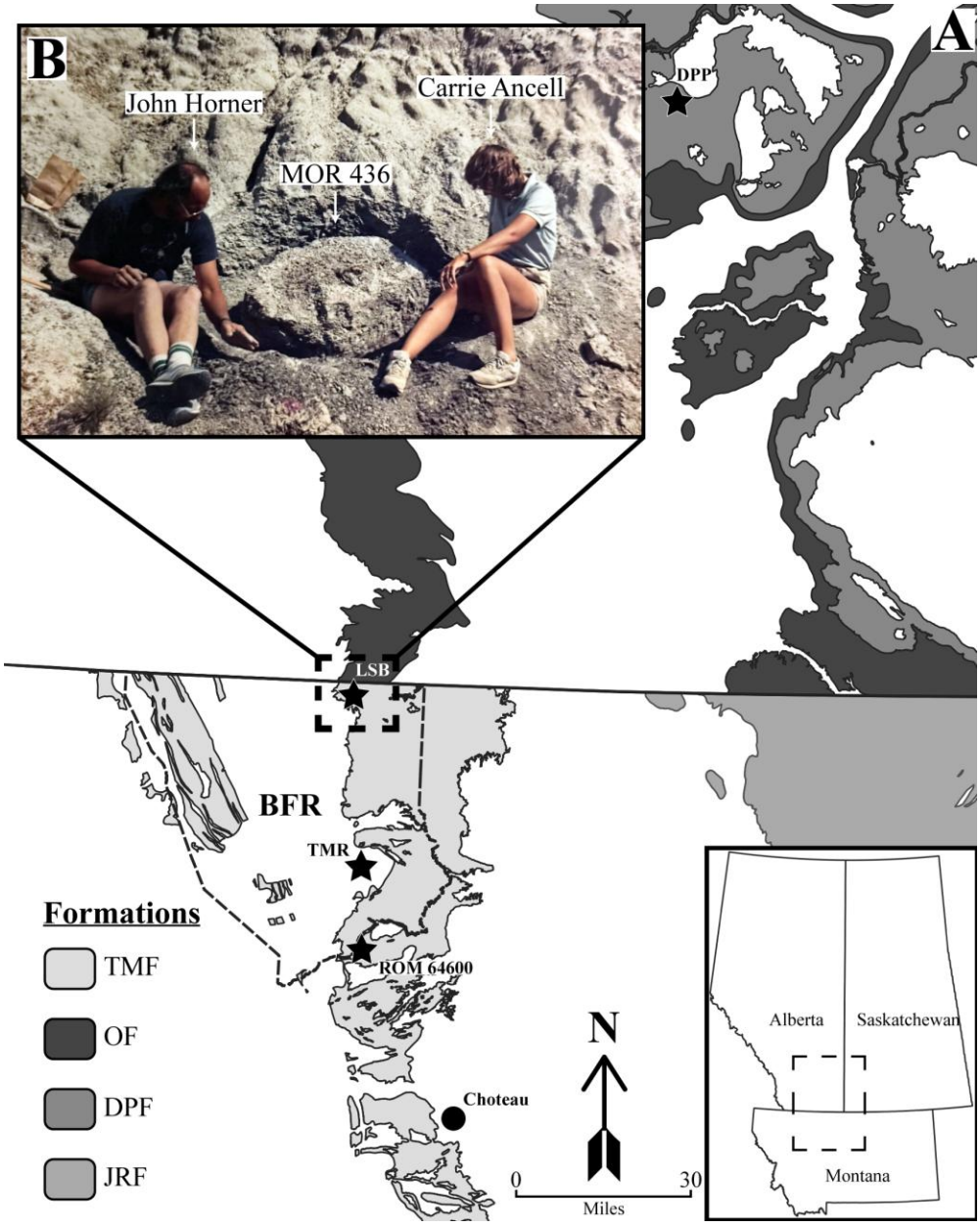


Figure 1. Geographic map of *Pikunidromeus* ancellae localities. (A) Regional geological formations with fossil localities symbolized by stars. Blackfeet Reservation outlined with a dashed border. Geological formation abbreviations: **DFP**, Dinosaur Park Formation; **JRF**, Judith River Formation; **OF**, Oldman Formation; **TMF**, Two Medicine Formation. *Pikunidromeus* fossil locality abbreviations: **DPP**, Dinosaur Provincial Park; **LSB**, Landslide Butte Field Area; and **TMR**, Two Medicine River Field Area. (B) Photograph of Carrie Ancell and John Horner near TM-019 during the collection of referred specimen MOR 436. Quarry image provided by Museum of the Rockies. [Planned for column width]

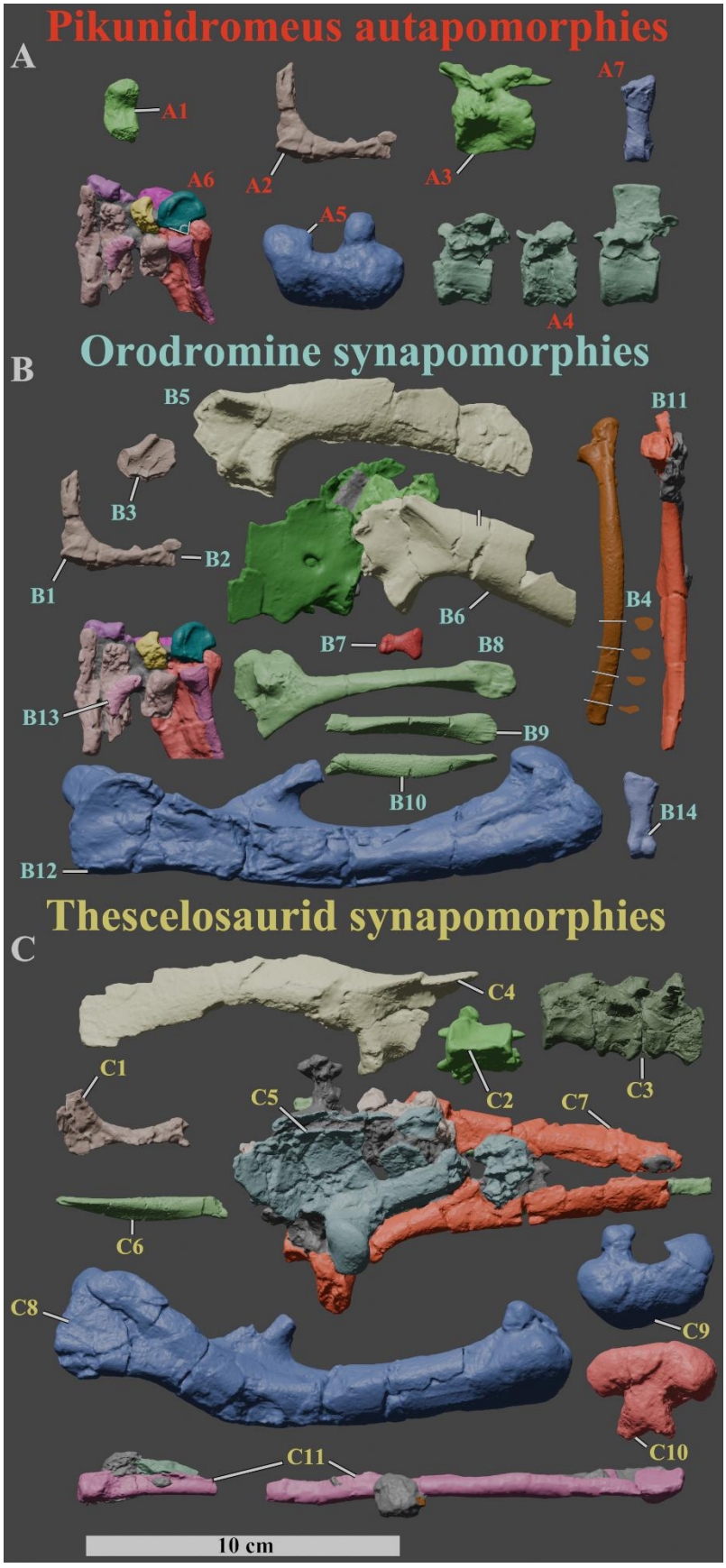

Pikunidromeus autapomorphies
A
A1
A2
A3
A4
A5
A6
A7
Orodromine synapomorphies
B
B1
B2
B3
B4
B5
B6
B7
B8
B9
B10
B11
B12
B13
B14
Thescelosaurid synapomorphies
C
C1
C2
C3
C4
C5
C6
C7
C8
C9
C10
C11
10 cm

Figure 2. *Pikunidromeus* diagnostic features. Figure rendered without texture. (A) *Pikunidromeus* autapomorphies. (A1) lack of transvers dorsal groove on atlantal intercentrum; (2) small, triangular, posterolaterally deflected jugal horn core; (A3) hypapophysis on ventral keel of cervical vertebrae four; (A4) transition of dorsal ribs from vertical to near horizontal articulation occurs between dorsal vertebrae six and eight; (A5) medial condyle of femur inflated and partially invading the posterior intercondylar sulcus on distal femur; (A6) an angle <120° formed between the tibial and fibular facets on the calcaneum; (7) averaged length/width ratio PI-I is 4.15. (B) Orodromine synapomorphies. (B1) presence of a jugal horn core; (B2) bifurcated maxillary ramus of the jugal; (B3) two nutrient foramen on the medial wall of the jugal; (B4) anterior dorsal rib sub-oval in cross section distally; (B5) length of scapula blade to minimum width shows a ratio between 6.0 and 7.3; (B6) posterior scapular flange; (B7) metacarpal I shows obliquely inclined, asymmetric distal condyles; (B8) anteriorly the prepubic process dorsoventrally expands it a large pad; (B9) anteroposteriorly trending striations on anterior terminus of prepubic process; (B10) prepubic process lateral inflection medially placed; (B11) lack of twist in the ischial shaft; (B12) no intertrochanteric notch; (B13) “mailbox flag” shaped metatarsal V; (B14) deep pit on the ventromedial shaft of P1-1 just proximal to the distal articular condyles. (C) Thescelosaurid synapomorphies. (C1) orbital rim on anterior margin of postorbital ramus of jugal; (C2) ventral keel on cervical vertebrae; (C3) location of the first chevron is on the distal end of the second caudal vertebra rather than the first; (C4) sharp scapular spine; (C5) rounded dorsal margin of the ilium in lateral view; (C6) laterally inflection of the prepubic process; (C7) lateral inflection of the ischial shaft into thin blade-like protuberance in the distal third; (C8) cranial expansion of the greater trochanter; (C9) no anterior intercondylar groove on distal femur; (C10) fibular condyle is larger than accessory condyle on tibia; (C11) a flange projects from the fibular shaft along the distal half of the fibula. Gray represents matrix in figure. [Planned for column width]

Table 1.1. Measurements for figured *Pikunidromeus* vertebrae (cm.).

Specimen	Vertebra type	# in series	Le(A/P)	Wc(M/L)	Hc(D/V)
MOR 473	Atlantal intercentrum	1	1.06	2.07	0.53
	Odontoid process	2	1.18	2.04	0.86
	Axis	2	2.63	-	1.27
	Cervical	3	2.66	1.26	1.56
		4	2.51	2.08	1.51
		5	2.4	2.15	1.63
		6	2.23	1.99	1.64
		7	2.24	2.1	1.64
		8	2.12	2.17	1.88
		9	2.22	1.99	1.73
	Dorsal	1	2.15	1.59	1.5
		2	2.12	1.6	1.64
		3	2.12	1.56	1.59
		4	2.42	1.62	1.47
		5	2.19	1.44	1.55
		6	2.08	1.62	1.52
		7	1.98	1.68	1.85
		8	1.98	1.71	1.54
		9	2	1.69	1.68
		10	2.11	1.76	1.68
		11	2.09	1.8	1.76
		12	2.14	1.87	1.89
		13	2.18	1.9	1.94
		14	2.27	2.21	2.03
	Sacral	1	2.32	2.36	2.01
		2	2.96	2.95	2.01
		3	2.14	2.53	1.58
		4	1.95	2.01	1.84
		5	2.07	1.97	1.83
		6	2.09	1.72	1.9
		7	2.09	2.14	1.77
	Caudal	1	1.94	1.9	1.81
		2	1.74	1.57	2.04
		3	2.11	1.67	1.91
		?	2.05	1.47	1.9
		?	2.22	1.25	1.88
		?	1.99	1.41	1.96
		?	1.66	1.55	2.27
	Distal caudal	?	1.96	1.17	1.3

Table 1.1 Continued.

Specimen	Vertebra type	# in series	Le(A/P)	Wc(M/L)	Hc(D/V)
ROM 64600	Anterior Caudal	?	1.86	2.13	1.89
	Caudal block 1	1	-	-	-
		2	-	-	-
		3	2.26	-	-
		4	2.32	-	-
		5	2.38	-	-
		6	2.51	-	1.65
		7	2.23	-	-
		8	2.23	-	1.49
		9	2.22	-	-
		10	2.18	-	1.52
		11	2.16	-	1.55
	Caudal block 2	1	2.21	-	1.52
		2	2.21	-	1.38
		3	2.18	-	1.38
		4	2.17	-	1.28
		5	2.14	-	1.29
		6	2.05	-	1.16
		7	2.11	-	1.16
		8	2.04	-	-
		9	2.03	0.72	1.09
	Isolated caudal	1	2.29	-	1.4

Table 1.2. Forelimb measurements (cm.).

Specimen	Element	L/R	Le(D/P)	Wp(M/L)	Wp(A/P)	Wd(M/L)	Wd(A/P)
MOR 473	Scapula	L	10.93	1.42	**3.91**	0.41	-
	Humerus	L	10.64	3.69	1.41	2.06	1.57
	Coracoid	L	5.41	1.29	-	0.3	-
	Ulna	L	8.13	1.34	1.93	0.68	1.42
	Radius	L	-	0.89	1.59	1.35	0.95
	Carpal 1	L	0.25	0.56	0.64	0.68	0.89
	Carpal 2	L	0.24	0.24	0.33	0.23	0.26
	Carpal 3	L	0.66	0.57	0.69	0.54	0.64
	Carpal 4	L	0.51	0.47	0.89	-	-
	Metacarpal 1	L	1.42	0.52	1.03	4.53	0.68
	Phalange 1	L	0.78	0.53	0.48	0.41	0.44
	Phalange 2	L	0.87	0.37	0.54	-	-
	Metacarpal II	L	1.69	0.6	0.83	0.47	0.67
	Phalange I	L	-	0.56	0.67	-	-
	Phalange II	L	0.61	0.477	0.55	0.31	0.52
	Digit III Phalange II	L	0.45	0.42	0.47	0.29	0.43
	Phalange III	L	0.4	33	0.42	0.24	0.4
	Metacarpal IV	L	**0.78+0.52**	0.38	0.53	0.41	0.57
	Phalange I	L	0.56	0.35	0.58	0.31	0.45
	Phalange II	L	0.56	0.34	0.46	0.26	0.36
	Phalange III	L	**0.55**	0.23	0.34	-	-
	Digit V Phalange II	L	0.47	0.34	0.53	0.3	0.49
	Scapula	R	12.96	1.43	5.08	0.43	-
	Humerus	R	10.46	3.25	1.51	2.04	1.54
	Corocoid	R	5.52	1.82	-	0.34	-
	Ulna	R	-	1.26	1.99	0.78	1.41
	Radius	R	-	-	-	1.04	1.3

Table 1.2 Continued.

Specimen	Element	L/R	Le(D/P)	Wp(M/L)	Wp(A/P)	Wd(M/L)	Wd(A/P)
ROM 64600	Scapula	L	-	0.93	**3.79**	-	-
	Humerus	L	**8.25**	-	-	1.92	1.49
	Coracoid	L	-	-	-	-	-
	Ulna	L	**6.17**	-	-	1.7	0.47
	Radius	L	**6.56**	-	-	1.42	0.8
	Metacarpal I	L	1.49	0.68	0.94	0.69	0.56
	Metacarpal II	?	-	-	-	-	0.74
	Phalange #?	?	-	-	-	0.68	0.56
	Phalange #?	?	0.72	0.52	0.63	0.32	0.54
	Phalange #?	?	-	0.61	0.73	-	-
	Scapula	R	-	1.04	**4.46**	-	-
	Humerus	R	11.54	-	2.69	1.42	1.79
	Coracoid	R	-	1.02	-	-	-
ROM 64601	Coracoid	R	-	0.79	-	-	-
MOR 436	Humerus	L	**6.42**	-	-	1.18	1.04
	Ulna	L	5.82	0.74	1.35	0.44	1.08
	Radius	L	5.91	0.67	0.9	0.66	0.85

Table 1.3. Pelvic measurements (cm.).

Specimen	Element	L/R	Le(A/P)	Wp(M/L)	Wp(D/V)	Wd(M/L)	Wd(D/V)
MOR 473	Prepubic process	L	**6.58**	0.32	0.97	0.55	0.91
	Ischium	L	**12.33**	0.57	3.97	-	-
	Prepubic process	R	**5.5**	0.31	1.01	-	-
ROM64600	Postacetabular Ilium	R	**6.17**	0.49	3.21	-	1.71
	Prepubic process	R	6.24	0.27	1.07	0.54	1.01
	Ischium	R	**10.89**	0.43	**4.04**	-	-

Table 1.4. Hindlimb measurements (cm.).

Specimen	Element	L/R	Le(D/V)	Wp(M/L)	Wp(A/P)	Wd(M/L)	Wd(A/P)
MOR 473	Femur	L	16.59	3.38	3.85	4.44	3.37
	Tibia	L	21.46	3.46	4.24	-	4.15
	Fibula	L	**5.43 + 6.27 + 8.33**	1.08	2.45	-	1.32
	Metatarsal I	L	**1.62**	-	-	1.06	0.79
	Phalange I	L	2.8	1.16	1.11	0.95	0.82
	Metatarsal II	L					
	Metatarsal III	L					
	Metatarsal IV	L					
	Metatarsal V	L	2.09	0.69	-	1.35	-
	Femur	R	17.72	3.62	**3.35**	4.49	3.08
	Tibia	R	20.03	3.35	4.37	2.15	4.13
	Fibula	R	**8.9**	1.06	2.37	-	-
	Digit I-Phalange II	R	1.98	0.76	0.72	-	-
	Metatarsal II	R	**1.78**	-	-	1.36	1.23
	Phalange II	R	2.32	1.47	1.28	0.95	0.92
	Phalange III	R	2.69	0.92	0.9	-	-
	Metatarsal III	R	**3.82**	-	-	1.82	1.35
	Phalange I	R	2.97	1.96	1.59	1.72	1.19
	Phalange II	R	2.73	1.27	1.23	1.29	0.98
	Phalange III	R	2.05	1.41	1.26	1.07	0.91
	Phalange IV	R	3.14	1.07	0.96	-	-
	Metatarsal IV	R	3.2	-	-	1.22	1.3
	Phalange I	R	2.11	1.38	1.33	1.1	1.27
	Phalange II	R	1.56	1.11	1.47	1.08	1.1
	Phalange III	R	1.59	1.01	1.13	0.8	0.95
	Phalange IV	R	1.33	0.97	1	0.84	0.91
	Phalange V	R	**1.86**	0.86	0.78	-	-

Table 1.4 Continued.

Specimen	Element	L/R	Le(D/V)	Wp(M/L)	Wp(A/P)	Wd(M/L)	Wd(A/P)
ROM 64600	Femur	L	17.29	2.99	3.8	2.38	2.39
	Tibia	L	21.67	2.56	4.94	3.83	2.11
	Fibula	L	**13.43 + 4.48**	1.04	2.28	0.86	1.42
	Metatarsal I	L	-	-	-	0.87	0.99
	Metatarsal III	L	-	-	-	1.77	1.45
	Femur	R	18.49	2.91	3.79	3.62	1.82
	Tibia	R	21.02	2.07	4.75	3.85	2.37
	Fibula	R	18.95	0.69	2.73	0.9	-
	Metatarsal I	R	5.75	-	0.88	1.03	0.93
	Phalange I	R	2.91	1.22	1.19	0.96	-
	Metatarsal II	R	-	-	-	1.34	1.42
	Phalange I	R	3.77	1.36	1.65	1.28	1.37
	Phalange II	R	2.17	1.34	1.54	1.12	1.02
	Phalange III	R	**2.59**	1.11	0.95	-	-
	Metatarsal III	R	-	-	-	1.75	1.31
	Phalange I	R	3.11	1.85	1.51	1.52	1.28
	Phalange II	R	2.57	1.6	1.41	-	-
	Phalange III	R	2.03	-	-	-	-
	Phalange IV	R	3.41	1.2	1.02	-	-
	Metatarsal IV	R	**7.46**	-	-	1.4	1.83
	Phalange I	R	2.01	1.32	1.44	1.21	1.11
	Phalange II	R	1.7	1.25	-	1.14	1.12
	Phalange III	R	1.53	1.23	-	-	-
	Phalange IV	R	1.33	1.1	1.24	1.05	0.86
	Phalange V	R	2.47	1.01	0.91	-	-

Table 1.4 Continued.

Specimen	Element	L/R	Le(D/V)	Wp(M/L)	Wp(A/P)	Wd(M/L)	Wd(A/P)
ROM 64601	Femur	L	-	-	2.72	3.21	-
	Metatarsal I	L	-	-	-	0.96	0.79
	DigitII.Phalange I	R	-	-	-	0.82	0.8
	Metatarsal III	R	-	-	-	1.32	0.99
	DigitIV.Phalange I	R	1.4	1.05	0.9	-	0.79
MOR 436	Femur	L	11.8	2.19	2.43	2.42	-
	Tibia	L	**11.5**	-	2.8	-	-
	Metatarsal I	L	**1.94**	-	-	0.89	0.88
	Phalange I	L	1.99	0.81	0.63	0.71	0.61
	Phalange II	L	**0.95**	-	-	-	-
	Metatarsal II	L	6.01	0.58	1.81	0.89	1.01
	Phalange I	L	2.11	0.83	1.05	0.88	0.82
	Phalange II	L	1.59	0.86	0.91	0.85	0.64
	Metatarsal III	L	6.77	0.79	1.22	1.03	0.87
	Phalange I	L	2.19	1.38	0.94	1.09	0.86
	Phalange II	L	1.72	1.04	0.89	1	7.62
	Phalange III	L	1.4	0.96	0.81	0.86	0.61
	Phalange IV	L	**1.56**	0.71	0.61	-	-
	Metatarsal IV	L	**3.35**	0.84	1.02	-	-
	Phalange I	L	1.37	1.1	0.98	0.86	0.8
	Phalange II	L	**1.24**	0.98	0.86	-	-
	Phalange III	L	1.2	0.89	0.91	0.78	0.73
	Phalange V	L	1.47	0.62	0.56	-	-
	Femur	R	12.2	-	-	1.98	-
	Tibia	R	**12.01**	-	-	-	-

Table 1.4 Continued.

Specimen	Element	L/R	Le(D/V)	Wp(M/L)	Wp(A/P)	Wd(M/L)	Wd(A/P)
MOR 530	Femur	L	-	-	-	3.58	2.37
	Tibia	L	-	-	-	3.49	-
	Fibula	L	-	-	-	1.17	0.54
	Tibia	R	-	-	-	3.36	1.71
	Fibula	R	-	-	-	1.01	-
	Metatarsal I	R	4.23	0.27	0.69	-	0.78
	Phalange I	R	2.13	-	0.94	0.75	0.59
	Metatarsal II	R	-	1.03	1.93	-	-
	Metatarsal III	R	7.57	-	1.68	1.46	1.22
	Metatarsal IV	R	6.39	1.26	1.33	-	-
	Phalange I	R	-	-	-	1.44	1.46
MOR 10925	Femur	R	8.7	-	-	-	-
MOR 10927	Femur	R	7.39	1.73	1.27	1.79	1.16
TMP1998.093.0014	Femur	R	13.19	-	-	3.08	-
TMP1997.080.0003	Femur	R	-	-	-	3.34	2.75

Table 2.1. Informal thescelosaurid taxa.

Informal taxon name	Formation	Member/section	Stage	Temporal Range
Landslide Butte Orodromine (=Pikunidromeus)	Two Medicine	Flag Butte	Campanian	75.25-76.25 Ma
BV Orodromine	Two Medicine	Flag Butte	Campanian	76.25 Ma
Judith River Orodromine (=Akanthodromeus)	Judith River	McClelland Ferry Member	Campanian	~77.9-78.59 Ma
Kaiparowits Orodromine	Kaiparowits	Lower, Middle	Campanian	~75.42-77.29 Ma
Wapiti Thescelosaurid	Wapiti	Unit 3	Campanian	73.6 Ma

Table 2.2. Indeterminate specimens of significance.

Indeterminate specimens	Formation	Member/section	Stage	Temporal Range
TMP2008.045.0004	Oldman	Lower	Campanian	~77.0-77.5 Ma
TMP2003.012.0135	Oldman	Upper	Campanian	~76.5 Ma
TMP1995.12.127	Dinosaur Park	-	Campanian	~76.0-76.4 Ma
MOR 554	Two Medicine	Hagans Crossing	Campanian	~79.6-80.16 Ma
Prince Creek thescelosaurids	Prince Creek	-	Campanian	~73.0 Ma

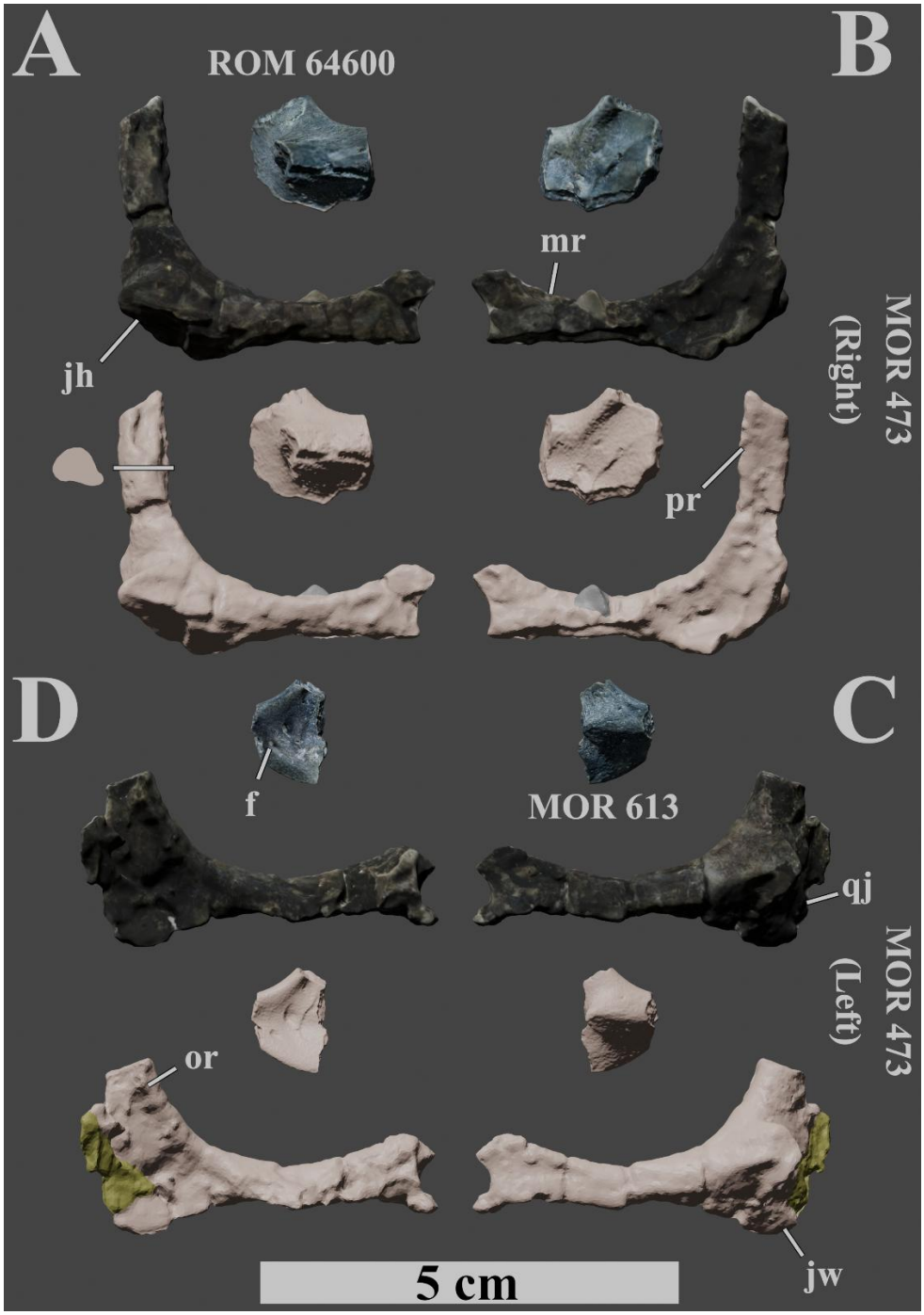


FIGURE 3: *Pikunidromeus* jugal rendered with and without texture. (A) Right jugal of MOR 473 and ROM 64600 in lateral view; (B) right jugal of MOR 473 and ROM 64600 in medial view; (C) left jugal of MOR 473 and right jugal of MOR 613 in lateral view; and (D) left jugal of MOR 473 and right jugal of MOR 613 in medial view. **Abbreviations: jh**, jugal horn; **jw**, jugal wing; **f**, foramen; **mr**, maxillary ramus; **or**, orbital rim; **pr**, postorbital ramus; **qj**, quadratojugal. [Planned for page width]

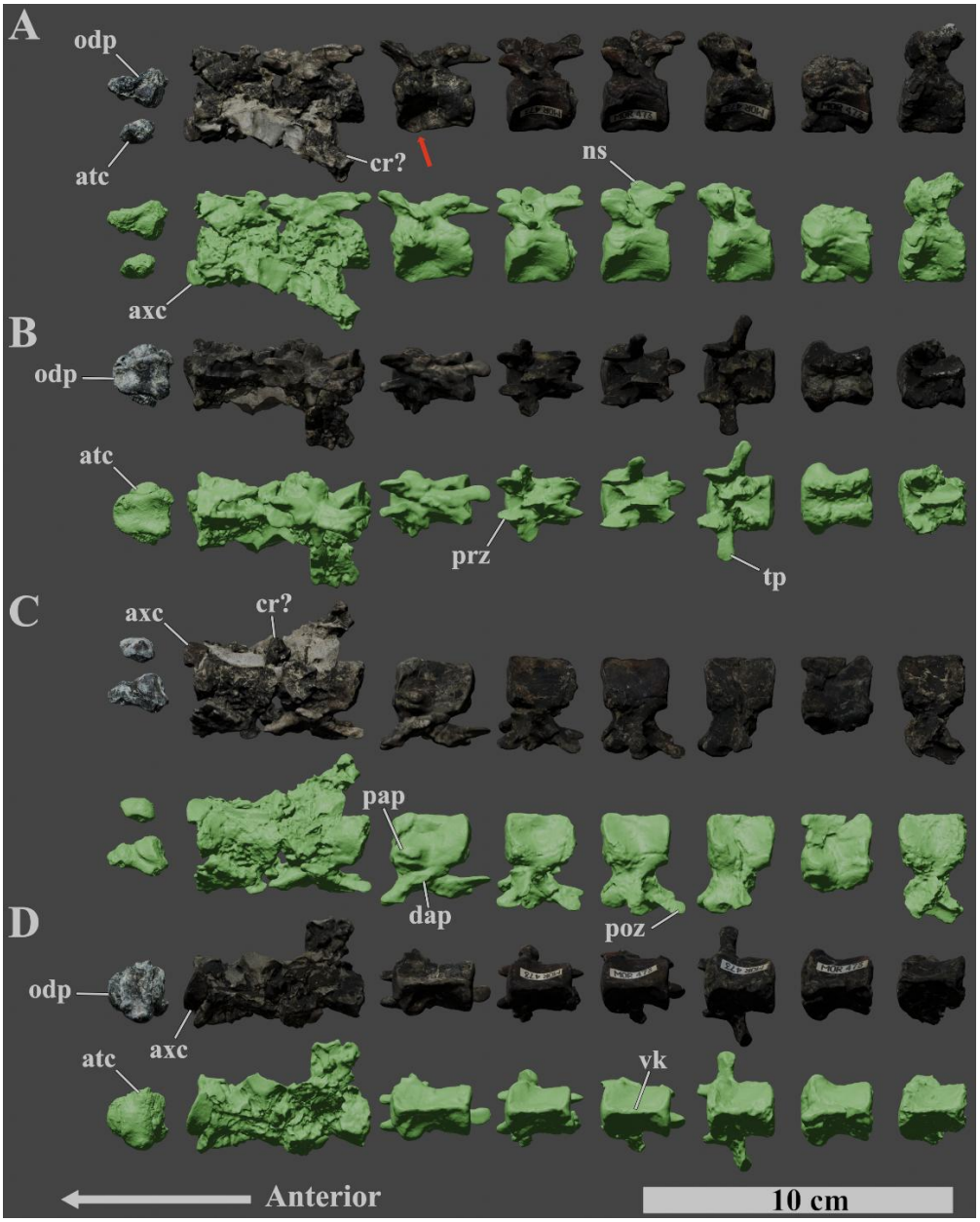


Figure 4. *Pikunidromeus* cervical series [MOR 473] rendered with and without texture. (A) Left lateral view, (B) dorsal view, (C) right lateral view, and (D) ventral view. Red arrow denotes potential hypapophysis-like structure. **Abbreviations: atc**, atlantal intercentrum; **axc**, axis intercentrum; **cr**, cervical rib; **dap**, diapophysis; **ns**, neural spine; **odp**, odontoid process; **pap**, parapophysis; **poz**, postzygapophysis; **prz**, prezygapophysis; **tp**, transverse process; **vk**, ventral keel. [Planned for page width]

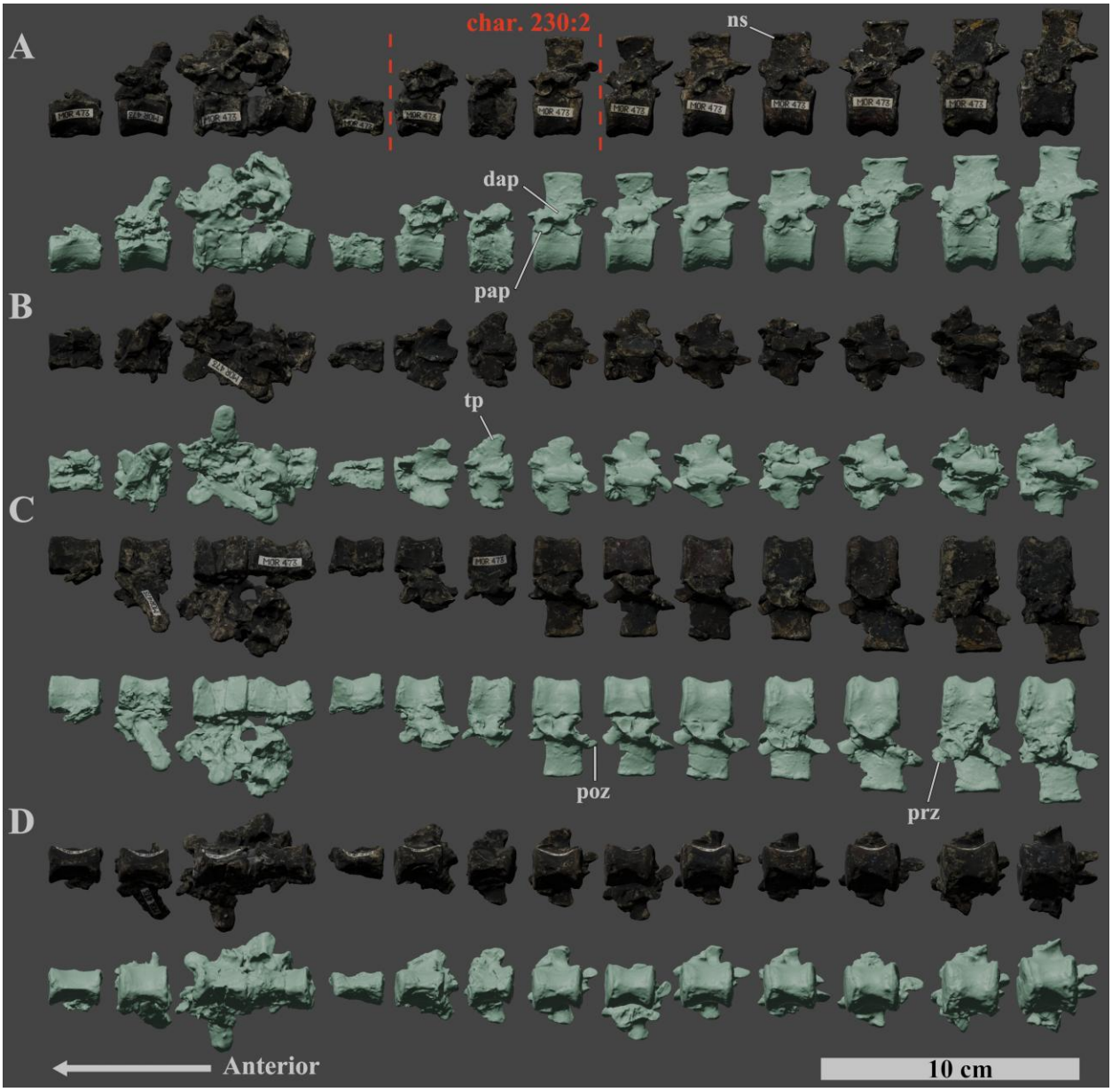


Figure 5. *Pikunidromeus* dorsal series [MOR 473] rendered with and without texture. (A) Left lateral view, (B) dorsal view, (C) right lateral view, and (D) ventral view. **Abbreviations: dap**, diapophysis; **ns**, neural spine; **pap**, parapophysis; **poz**, postzygapophysis; **prz**, prezygapophysis; **tp**, transverse process. [Planned for page width]

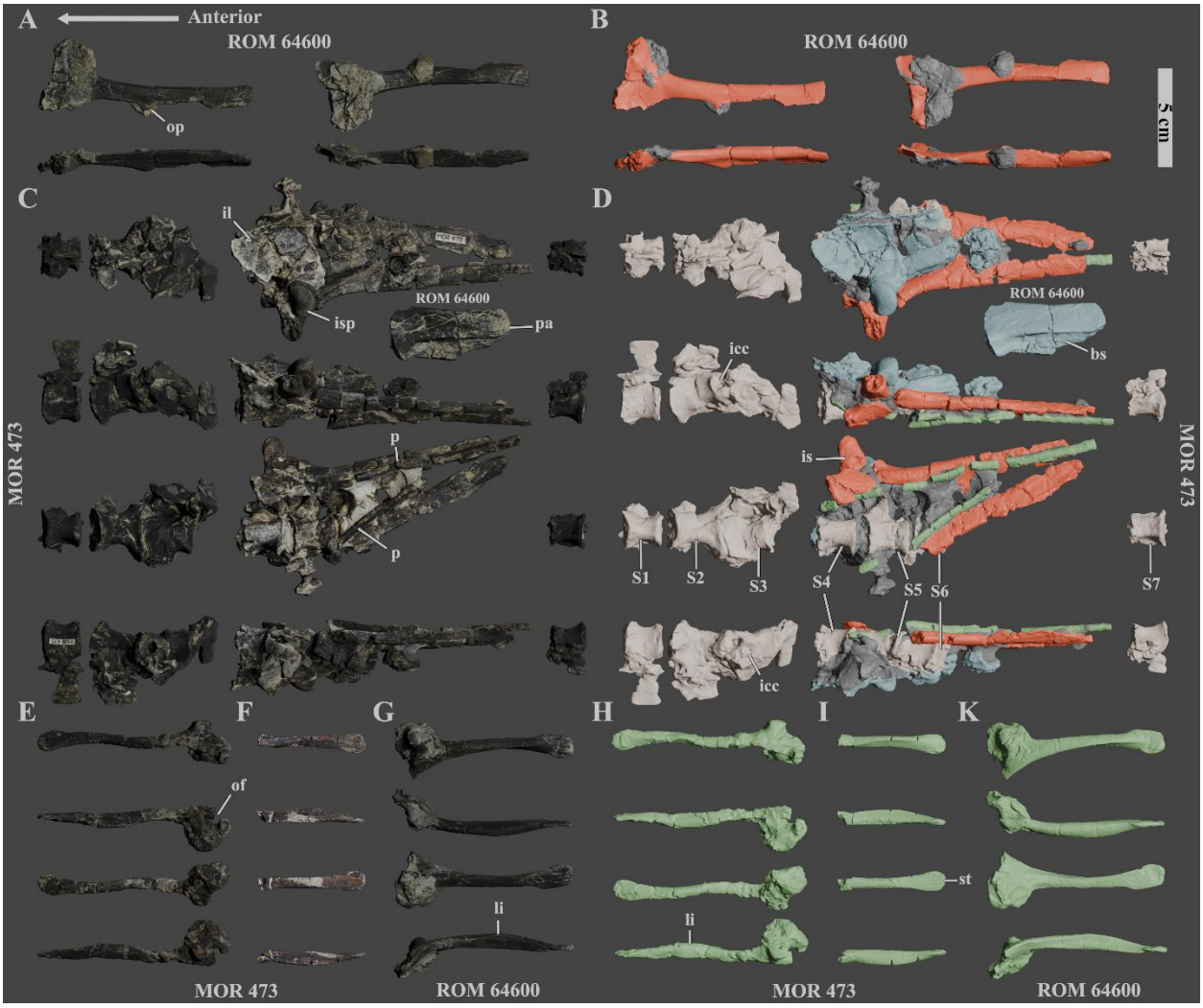


Figure 6. *Pikunidromeus* pelvis and sacral vertebrae rendered with and without texture. (A-B) ROM 64600 right ischium, (C-D) ROM 64600 postacetabular process of ilium and MOR 473 sacral series and pelvic elements, (E-F, H-I) MOR 473 left and right prepubic processes, (G, K) ROM 64600 right prepubic process. Gray represents matrix. **Abbreviations: bs**, brevis shelf; **icc**, intercentrum cavities; **il**, ilium; **is**, ischium; **isp**, ischiac peduncle; **li**, lateral inflection; **of**, obturator foramen; **op**, obturator process; **p**, pubis; **pa**, postacetabular process; **st**, striations; **S#**, sacral vertebra number. [Planned for page width]

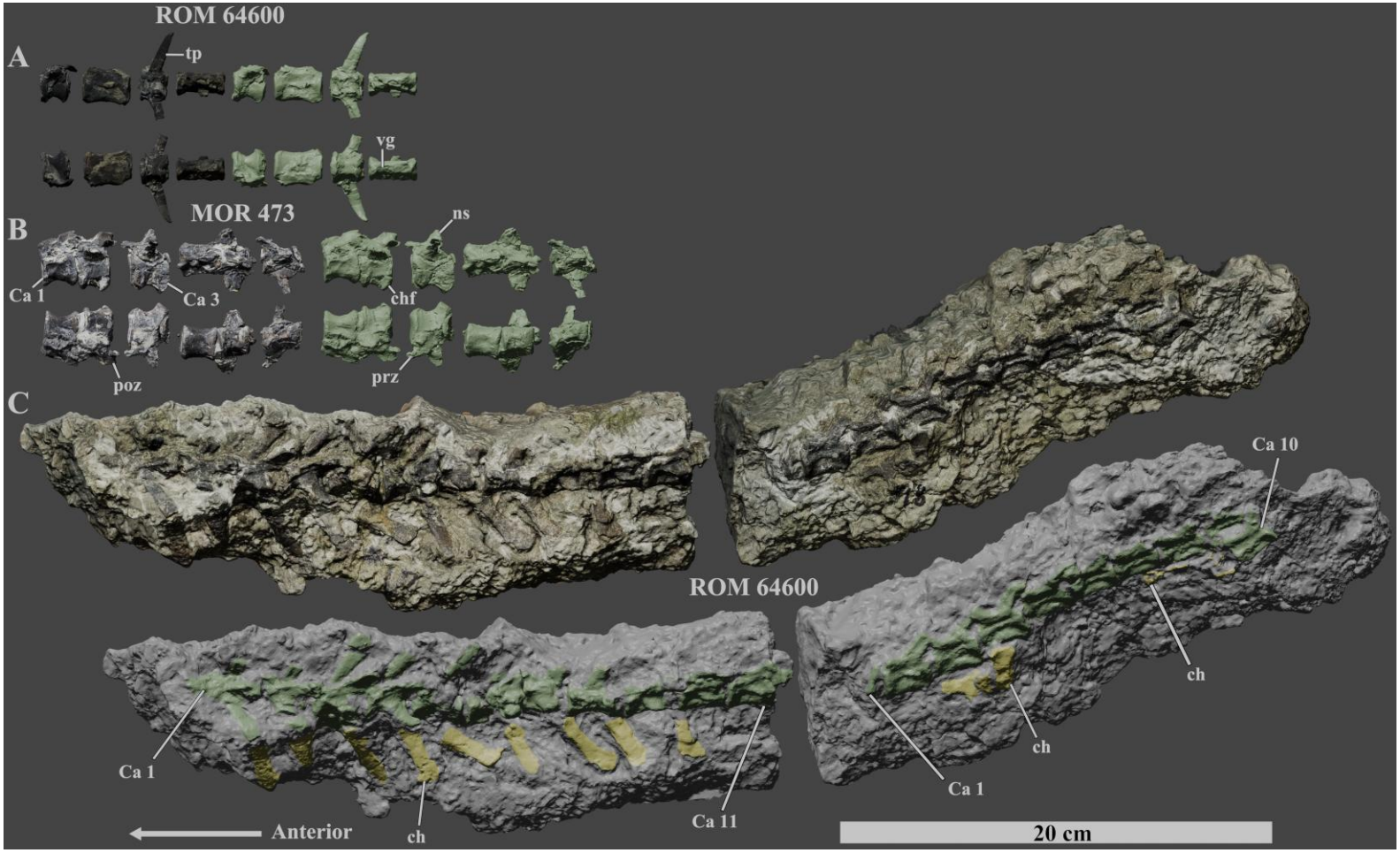


Figure 7. *Pikunidromeus* caudal series rendered with and without texture. (A) ROM 64600 anterior and distal caudal vertebrae of uncertain axial placement, (B) MOR 473 caudal vertebrae 1 through 3, (C) ROM 64600 caudal series in dorsolateral view, series is broken up into two blocks with at least two vertebrae separating them. Gray represents matrix. **Abbreviations: ch**, chevron; **chf**, chevron facet; **ns**, neural spine; **poz**, postzygapophysis; **prz**, prezygapophysis; **tp**, transverse process; **vg**, ventral groove. [Planned for page width]

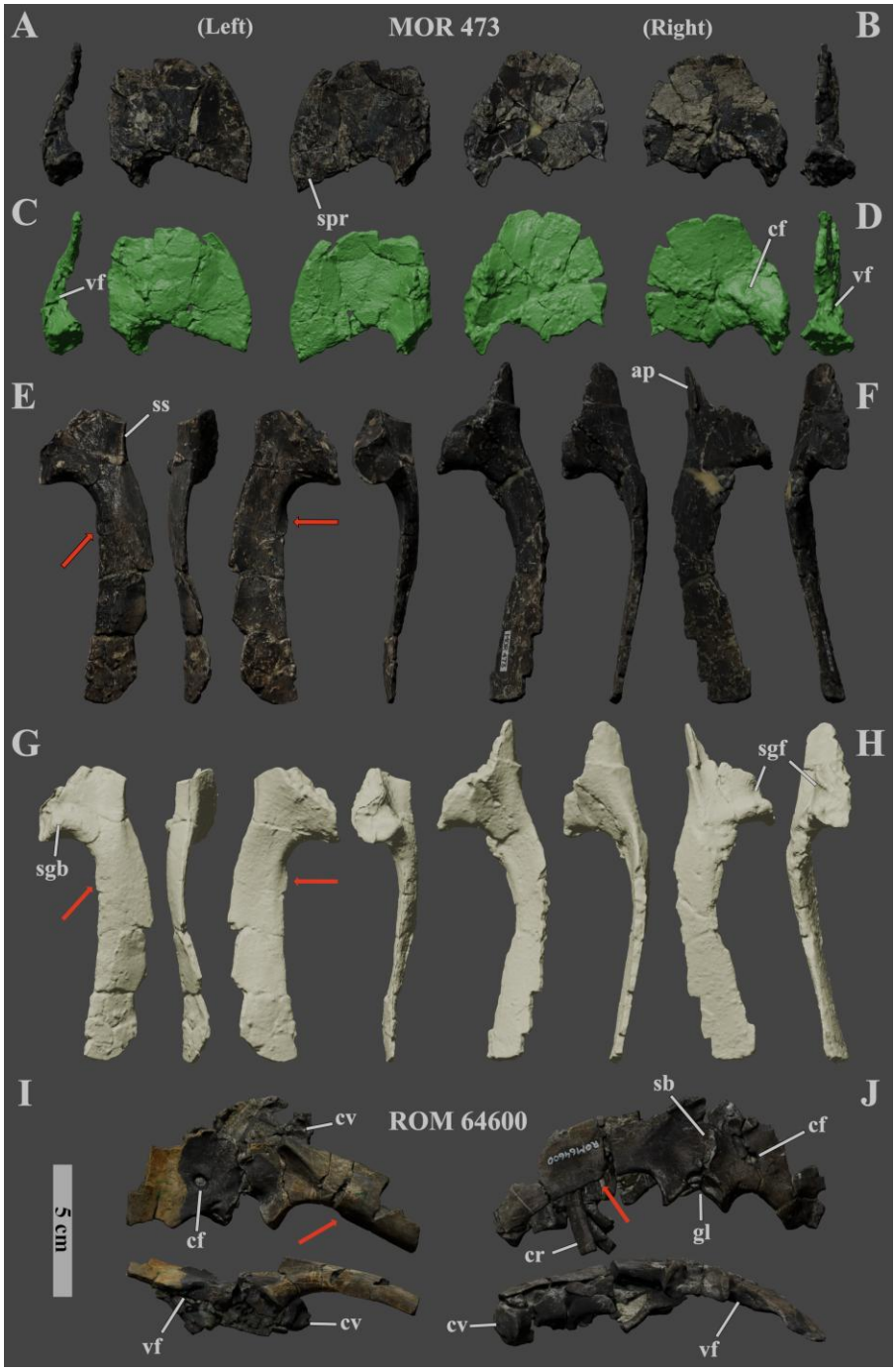


Figure 8. *Pikunidromeus* scapulae and coracoids rendered with and without texture. (A-D) MOR 473 left and right coracoids, (E-H) MOR 473 left and right scapulae, and (I-J) ROM 64600 left and right scapulae and coracoids. Red arrows denote posterior ventral flange of the scapula. **Abbreviations: ap**, acromion process; **cf**, coracoid foramen; **cr**, cervical rib; **cv**, cervical vertebra; **gl**, glenoid fossa; **sb**, supraglenoid boss; **sgb**, supraglenoidal buttress; **sgf**, supraglenoid fossa; **spr**, sternal process; **ss**, scapular spine; **vf**, ventral fossa. [Planned for page width]

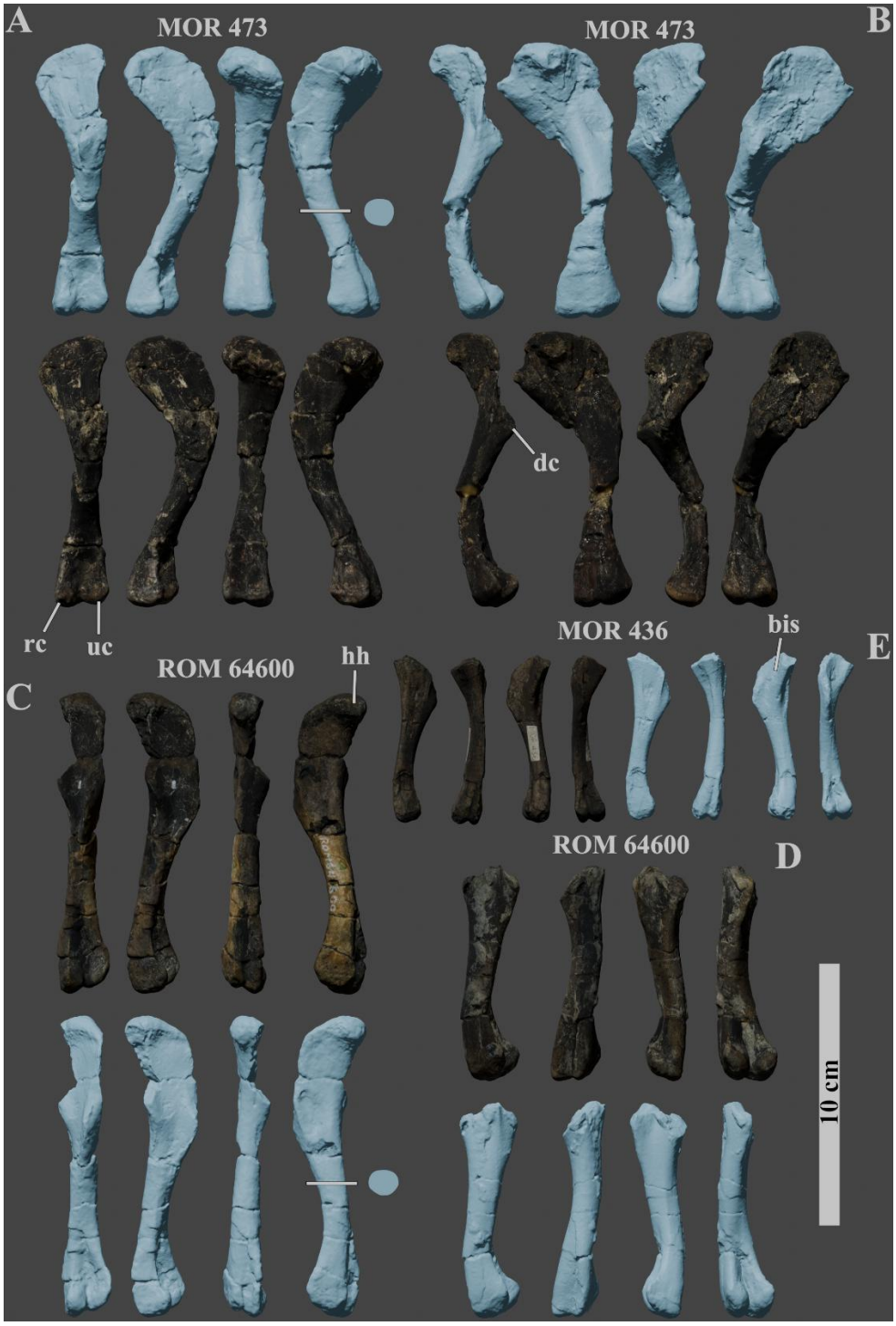


Figure 9. *Pikunidromeus* humeri rendered with and without texture. (A-B) MOR 473 left and right humeri, (C-D) ROM 64600 left and right humeri, and (E) MOR 436 right humerus. **Abbreviations: bis,** bicipital sulcus**; dc**, deltopectoral crest; **hh**, humeral head olecranon process; **rc**, radial condyle; **uc**, ulnar condyle. [Planned for page width]



Figure 10. *Pikunidromeus* forearm. Specimens rendered with and without texture. (A-B) MOR 473 left and right radii and ulnae without texture, (C-D) MOR 473 left and right radii and ulnae with texture, (E) ROM 64600 left radii and ulnae, (F) MOR 436 left radii and ulnae texture, (G) ROM 64600 left radii without texture, and (H) MOR 436 left radii without texture. Gray represents matrix. **Abbreviations: op**, olecranon process; **r**, radius; **u**, ulna. [Planned for page width]

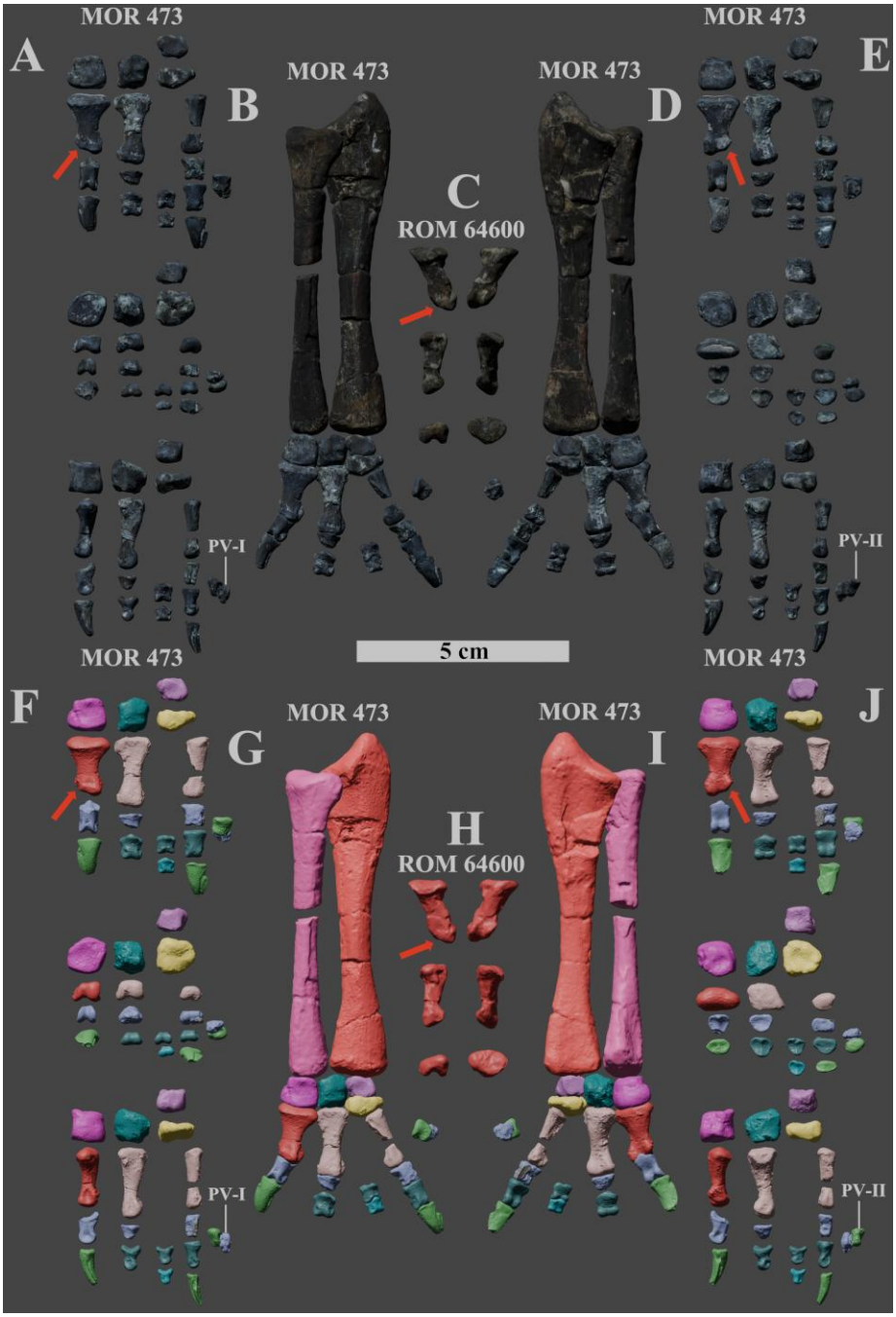


Figure 11. *Pikunidromeus* manus. Skeletal elements rendered with and without texture. (A, E) MOR 473 metacarpals and manual phalanges, (B, D) MOR 473 manus figured with left forearm and lateral and medial views, (E) ROM 64600 metacarpal I, (F, J) MOR 473 metacarpals and manual phalanges, (G, I) MOR 473 manus figured with left forearm and lateral and medial views, and (H) ROM 64600 metacarpal I. Red arrows denote obliquely inclined, asymmetric articular condyles of metacarpal I. Phalanges denoted by roman numerals. Gray represents matrix. [Planned for page width]



Figure 12. *Pikunidromeus* femora rendered with texture. (A1) left femora (n=5) and (B1) right femora (n=9). Arrows denote swollen inflection of medial condyle (char. 359:1). **Abbreviations: df,** distal femur; **f**, foramen **fi,** fibula; **ft**, fourth trochanter; **gt**, greater trochanter; **ic,** posterior intercondylar groove; **lc**, lateral condyle; **lt**, lesser trochanter; **mc**, medial condyle; **s**, sulcus; **ti**, tibia. [Planned for page width]

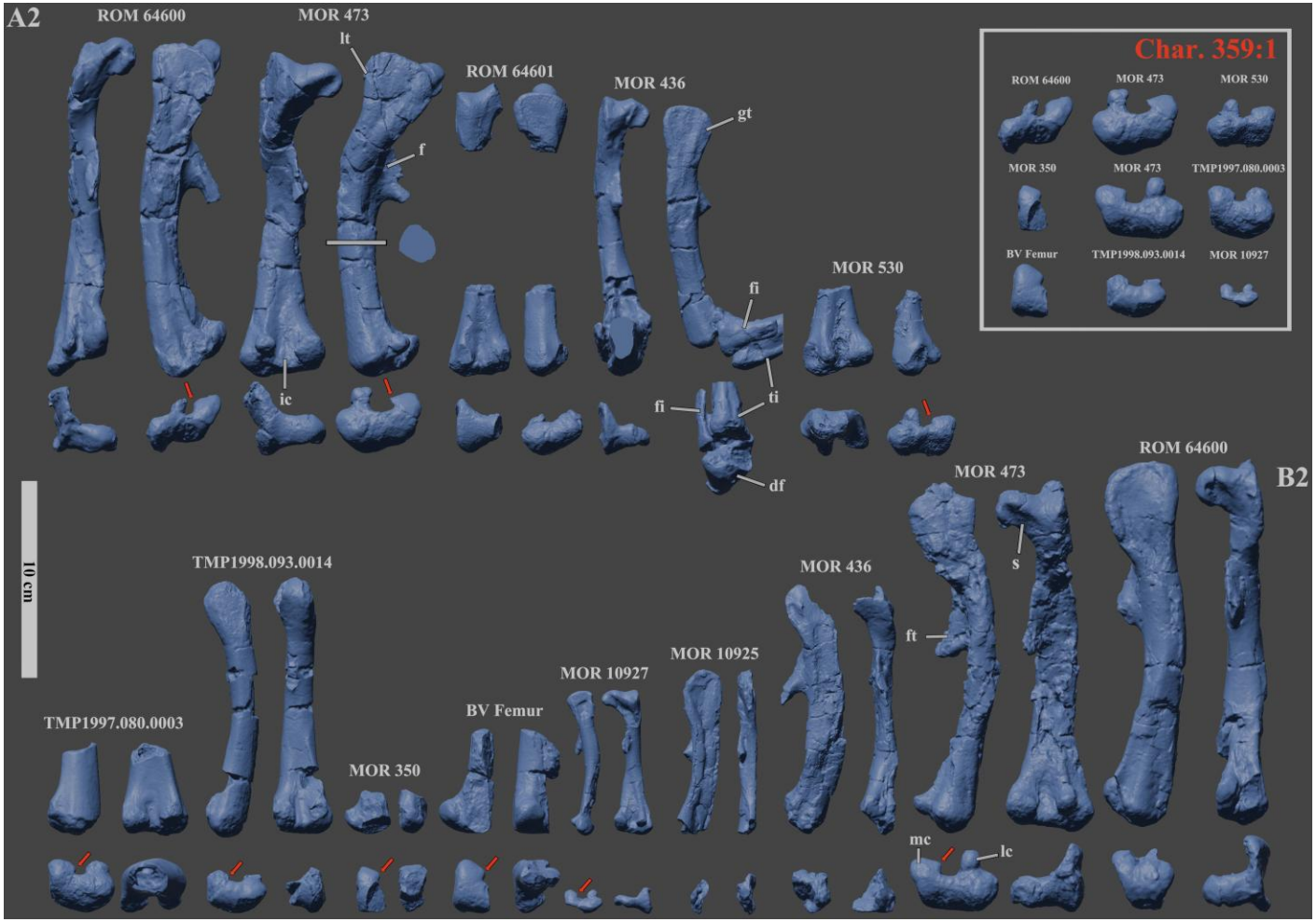


Figure 13. *Pikunidromeus* femora rendered without texture. (A1) left femora (n=5) and (B1) right femora (n=9). Arrows denote swollen inflection of medial condyle (char. 359:1). **Abbreviations: df,** distal femur; **f**, foramen **fi,** fibula; **ft**, fourth trochanter; **gt**, greater trochanter; **ic,** posterior intercondylar groove; **lc**, lateral condyle; **lt**, lesser trochanter; **mc**, medial condyle; **s**, sulcus; **ti**, tibia. [Planned for page width]



Figure 14. *Pikunidromeus* tibiae rendered with and without texture. (A, B) left tibia (n=4) in (left to right) lateral and anterior views, then below in proximal and distal views; and (C, D) right tibia (n=3) in (left to right) lateral and anterior views, then below in proximal and distal views. **Abbreviations: ac,** accessory condyle; **as,** astragalus; **ca**, calcaneum; **cc**, cnemial crest; **fc**, fibular condyle; **fe,** femur; **fi,** fibula; **ic**, inner condyle; **im**, inner malleolus; **ldt**, lateral distal tarsal; **mdt**, medial distal tarsal; **mt**, metatarsal; **om**, outer malleolus. [Planned for page width]

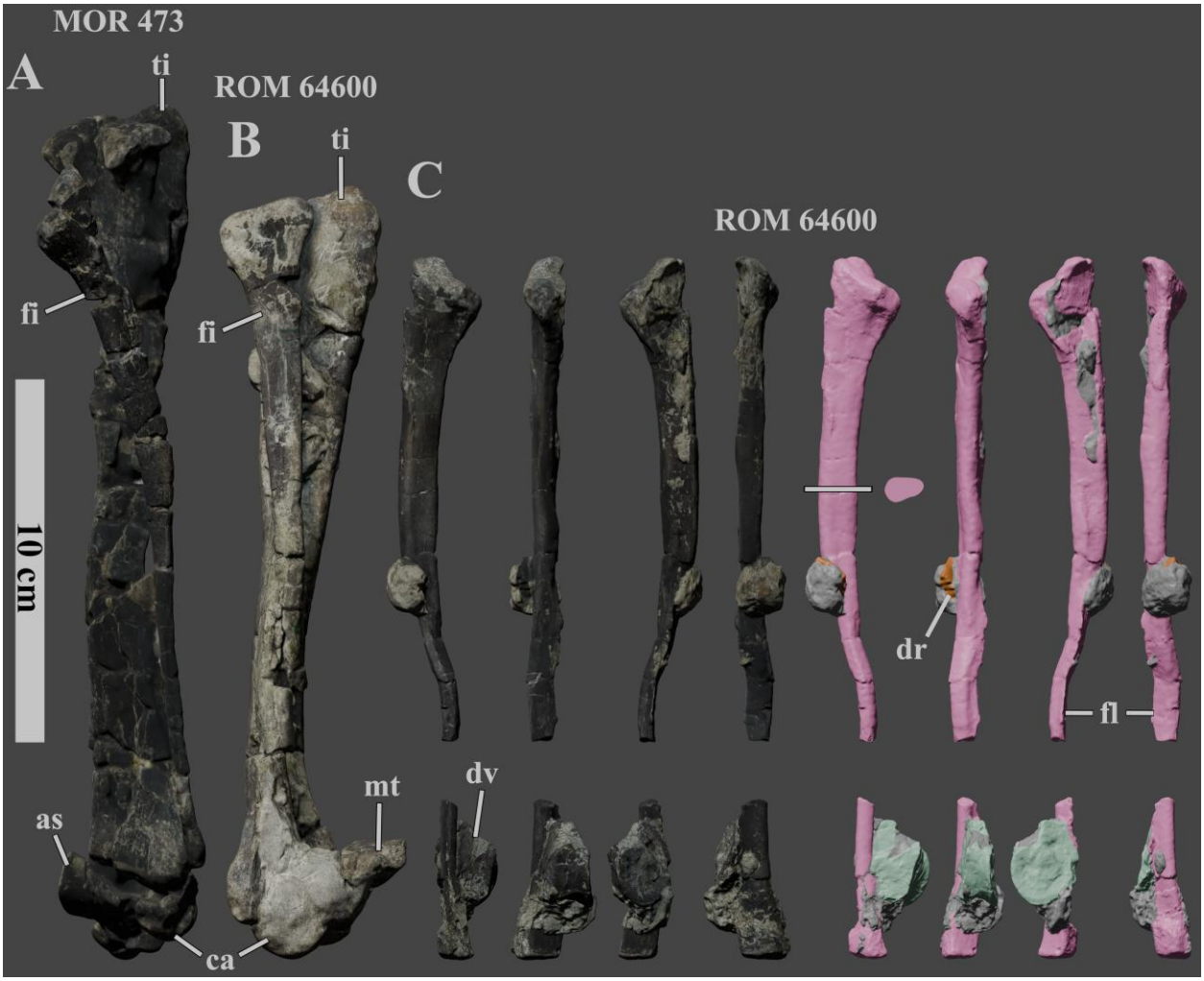


Figure 15. *Pikunidromeus* fibulae rendered with and without texture. (A) MOR 473 right tibia and fibula, (B) ROM 64600 right tibia and fibula, and (C) ROM 64600 left fibula. Gray represents matrix **Abbreviations: as,** astragalus**; ca**, **calcaneum; dr**, dorsal rib; **dv,** dorsal vertebra; **fi,** fibula; **fl,** medial flange; **mt**, metatarsal; **ti**, tibia. [Planned for page width]

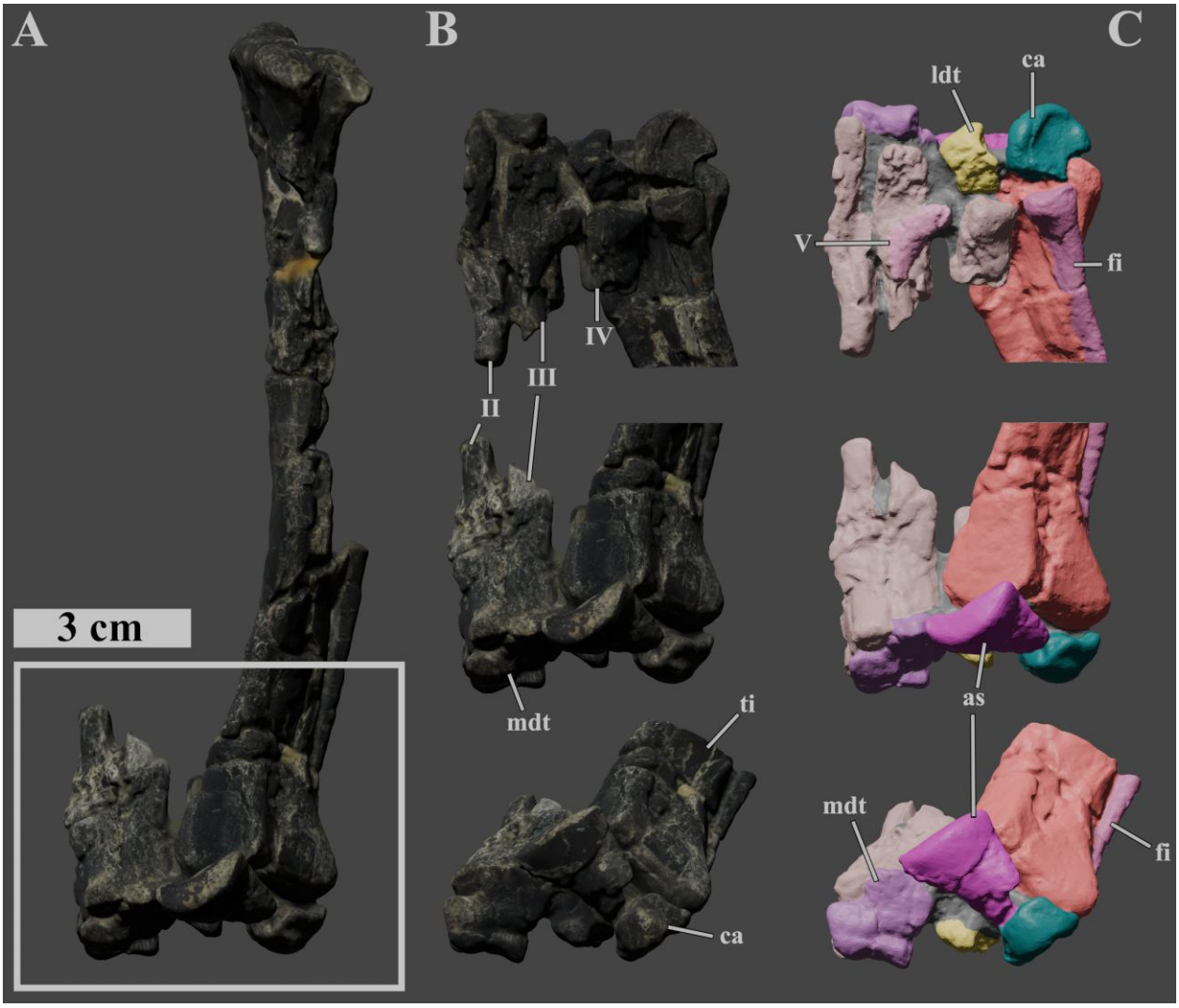


Figure 16. MOR 473 tarsals rendered with and without texture. (A) MOR 473 right tibia, fibula, tarsals, and the proximal portions of metatarsal II-V, (B) in three views with texture; posterior, anterior, and distal, and (C) in three views without texture; posterior, anterior, and distal. Metatarsals denoted by roman numerals. Gray represents matrix. **Abbreviations: as,** astragalus**; ca,** calcaneum**; fi,** fibula; **ldt**, lateral distal tarsal; **mdt**, medial distal tarsal; **ti**, tibia. [Planned for page width]

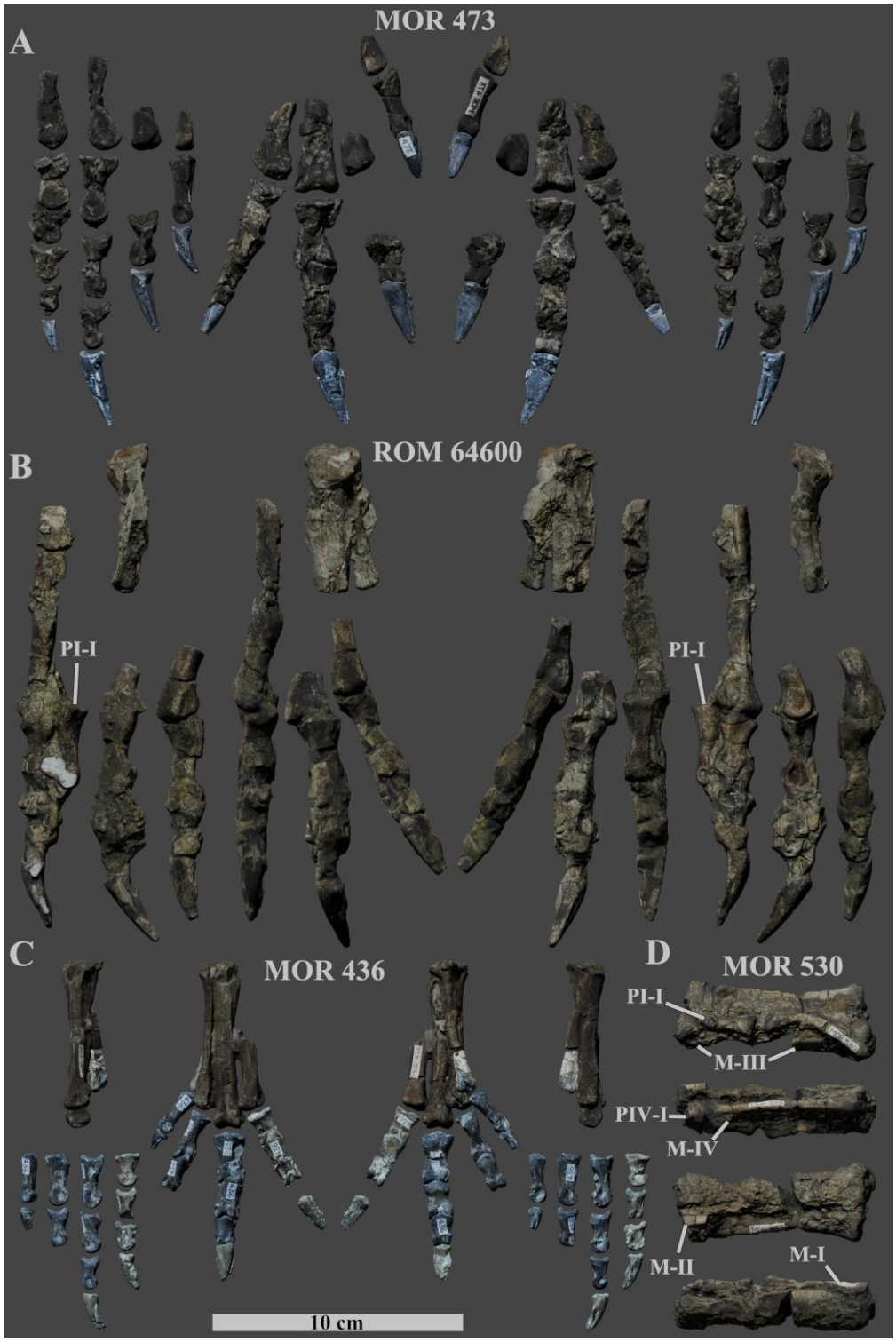


Figure 17. *Pikunidromeus* pes rendered with texture. (A) MOR 473 right pes, (B) ROM 64600 right pes, (C) MOR 436 left pes, and (D) MOR 530 left pes. Metatarsals and phalanges denoted by roman numerals. [Planned for page width]

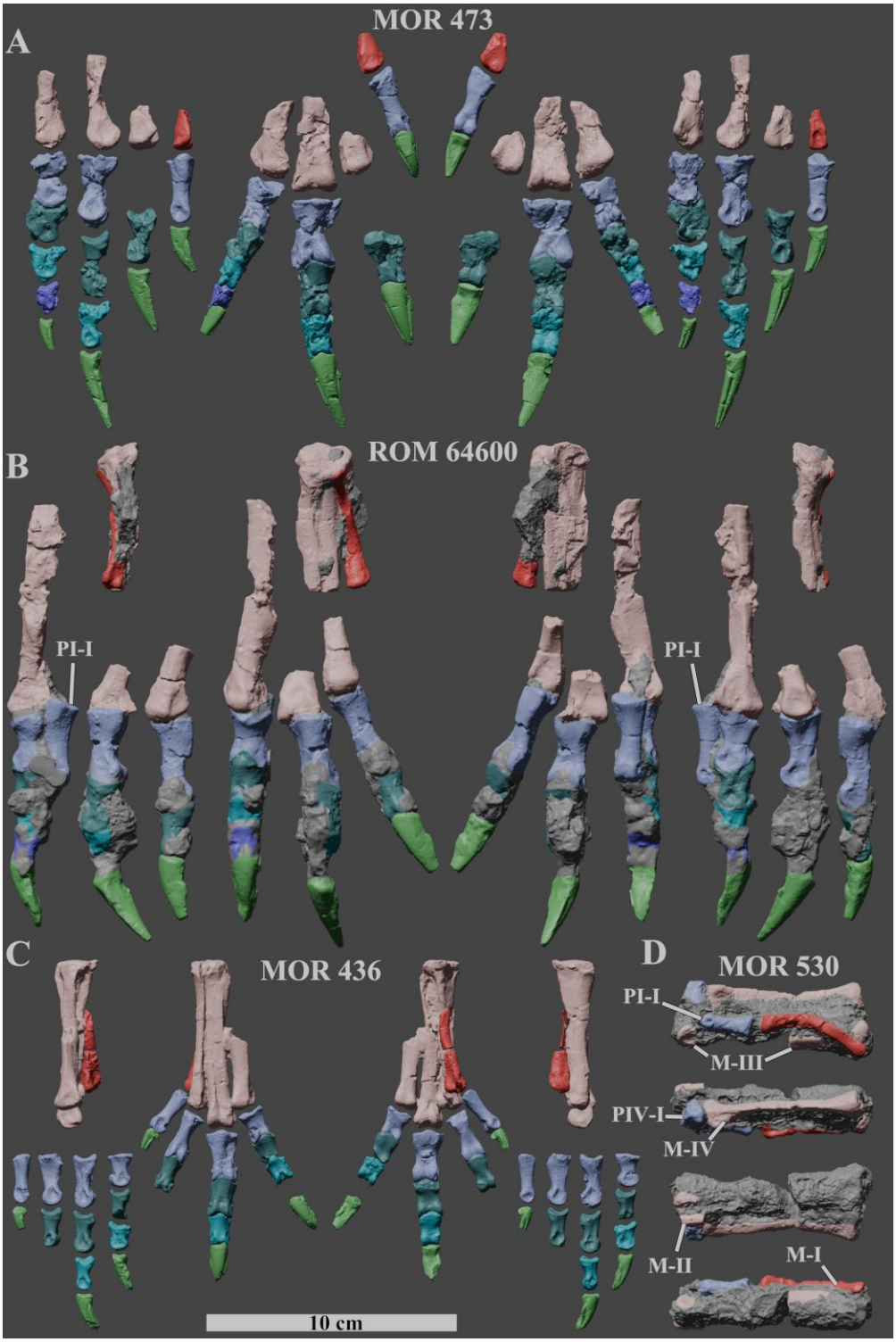


Figure 18. *Pikunidromeus* pes rendered without texture. (A) MOR 473 right pes, (B) ROM 64600 right pes, (C) MOR 436 left pes, and (D) MOR 530 left pes. Metatarsals and phalanges denoted by roman numerals. Gray represents matrix. [Planned for page width]

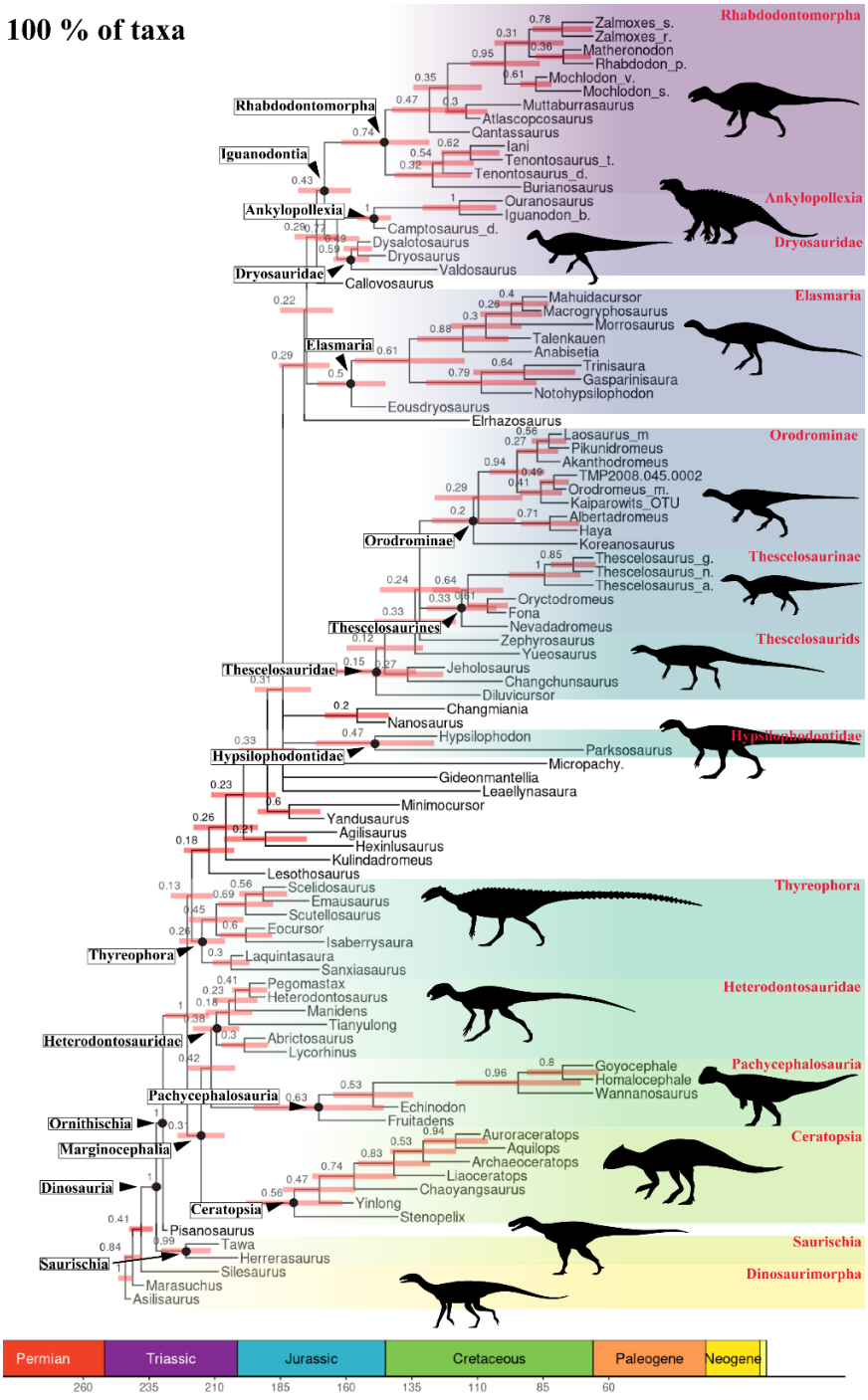


Figure 19. Time-calibrated consensus tree resulting from phylogenetic Bayesian analysis of early diverging ornithischian dinosaurs using an updated version of the Avrahami et al. (2024). Branch lengths are scaled by time in millions of years. Numbers represent posterior probability of support for each node. Red bars illustrate the 95% credible interval for the estimated node ages. 100% of the taxa in the character matrix included. Silhouettes are all downloaded from Phylopic.org. [Planned for page width]

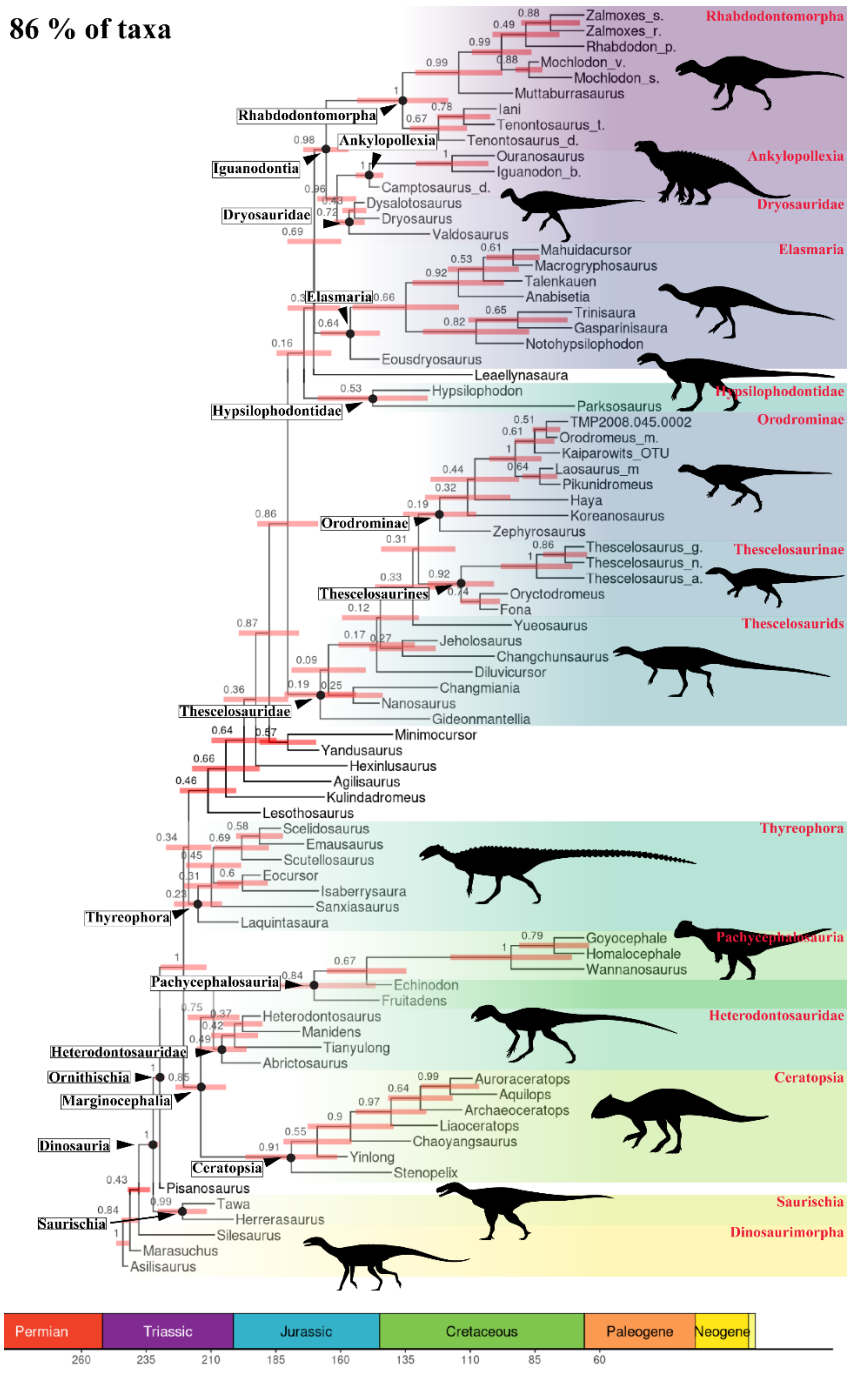


Figure 20. Time-calibrated consensus tree resulting from phylogenetic Bayesian analysis of early diverging ornithischian dinosaurs using an updated version of the Avrahami et al. (2024). Branch lengths are scaled by time in millions of years. Numbers represent posterior probability of support for each node. Red bars illustrate the 95% credible interval for the estimated node ages. 86 % of the taxa in the character matrix included in analysis. Taxa lacking 90% of the characters culled. Silhouettes are all downloaded from Phylopic.org. [Planned for page width].

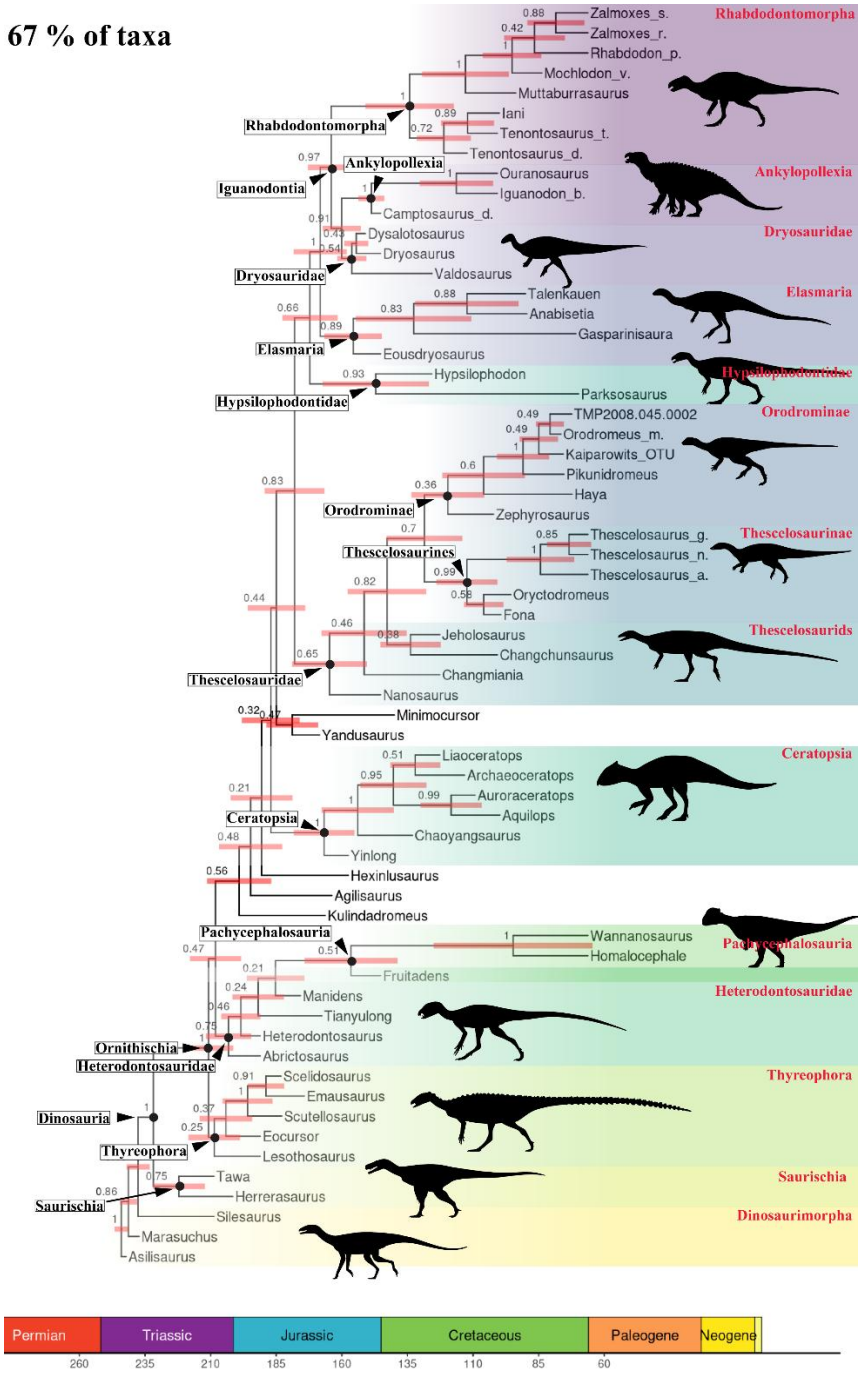


Figure 21. Time-calibrated consensus tree resulting from phylogenetic Bayesian analysis of early diverging ornithischian dinosaurs using an updated version of the Avrahami et al. (2024). Branch lengths are scaled by time in millions of years. Numbers represent posterior probability of support for each node. Red bars illustrate the 95% credible interval for the estimated node ages. 67 % of the taxa in the character matrix included in analysis. Taxa lacking 80% of the characters culled. Silhouettes are all downloaded from Phylopic.org. [Planned for page width].

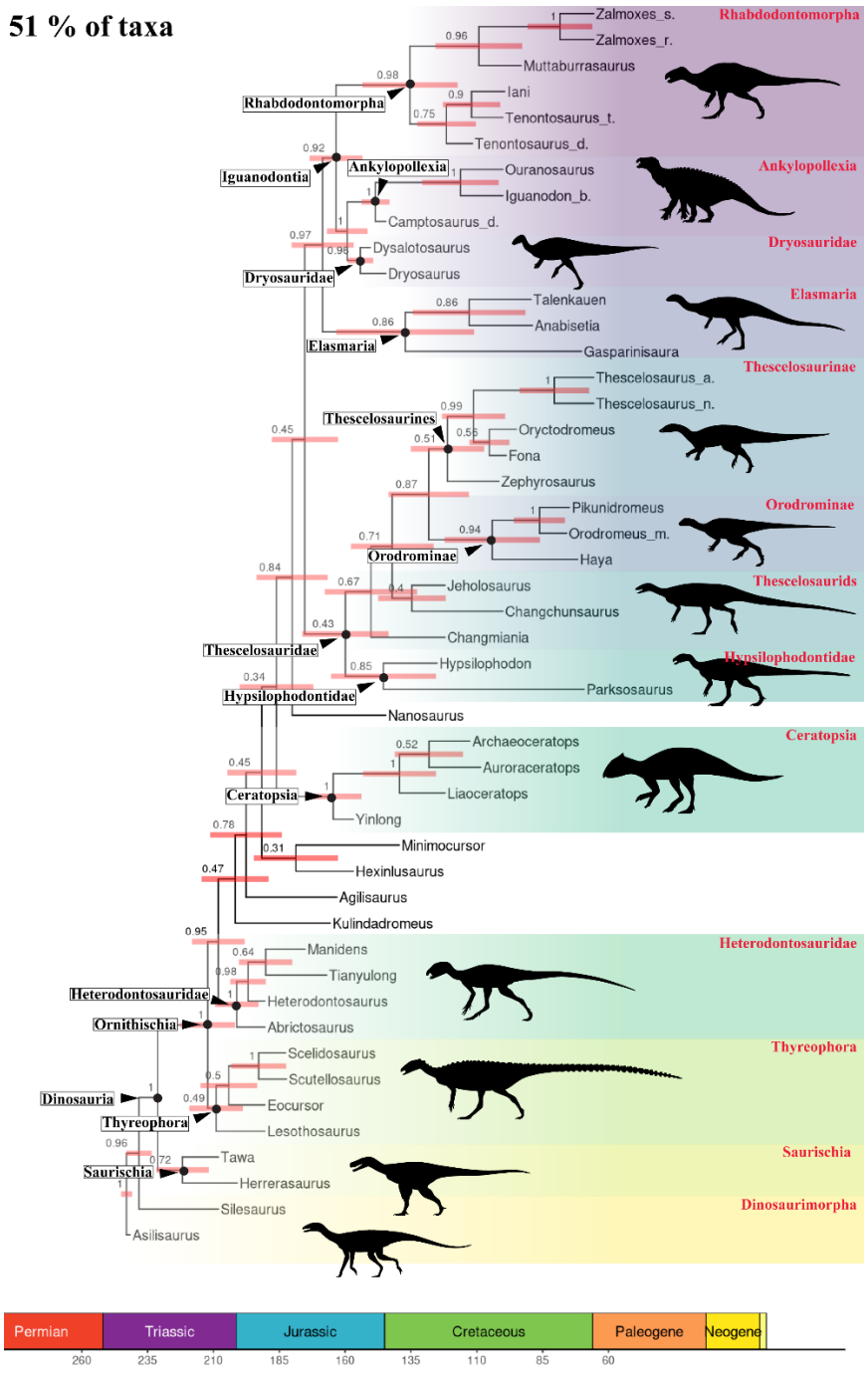


Figure 22. Time-calibrated consensus tree resulting from phylogenetic Bayesian analysis of early diverging ornithischian dinosaurs using an updated version of the Avrahami et al. (2024). Branch lengths are scaled by time in millions of years. Numbers represent posterior probability of support for each node. Red bars illustrate the 95% credible interval for the estimated node ages. 51 % of the taxa in the character matrix included in analysis. Taxa lacking 70% of the characters culled. Silhouettes are all downloaded from Phylopic.org. [Planned for page width].

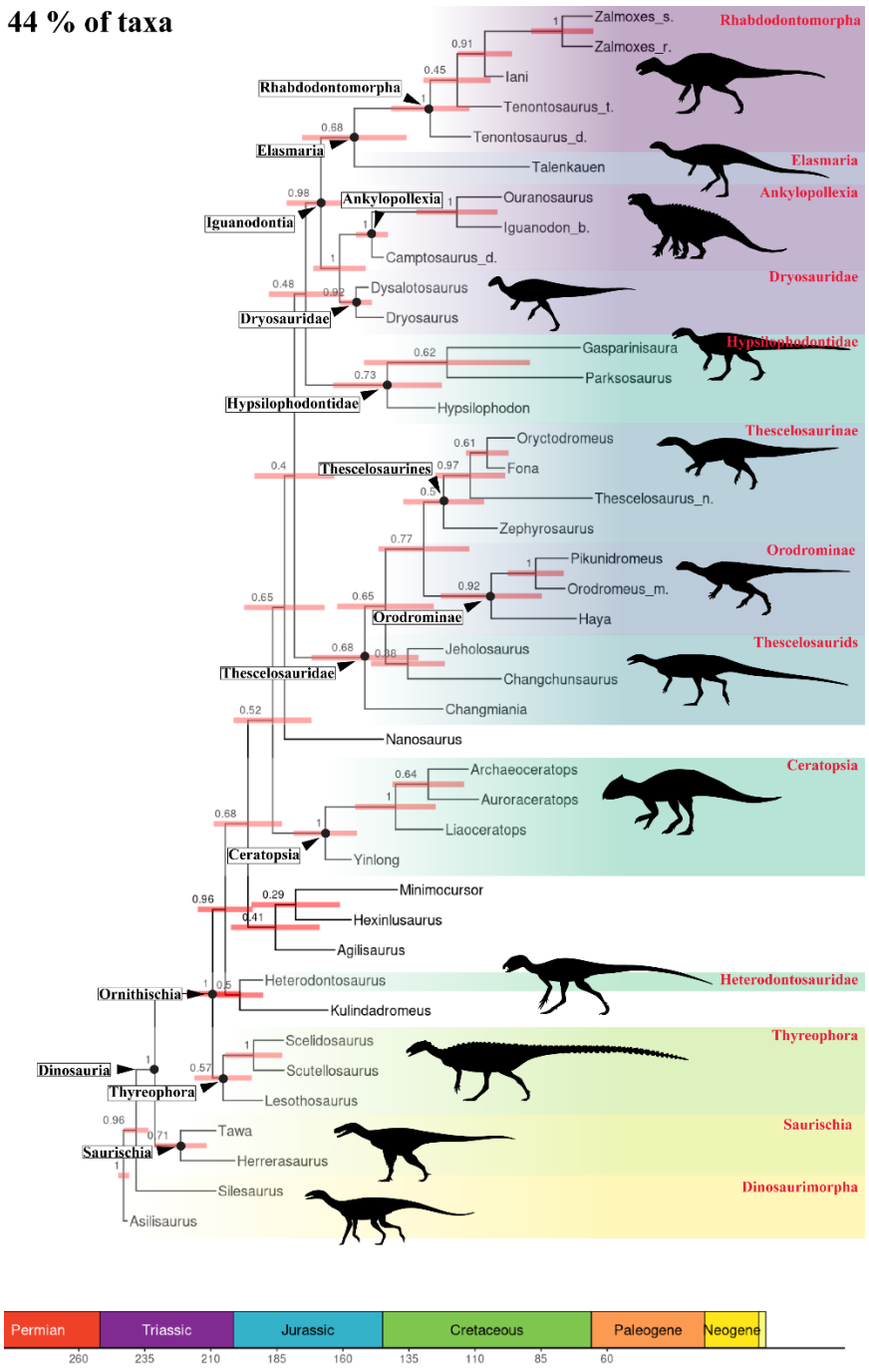


Figure 23. Time-calibrated consensus tree resulting from phylogenetic Bayesian analysis of early diverging ornithischian dinosaurs using an updated version of the Avrahami et al. (2024). Branch lengths are scaled by time in millions of years. Numbers represent posterior probability of support for each node. Red bars illustrate the 95% credible interval for the estimated node ages. 44 % of the taxa in the character matrix included in analysis. Taxa lacking 60% of the characters culled. Silhouettes are all downloaded from Phylopic.org. [Planned for page width].

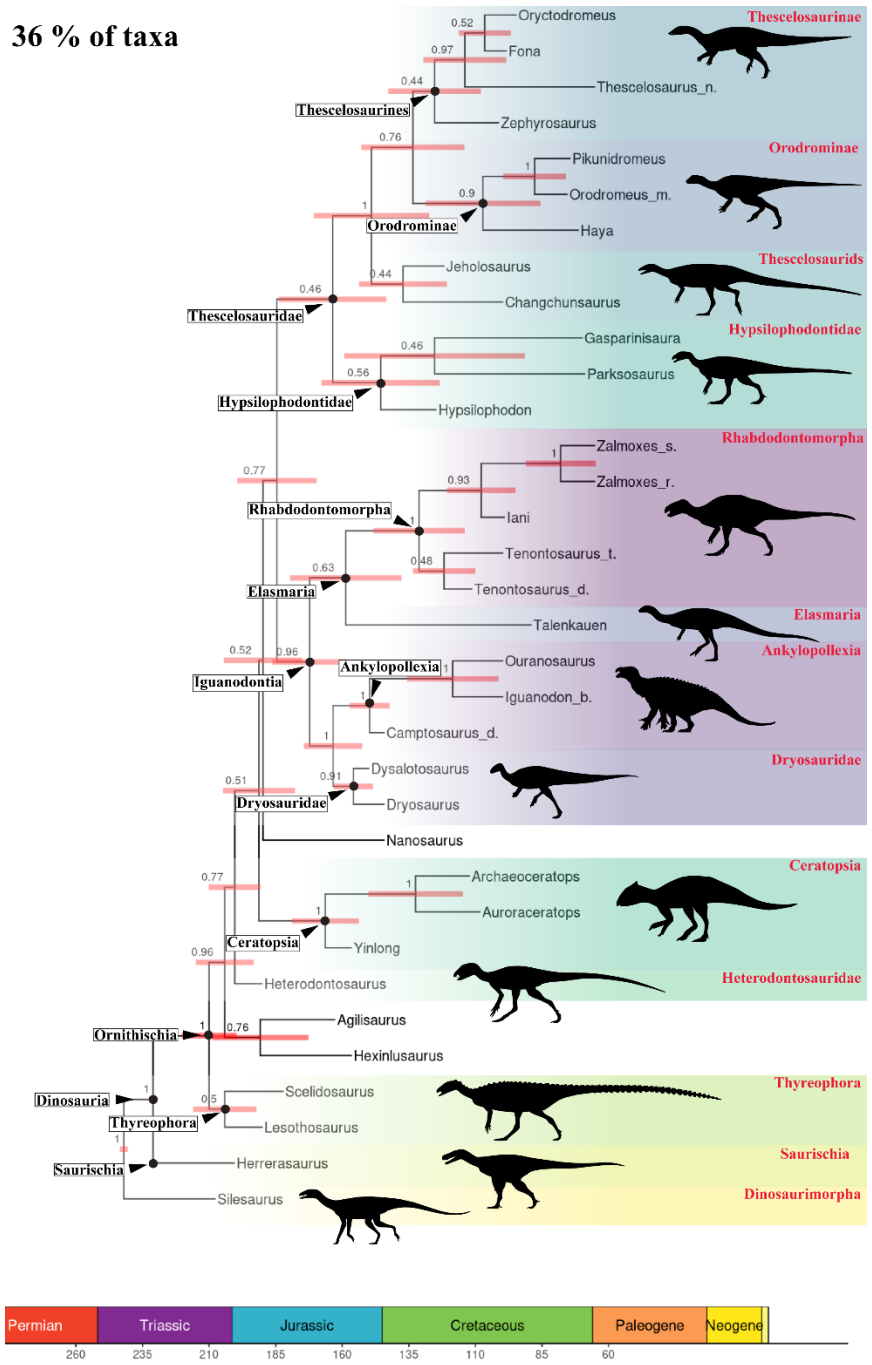


Figure 24. Time-calibrated consensus tree resulting from phylogenetic Bayesian analysis of early diverging ornithischian dinosaurs using an updated version of the Avrahami et al. (2024). Branch lengths are scaled by time in millions of years. Numbers represent posterior probability of support for each node. Red bars illustrate the 95% credible interval for the estimated node ages. 36 % of the taxa in the character matrix included in analysis. Taxa lacking 50% of the characters culled. Silhouettes are all downloaded from Phylopic.org. [Planned for page width].

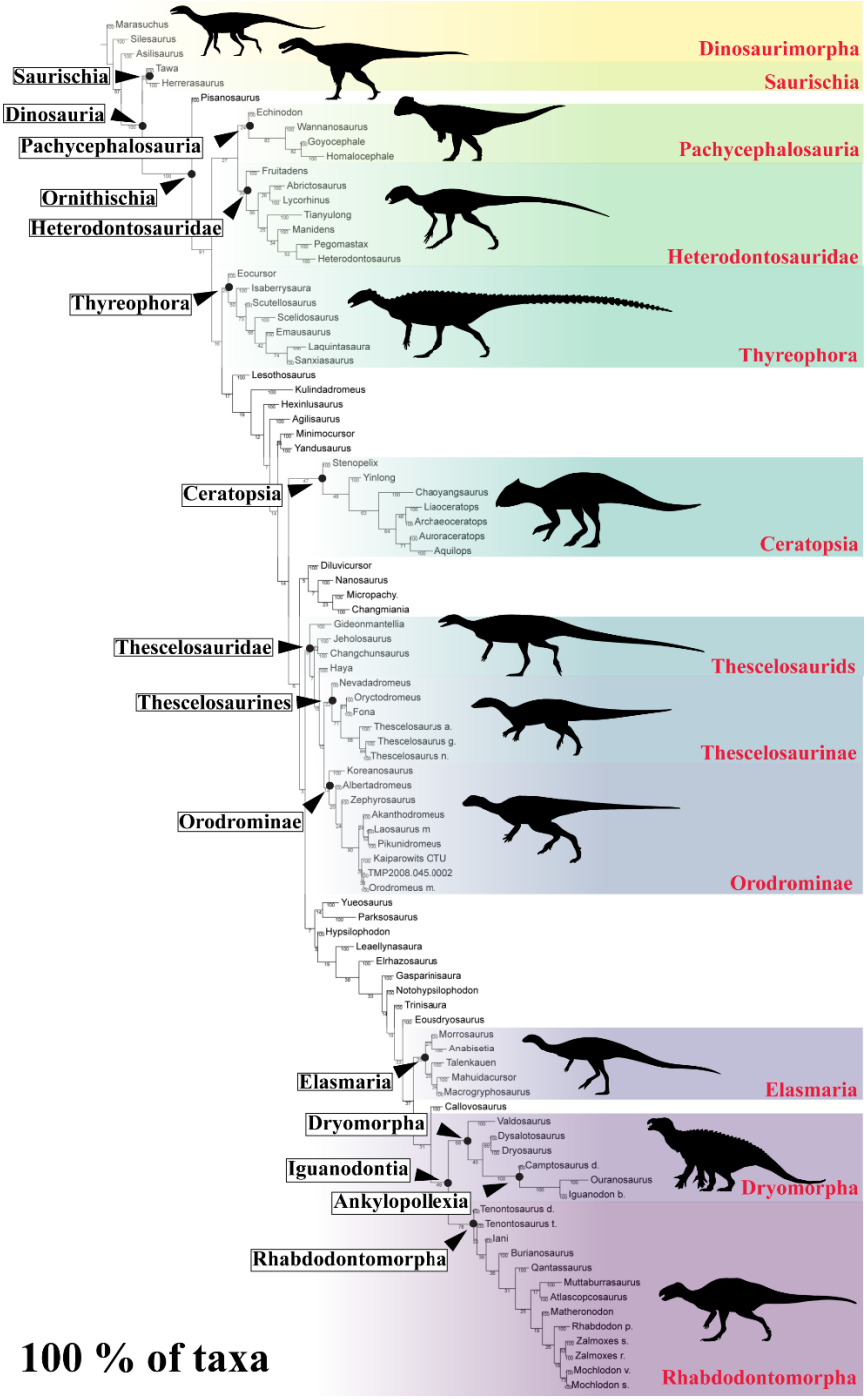


Figure 25. Non-time calibrated phylogenetic Bayesian analysis of early diverging ornithischian dinosaurs using an updated version of the Avrahami et al. (2024). Numbers represent posterior probability of support for each node. 100 % of the taxa in the character matrix included in analysis. Silhouettes are all downloaded from Phylopic.org. [Planned for page width].

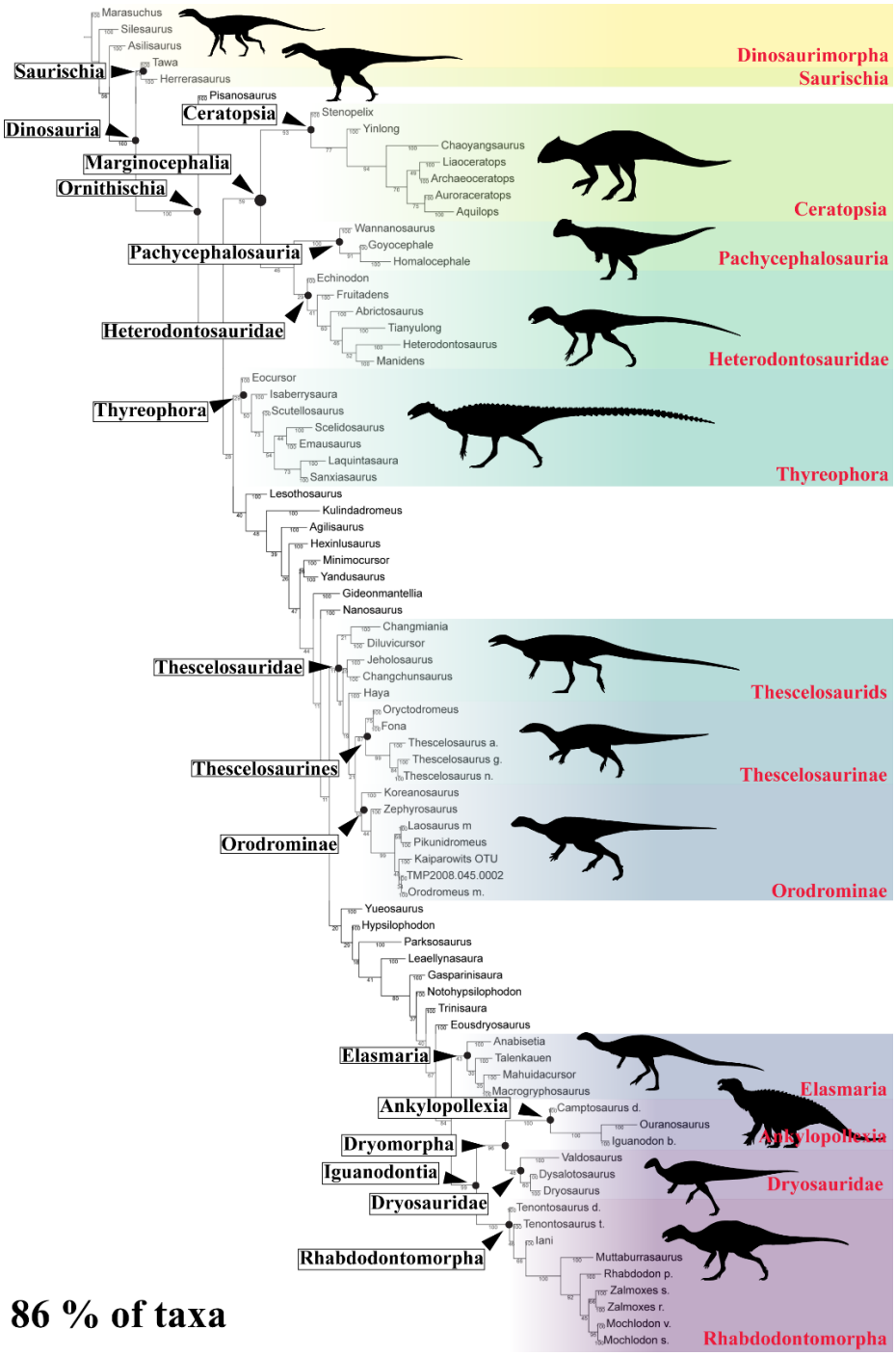


Figure 26. Non-time calibrated phylogenetic Bayesian analysis of early diverging ornithischian dinosaurs using an updated version of the Avrahami et al. (2024). Numbers represent posterior probability of support for each node. 86 % of the taxa in the character matrix included in analysis. Taxa lacking 90% of the characters culled. Silhouettes are all downloaded from Phylopic.org. [Planned for page width]

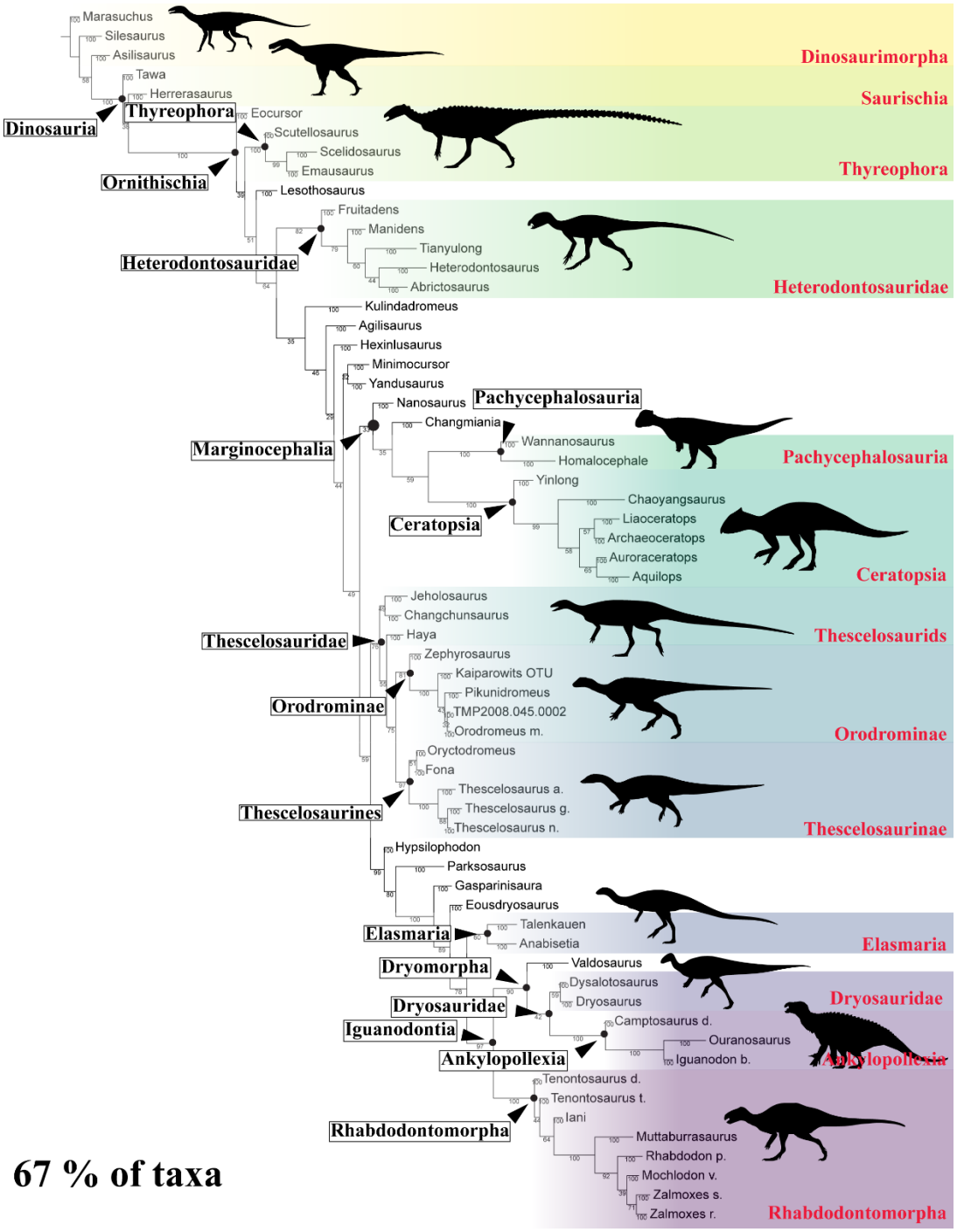


Figure 27. Non-time calibrated phylogenetic Bayesian analysis of early diverging ornithischian dinosaurs using an updated version of the Avrahami et al. (2024). Numbers represent posterior probability of support for each node. 67 % of the taxa in the character matrix is included in analysis. Taxa lacking 80% of the characters culled. Silhouettes are all downloaded from Phylopic.org. [Planned for page width]

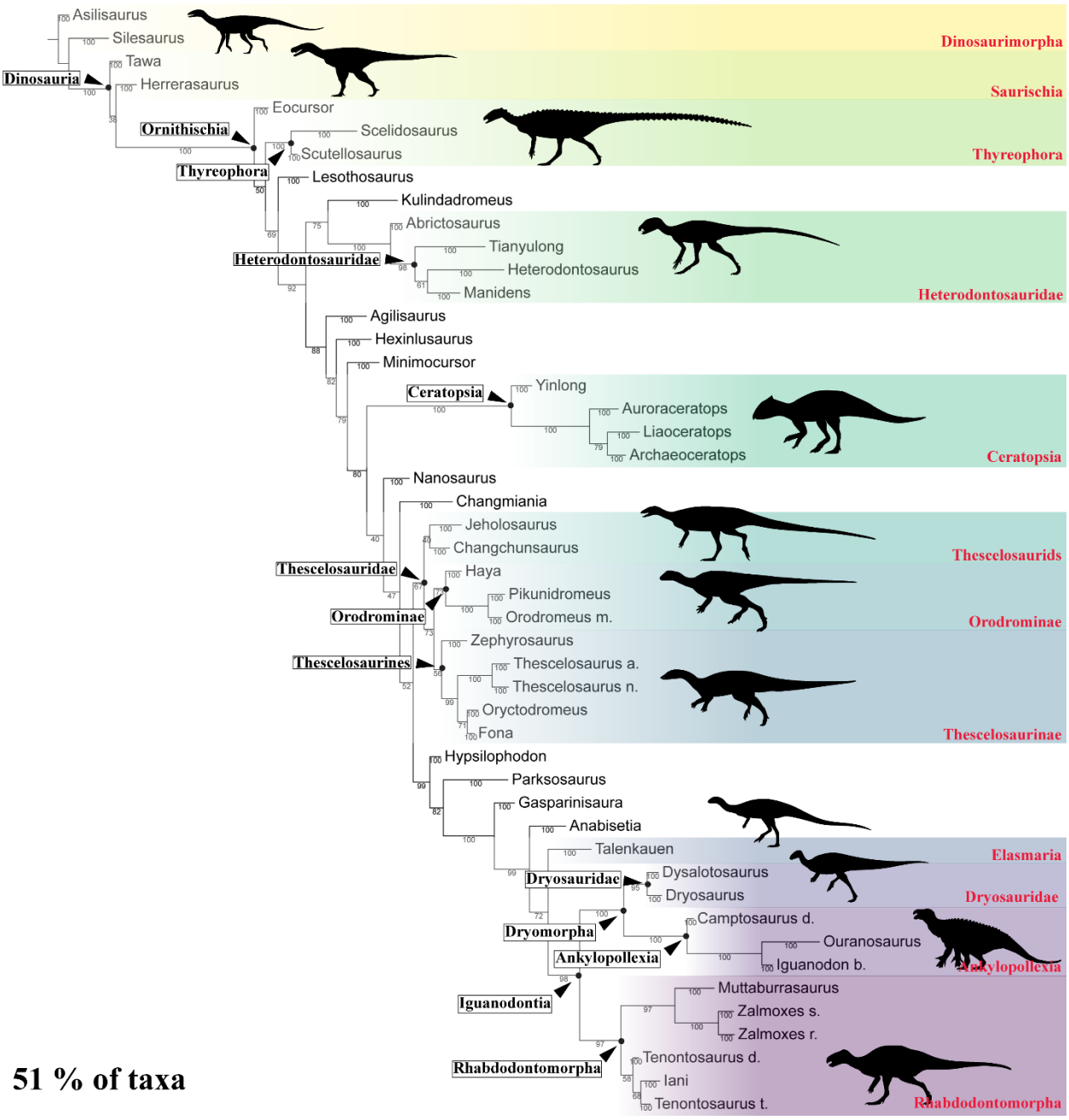


Figure 28. Non-time calibrated phylogenetic Bayesian analysis of early diverging ornithischian dinosaurs using an updated version of the Avrahami et al. (2024). Numbers represent posterior probability of support for each node. 51 % of the taxa in the character matrix included in analysis. Taxa lacking 70% of the characters culled. Silhouettes are all downloaded from Phylopic.org. [Planned for page width]

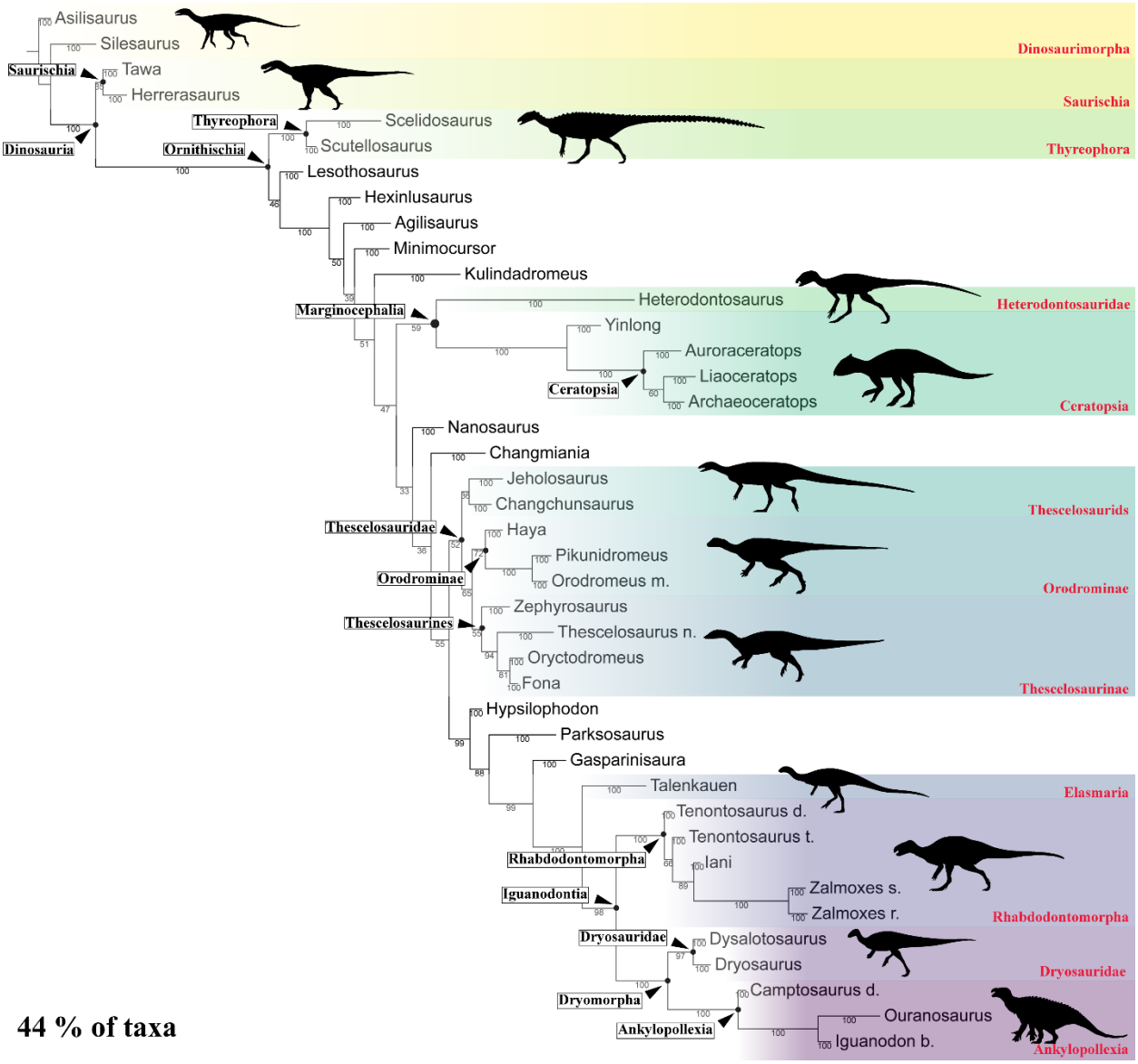


Figure 29. Non-time calibrated phylogenetic Bayesian analysis of early diverging ornithischian dinosaurs using an updated version of the Avrahami et al. (2024). Numbers represent posterior probability of support for each node. 44 % of the taxa in the character matrix included in analysis. Taxa lacking 60% of the characters culled. Silhouettes are all downloaded from Phylopic.org. [Planned for page width]

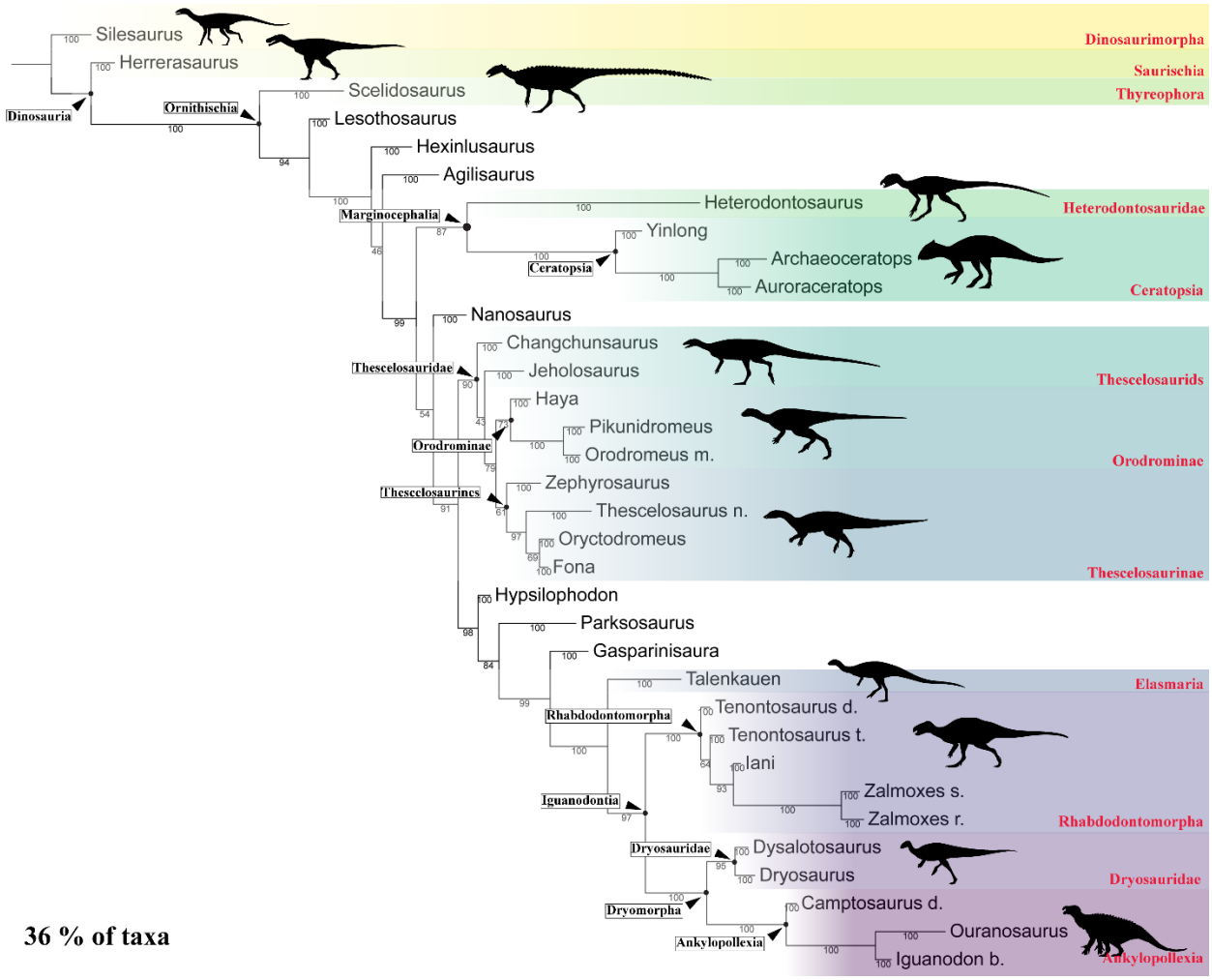


Figure 30. Non-time calibrated phylogenetic Bayesian analysis of early diverging ornithischian dinosaurs using an updated version of the Avrahami et al. (2024). Numbers represent posterior probability of support for each node. 36 % of the taxa in the character matrix included in analysis. Taxa lacking 50% of the characters culled. Silhouettes are all downloaded from Phylopic.org. [Planned for page width]

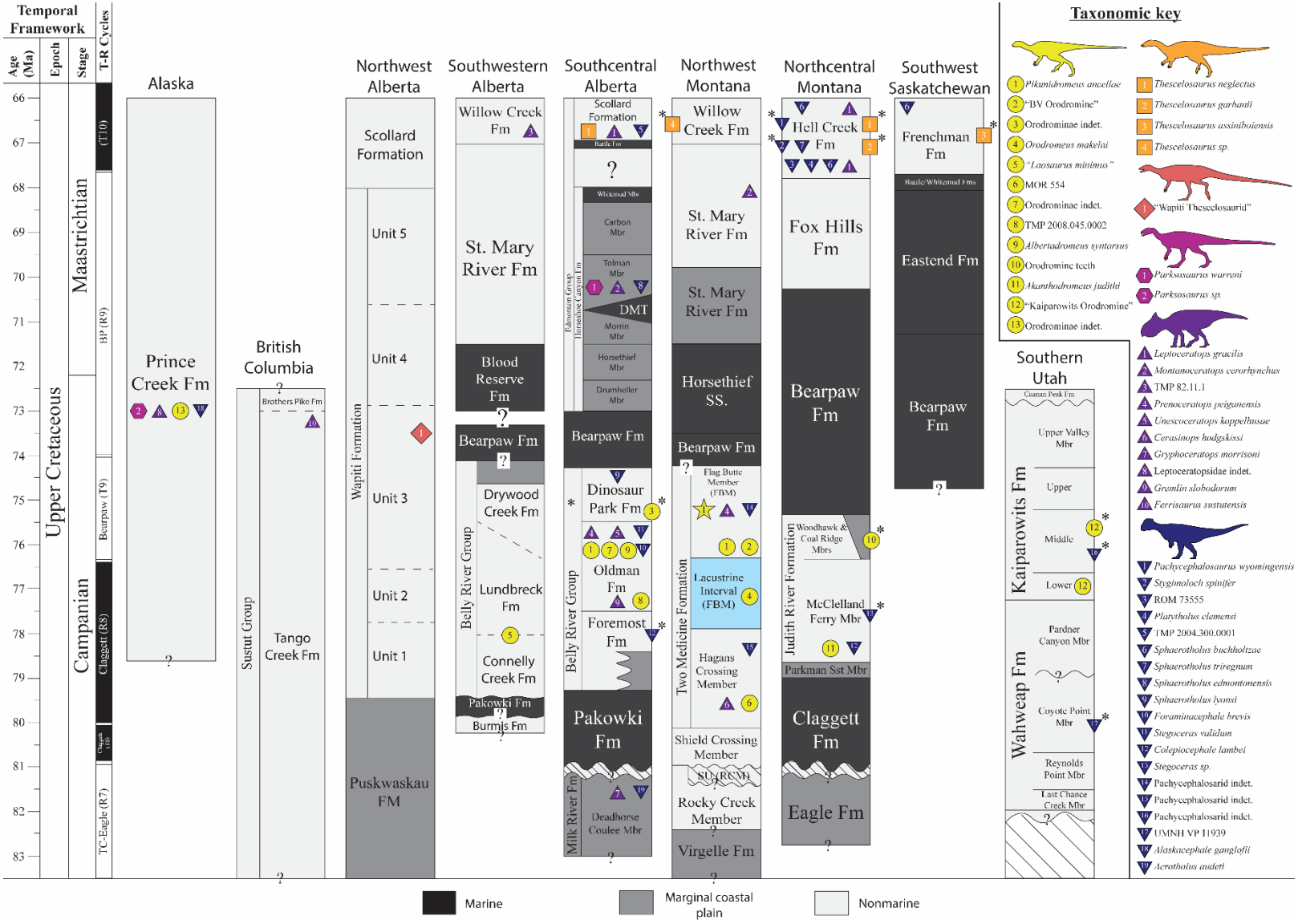

Temporal Framework
Age (Ma)
Epoch
Stage
T-R Cycles
Upper Cretaceous
Campanian
Maastrichtian
(T10)
BP (R9)
Bearpaw (T9)
Claggett (R8)
Claggett (T8)
TC-Eagle (R7)
Alaska
Prince Creek Fm
British Columbia
Brothers Pike Fm
Sustut Group
Tango Creek Fm
Northwest Alberta
Scollard Formation
Wapiti Formation
Unit 5
Unit 4
Unit 3
Unit 2
Unit 1
Puskwaskau FM
Southwestern Alberta
Willow Creek Fm
St. Mary River Fm
Blood Reserve Fm
Bearpaw Fm
Belly River Group
Drywood Creek Fm
Lundbreck Fm
Connelly Creek Fm
Pakowki Fm
Burmis Fm
Southcentral Alberta
Scollard Formation
Battle Fm
Whitemud Mbr
Carbon Mbr
Tolman Mbr
DMT
Morrin Mbr
Horsethief Mbr
Drumheller Mbr
Edmonton Group
Horseshoe Canyon Fm
Bearpaw Fm
Dinosaur Park Fm
Oldman Fm
Foremost Fm
Belly River Group
Pakowki Fm
Milk River Fm
Deadhorse Coulee Mbr
Northwest Montana
Willow Creek Fm
St. Mary River Fm
Horsethief SS.
Bearpaw Fm
Flag Butte Member (FBM)
Two Medicine Formation
Lacustrine Interval (FBM)
Hagans Crossing Member
Shield Crossing Member
SUNRCVD
Rocky Creek Member
Virgelle Fm
Northcentral Montana
Hell Creek Fm
Fox Hills Fm
Bearpaw Fm
Woodhawk & Coal Ridge Mbrs
Judith River Formation
McClelland Ferry Mbr
Parkman Sst Mbr
Claggett Fm
Eagle Fm
Southwest Saskatchewan
Frenchman Fm
Battle/Whitemud Fms
Eastend Fm
Bearpaw Fm
Southern Utah
Cuanan Peak Fm
Kaiparowits Fm
Upper Valley Mbr
Upper
Middle
Lower
Wahweap Fm
Pardner Canyon Mbr
Coyote Point Mbr
Reynolds Point Mbr
Last Chance Creek Mbr
Taxonomic key
1 Pikunidromeus ancellae
2 "BV Orodromine"
3 Orodrominae indet.
4 Orodromeus makelai
5 "Laosaurus minimus"
6 MOR 554
7 Orodrominae indet.
8 TMP 2008.045.0002
9 Albertadromeus syntarsus
10 Orodromine teeth
11 Akanthodromeus judithi
12 "Kaiparowits Orodromine"
13 Orodrominae indet.
1 Thescelosaurus neglectus
2 Thescelosaurus garbanii
3 Thescelosaurus assiniboiensis
4 Thescelosaurus sp.
1 "Wapiti Thescelosaurid"
1 Parksosaurus warreni
2 Parksosaurus sp.
1 Leptoceratops gracilis
2 Montanoceratops cerorhynchus
3 TMP 82.11.1
4 Prenoceratops pieganensis
5 Unescoceratops koppelhusae
6 Cerasinops hodgskissi
7 Gryphoceratops morrisoni
8 Leptoceratopsidae indet.
9 Gremlin slobodorum
10 Ferrisaurus sustutensis
1 Pachycephalosaurus wyomingensis
2 Stygimoloch spinifer
3 ROM 73555
4 Platytholus clemensi
5 TMP 2004.300.0001
6 Sphaerotholus buchholtzae
7 Sphaerotholus triregnum
8 Sphaerotholus edmontonensis
9 Sphaerotholus lyonsi
10 Foraminacephale brevis
11 Stegoceras validum
12 Colepiocephale lambei
13 Stegoceras sp.
14 Pachycephalosarid indet.
15 Pachycephalosarid indet.
16 Pachycephalosarid indet.
17 UMNH VP 11939
18 Alaskacephale gangloffi
19 Acrotholus audeti
Marine
Marginal coastal plain
Nonmarine

Figure 31. Stratigraphic section of Late Cretaceous northern Laramidia and southern Utah, with orodromine (red), thescelosaurine (purple), thescelosaurid (blue), *Parksosaurus* (dark orange), leptoceratopsid (light orange), and pachycephalosaurid (yellow) occurrences denoted. *Pikunidromeus ancellae* holotype symbolized by a star. Marginalized taxon/specimen occurrences straddle the column edge signify uncertain placement within respective formations. Positioning on the column border is not reflective of stratigraphic positioning in the formation. For indeterminate forms, specimen numbers are preferentially shown if known. Pachycephalosaurid #13 represents a handful of undescribed specimens informally designated *Stegoceras sp*. from the Judith River Formation reposited at the MOR. This chronostratigraphic framework synthesizes data provided in Jerzykiewicz and Norris (1995), Fowler (2017), Arbour et al. (2020), Ramezani et al. (2022), and Rogers et al. (2024). Orodromine taxon/specimen occurrences drawn from Brown et al. (2013), Druckenmiller et al. (2021), Hudgins (2021), Rogers et al. (2024), personal communications with C. Brown, and this study; *Thescelosaurus* taxa sourced from Morris (1976) and Brown et al. (2011); thescelosaurid #1 (="Wapiti Thescelosaurid") was described in Hudgins (2021); *Parksosaurus* temporal occurrences obtained from Brown and Druckenmiller (2011), Druckenmiller et al. (2021), Hudgins (2021), and Sues et al (2023); leptoceratopsid taxon/specimen occurrences compiled using data from Brown et al. (2012), Evans et al. (2013), Druckenmiller et al. (2021), Ryan et al. (2023), and Rogers et al. (2024); pachycephalosaurid taxon/specimen data informed from Sullivan (2006). Schott et al. (2009), Evans et al. (2015), Mallon et al. (2015); Schott and Evans (2017), Dyer et al. (2022), Horner et al. (2022), Woodruff (2022), Woodruff and Schott (2023), Rogers et al. (2024), and personal observations of undescribed Judith River pachycephalosaurid specimens at the MOR. Silhouettes sourced from Phylopic.org

Literature Cited

Agnolin, F. L., & Varricchio, D. (2012). Systematic reinterpretation of *Piksi barbarulna* Varricchio, 2002 from the Two Medicine Formation (Upper Cretaceous) of Western USA (Montana) as a pterosaur rather than a bird. *Geodiversitas*, 34(4), 883-894.

Agnolín, F. L., Herrera, G. Á., Rolando, M. A., Motta, M., Rozadilla, S., Verdiquio, L., ... & Novas, F. E. (2024). Fossil vertebrates from the Cerro Fortaleza Formation (Upper Cretaceous), Santa Cruz Province, Argentina. *Cretaceous Research*, *154*, 105735.

Alcober, O. A. & Martinez R. N. (2010). A new herrerasaurid (Dinosauria, Saurischia) from the Upper Triassic Ischigualasto Formation of northwestern Argentina. *ZooKeys*, 63(2), 55-87. https://doi.org/10.3897/zookeys.63.550

Andrzejewski, K. A., Winkler, D. A., & Jacobs, L. L. (2019). A new basal ornithopod (Dinosauria, Ornithischia) from the Early Cretaceous of Texas. *PloS one*, 2019(3), e0207935-e0207935. https://doi.org/10.1371/journal.pone.0207935

Arbour, V. M., Evans, D. C., Simon, D. J., Cullen, T. M., & Braman, D. (2020). Cretaceous flora and fauna of the Sustut Group near the Sustut River, northern British Columbia, Canada. *Canadian Journal of Earth Sciences*, *57*(6), 671-680.

Avrahami, H. M., Makovicky, P. J., Tucker, R. T., & Zanno, L. E. (2024). A new semi-fossorial thescelosaurine dinosaur from the Cenomanian-age Mussentuchit Member of the Cedar Mountain Formation, Utah. *The Anatomical Record*.

Avrahami, H. M., Lindsey, K. P., & Herzog, L. (2023). Advances in 3D surface scanning: Mobile device applications set a new standard for digitization of fossils and museum artifacts. *Journal of Vertebrate Paleontology* Program Abstract 83:77.

Averianov, A. O., Voronkevich, A. V., Leshchinskiy, S. V., & Fayngertz, A. V. (2006). A ceratopsian dinosaur *Psittacosaurus sibiricus* from the Early Cretaceous of West Siberia, Russia and its phylogenetic relationships. *Journal of Systematic Palaeontology*, *4*(4), 359-395.

Baron, M. G., Norman, D. B., & Barrett, P. M. (2017). Postcranial anatomy of *Lesothosaurus diagnosticus* (Dinosauria: Ornithischia) from the Lower Jurassic of southern Africa: implications for basal ornithischian taxonomy and systematics. *Zoological Journal of the Linnean Society*, *179*(1), 125-168.

Barrett, P. M., Butler, R. J., & Knoll, F. (2005). Small-bodied ornithischian dinosaurs from the Middle Jurassic of Sichuan, China. *Journal of Vertebrate Paleontology*, 25(4), 823-834.

Barrett, P. M. & Han, F. -L. (2009) Cranial anatomy of *Jeholosaurus shangyuanensis* (Dinosauria: Ornithischia) from the Early Cretaceous of China. Zootaxa, 2072, 31-55.

Barrett, P. M. (2016). A new specimen of *'Valdosaurus canaliculatus'* (Ornithopoda: Dryosauridae) from the Lower Cretaceous of the Isle of Wight, England. *Memoirs of Museum Victoria*, *74*, 29-48.

Barta, D. E., & Norell, M. A. (2021). The osteology of *Haya griva* (Dinosauria, Ornithischia) from the Late Cretaceous of Mongolia. *Bulletin of the American Museum of Natural History*, 445 (1), 1-112. https://doi.org/10.1206/0003-0090.445.1.1

Becerra, M. G., Pol, D., Porro, L. B., Paulina-Carabajal, A., & Rauhut, O. W. (2022). Craniomandibular osteology of *Manidens condorensis* (Ornithischia: Heterodontosauridae) from the upper Lower Jurassic of Argentina. *Journal of Vertebrate Paleontology*, *42*(3), e2181087.

Boulenger GA. 1881. *Iguanodon bernissartensis*. p. 606. In: Beneden P-J, ed. *Sur l'arc pelvien chex les dinosauriens de Bernissart. Bulletin de l'Académie royal de Belgique 3 Sér. 1*. Brussels, Belgium: Académie royal de Belgique, 600–608.

Boyd, C. A. (2012). *Taxonomic revision of latest Cretaceous North american basal neonithischian taxa and a phylogenetic analysis of basal ornithischian relationships* University of Texas - Austin.

Boyd, C. A., Brown, C. A., Scheetz, R. D., & Clarke, J. A. (2009). Taxonomic revision of the basal Neornithischian taxa *Thescelosaurus* and *Bugenasaura*. *Journal of Vertebrate Paleontology*, 29, 758-770.

Boyd, C. A. (2014). The cranial anatomy of the neornithischian dinosaur *Thescelosaurus neglectus*. *PeerJ*, 2, e669.

Boyd, C. A. (2015). The systematic relationships and biogeographic history of ornithischian dinosaurs. *PeerJ*, 3, e1523.

Brochu, C. A. (1996). Closure of neurocentral sutures during crocodilian ontogeny; implications for maturity assessment in fossil archosaurs. *Journal of Vertebrate Paleontology*, 16(1), 49-62. https://doi.org/10.1080/02724634.1996.10011283

Brown, B. (1914). *Leptoceratops*, a new genus of Ceratopsia from the Edmonton Cretaceous of Alberta. *Bulletin of the AMNH*; v. 33, article 36.

Brown, C. M., Boyd, C. A., & Russell, A. P. (2011). A new basal ornithopod dinosaur (Frenchman Formation, Saskatchewan, Canada), and implications for late Maastrichtian ornithischian diversity in North America. *Zoological Journal of the Linnean Society*, 163(4), 1157-1198.

Brown, C. M., & Druckenmiller, P. (2011). Basal ornithopod (Dinosauria: Ornithischia) teeth from the Prince Creek formation (early Maastrichtian) of Alaska. *Canadian Journal of Earth Sciences*, *48*(9), 1342-1354.

Brown, C. M., Evans, D. C., Campione, N. E., O'Brien, L. J., & Eberth, D. A. (2013). Evidence for taphonomic size bias in the Dinosaur Park Formation (Campanian, Alberta), a model Mesozoic terrestrail alluvial-paralic system. *Palaeogeography, palaeoclimatology, palaeoecology*, 372 (S1), 180-122. https://doi.org/10.1016/j.palaeo.2012.06.027

Brown, C. M., Evans, D. C., Ryan, M. J., & Russell, A. P. (2013). New data on the diversity and abundance of small-bodied ornithopods (Dinosauria, Ornithischia) from the Belly, River Group (Campanian) of Alberta. *Journal of vertebrate paleontology*, 33(3), 495-520. https://doi.org/10.1080/02724634.2013.746229

Butler, R. J., Jin, L., Chen, J., & Godefroit, P. (2011). The postcranial osteology and phylogenetic position of the small ornithischian dinosaur *Changchunsaurus parvus* from the Quantou Formation (Cretaceous, Aptian-Cenomanian) of Jilin Provine, north-eastern China. *Palaeontology*, 54(3), 667-683. https://doi.org/10.1111/j.1475-4983.2011.01046.x

Button, D. J. & Zanno, L. E. (2023). Neuroanatomy of the late Cretaceous *Thescelosaurus neglectus* (Neornithischia: Thescelosauridae) reveals novel ecological specialisations within Dinosauria. Scientific Reports, 13(1), 19224-19224. https://doi.org/10.1038/s41598-023-45658-3

Carpenter, K., & Wilson, Y. (2008). A new species of *Camptosaurus* (Ornithopoda: Dinosauria) from the Morrison Formation (Upper Jurassic) of Dinosaur National Monument, Utah, and a biomechanical analysis of its forelimb. *Annals of Carnegie Museum*, 76(4), 227-

263.

Carpenter, K., & Galton, P. (2018). A photo documentation of bipedal ornithischian dinosaurs from the Upper Jurassic Morrison Formation, USA. *Geology of the Intermountain West*, 5, 167-207.

Chanthasit, P. (2010). *The ornithopod dinosaur Rhabdodon from the Late Cretaceous of France: anatomy, systematics and paleobiology* (Doctoral dissertation, Université Claude Bernard-Lyon I).

Chin, K. (2007). The paleobiological implications of herbivorous dinosaur coprolites from the Upper Cretaceous Two Medicine Formation of Montana: why eat wood?. *Palaios*, 22(5), 554-566.

Cooper, M. R. 1985. A revisoin of the ornithischian dinosaur *Kangnasaurus coetzeei* Haughton, with classification of the Ornithischia. *Annals of the South African Museum*. 95, 281-317.

Coria, R. A., & Salgado, L. (1996). A basal iguanodontian (Ornithischia: Ornithopoda) from the Late Cretaceous of south America. *Journal of Vertebrate Paleontology*, 16(3), 445-457.

Coria, R. A., & Calvo, J. O. (2002). A new iguanodontian ornithopod from Neuquén Basin, Patagonia, Argentina. *Journal of Vertebrate Paleontology*, *22*(3), 503-509.

Coria, R. A., Moly, J. J., Reguero, M., Santillana, S., & Marenssi, S. (2013). A new ornithopod (Dinosauria; Ornithischia) from Antarctica. *Cretaceous Research*, *41*, 186-193.

Cruzado-Caballero, P., Gasca, J. M., Filippi, L. S., Cerda, I. A., & Garrido, A. C. (2019). A new ornithopod dinosaur from the Santonian of Northern Patagonia (Rincón de los Sauces, Argentina). *Cretaceous Research*, *98*, 211-229.

Druckenmiller, P. S., Erickson, G. M., Brinkman, D., Brown, C. M., & Eberle, J. J. (2021). Nesting at extreme polar latitudes by non-avian dinosaurs. *Current Biology*, 31(16), 3469-3478.

Dyer, A., Powers, M., & Currie, P. (2022). Problematic putative pachycephalosaurids: Synchrotron μCT imaging shines new light on the anatomy and taxonomic validity of *Gravitholus albertae* from the Belly River Group (Campanian) of Alberta, Canada. *Vertebrate Anatomy Morphology Palaeontology*, *10*(1).

Dzik, J. (2003). A beaked herbivorous archosaur with dinosaur affinities from the early Late Triassic of Poland. *Journal of Vertebrate Paleontology*, *23*(3), 556-574.

Evans, D. C., Williamson, T., Loewen, M. A., & Kirkland, J. I. (2013). Review of pachycephalosaurian dinosaurs from Grand Staircase-Escalante National Monument, southern Utah. *At the Top of Grant Staircase: The Late Cretaceous of Southern Utah*, 482-487.

Evans, D. C., Vavrek, M. J., & Larsson, H. C. (2015). Pachycephalosaurid (Dinosauria: Ornithischia) cranial remains from the latest Cretaceous (Maastrichtian) Scollard Formation of Alberta, Canada. *Palaeobiodiversity and Palaeoenvironments*, *95*, 579-585.

Forster, C. A., de Klerk, W. J., Poole, K. E., Chinsamy-Turan, A., Roberts, E. M., & Ross, C. F. (2023). *Iyuku raathi*, a new iguanodontian dinosaur from the Early Cretaceous Kirkwood Formation, South Africa. *The Anatomical Record*, 306(7), 1762-1803.

Fowler, D. W. (2017). Revised geochronology, correlation, and dinosaur stratigraphic ranges of the Santonian-Maastrichtian (Late Cretaceous) formations of the Western Interior of North America. *PloS one*, *12*(11), e0188426.

Freimuth, W. J., & Varricchio, D. J. (2019). Insect trace fossils elucidate depositional environments and sedimentation at a dinosaur nesting site from the Cretaceous (Campanian) Two Medicine Formation of Montana. *Palaeogeography, Palaeoclimatology, Palaeoecology,* 534, 109262.

Freimuth, W. J., Varricchio, D. J., & Chin, K. (2021). Paleoenvironmental implications of invertebrate fecal pellets (Edaphichnium isp.) at an ichnofossil-rich dinosaur nesting locality, Upper Cretaceous Two Medicine Formation, Montana, USA. *Palaios*, 36(9), 283-300.

Fricke, H. C., Foreman, B. Z., & Sewall, J. O. (2010). Integrated climate model-oxygen isotope evidence for a North American monsoon during the Late Cretaceous. *Earth and Planetary Science Letters*, 289(1-2), 11-21.

Fuentes, F., DeCelles, P. G., & Constenius, K. N. (2012). Regional structure and kinematic history of the Cordilleran fold-thrust belt in northwestern Montana, USA. *Geosphere*, 8(5), 1104-1128.

Galton, P. M., & Jensen, J. A. (1973). Skeleton of a hypsilophodontid dinosaur (*Nanosaurus* (?) *rex*) from the Upper Jurassic of Utah. *Brigham Young University Geology Studies*, 20(4), 137-157.

Galton, P. M. (1975). The ornithischian dinosaur *Hypsilophodon* from the Wealden of th Isle of Wight. Bulletin of the British Museum (Natural History) Geology, 25(1), 1-152.

Galton, P. M. (1978). Fabrosauridae, the basal family of ornithischian dinosaurs (Reptilia: Ornithopoda). *Paläontologische Zeitschrift*, 52(1), 138-159.

Galton, P. M. (1981). *Dryosaurus*, a hypsilophodontid dinosaur from the Upper Jurassic of North America and Africa postcranial skeleton. *Paläontologische Zeitschrift*, 55(3), 271-312.

Galton, P. M., & Taquet, P. (1982). *Valdosaurus*, a hypsilophodontid dinosaur from the Lower Cretaceous of Europe and Africa. *Geobios*, 15(2), 147-159.

Gates, T. A., Lund, E. A., Boyd, C. A., DeBlieux, D. D., Titus, A. L., Evans, D. C., Getty, M. A., Kirkland, J. I., & Eaton, J. G. (2013). Ornithopod Dinosaurs from the Grand Staircase-Escalante National Monument Region, Utah, and Their Role in Paleobiogeographic and Macroevolutionary Studies. In (pp. 463). Indiana University Press.

Gilmore, C. W. (1913). A new dinosaur from the Lance Formation of Wyoming: Smithson. *Misc. Coll*, 61, 1-5.

Gilmore, C. W. (1915). Osteology of *Thescelosaurus*, an orthopodous dinosaur from the Lance Formation of Wyoming. *Proceedings of the United States National Museum*.

Gilmore, C. W. (1924). A new species of *Laosaurus*, an ornithischian dinosaur from the Cretaceous of Alberta. Royal Society of Canada.

Godefroit, P., Sinitsa, S. M., Dhouailly, D., Bolotsky, Y. L., Sizov, A. V., McNamara, M. E., ... & Spagna, P. (2014). A Jurassic ornithischian dinosaur from Siberia with both feathers and scales. *Science*, 345(6195), 451-455.

Han, F., Barrett, P. M., Butler, R. J., & Xu, X. (2012). Postcranial anatomy of *Jeholosaurus shangyuanensis* (Dinosauria, Ornithischia) from the Lower Cretaceous Yixian Formation of China. *Journal of Vertebrate Paleontology*, 32(6), 1370-1395.

Hannebaum, Z. J., Varricchio, D. J., and Krumenacker, L. J. (2023). Beneath the feet of giants: a case study of the population dynamics of *Oryctodromeus cubicularis* and *Orodromeus*

makelai, two potential burrowing dinosaurs. 83rd Annual Meeting – Society of Vertebrate Paleontology, Cincinnati, Ohio.

Hannebaum, Z. J., Varricchio, D. J., Scheetz, R., Brown, C. M., and Avrahami, H. M. (2024). The three species problem: a revise look at the systematics and phylogenetic relationships of neornithischian dinosaurs in the Upper Cretaceous Two Medicine Formation of northcentral Montana. 84rd Annual Meeting – Society of Vertebrate Paleontology

Hannebaum, Z. J., Varricchio, D. J., Scheetz, R., Brown, C. M., and Avrahami, H. (2024). The three species problem: a revised look at the systematics and phylogenetic relationships of neornthischian dinosaurs in the Upper Cretaceous Two Medicine Formation of northcentral Montana. *Journal of Vertebrate Paleontology Program Abstracts*, (2024).

He, X. L., & Cai, K. (1984). The Middle Jurassic Dinosaurian Fauna from Dashanpu, Zigong, Sichuan. Vol 1, The Ornithopod Dinosaurs. *Chengdu: Sichuan Scientific and Technological Publishing House*, 71, 1-66.

Herne, M. C., Tait, A. M., Weisbecker, V., Hall, M., Nair, J. P., Cleeland, M., & Salisbury, S. W. (2018). A new small-bodied ornithopod (Dinosauria, Ornithischia) from a deep, high-energy Early Cretaceous river of the Australian–Antarctic rift system. *PeerJ*, *5*, e4113.

Horner, J. R., & Weishampel, D. B. (1988). A comparative embryological study of two ornithischian dinosaurs. *Nature*, 332(6161), 256-257.

Horner, J. R., Schmitt, J. G., Jackson, F. D., & Hanna, R. (2001). Bones and rocks of the Upper Cretaceous Two Medicine-Judith River clastic wedge complex. *In Guidebook for the Field Trips, Society of Vertebrate Paleontology 61st Annual Meeting, Montana*. Museum of the Rockies Occasional Paper (No. 3, pp. 1-14).

Horner, J. R., Goodwin, M. B., & Myhrvold, N. (2011). Dinosaur census reveals abundant Tyrannosaurus and rare ontogenetic stages in the Upper Cretaceous Hell Creek Formation (Maastrichtian), Montana, USA. *PLoS One*, *6*(2), e16574.

Horner, J. R., Goodwin, M. B., & Evans, D. C. (2022). A new pachycephalosaurid from the Hell Creek Formation, Garfield County, Montana, USA. *Journal of Vertebrate Paleontology*, *42*(4), e2190369.

Hudgins, M. N. (2021*). The Paleobiology, Paleoecology, and Evolution of Thescelosauridae (Ornithischia) from Alberta, Canada*. University of Alberta.

Hudgins, M. N., Currie, P. J., & Sullivan, C. (2022). Dental assessment of *Stegoceras validum* (Ornithischia: Pachycephalosauridae) and *Thescelosaurus neglectus* (Ornithischia: Thescelosauridae): paleoecological inferences. *Cretaceous Research*, *130*, 105058.

Huh, M., Lee, D.-G., Kim, J.-K., Gwangju, Lim, J.-D., Daejeon, & Godefroit, P. (2010). A new basal ornithopod dinosaur from the Upper Cretaceous of South Korea. *Neues Jahrbuch für Geologie und Paläontologie. Abhandlungen, 259(1), 1-24.*, *259*, 1-24. https://doi.org/10.1127/0077-7749/2010/0102

Huxley, T. H. (1870). On *Hypsilophodon foxii*, a new dinosaurian from the Wealden of the Isle of Wight. *Quarterly Journal of the Geological Society*, 26(1-2), 3-12.

Ibiricu, L. M., Martínez, R. D., Luna, M., & Casal, G. A. (2014). A reappraisal of *Notohypshilophodon comodorensis* (Ornithischia: Ornithopoda) from the Late Cretaceous of Patagonia, Argentina. *Zootaxa*, 3786 (4), 401-422.

Jerzykiewicz, T., & Norris, D. K. (1994). Stratigraphy, structure and syntectonic sedimentation of the Campanian'Belly River'clastic wedge in the southern Canadian Cordillera. *Cretaceous Research*, *15*(4), 367-399.

Jin, L., Jun, C., Zan, S., Butler, R. J., & Godefroit, P. (2010). Cranial anatomy of the small ornithischian dinosaur *Changchunsaurus parvus* from the Quantou Formation (Cretaceous, Aptian-Cenomanian) of Jilin Province, northeastern China. Journal of vertebrate paleontology, 30(1), 196-214. https://doi.org/10.1080/02724630903412372

Kauffman, E. G. (1977). Geological and biological overview: Western Interior Cretaceous basin. The Mountain Geologist.

Krumenacker, L. J. (2017). *Osteology, phyloheny, taphonomy, and ontogenetic histology of Oryctodromeus cubicularis, from the middle Cretaceous (Albian-Cenomanian) of Montana and Idaho*. Montana State Univerisity – Bozeman, College of Letters and Science.

Krumenacker, L. J., Varricchio, D., J., Organ, C., Gardner, J. D., Britt, B. B., & Boyd, C. (2024). Osteology and phylogenetic relationships of the mid-Cretaceous neornithischian dinosaur *Oryctodromeus cubicularis* Varricchio, 2007. Journal of Vertebrate Paleontology. https://doi.org/10.1080/027724634.2024.2330581

Kutter, M. M. (2004). *New material of Zephyrosaurus schaffi (Dinosauria; Ornithischia) from the Cloverly Formation (Aptian-Albian) of Montana and the phylogeny of Hypsilophodontidae*. College of the Pacific – Stockton, Department of Biological Scienece.

Lageson, D. R., Schmitt, J. G., Horton, B. K., Kalakay, T. J., & Burton, B. R. (2001). Influence

of Late Cretaceous magmatism on the Sevier orogenic wedge, western Montana. *Geology*, 29(8), 723-726.

Lorenz, J. & Gavin, W. (1984). *Geology of the Two Medicine Formation and the sedimentology of a dinosaur nesting ground*. Montana Geological Society Field Conference Northwestern Montana.

Li, N., Dai, H., Tan, C., Hu, X., Wei, Z., Lin, Y., Wei, G., Li, D., Meng, L., Hao, B., You, H., & Peng, G. (2021). A neornithischian dinosaur from the Middle Jurassic Xintiangou Formation of Yunyang, Chongquing, China: the earliest record in Asia. Historical Biology, 33(7), 1089-1102. https://doi.org/10.1080/08912963.2019.1679129Maidment, S. C., & Barrett, P. M. (2011). The locomotor musculature of basal ornithischian dinosaurs. *Journal of Vertebrate Paleontology*, 31(6), 1265-1291.

Makovicky, P. J., Kilbourne, B. M., Sadleir, R. W., & Norell, M. A. (2011). A new basal ornithopod (Dinosauria, Ornithischia) from the Late Cretaceous of Mongolia. *Journal of Vertebrate Paleontology*, 31(3), 626-640. https://doi.org/10.1080/02724634.2011.557114

Mallon, J. C., Evans, D. C., Tokaryk, T. T., & Currie, M. L. (2015). First pachycephalosaurid (Dinosauria: Ornithischia) from the Frenchman Formation (upper Maastrichtian) of Saskatchewan, Canada. *Cretaceous Research*, *56*, 426-431.

Manitkoon, S., Deesri, U., Khalloufi, B., Nonsrirach, T., Suteethorn, V., Chanthasit, P., ... & Buffetaut, E. (2023). A New Basal Neornithischian Dinosaur from the Phu Kradung Formation (Upper Jurassic) of Northeastern Thailand. *Diversity*, 15(7), 851.

Morris, W. J. (1976). Hypsilophodont dinosaurs: a new species and comments on their systematics. *Athlon: essays on Palaeontology in Honour of Loris Shano Russell. Toronto: Royal Ontario Museum*, 93-113.

Maryanska, T. E. R. E. S. A., & Osmólska, H. (1974). Pachycephalosauria, a new suborder of ornithischian dinosaurs. *Palaeontologia Polonica*, 30, 45-102.

Matson, C. C. (2010). *Paleoenvironments of the Upper Cretaceous Dinosaur Park Formation in southern Alberta, Canada* (Doctoral dissertation, University of Calgary, Department of Geoscience).

Matheron P. 1869. Notice sur les reptiles fossiles des dépôts fluvio-lacustres crétacés du bassin à lignite de Fuveau. In: *Mémoires de l'Académie des Sciences, Belles-Lettres, et Arts de Marseille 1868–1869*. 345–379.

Mayo, K., Silva, R. L., & Durkin, P. R. (2023). Paleoenvironmental reconstruction of Late Cretaceous rivers, Dinosaur Park Formation, Alberta, Canada. *Sedimentary Geology*, 457, 106499.

Moore, B. R. S. (2021). *The postcranial anatomy of pachycephalosaurs (Ornithischia: Pachycephalosauria) and its phylogenetic and myological implications* (Doctoral dissertation, Carleton University).

Morschhauser, E. M., Li, D., You, H., & Dodson, P. (2018). Cranial Anatomy of the Basal Neoceratopsian *Auroraceratops* rugosus (Ornithischia: Ceratopsia) from the Yujingzi Basin, Gansu Province, China. *Journal of Vertebrate Paleontology*, 38(sup1), 36-68.

Morschhauser, E. M., You, H., Li, D., & Dodson, P. (2018). Postcranial morphology of the basal neoceratopsian (Ornithischia: Ceratopsia) Auroraceratops rugosus from the Early

Cretaceous (Aptian–Albian) of northwestern Gansu Province, China. *Journal of Vertebrate Paleontology*, *38*(sup1), 75-116.

Norman, D. B., Sues, H. -D., Witmer, L. M., & Coria, R. A. (2004). Basal Ornithopoda. In D. B. Weishampel, P. Dodson, and H. Osmólska (editors), The Dinosauria: 413-437. Berkeley: Unversity of California Press.

Norman, D. B., Crompton, A. W., Butler, R. J., Porro, L. B., & Charig, A. J. (2011). The Lower Jurassic ornithischian dinosaur *Heterodontosaurus tucki* Crompton & Charig, 1962: cranial anatomy, functional morphology, taxonomy, and relationships. *Zoological Journal of the Linnean Society*, 163(1), 182-276.

Owens, R. 1842. Report on British fossil reptiles. Part II. *Report for the British Association for the Advancement of Science*, 11, 60-204.

Pol, D., Rauhut, O. W., & Becerra, M. (2011). A Middle Jurassic heterodontosaurid dinosaur from Patagonia and the evolution of heterodontosaurids. *Naturwissenschaften*, 98, 369-379.

Porro, L. B., Witmer, L. M., & Barrett, P. M. (2015). Digital preparation and osteology of the skull of *Lesothosaurus diagnosticus* (Ornithischia: Dinosauria). *PeerJ*, 3, e1494.

Ramezani, J., Beveridge, T. L., Rogers, R. R., Eberth, D. A., & Roberts, E. M. (2022). Calibrating the zenith of dinosaur diversity in the Campanian of the Western Interior Basin by CA-ID-TIMS U-Pb geochronology. *Scientific Reports*, 12(1). 16026-16026. https://doi.org/10.1038/s41598-022-19896-w.

Rich, T. H., Galton, P. M., & Vickers-rich, P. (2010). The holotype individual of the ornithopod dinosaur *Leaellynasaura amicagraphica* Rich & Rich, 1989 (late Early Cretaceous,

Victoria, Australia). *Alcheringa: An Australasian Journal of Palaeontology*, 34(3), 385-396.

Rogers, R. R. (1990). Taphonomy of three dinosaur bone beds in the Upper Cretaceous Two Medicine Formation of northwestern Montana: evidence for drought-related mortality. *Palaios*, 394-413.

Rogers, R. R., Swisher, C. C. III, & Horner, J. R. (1993). $^{40}Ar/^{39}Ar$ ad correlation of the nonmarine Two Medicine Formation (Upper Cretaceous), northwestern Montana, U.S.A. *Canadian journal of earth sciences*, 30(5), 1066-1075.

Rogers, R., Horner, J., Ramezani, J., Roberts, E., and Varricchio. D. (2024). Updating the Upper Cretaceous (Campanian) Two Medicine Formation of Montana: Lithostratigraphic revisions, new CA-ID-TIMS U-Pb ages, and a calibrated framework of dinosaur occurances. *The Geologial Society of America Bulletin*.

Rozadilla, S., Agnolin, F. L., Novas, F. E., Rolando, A. M. A., Motta, M. J., Lirio, J. M., & Isasi, M. P. (2016). A new ornithopod (Dinosauria, Ornithischia) from the Upper Cretaceous of Antarctica and its palaeobiogeographical implications. *Cretaceous Research*, *57*, 311-324.

Rozadilla, S., Agnolín, F. L., & Novas, F. E. (2019). Osteology of the Patagonian ornithopod *Talenkauen santacrucensis* (Dinosauria, Ornithischia). *Journal of Systematic Palaeontology*, *17*(24), 2043-2089.

Rozadilla, S., Cruzado-Caballero, P., & Calvo, J. O. (2020), Osteology of Ornithopod *Macrogryphosaurus gondwanicus* (Dinosauris, Ornithischia) from the Upper Cretaceous of Patagonia, Argentina. *Cretacesous research*, 108, 104311.

Ruiz-Omeñaca, J. I., Canudo, J. I., Cuenca-Bescós, G., Cruzado-Caballero, P., Gasca, J. M., & Moreno-Azanza, M. (2012). A new basal ornithopod dinosaur from the Barremian of Galve, Spain. *Comptes Rendus Palevol*, 11(6), 435-444.

Russell, L. S. (1949). The relationships of the Alberta Cretaceous dinosaur" *Laosaurus*" *minimus* Gilmore. *Journal of Paleontology*, 518-520.

Ryan, M. J., Evans, D. C., Currie, P. J., Brown, C. M., & Brinkman, D. (2012). New leptoceratopsids from the upper Cretaceous of Alberta, Canada. *Cretaceous Research*, *35*, 69-80.

Ryan, M.J. L. Micucci, H. Rizo, C. Sullivan, Y.-N. Lee, and D. C. Evans. 2023. A new Late Cretaceous leptoceratopsid (Dinosauria: Ceratopsia) from the Oldman Formation (Campanian) of Alberta, Canada. In Y.-N. Lee, Ed., Windows into Sauropsid and Synapsid Evolution: Essays in Honor of Prof. Louis L. Jacobs, pp. 151-165. Dinosaur Science Center Press: Hwaseong City, South Korea.

Salgado, L., Coria, R. A., & Heredia, S. E. (1997). New materials of *Gasparinisaura cincosaltensis* (Ornithischia, Ornithopoda) from the Upper Cretaceous of Argentina. *Journal of Paleontology*, 71(5), 933-940.

Salgado, L., Canudo, J. I., Garrido, A. C., Moreno-Azanza, M., Martínez, L. C., Coria, R. A., & Gasca, J. M. (2017). A new primitive Neornithischian dinosaur from the Jurassic of Patagonia with gut contents. *Scientific Reports*, 7(1), 1-10.

Sampson, S. D. (1995). Two new horned dinosaurs from the Upper Cretaceous Two Medicine Formation of Montana; with a phylogenetic analysis of the Centrosaurinae (Ornithischia: Ceratopsidae). *Journal of vertebrate paleontology*, 15(4), 743-760.

Santa Luca, A. P. (1980). The postcranial skeleton of *Heterodontosaurus tucki* (Reptilia, Ornithischia) from the Stormberg of South Africa. Annals of the South African Museum. 79: 159-211.

Scheetz, R. D. (1999). *Osteology of Orodromeus makelai and the phylogeny of basal ornithopod dinosaurs*. Montana State University-Bozeman.

Schott, R. K., Evans, D. C., Williamson, T. E., Carr, T. D., & Goodwin, M. B. (2009). The anatomy and systematics of *Colepiocephale lambei* (Dinosauria: Pachycephalosauridae). *Journal of Vertebrate Paleontology*, *29*(3), 771-786.

Schott, R. K., & Evans, D. C. (2017). Cranial variation and systematics of *Foraminacephale brevis* gen. nov. and the diversity of pachycephalosaurid dinosaurs (Ornithischia: Cerapoda) in the Belly River Group of Alberta, Canada. *Zoological Journal of the Linnean Society*, *179*(4), 865-906.

Seeley H. G. 1887. On the classification of the fossil animals commonly named Dinosauria. *Proceedings of the Royal Society of London*, 43, 481-494.

Sereno, P. C. (2012). Taxonomy, morphology, masticatory function and phylogeny of heterodontosaurid dinosaurs. *ZooKeys*, (226), 1.

Sereno, P. C., & Novas, F. E. (1994). The skull and neck of the basal theropod *Herrerasaurus ischigualastensis*. *Journal of Vertebrate Paleontology*, 13(4), 451-476.

Sharp, A. C., Siu, K., & Rich, T. H. (2017). Revealing the skeleton of the polar dinosaur *Leaellynasaura amicagraphica* using synchrotron computed tomography. In *Society of Vertebrate Paleontology 77th Annual Meeting, Meeting Program and Abstracts* (Vol. 193).

Sternberg, C. M. 1937. A classification of *Thescelosaurus*, with a description of a new species. *Geological Society of America, Proceedings and Abstracts*, 1936-375.

Sues, H. D. (1980). Anatomy and relationships of a new hypsilophodontid dinosaur from the Lower Cretaceous of North America. *Palaeontographica. Abt. A, Palaozoologie-Stratigraphie*, 169, 51-72.

Sues, H. D., Evans, D. C., Galton, P. M., & Brown, C. M. (2023). Anatomy of the neornithischian dinosaur *Parksosaurus warreni* (Parks, 1926) from the Upper Cretaceous (lower Maastrichtian) Horseshoe Canyon Formation of Alberta, Canada. *Cretaceous Research*, 141, 105369.

Sullivan, R. M. (2006). A taxonomic review of the Pachycephalosauridae (Dinosauria: Ornithischia). *New Mexico Museum of Natural History and Science Bulletin*, *35*(47), 347-365.

Varricchio, D. J. (2002). A new bird from the Upper Cretaceous Two Medicine Formation of Montana. *Canadian Journal of Earth Sciences*, 39(1), 19-26.

Varricchio, D. J., Martin, A. J., & Katsura, Y. (2007). First trace and body fossil evidence of a burrowing, denning dinosaur. *Proceedings of the Royal Society. B, Biological sciences*, 274(1616), 1361-1368. https://doi.org/10.1098/rspb.2006.0443.

Verdú, F. J., Royo-Torres, R., Cobos, A., & Alcalá, L. (2018). New systematic and phylogenetic data about the early Barremian *Iguanodon galvensis* (Ornithopoda: Iguanodontoidea) from Spain. *Historical Biology*, 30(4), 437-474.

Weishampel, D. B., & Heinrich, R. E. (1992). Systematics of hypsilophodontidae and basal Iguanodontia (Dinosauria: Ornithopoda). *Historical Biology*, 6(3), 159-184.

Weishampel, D. B., Jianu, C. M., Csiki, Z., & Norman, D. B. (2003). Osteology and phylogeny of *Zalmoxes* (n.g.), an unusual euornithopod dinosaur from the latest Cretaceous of Romania. *Journal of Systematic Palaeontology*, *1*(2), 65-123.

Wilson, J. A. (2006). Anatomical nomenclature of fossil vertebrates: standardized terms or 'lingua franca'?. *Journal of Vertebrate Paleontology*, 26(3), 511-518.

Wolff, E., & Horner, J. R. (2003). The first occurrence of *Orodromeus makelai* postcrania from the Late-Campanian Judith River Formation of eastern Montana. *Journal of Vertebrate Paleontology*, 23(3), 122.

Woodruff, D. C. (2022). *New insights into pachycephalosaurian (Dinosauria: Ornithischia) anatomy, functional morphology, and evolution* (Doctoral dissertation, University of Toronto (Canada)).

Woodruff, D. C., Schott, R. K., & Evans, D. C. (2023). Two new species of small-bodied pachycephalosaurine (Dinosauria, Marginocephalia) from the uppermost Cretaceous of North America suggest hidden diversity in well-sampled formations. *Papers in Palaeontology*, *9*(6), e1535.

Xu, X., Forster, C. A., Clark, J. M., & Mo, J. (2006). A basal ceratopsian with transitional features from the Late Jurassic of northwestern China. *Proceedings of the Royal Society B: Biological Sciences*, 273(1598), 2135-2140.

Yang, Y., Wu, W., Dieudonné P.-E., & Godefroit, P. (2020). A new basal ornithopod dinosaur from the Lower Cretaceous of China. PeerJ (San Francisco, CA), 8, e9832-e9832. https://doi.org/10.7717/peerj.9832

Zanno, L. E., Gates, T. A., Avrahami, H. M., Tucker, R. T., & Makovicky, P. J. (2023). An early-

diverging iguanodontian (Dinosauria: Rhabdodontomorpha) from the Late Cretaceous of North America. *Plos one*, 18(6), e0286042.

Zheng, W., Jin, X., Shibata, M., Azuma, Y., & Yu, F. (2012). A new ornithischian dinosaur from the cretaceous Liangtoutang formation of Tiantai, Zhejiang Province, China. *Cretaceous Research*, *34*, 208-219.

CHAPTER FOUR

THE OSTEOLOGY OF *ORODROMEUS MAKELAI* AND A REVIEW OF ORODROMINE SYSTEMATICS

Contribution of Authors and Co-Authors

Manuscript in Chapter 4

Author: Zakaria Hannebaum

Conceived the study, performed analyses, interpreted results, and wrote the manuscript.

Co-Author: Brendan Clark

Contributions: Performed segmentation of CT imagery

Co-Author: David J. Varricchio

Contributions: Conceived the study, discussed results and implications, and edited manuscript drafts.

Co-Author: Rodney Scheetz

Contributions: Provided preliminary descriptions of specimens, edited manuscript drafts.

Co-Author: Caleb Brown

Contributions: Provided access and preliminary descriptions of specimens, discussed results and implications, edited manuscript drafts.

Co-Author: Haviv Avrahami

Contributions: Procured CT imaging of MOR 294, 1136, and 1141, aided in phylogenetic analysis, edited manuscript drafts.

Manuscript Information

Zakaria J. Hannebaum, Brenan Clark, David J. Varricchio, Rodney Scheetz, Caleb Brown, and Haviv Avrahami.

Journal of Vertebrate Paleontology

☒ Prepared for submission to a peer-reviewed journal
☐ Officially submitted to a peer-reviewed journal
☐ Accepted by a peer-reviewed journal
☐ Published in a peer-reviewed journal

Abstract

Orodromines are a group of small bodied early diverging ornithischians which proliferated rapidly in northern Laramidia during the Campanian but disappeared just as quickly prior to the climax of the Bearpaw Sea transgression. *Orodromeus makelai* is the most well-sampled orodromine, as hundreds of non-tooth specimens have been assigned to this taxon from the Two Medicine Formation. For forty years, all orodromine skeletal material collected in the Two Medicine fell under the taxonomic purview of *Orodromeus makelai*. The recent recognition of a new orodromine, *Pikunidromeus ancellae*, from material once considered *Orodromeus makelai*, warrants revisiting the rest of the assemblage. *Orodromeus makelai* lacks a published osteology, and instead much of the published acknowledgements of this taxon rely on an unpublished doctoral thesis. Exacerbating osteological uncertainties, the only published description for *Orodromeus makelai* is its initial description, which is limited, focused on juvenile skeletal material, and erroneously includes troodontid embryonic material. Here we present an updated diagnosis for *Orodromeus makelai* and demonstrate its temporal restriction to the lacustrine interval of the Flagg Butte Member of the Two Medicine Formation, with no obvious overlap with any other orodromines in the formation. We also provide comments on a pervasive problem plaguing Orodrominae systematics, the proliferation of informal taxa. We broadly survey these taxa/specimens within a new systematic framework constrained here for *Orodromeus makelai* and other recently described orodromines.

Introduction

Orodromeus makelai is a pivotal early diverging ornithischian taxon upon which much of the anatomical, taxonomic, and phylogenetic consensus pertaining to the early evolution of ornithischian (hereafter SBEDO, sensu Avrahami et al., 2024) lineages hinges. However, the lack of a published description (Scheetz, 1999) creates significant inconsistencies in character coding and facilitates the persistence of an informal *Orodromeus* osteology to pervade phylogenetic and osteological analyses. Furthermore, the only published diagnosis for *Orodromeus makelai* leans heavily on juvenile materials (Horner and Weishampel, 1988) dated in the modern SBEDO context, and further muddied by the inclusion of egg and embryonic material, which were later rectified as troodontid (Weishampel and Horner, 1996). Hundreds of non-tooth specimens collected over the last 40 years from the Two Medicine Formation in northcentral Montana fall under the taxonomic purview of *Orodromeus*; however, recent work contradicts this monospecific designation for some of the Two Medicine orodromine assemblage (Chapter 3). An updated chronostratigraphic framework for the Two Medicine Formation (Rogers et al., 2025) demonstrates distinct temporally restricted orodromine morphotypes in the assemblage. *Pikunidromeus ancellae* represents the youngest morphotype in the Two Medicine Formation, restricted to the Flagg Butte Member above the lacustrine interval, while *Orodromeus makelai* specimens are constrained to only the lacustrine interval. Furthermore, another informal taxon represented only by jugal horns called the “BV Orodromine” overlaps with *Pikunidromeus* at site TM-088 and illustrates a pervasive problem with orodromine taxonomy, the prevalence of informal taxon names. Here we reevaluate *Orodromeus makelai*, presenting an updated diagnosis, and perform a systematic review of orodromine informal and problematic taxa like the

aforementioned “BV Orodromine”, the “Kaiparowits Orodromine” (Boyd, 2012), the fragmentary *Albertadromeus syntarsus* (Brown et al., 2013), and the likely dubius *Laosaurus minimus* (Gilmore, 1924). We also revisit indeterminate specimens presented by Brown et al. (2013) and resolve some taxonomic affinities there.

Materials and methods

SBEDOs is an acronym which stands for small-bodied early diverging ornithischians. It was recently coined by Avrahami et al. (2024) and references a “grade” of distantly related early diverging ornithischian lineages exhibiting similar body plans (i.e. bipedal, small-bodied, similar dentition, etc.), this “grade” does not include marginocephalians or thyreophorans. Over the years, other researchers have used different terms to describe such dinosaurs calling them “Fabrosaurids” (Galton, 1978), “Hypsilophodontids” (Weishampel and Heinrich, 1992), or “basal ornithopods” (Norman et al., 2004). Unlike the SBEDOs acronym, these earlier terms tried to group unrelated taxa within a phylogenetic context. We follow the naming schemes denoted in Brochu (1996) for vertebral ossification when describing vertebral fusion. Anatomy is discussed using the Romerian anatomical and directional terms for fossil vertebrates, in preference of veterinarian terms like rostral or caudal to limit misunderstandings (Wilson, 2006) as rostral bones are a derived feature of ceratopsians, which thescelosaurids lack.

We follow the naming schemes denoted in Brochu (1996) for vertebral ossification types when describing vertebral fusion. Anatomy is discussed using the Romerian anatomical and directional terms for fossil vertebrates, in preference of veterinarian terms like rostral or caudal to limit misunderstandings (Wilson, 2006) as rostral bones are a derived feature of ceratopsians, which thescelosaurids lack. The supraorbitals are often referred to as palpebrals in early

diverging ornithischians dinosaurs (Coria and Salgado, 1996; Norman et al., 2011, Xu et al., 2006). We follow Barta and Norell (2021), sensu Salgado et al. (2017), and refer to the palpebrals as supraorbitals, specifically the anterior supraorbital and posterior supraorbital (respectively =accessory supraorbital; and =postpalpebral). Specimens are defined here as any independent occurrence of an individual represented from a single non-toothed element to associated skeletal materials.

The specimens discussed here are curated, and accessed, at the Museum of the Rockies in Bozeman, Montana, United States. Specimens in this study were digitally imaged using the photogrammetry application called Abound (v. 3.0.0) on an iPhone 13 Mini and 16 Pro Max, using a macro-lens at times, following the workflow outlined by Avrahami et al. (2023). The MOR's Creaform model Go!SCAN 20 supplemented Abound in digitally imaging some elements and meshes were processed in VXelements v.11. Digital models were assembled in Blender v.4.3. The geological map was created using QGIS (v. 3.34.1) with GIS data sourced from the Montana Bureau of Mines and Geology, Montana State Library, Canadian Census, and geoBoundaries.org. Adobe Photoshop v.25.12 and Illustrator v.28.7.1 were employed to create final versions of some figures.

Institutional Abbreviations

BYU, Brigham Young University, Provo, Utah, United States; **CMN,** Canadian Museum of Nature; **IGM**, Institute of Geology, Mongolian Academy of Sciences, Ulaan Baatar, Mongolia; **IMNH**, Idaho Museum of Natural History, Pocatello, Idaho, United States; **IVPP,** Institute of Vertebrate Paleontology and Paleoanthropology, Beijing, China; **LACM**, Los Angeles County Museum of Natural History, Los Angeles, California, United States; **MCZ**,

Museum of Comparative Zoology, Harvard University, Cambridge, Massachusetts, United States; **MOR**, Museum of the Rockies, Bozeman, Montana, United States; **NCSM**, North Carolina Science Museum, Raleigh, North Carolina, United States; **NHMUK**, The Natural History Museum, London, United Kingdom; **NMV**, Museums Victoria (formerly, National Museum of Victoria), Melbourne, Victoria, Australia; **OMNH**, Oklahoma Museum of Natural History, Norman, Oklahoma, United States; **PU**, Princeton University, Princeton, New Jersey, United States; **ROM**, Royal Ontario Museum, Toronto, Canada; **RSM**, Royal Saskatchewan Museum, Regina, Saskatchewan, Canada; **TMP**, Royal Tyrrell Museum of Paleontology, Drumheller, Alberta, Canada; **USNM**, United States National Museum, Washington, D. C., United States; **YPM**, Yale Peabody Museum, New Haven, Connecticut, United States.

Systematic Paleontology

DINOSAURIA Owen, 1842

ORNITHISCHIA Seeley, 1887

NEORNITHISCHIA Cooper, 1985 (sensu Madzia et al., 2021)

THESCELOSAURIDAE Sternberg, 1937 (sensu Madzia et al., 2021)

ORODROMINAE Brown et al., 2013 (sensu Madzia et al., 2021)

ORODROMEUS Horner and Weishampel, 1988

(Figs 2-23)

Type Species—*Orodromeus makelai*

Diagnosis—As for type.

ORODROMEUS makelai (sensu Horner and Weishampel 1988)

Holotype—MOR 294

Paratype—MOR 1141

Referred specimens—PU 22440, PU 22445, PU 23246, PU 23442, PU23443, PU 23246, PU 23257; PU 23408, PU 23409, PU 22412, PU 23431, PU 23432, PU 23248, PU 23247; MOR 248, MOR 251, MOR 252, MOR 253, MOR 254, MOR 255, MOR 256, MOR 257, MOR 272, MOR 303, MOR 331, MOR 401, MOR 402, MOR 403, MOR 404, MOR 405, MOR 406, MOR 407, MOR 408, MOR 623, MOR 685, MOR 974, MOR 994, MOR 1003, MOR 1136, MOR 1177, MOR 2726;F#7-7-99-29, F#7-17-15-14, F#7-17-11-10, F#14-14, F#7-17-11-110-17, F#77-14-10, "Jacket A", F#7-10-16-14, F#7-23-15-29, F#7-26-15-39, F#06.26.95; and all of the unnumbered orodromine specimens from the Willow Creek Anticline.

Revised diagnosis—A SBEDO differentiated by the following combinations of morphological characters with autapomorphies denoted by *: nasal, lacrimal, prefrontal, and supraorbitals all contribute to a single composite supraorbital ridge*; anterior and posterior supraorbitals present; anterior supraorbital lower in the orbit than the posterior supraorbital*; large dorsally inflected jugal horn (=boss)*; two nutrient foramina medial to jugal horn; a ovoid foramen piercing the pterygoid wing of the quadrate; pronounced ventromedial process on dentary; lateral fossa on angular-surangular contact*; transverse dorsal groove on atlantal intercentrum; ventral groove on atlantal intercentrum*; subequal capitulate processes on anterior cervical ribs transition posteriorly to an elongate capitulum*; vertical to horizontal transition of dorsal rib articulation occurs between dorsal vertebrae five and six*; sub-oval distal cross-section in anterior dorsal ribs; caudal vertebrae transverse processes to centrum length ratio of 0.72; intercentrum cavity between sacral vertebrae two and three; epaxial tendons present but no hypaxial; posterior scapular flange; ventral fossa on coracoid; preacetabular process length to

total ilium length ratio of 0.35*; curved dorsal margin of the ilium; prepubic process anterior terminus striated; prepubic process dorsoventrally expanded into pad; ischial shaft lack lateral blade-like protrusion in distal third*; no intertrochanteric cleft on femur; no medial inflection of distal femur medial condyle; medial flange on distal half of fibula; forked ascending process of astragalus; large foramen pierces the lateral face of the medial distal tarsal*; short “mailbox flag” shaped metatarsal V*; deeply incising ventromedial pit penetrating shaft of PI-I.

Horizon—The Upper Cretaceous nonmarine Two Medicine Formation represents proximal deposition within a retroarc foreland basin called the Western Interior Basin (WIB), locally part of an eastward thinning clastic wedge which included the Belly River Group and Judith River Formation (Fuentes et al., 2012; Kauffman, 1977). The Two Medicine Formation is subdivided into four members: the Rocky Creek, Shields Crossing, Hagans Crossing, and Flag Butte Members (Rogers et al., 2025). Deposition was heavily influenced throughout by western transgressive and regressive cycles of the Western Cretaceous Interior Seaway (WICS) which bisected North America north to south. Temporally, deposition encompasses much of the Campanian at a paleolatitude of 56ºN occurring between ca. 82.4 Ma. to 74.4 Ma. (Lorenz and Gavin, 1984; Fricke et al., 2010; Rogers et al., 2025). Siliciclastic detritus derived from the North American Cordillera dominates, deposited primarily in eastward flowing fluvial and lacustrine systems, with periodic influxes of effusive volcaniclastics sourced from the Elkhorn Mountain Volcanic Field (Lorenz and Gavin, 1984; Rogers et al., 1993; Lageson et al., 2001; Horner et al., 2001). Paleoclimatic conditions were semi-arid and influenced greatly by monsoonal regimes as evidenced by abundant caliche nodules, growth interruptions in conifer wood, herbivorous dinosaur coprolites, invertebrate traces, and taphonomic data supporting

episodic drought (Freimuth et al., 2019; Freimuth et al., 2021; Lorenz and Gavin, 1984; Rogers, 1990; Chin, 2007; Fricke et al., 2010). *Orodromeus makelai* specimens are restricted to the lacustrine interval of the Flag Butte Member (ca. 76.99 Ma to 76.5 Ma; Rogers et al., 2025) and are recovered primarily from three localities in the Willow Creek Anticline [TM-006, TM-024, and TM-160].

Comments—Many of the *Orodromeus makelai* specimens discussed in this description will be loosely referred to as juveniles, subadults, and adults. These assumptions are informed by the histological sampling of Two Medicine orodromines in Horner et al. (2009), in conjunction with overall proportional size disparities. A few specimen numbers represent multiple individuals; MOR 248 encompasses three individuals of multiple ontogenetic stages, their temporal relationships with each other is still being investigated, and MOR 623 consists of two similarly sized individuals found in cooccurrence.

Description

Cranium

Skull—A general description of skull elements follows. A more detailed cranial osteology and will encompass the noticeable omissions here (Hannebaum et al., in prep). Three skulls compose the bulk of this description, the holotype specimen [MOR 294], MOR 1136, and MOR 1141; supplemented by isolated pertinent cranial elements.

Premaxilla—This dentigerous bone is best represented by the *Orodromeus* specimen [MOR 1141], but a small premaxillary fragment retaining some teeth is also recovered with MOR 623. The premaxilla remains an unfused structure in *Orodromeus* [MOR 1141], a condition shared with all specimens of *Fona* (Avrahami et al., 2024) and differing from other

thescelosaurids like *Oryctodromeus* (Krumenacker et al., 2024), *Zephyrosaurus* (Sues, 1980), *Changchunsaurus* (Jin et al., 2010), *Haya* (Barta and Norell, 2021), and *Thescelosaurus neglectus* (Boyd, 2014). The ascending subnarial process of the premaxilla is lacking in MOR 1141, but its rounded broken base is centrally placed on the anterodorsal surface of the premaxilla. Posteriorly, the subnarial process ascends to meet the naris and curves slightly posteriorly distally without contacting the lacrimal. Many thescelosaurids develop rugose premaxillae surfaces (Barrett and Han, 2009; Boyd, 2014; Jin et al., 2010; Krumenacker et al., 2024; Sues et al., 1980). *Orodromeus* lacks surface rugosities on the premaxilla, nor does it display the mediolaterally expanded shelf on the anterior tip, a condition shared with *Haya* and *Fona* (Avrahami et al., 2024; Barta and Norell, 2021). The left premaxilla in MOR 1141 exhibits five premaxillary teeth which contrast with the right, which displays seven. This inconsistent tooth count likely means a portion of the posterior premaxilla is missing on the left premaxilla in MOR 1141; furthermore, the anterior-most three teeth of the left premaxilla are exceptionally closely packed together. We postulate the first two premaxilla teeth on the left side may be pathologic or abnormal, but this assessment is preliminary.

Maxilla—Posterior to the premaxilla lies the dentigerous maxilla, which is a large centrally positioned bone within the snout which facilitates a plethora of contacts with other cranial bones starting anteriorly with the aforementioned premaxilla, the nasal dorsally, the lacrimal over much of its anterodorsal border, the palatine, and posteriorly with the maxillary ramus of the jugal. Two *Orodromeus* specimens present beautifully preserved maxilla [MOR 294 and 1141]. MOR 294 lacks an associated premaxilla, but the maxillary anterior process, which articulates with the premaxilla, is beautifully preserved in the right maxilla. This process is

triangular in lateral profile, and longer anterodorsally than dorsoventrally tall. This process lacks maxillary teeth, creating a short diastema between the anterior maxillary teeth and posterior premaxillary teeth. In MOR 1141, this process contacts the premaxilla medially. A deep circular fossa (=anterior/rostral maxillary fossa) straddles the premaxilla-maxilla contact, anterior to the first maxillary tooth. This fossa expression is comparable to *Thescelosaurus neglectus* specimen NCSM 15728 but appears more elliptical in MOR 979. *Fona* (Avrahami et al., 2024), *Isaberrysaura* (Salgado et al., 2017), and at least one specimen of *Haya* (Avrahami et al., 2024) all present the anterior maxillary fossa posterior to the most anterior maxillary tooth. The ascending dorsal process of the maxilla slots against a mediolaterally thin expansion of the nasal which descends from the below the lateral nasal ridge. The maxillary tooth row is medially offset, with a prominent ledge (=buccal ridge) extended laterally. The buccal ridge runs the long axis of the maxilla [MOR 294] and posteriorly aligns with the lacrimal and jugal. A ventral row of nutrient foramina trend in parallel to the buccal ridge and are visible in both maxilla of MOR 1141; however, their total number is unclear. In MOR 294, at least six obvious nutrient foramina are just ventral to the buccal ridge, with none laterally placed, which contrast with the extensive foraminate buccal ridge in *Thescelosaurus neglectus* (Boyd, 2014). The maxilla houses the antorbital fenestra near dorsally and just anterior to lacrimal. There is no maxillary fenestra in *Orodromeus* [MOR 294 and 1141], which is the shared condition of most thescelosaurids (Barret and Han, 2009; Boyd, 2014; Jin et al., 2010) excluding *Haya* (Barta and Norell, 2021) and perhaps *Fona* (Fig. 3, Avrahami et al., 2024).

Nasal—These thin and delicate plate-like bones are best represented by MOR 1141 but have collapsed inward into the nasal cavity in the physical specimen. MOR 1141 was μCT

imaged. During post processing, specifically post-segmentation of μCT imaging, we isolated each nasal fragment mesh individually and retroactively returned these meshes back to their original placement within the animation software Blender v.4.3. No retrodeformation modification of bones were attempted (i.e. straightening deformities).

The paired nasals of *Orodromeus* are unfused along the midline internasal suture. They lack most of their anterior portions [MOR 1141]. Anterolaterally, they contact the subnarial processes of the premaxilla and marginate the naris dorsally. A bilateral ridge originates at the subnarial contact and emanating from the lateral face of the naris before continuing posteriorly across the prefrontal, lacrimal, and anterior supraorbital. There is no obvious midline elliptical fossa on the dorsal surface of the nasals, but its presence or absence is difficult to assess in MOR 1141 presently. No foramina are observed on either the dorsal or lateral faces of the nasals. This condition contrasts with the extensive foramina coverage across both these surfaces in *Jeholosaurus* and *Thescelosaurus neglectus* (Barret and Han, 2009; Boyd, 2014), and the sparsely foraminate nasals of *Fona* and *Haya* (Avrahami et al., 2024; Barta and Norrell, 2021). The nasals likely contacted the lacrimal along a small margin on the posteroventral corner [MOR 294 and 1141]. The maxilla-nasal contact was relatively extensive in comparison. Ventrally, both left and right nasals present a thin expansion, ventral to the nasal lateral ridge, which medially overlapped the ascending dorsal process of the maxilla. The nasal-frontal suture is perpendicular to the sagittal plane of the skull and straight. This unfused suture is framed by the left and right prefrontals laterally.

Prefrontal—The prefrontal is a blade-shaped bone which tapers dorsally and frames the anterodorsal margins of the orbit. Two *Orodromeus* specimens retain prefrontals [MOR 294 and

1141]. The prefrontal articulates with the frontal dorsally through its reception along the along a long oblique sutural surface framing the anterolateral corner of the frontal. The prefrontal descends ventrally and thickens anteroposteriorly, but also mediolaterally, facilitating the continuation of a prominent lateral ridge trending from the nasals which articulate broadly along the prefrontal anterior margin. The prefrontal does not appear to contact the maxilla as seen in *Haya* and *Parksosaurus* (Barta and Norell, 2021; Sues et al., 2023). On the posteroventral corner of the prefrontal a circular rugose depression accommodates the anterior supraorbital. The medial surface of the prefrontal is concave and ventromedially indented for reception of the dorsal margin of the lacrimal. The orbital margin of the prefrontal juts medially, forming a rim, as is also seen in posterior opposition within the orbit, manifested by the orbital rim of the postorbital ramus of the jugal. The prefrontal foramen is present along the lateromedial edge of the prefrontal dorsal to the supraorbital depression. Avrahami et al. (2024) notes this foramen is a proposed autapomorphy of *Thescelosaurus neglectus* but is now documented in *Fona* and *Haya*.

Supraorbital—A proposed synapomorphy of Orodrominae is the presence of a single anterior supraorbital (Avrahami et al., 2024), as some other thescelosaurids display both anterior and posterior (=accessory) supraorbitals (Barta and Norell, 2021; Boyd, 2014). Here, we confirm, for the first time, a posterior supraorbital for *Orodromeus makelai* [MOR 1141]. This calls into question validity of this synapomorphy, and with its recognition here, opens the door for further documentation of their presence in other orodromines. The posterior supraorbital is small and rod-like with a medially flattened face where it presses against the lateral face of the postorbital. Barta and Norell (2021) noted the rugosity observed on the lateral surface of the orbital postorbital protuberance in some thescelosaurids and *Hexinlusaurus* likely would be

where a posterior supraorbital articulates (if it is found to exist in these taxa). We agree and place the proposed posterior supraorbital in MOR 1141 in this position. This posterior supraorbital closely matches the morphology of the posterior supraorbital seen in multiple *Haya* specimens (Barta and Norell, 2021). The anterior supraorbital does not contact the posterior supraorbital but does extend roughly halfway across the anteroposterior length of the orbit. Scheetz (1999) proposed ontogenetic change in the length of the anterior supraorbitals, being longer in adult specimens. However, specimens are not listed in Table 1 where this statement is made, nor is it clarified if supraorbital length is a proportional assessment in relation to the total anteroposterior length of the orbit, which we believe was the intention. Only two specimens preserve anterior supraorbitals with a complete enough orbit to assess this proposed change (MOR 294 and 1141). There does appear to be a decrease in this ratio through ontogeny; however, a sample of two does not offer strong support. MOR 1141 demonstrates a supraorbital length to orbit length ratio of 0.55 and MOR 294 exhibits a ratio of 0.59, illustrating a slight proportional increase in anterior supraorbital length through ontogeny. The overall morphology of the anterior supraorbital is rather consistent with other thescelosaurids like *Fona* (Avrahami et al., 2024) and *Haya* (Barta and Norell, 2021). Notably, the anterior supraorbital straddles the contact between the prefrontal and lacrimal, received by a rounded socket on the orbit side of the prefrontal.

This articulation illuminates two observations about the more anterior portions of the skull and perhaps distinguishes orodromines from their thescelosaurine and thescelosaurid cousins. First, lateral expressions of the nasal, prefrontal, lacrimal, and anterior supraorbital form a distinctive ridge observable on both sides of the skull [MOR 1141] making their expression unlikely to be a taphonomic artifact. We denote this ridge the supraorbital ridge. This

supraorbital ridge lacks any rugose surface texturing and is smooth, nor are any foramina observed. A similar, but less developed, composite supraorbital ridge is expressed more dorsal in *Fona* (Fig. 3, Avrahami et al., 2023) and *Changmiania* (Yang et al., 2020). The skull of *Lesothosaurus* laterally bulges without forming any supraorbital ridge [NHMUK PV RU B17]. The second novelty of *Orodromeus* [MOR 294 and 1141] is how low in the orbit the anterior supraorbital is placed in relation to the posterior supraorbital, which is not documented in other thescelosaurids. This would have facilitated an obliquely angled cartilaginous extension (Maidment and Porro, 2010) in a posteriorly upward trending supraorbital ridge spanned much of the anterior orbit. This differs from thescelosaurids like *Fona* (Avrahami et al., 2024), *Haya* (Barta and Norell, 2021), and *Thescelosaurus neglectus* [MOR 979, NCSM 15728] with supraorbitals placed high in the orbit.

Lacrimal—The lacrimal frames the anteroventral corner of the orbit and is largely complete in MOR 294, but fragmentary in MOR 1141. In lateral view, the lacrimal is posteriorly concave and contacts many other elements along its length like the maxilla, jugal, nasals, prefrontal, and supraorbital. Dorsally, at the prefrontal suture, the large lacrimal duct is visible in the CT imaging for MOR 1141 trending anteroposterior. In the physical specimen, the antorbital fenestra appears medially walled in MOR 1141, but at the present resolution of our obtained CT imaging, segmentation fails to capture the extremely mediolaterally thin bone forming this wall. This leaves any the total extent of the lacrimal contributions to the medially walled antorbital fenestra ambiguous. At a cursory glance, MOR 294 seems at odds with MOR 1141, as the fenestra is completely open hinting there may be some ontogenetic control at play during the development of the antorbital fenestra. However, again, this conclusion is speculative since much

of the lacrimal and maxilla fenestra margins show evidence of fracturing. A medial wall may likely have been present but lost during decay/fossilization or alternatively during the discovery/preparation of MOR 294. The closest thescelosaurid proxy may be *Jeholosaurus*, which demonstrates a significant posteroventral expansion of the lacrimal into the antorbital fenestra, forming this medial wall, but retaining an open posteroventral corner in the antorbital fenestra (Fig. 16, Bertozzo et al., 2025). At least one *Haya* specimen exhibits an antorbital fenestra partially invaded by a transversely thin expansion of the lacrimal [IGM 100/2017], like the condition presented for *Hypsilophodon* (Galton, 1975).

Jugal—Several jugals from the Willow Creek Anticline provide clarification of the distinct morphology, and ontogenetic development, of the large jugal horn cores observed in *Orodromeus*. Jugal horns are characteristic of orodromines amongst SBEDOs, convergently shared with Heterodontosaurs (Becerra et al., 2023; Santa Luca, 1980) and neoceratopsians (Averianov et al., 2006; Morschhauser et al., 2018). Orodromine jugal horns project from the lateral face of the jugal, with the angled deflection of the horn varying between taxa. In *Akanthodromeus*, the jugal horn projects laterally and is conspicuous in its large size and pyramidal shape (Chapter 2); the jugal horn of *Pikunidromeus* contrasts in its posterolateral deflection, small size, and triangular shape (Chapter 3); the “Kaiparowits Orodromine” presents a sub-triangular horn, also posterolaterally deflected, with a distinct singular ventral ridge and ovoid cross-section (Boyd, 2012); the “BV Orodromine” is subconical, very rugose, with a slight posterodorsal inflection to its sharp terminus; and distinct from other orodromine is the temporally oldest species *Zephyrosaurus*, which displays multiple specimens with a wedge-shaped posterolaterally deflected horn core [OMNH 34832, YPM 56695, and MCZ 4394].

The jugal horn of *Orodromeus* stands out amongst the crowd in its steep posterodorsal deflection and sub-conical cross-section [MOR 1141]. Most eminent are the distinctive ridges encircling the external horn surface anteriorly, ventrally, posteriorly, and dorsally. These ridges are not uniform in their expression, with the ventral ridge most eminent, as is the case in the "Kaiparowits Orodromine" (Boyd. 2012). In *Orodromeus*, the horn surface separating the dorsal and anterior ridges is flat contrasting with *Pikunidromeus* where this horn surface is rounded [MOR 473 and ROM 64600]. A deeply incising concavity separates the anterior and ventral jugal horn ridges in *Orodromeus*. This concavity is shared with some specimens of *Pikunidromeus*, but markedly in *Pikunidromeus* this concavity is variable in its expression, even within the same individual [MOR 473] which may be attributable to some taphonomic alteration. In the "BV Orodromine", a shallow groove on the anteroventral horn surface corresponds to the location of the deeply incising concavity seen in *Orodromeus*. MOR 1136 preserves an incomplete disarticulated right jugal which exhibits two nutrient foramina on the medial wall, opposite the jugal horn.

Juvenile *Orodromeus* specimens [MOR 294, 647, 1136, F#7.7.99.28] demonstrate changes in horn morphology and size through ontogeny. In juvenile specimens, the jugal horns are proportionally small and conical with only slight depressions on the anteroventral face of the horn [MOR 294, 647, 1136, F#7.7.99.28] which differs from the distinctly rugose surface of a juvenile "BV Orodromine" specimen, and the juveniles of *Pikunidromeus* which display a distinctly triangular morphology [MOR 436 and 613]. In juvenile *Orodromeus*, the horns are posterolaterally deflected from the lateral face of the jugal with no dorsal curve as seen in the adult condition [MOR 1141]. These juveniles also lack any of the discrete ridging observed in

MOR 1141. This demonstrates a trend through ontogeny from a small, conical, posterolateral deflected horn; to a large, upturned, subconical jugal horn with conspicuous ridging.

The overall morphology of *Orodromeus* jugals follow the triradiate blueprints of other orodromines like *Pikunidromeus* (Chapter 3). The maxillary ramus floors the orbit and is best preserved in the holotype specimen, MOR 294. In lateral profile, the maxillary process is elongate and slender which distinctly bifurcates anteriorly. Bifid maxillary processes previously were only documented in *Pikunidromeus* (Chapter 3), the thescelosaurid *Haya* (Barta and Norell, 2021), and *Heterodontosaurus* (Norman et al., 2011) among SBEODs. Few orodromines preserve maxillary rami and they have often been characterized as being tapered (char. 51:0, 67:1); however, with the revelation of a shared bifid condition between *Orodromeus* and *Pikunidromeus*, this suggests it may be the synapomorphic condition of the group. The postorbital ramus of the jugal articulates with the ventral process of the postorbital bone in a laterally placed socket [MOR 294, 1141]. Do note, in MOR 1141 two lines transect the postorbital ramus in the rendered model, an error in the procured μCT imaging. A prominent orbital rim emanates from the anteromedial margin of the postorbital ramus, a feature characteristic of orodromines like *Pikunidromeus* (Chapter 3) and *Akanthodromeus* (Chapter 2), the "BV Orodromine", the "Kaiparowits Orodromine" (Boyd, 2012), and *Zephyrosaurus* [OMNH 34832, YPM 56695, MCZ 4394]. The jugal wing is broad in *Orodromeus* and bifurcates posteriorly [MOR 1141], as in *Pikunidromeus* (Chapter 3), *Haya* (Barta and Norell, 2021), *Minimocursor* (Manitkoon et al., 2023), and potentially *Akanthodromeus* (Chapter 2).

Quadratojugal—The quadratojugal is a transversely flattened sheet-like bone posterior to the jugal, which articulates with the quadrate and jugal. Two specimens [MOR 294 and 1141]

preserve quadratojugals in relative life position, where it frames the posteroventral corner of the infratemporal fenestra. In MOR 294, the jugal-quadratojugal connection is unclear but is potentially illuminated in MOR 1141. Most SBEDOs demonstrate a laterally seamless jugal-quadratojugal contact, where the jugal wing (of the jugal) does not contact the medial or ventral surfaces of the quadratojugal. This condition contrasts with *Fona*, *Thescelosaurus neglectus*, *Changmiania*, and *Jeholosaurus*, which exhibit bifurcated jugal wings, of which the ventral process contacts the ventral medial surface of the quadratojugal (Avrahami et al., 2024). *Orodromeus* specimen MOR 1141 appears to display the latter condition, where the quadratojugal overlaps the lateral surface of the ventral process of the bifid jugal wing. It is unclear at the current scan resolution obtained for MOR 1141 whether the ventral prong of the jugal wing slots into a groove along the ventral margin of the quadratojugal. A foramen is centrally placed in the quadratojugal. This foramen may enlarge through ontogeny, as it miniscule in MOR 294 when compared to the adult condition [MOR 1141]. The central placement of the quadratojugal foramen differs from the more posterior location seen in some specimens of *Jeholosaurus* (Bertozzo et al., 2025).

Postorbital—Three specimens retain postorbitals [MOR 294, 1136, and 1141]. These triradiate shaped bones frame the posterodorsal corner of the orbit, with a broad triangular protuberance emanating into the orbit anteriorly. The protuberance likely anchored the posterior supraorbital and a cartilaginous structure which extended across the orbit to the single supraorbital anteriorly situated in the orbit. The postorbital frontal process contacts the frontal anterodorsally and is received by a triangular sutural surface (sensu Brown et al., 2013). Just posterior, the postorbital squamosal process makes brief connections with the parietal and

squamosal and marginates the anterodorsal corner of the infratemporal fenestra. The ventral process of the postorbital descends to meet the postorbital ramus of the jugal, which together form the temporal bar. Medially, the laterosphenoid socket straddles the frontal-postorbital contact.

Quadrate—Two relatively complete [MOR 294, 1136], and one incomplete left quadrate [MOR 1141], are recovered for *Orodromeus*. This bone is dorsoventrally elongate and posteriorly inclined in its upper half. The quadrate articulates dorsally with the squamosal in a rounded and transversely narrow end. Two thin flanges project anteriorly, beginning just ventral to the dorsal end of the quadrate, and widest just dorsal to the distal articular condyles. They are best observed in the segmented CT models of MOR 1136. The lateral flange (=quadratojugal wing) extends anteriorly to its contact with the quadratojugal, where in MOR 294 it appears the quadratojugal overlaps the lateral face of the quadratojugal wing. Just medial to this contact in MOR 294, is a dorsoventrally inclined elongate “blind pocket”. This blind pocket is also obvious and in like location in *Zephyrosaurus* [MCZ 4394]. *Orodromeus* specimen MOR 1136 distinctly lacks this blind pocket on the lateral face of its quadrate, hinting at some variability in its expression between individuals. The medial wing (=pterygoid wing) similarly projects anteriorly to meet the quadrate wing of the pterygoid [MOR 1136]. The pterygoid wing exhibits an apparent ovoid foramen visible in both CT imagery and the physical specimen [MOR 1136]. A pterygoid wing foramen is also conspicuous in *Zephyrosaurus* specimen MCZ 4394. This differs from the dorsoventrally elongate fossa reported in the thescelosaurines *Fona* (Avrahami et al., 2024), *Oryctodromeus* (Krumenacker et al., 2024), and *Thescelosaurus neglectus* (Boyd, 2012). Ventrally, the quadrate mediolaterally widens into subequal rounded condyles, which are

received by the surangular and articular bones of the lower jaw.

Squamosal—The left and right squamosals are only partially revealed in MOR 294, limiting current interpretation. The squamosal frames the posterodorsal corner of the supratemporal fenestra and is crescentic in lateral profile. A dorsoventrally tapering process proceeds anteriorly to meet the posterior process of the postorbital. Posteriorly a deep socket receives the rounded dorsal end of the quadrate. A ventral process (=prequadratic process) descends along the anterior third of the quadrate, high above the quadratojugal.

Parietal—Specimens MOR 294 and 1136 both preserve fully fused parietals, but much of the following description will lean heavily on the exceptionally preservation 1136. Though Avrahami et al. (2024) states MOR 1136 lacks a parietal sagittal crest, we note this statement was likely made in error, as a sagittal crest arises clearly from the dorsal surface of the parietal in MOR 1136. The sagittal crest is placed along the midline of the parietal, trends anteroposteriorly, before bisects anteriorly into divergent lateral trajectories at the frontal sutural contact. The parietal sagittal crest of *Orodromeus* is a shared condition with *Pikunidromeus* [MOR 473], but also more broadly in SBEDOs, more notable is the rare SBEDO taxa that lack this crest like *Fona* (Avrahami et al., 2024), *Lesothosaurus* (Porro et al., 2015), and *Kulindadromeus* (Supp. materials, Godefroit et al., 2014). In dorsal and ventral views, the parietal is hourglass shaped and posteriorly flares laterally into two thin “wings”. Ventrally, the parietal is concave, which molds the posterior portion of the brain, most prominently eminent is the cerebellum. The parietal-frontals contact is extensive and evidenced by an interdigitating suture. In dorsal view, this sutural contact is slightly W-shaped, with the center inflection coming to a point at the frontal suture [MOR 1136 and 1141].

Frontal—The paired frontals of *Orodromeus* are unfused along their midline suture, and trapezoidal in dorsal profile with a curved lateral orbital margin. MOR 1136 is a juvenile specimen demonstrating immaculate preservation of a minimally altered frontal pair. In fact, frontals are quite well represented for *Orodromeus* and span an ontogenetic spectrum from small juveniles [MOR 248] to likely adults [MOR 1141]. Do note, the rendered model of MOR 1141 exhibits two lines bisecting the left frontal, these lines are not real and just an error of the μCT imaging. The right frontal of the smallest specimen [MOR 248] is quite arched dorsally and anteroposterior short. This dorsal inclination decreases through ontogeny and the frontals length [MOR 1141]; however, the frontals do not flatten completely over the orbit. This contrasts with thescelosaurines where this flattened profile is widespread and demonstrated by *Fona*, *Thescelosaurus neglectus* (Boyd, 2014), *Thescelosaurus assiniboiensis* (Brown et al., 2011). Notably, the early orodromine *Zephyrosaurus* (Sues, 1980) shares this flattened frontal condition [MCZ 4392]. To quickly note, MOR 623 recovers a left frontal which is flat. This is not authentic morphology instead resulting from post-burial crushing, which is evident across much of this specimen. The frontals of *Orodromeus* are more mediolaterally narrow than *Pikunidromeus* (pers. observ.), and *Zephyrosaurus* (Sues, 1980). The concave orbital margin is finely striated in *Orodromeus*, signifying soft tissue attachments which likely descended to connect with the supraorbitals. *Orodromeus* frontals lack the spatter of splinter-like foramina across the dorsal surface as seen in at least one *Pikunidromeus* specimen [MOR 995], nor does it display the vascular surface of an indeterminate orodromine frontal from the Oldman Formation [TMP 2003.012.0135].

Predentary—Incomplete predentaries are accounted for in two *Orodromeus* specimens

[MOR 1136 and MOR 1141]. The predentary is a separate ossification anterior to the mandibular symphysis and is the plesiomorphic condition omnipresent in Ornithischia. When comparing the adult Orodromeus specimen to 1141 to presumed other non-juvenile thescelosaurid specimens, *Orodromeus* [MOR 1141] stands out with a relatively anteroposteriorly short predentary, akin to *Haya* [IGM 100/2017]. Other thescelosaurids like *Changchunsaurus* (Jin et al., 2010) and *Jeholosaurus* [IVPP V15716] exhibit comparatively elongate and dorsoventrally narrow predentaries. The predentary demonstrates a descending ventral process which inserts into a squarish socket framed at the mandibular symphysis (=Meckelian groove) and is posteriorly framed by the prominent medial process of the dentary (sensu Brown et al., 2013). The ventral process of the predentary is not posteriorly bifurcated as in *Changchunsaurus* (Jin et al., 2010). In *Orodromeus*, at the predentary-dentary symphysis, the predentary surface exhibits two sulci, separated by a medial ridge, these sulci accommodate the unfused dentaries along the mandibular symphysis. The predentary-dentary symphysis itself is a dynamic connection with at least three different proposed morphotypes evident across Ornithischia (Nabavizadeh and Weishampel, 2016). *Orodromeus* exhibits a predentary-dentary joint (PDJ) morphotype I as defined in (Nabavizadeh and Weishampel, 2016).

Dentary—Three *Orodromeus* specimens retain well preserved dentaries [MOR 294, 1136, and 1141]. The dentary is an elongate dentigerous dorsoventrally narrow bone which comprises roughly two thirds of the mandible. It articulates with the predentary anteriorly, splenial and coronoid medially, and posteriorly with the angular and surangular. Each dentary is medioventrally twisted anteriorly and joins together in the mandibular symphysis. Anteriorly, the dentary is pointed with two distinct facets for reception of the dorsal and ventral processes of the

predentary. A large protuberance projects ventrally from each dentary of the mandibular symphysis and frame the posterior border of a rectangular sulcus for reception of the predentary ventral process. This ventral protuberance, the “medial process” (sensu Brown et al., 2013), is pronounced in *Orodromeus* [MOR 1136, 1141], more so than in *Pikunidromeus* (pers. observ.) and *Haya* (Barta and Norell, 2021). This pronounced medial process is a condition shared between a handful of indeterminate orodromine dentaries from the Two Medicine Formation fossil locality (TM-088) and another from the Oldman Formation of Alberta [TMP 1997.128.0002]. TMP 1997.128.0002 differs from *Orodromeus*, in that the mandibular process is gently curved and not the abrupt descending protuberance seen in MOR 1141. TMP 1997.128.0002 further contrasts in its demonstration of a plethora of nutrient foramina framing the mandibular symphysis laterally, a condition shared with *Haya* (Barta and Norell, 2021). *Haya* exhibits paired mental foramina within a lateral groove that receives the predentary. These paired mental foramina are not observed in the *Orodromeus* specimen [MOR 1141], but a single foramen may be present in MOR 1136.

Surangular—The morphology of the surangular in *Orodromeus* is best represented by specimens MOR 294 and 1141. In MOR 1141, the μCT resolution makes it appear as a large cavity pierces the surangular centrally; however, this is just an artifact of the μCT imaging. The splenial is roughly trilateral in shape and contributes to a significant portion of the post-dentary. The ascending coronoid process of the dentary frames the anterodorsal border of the surangular. Ventrally, the angular confines the surangular and shares claim to a large fossa which straddles their contact. The surangular maintains a significant contribution to the lateral portion of the glenoid which cups the articular condyles of the quadrate in the retroarticular joint. The lateral

process of the surangular arises just anterior to the glenoid and is a large boss in *Orodromeus*. Two clearly defined ovoid foramen pierce the surangular in lateral view [MOR 1141]. The largest is just ventral to the dentary-surangular contact, even with the apex of the coronary process, and the second just anteromedial to the glenoid. Zanno et al. (2023) details the many inconsistencies in foraminal nomenclature in application to the ornithischian surangular. Following their example, we reference the ovoid foramen posterior to the lateral dentary-surangular contact as the "surangular foramen", while we diverge slightly and refer to second foramen that lies anterior to the lateral boss as the "lateral boss foramen" until the internal branching structure of the neurovascular canals proximal to the lateral boss can be investigated in detail in future work (Hannebaum et al., in prep).

Angular—The angular is a narrow canoe-shaped bone framing the ventrolateral border of the post-dentary region of the mandible. It is well preserved in MOR 294, 1136, and 1141. The angular is sharply pointed anteriorly in one specimen and appears to slot into a tongue and groove connection with the dentary [MOR 1136]. This tongue and groove connection is shared with Haya, along with the pointed anterior tip which is shared more broadly in SBEDOs. When comparing MOR 1136 to the two other *Orodromeus* specimens [MOR 294 and 1141] some variability in the expression of the pointed tip of the angular arises. In both MOR 294 and 1141, this pointed tip is more dorsally placed and lies at the anterodorsal angular-surangular junction, while in MOR 1136 this sharp anterior tip is more ventrally placed. The angular thins posteriorly before progressing into a dorsally convex posterolateral profile when nearing the retroarticular joint. The lateral surface of the angular presents a shallow fossa which extends onto the ventral surangular. This fossa is also documented in *Thescelosaurus neglectus* (Boyd, 2014) but is

deeper and anteroposterior longer in that taxon.

Splenial—The splenial is represented in the *Orodromeus* juvenile holotype [MOR 294] and the specimen MOR 1141. This sheet-like mediolaterally thin bone is partially obscured by matrix and bone in both specimens hindering interpretations of its complete morphology. Still, the splenial appears to be triangular in medial profile as in other SBEDOs. In MOR 1141, the ventral margin of the mandible shows the splenial closely follows the Meckelian groove through its length starting just posterior to the ventral mandibular process. In both specimens, it is closely appressed against the medial faces of the dentary, surangular, and angular, and contacts the prearticular posteriorly. Its posterior connection with the prearticular is extremely difficult to discern in MOR 294. The splenial appears bifurcated posteriorly, and if true, shows an extensive contact contrasting with the smaller forked connection observed in *Changchunsaurus* (Jin et al., 2010).

Prearticular—The *Orodromeus* holotype specimen [MOR 294] and MOR 1136 retain the prearticular. The prearticular is a thin strap-like bone, medial to the surangular, posterior to the splenial, and contributes to the medioanteriorly to the glenoid. The angular frames its ventral margin, and the articular articulates posteriorly. There is no obvious foramen near the suture contact with the angular as there is in *Haya* (Barta and Norell, 2021).

Articular—The articular is the posterior most bone in the mandible and is retained only in the holotype specimen [MOR 294]. The articular is bulky and roughly pyramidal in shape. The articular contributes to the saddle-shaped glenoid dorsoposteriorly which cups the ventral articular condyles of the quadrate. No foramen is visible along the medial face of the articular as is seen in *Fona* (Avrahami et al., 2024) and a specimen of *Psittacosaurus mongoliensis* (Barta

and Norell, 2021).

Axial skeleton

Cervical vertebrae—The *Orodromeus* holotype specimen [MOR 294] is the only specimen which preserves a complete cervical series for this taxon. MOR 294 exhibits a count of nine cervical vertebrae, which is consistent with most SBEDOs, excluding *Changmiania* and *Macrogryphosaurus* which present alternative cervical counts of six and ten respectively (Rozadilla et al., 2020; Yang et al., 2020). MOR 623 and 1141 both offer incomplete cervical series, but as with much of MOR 623, the cervical vertebrae recovered suffer from post-burial deformation. Small foramina dot the lateral faces of the cervical vertebrae in MOR 294 and 1141 in contrast with *Pikunidromeus* (Chapter 3). The neurocentral sutures are fully open in MOR 294 but are fully closed in MOR 623 and a posterior cervical of uncertain positioning in MOR 1141. Cervical vertebrae two and three of MOR 1141 appear to possess open neurocentral sutures. Cervical vertebrae are also recovered in isolation at fossil localities like Egg Mountain (TM-006), but the description instead will focus on the partial associated series listed above, only supplemented by isolated material when pertinent.

As a disclaimer, MOR 623 represents at least two similarly sized subadult specimens found in co-occurrence. Unfortunately, the absence of field or preparation notes makes any original articulation or association between elements impossible to know. Therefore, when discussing MOR 623 for description we will mainly reference it as its number without attempting to distinguish the composite individuals from each other; outside of the femora.

Atlas—Only the atlantal intercentrum is representative of the atlas complex in *Orodromeus* [MOR 623 and MOR 1141]. This small bone is sub-crescentic in anterior view with

distinctive collateral bosses (=parapophyses) marking the ventral attachments of the atlantal ribs. Collateral depressions mark the dorsolaterally extremities indicating articulation site for the atlantal neural arches. Anteriorly, the intercentrum is sharply lipped [MOR 11141] for reception of the occipital condyle.

The atlantal intercentrum of *Orodromeus* [MOR 623, MOR 1141] is strikingly distinct from the atlantal intercentrum of *Pikunidromeus* [MOR 473]. In *Pikunidromeus*, the stout atlantal intercentrum is rectangular in profile in dorsal view, while in *Orodromeus* it is V-shaped. The concave dorsal surface of the intercentrum in *Orodromeus* is deeply transversely grooved and accompanied by small foramina; however, the latter observation is tentative and difficult to confirm without CT imaging of the atlantal intercentrum. A similar transverse dorsal groove is also present in *Fona* (Fig. 9, Avrahami et al., 2024) *Oryctodromeus* [MOR 1642], and *Haya* (Fig. 31, Barta and Norell, 2021). *Pikunidromeus* specimen MOR 473 lacks this groove completely and does not display any apparent foramina on its external surfaces. The transverse dorsal groove would have received the sharp anteroventral ridge on the odontoid process, which is poorly developed on the odontoid of *Pikunidromeus* [MOR 473]. The atlantal intercentrum of *Orodromeus* is dorsoventrally thickened in comparison to *Pikunidromeus*. There is a ventral groove as documented in *Jeholosaurus* (Han et al., 2012), notably absent in *Pikunidromeus* [MOR 473].

Axis—Only the juvenile holotype specimen [MOR 294] illuminates the complete layout of the axis in *Orodromeus*, while the odontoid process of the axis is recovered in MOR 623. In MOR 294, the odontoid process and axial intercentrum are cemented by matrix to the axis centrum anteriorly and are not coossified. The dorsal margin of the neural arch of the axis is

lacking along most of its length but posteriorly is retained. This insight shows the dorsal margin of the neural arch was likely inclined acutely in relation to the long axis of the centrum, this contrast with the horizonal orientation of the neural arch in *Fona* (Avrahami et al., 2024). In MOR 623, the ventral groove of the odontoid process presents a linear series of collateral foramina. The axis centrum in *Orodromeus* exhibits an amphiplatyan condition like *Pikunidromeus* (Chapter 3) and *Jeholosaurus* (Han et al., 2012).

Cervical vertebrae three to nine—Posterior to the unfused atlas-axis complex the cervical centra transition from the amphiplatyan condition and start progressing quickly to a sightly amphicoelous centra starting with cervical four in *Orodromeus*. Each centrum face is D-shaped. Cervical vertebrae four is a transitional locus in *Pikunidromeus* [MOR 473]; however, the change in *Orodromeus* does not appear as drastic in comparison (MOR 294, 623, and 1141). Centrum four in *Orodromeus* does not present a ventral hypapophysis-like structure, but with a clear caveat to this statement. It is unclear if this structure is under some ontogenetic control in *Pikunidromeus*, if so, then we would expect *Orodromeus* juvenile specimen MOR 294 and potential subadult 623 to lack this structure, but MOR 1141 whose skull and vertebrae are comparable in size to a presumed adult specimen of *Pikunidromeus* [MOR 473] would be the specimen we turned to for confirmation of this proposed autapomorphic character of *Pikunidromeus*. The problem is MOR 1141 is missing the ventral section of the centrum that would correspond to this proposed hypophysis. Only further discoveries of adult aged *Orodromeus* with cervical vertebrae four will illuminate if this structure is a true autapomorphy of *Pikunidromeus*. Small nutrient foramina dot the lateral faces of the cervical vertebrae in immature *Orodromeus* specimens MOR 294 and 623, but not in the presumed adult [MOR

1141]. This pattern of cervical foramina loss with maturity is also seen in *Pikunidromeus* (Chapter 3).

Cervical ribs—There are several cervical ribs in articulation along the lateral faces of cervical vertebra three and four in MOR 1141. The capitulum and tuberculum of the post-axial cervical ribs are subequal in length until cervical vertebrae number six [MOR 294 and 1141]. This lengthening of the capitulum in relation to the turberculum contrasts with the trend seen in *Pikunidromeus* [MOR 473], where the capitulum is longer than the tuberculum in every cervical rib. Subequal capitate processes may also be present anteriorly in *Jeholosaurus* judging by the posistioning of the anterior diaphysis and parapophysis (Fig 1, Han et al., 2012) before lengthing the capitumul posteriorly. Each cervical vertebrae displays a sharp ventral keel on the centrum which a feature common in SBEDOs.

Dorsal vertebrae—No complete dorsal series is available for *Orodromeus* with only two specimens presenting any sizable portions of the series [MOR 294 and 623]. MOR 294 preserves ten total dorsal vertebrae, while MOR 623 retains only eight dorsal vertebrae. In MOR 623, extensive post-burial deformation of the dorsal vertebrae further complicates their interpretation and makes specific placements within the series tentative. *Pikunidromeus* demonstrates the only complete dorsal series of an orodromine and presents a dorsal series count of fourteen vertebrae (Chapter 3), a count likely reflected in *Orodromeus* as well. The centra of the dorsal vertebrae are sightly amphicoelous. The anterior three dorsal vertebrae retain a slightly ventrally keeled centrum which disappears in the subsequent vertebrae. The neural spine of each dorsal vertebrae is centered over each centra. Small nutrient foramina pierce the collateral faces in MOR 294 and 623.

A key distinction between *Orodromeus* and *Pikunidromeus* is the angled transition of rib dorsal rib articulation to the axial column. MOR 294 shows this transition of a more vertical rib articulation to one which is horizontal occurring between dorsal vertebrae five and six [char. 230:1], while in *Pikunidromeus* specimen MOR 473 this transition occurs between dorsal vertebrae six and eight [char. 230:2] (Chapter 3). The neurocentral sutures are closed in dorsal vertebrae 11 through 14 and partially open in the rest in specimen MOR 623, whereas MOR 294 demonstrates all open neurocentral sutures through its dorsal series.

Dorsal ribs—Only a handful of dorsal ribs are retained, and their morphology is best exemplified in *Orodromeus* specimens MOR 294, 623, and 1136. Importantly, the anterior dorsal ribs demonstrate a sub-oval distal cross-section. This sub-oval cross-section is a synapomorphy of orodromines and observed is observed here in *Orodromeus* (Chapter 3; Avrahami et al., 2024).

Sacral vertebrae—There are seven sacral vertebrae in *Orodromeus* as demonstrated in MOR 294 and 623. Sacral count is determined by observations of sacralized centra faces (sensu Avrahami et al., 2024). These sacralized faces are characterized by an irregular scalloped texture on the centrum face. In MOR 623, sacral vertebra one is not fused to two, but vertebrae two through four are fused together at their centrum faces in conjunction with the neural processes. Sacral vertebrae five is not fused to vertebra four or six, but sacral vertebrae six and seven are fused each other. This ossification of the sacral series is similar to the juvenile *Orodromeus* holotype specimen [MOR 294] where sacral vertebrae two through five are fused at their centra faces. The intercentral cavity is a proposed autapomorphy observed in one *Fona* specimen (Avrahami et al., 2024); however, this cavity, located at the ventrolateral boundary of sacral vertebrae two and three, is also present in a presumed adult specimen of *Pikunidromeus* [MOR

473], and may be seen in the holotype adult *Oryctodromeus* specimen [MOR 1636a] potentially indicating it is instead a thescelosaurid synapomorphy in skeletally mature specimens; CT imaging of the sacral series is needed to confirm this as surface-level inspections of important specimens are often hindered by matrix.

Avrahami et al. (2024) surmised this intercentral cavity may be a taphonomic artifact. This inference is potentially corroborated by *Orodromeus* specimens MOR 294, 623, and PU 23409, and the contextual morphology provided by these three specimens showcase a potential ontogenetic, or taphonomic, pathway to the intercentral cavity in thescelosaurids. MOR 294 and PU 23409, both juveniles, present collateral ventral sockets at the sutural division of vertebrae two and three. MOR 623, potential subadult specimens, instead show theses "sockets" have migrated dorsally and are more laterally placed as in *Fona* specimen [NCSM 36218]. The right "socket" is covered by matrix and consolidate, but the left "socket" of MOR 623 shows a mix of thin plated bone and matrix infilling the space. We propose two scenarios; (1) the ventral collateral intercentral sockets migrate to a more lateral placement from juveniles to adults, while the wall of this socket thins, thus is easily lost during burial resulting in this cavity, and (2) the collateral intercentral sockets seen in the sacrum of juveniles migrates dorsally through ontogeny, the medial wall of this socket thinning in conjunction until completely lost in adults. As mentioned above, really the only way to investigate this further is by obtaining CT imaging for specimens of *Orodromeus*, *Pikunidromeus*, *Fona*, *Oryctodromeus*, *Thescelosaurus*, and likely other proposed thescelosaurids, to investigate the validity of the intercentral cavity discussed here. Small foramina mark the lateral faces of the sacral centra in MOR 294 and 623, but also

ventrally in PU 23431. The sacral vertebrae exhibit sightly amphicoelous centra. The neurocentral sutures are all closed in the sacral vertebrae of MOR 623.

Caudal vertebrae—The *Orodromeus* holotype specimen [MOR 294] retains the first three caudal vertebrae in articulation with sacral vertebrae seven, while MOR 623 presents the anterior most five caudal vertebrae in conjunction with two posterior caudals of uncertain placement. The caudal vertebrae are distinguished from the rest of the axial column through their exhibition of a prominent ventral groove. The transverse processes of the anterior caudal vertebrae in *Orodromeus* [MOR 623] are proportionally long and exhibit a centrum length to transverse process length ratio of (0.72). This ratio is rather spread out over a spectrum in thescelosaurids with no apparent phylogenetic consistency. *Orodromeus* falls middling on this spectrum of ratios between the very elongate transverse processes seen in *Pikunidromeus* (0.65) [ROM 64600] and *Fona* (0.64), and the shortened transverse processes of *Oryctodromeus* (0.93) [MOR 1642], and the potential Australian thescelosaurid *Diluvicursor* (0.91). This proportional measurement was obtained measuring from the base of a single transverse process to its lateral most extent, coupled with the centrum length. Small nutrient foramina mark the lateral faces of the caudal centra in *Orodromeus*, and the caudal centra continues to exhibit a sightly amphicoelous condition.

Chevrons—Two *Orodromeus* specimen preserves a limited string of articulated caudal vertebrae with the chevrons in place and complete [MOR 252 and 294], MOR 294 preserves a single chevron in articulation. Isolated chevrons of uncertain placement are recovered with MOR 623. *Orodromeus* appears to follow the overall morphological trend observed in the caudal series of *Pikunidromeus* [ROM 64600] and *Haya* [IGM 100/2015] where proximal chevrons are

elongate and anteroposteriorly narrow, before gradually shortening dorsoventrally and anteroposteriorly thicken into a paddle-shaped lateral profile. There is one discernable distinction manifest in *Orodromeus* holotype MOR 294 which other thescelosaurids lack: a vestigial first chevron at the ventral margination between caudal vertebrae one and two. This vestigial first chevron is rounded and shows no division, or the beginnings of one, to accommodate a ventral haemal canal. A vestigial first chevron is also reported for an individual of *Alligator mississippiensis* in Erickson et al. (2005) and is remarkable in its similarity to the one still in articulation in MOR 294. MOR 623 exhibits potential diminished articular facets for receiving the first chevron on the first caudal vertebra; however, there is no vestigial first chevron retained with this specimen. The interspecific variability of not only the inception of the first chevron along the caudal series, but also the presence of a vestigial first chevron in *Alligator mississippiensis*, may suggest first chevron commencement is variable more broadly in archosaurs, corroborated by observations in tyrannosaurs (Erickson et al., 2005). Furthermore, in *Jeholosaurus* the emergence of the first chevron is documented to be intraspecifically variable and can occur at vertebrae two or three (Han et al., 2012). This added support for the variability in the emergence of the first chevron warrants our hesitation in designating a vestigial first chevron as a true autapomorphy of *Orodromeus makelai*.

Ossified tendons—Epaxial ossified tendons bundles are present in MOR 294 arranged parallel to the neural spines of vertebrae. In-situ, these tendons run lateral to each neural spine extending specifically from dorsal vertebra twelve to sacral vertebra seven [MOR 294]. Disarticulated epaxial tendons are recovered with *Orodromeus* specimens MOR 623 and PU 23442. There is no evidence for hypaxial tendons in any *Orodromeus* specimens, nor in any other

orodromine specimens retaining ossified tendons (Chapter 3; Brown et al., 2013), which is a condition shared with the thescelosaurid *Haya* (Barta and Norell, 2021) and *Changmiania* (Yang et al., 2020). Overall, these observations support previous observations distinguishing orodromines and thescelosaurines (Avrahami et al., 2024; Brown et al., 2013). Thescelosaurines like *Oryctodromeus* (Krumenacker et al., 2024), *Fona*, *Thescelosaurus neglectus*, and *Thescelosaurus assiniboiensis* (Avrahami et al., 2024) exhibit both hypaxial and epaxial ossified tendons, with both completely sheathing the tail in *Oryctodromeus* (Krumenacker et al., 2024), while orodromines appear to lack any hypaxial tendons (Chapter 3; Brown et al., 2013). Instead, longitudinally arranged epaxial tendon bundles typify Orodrominae, though, it is worth considering the variability of tendon preservation between specimens broadly in Ornithischia and demonstrated here between *Orodromeus* specimens.

Sternum—A handful of *Orodromeus* specimens preserve sternal plates [MOR 294, F#08.05.95 "Frankie's *Orodromeus*", and MOR 623]. These sternal plates showcase degrees of interspecific variability but generally fit the same morphologic profile. Differences between specimens may also be attributable to some taphonomic distortion, as MOR 623 shows extensive post-burial alterations across much of its assigned material attributed to compression, alternations obviously shared with F#08.05.95. The sternal plates have long been characterized as crescent-shaped; however, when compared to other SBEDOs, like *Parksosaurus* (Sues et al., 2023), it's apparent here that *Orodromeus* sternal plates do not fit neatly into this characterization and instead exhibit a weekly crescentic outline and is much more quadrilateral in dorsal/ventral profile. Small facets for reception of the coracoid mark the anterolateral corners, while each sternal is posteriorly rounded.

Appendicular skeleton

Scapula—Only a handful of scapulae are accounted for in *Orodromeus*. The available examples are relatively complete and provide excellent insight into its morphology; however, it's important to note post-burial compression has altered some of these specimens, often in subtle ways [MOR 623]. For descriptive purposes, we join Avrahami et al. (2024), Rozadilla et al. (2019), and Chapter 3 in discussing scapulae with the long axis dorsoventrally oriented. The scapula of *Orodromeus* is elongate, mediolaterally compressed along the blade, and anteroposteriorly flared distally. The lateral profile of the scapula is relatively straight, as in *Pikunidromeus*, unlike the ventrally downturned scapulae of thescelosaurines like *Fona* (Avrahami et al., 2024), *Oryctodromeus* (Krumenacker et al., 2024), and *Thescelosaurus neglectus* [MOR 979 and 1193]. This orodromine scapular profile is rather similar, though there is a significant body-size disparity, to the elasmerian *Mahuidacursor* (Cruzado-Caballero et al., 2019). The proximal sutural surface which meets the coracoid mirrors *Pikunidromeus* in its mediolateral robustness (Chapter 3), cumulating in a prominent lateral swelling denoted as the supraglenoid boss [MOR 294 and 623]. The deltoid fossa subdivides posteroventrally into the supraglenoidal fossa, framed by an enlarged supraglenoidal buttress, as in *Pikunidromeus* and *Yueosaurus* (Chapter 3; Zheng et al., 2012). The acromion process is well-developed with a sharp scapular spine running its long axis, a shared trait with *Pikunidromeus* (Chapter 3), *Changmiania* (Yang et al., 2020), *Fona* (Avrahami et al., 2024), *Thescelosaurus neglectus* [MOR 1183], and *Oryctodromeus* (Krumenacker et al., 2024). Avrahami et al. (2024) suggests the scapular spine is ventrally folded in two *Orodromeus* specimens [MOR 294 and 623] like in *Oryctodromeus* [MOR 1636a and 1642], Chapter 3 argues against this characterization, and we confer with the latter. Really only one *Orodromeus* specimen presents this "folded" scapular spine, MOR 623,

and upon close examination it is apparent the acromion process exhibits signs of post-burial crushing exemplified by a patchwork of fractures crisscrossing this process enabling it to be inset into the proximal scapula in conjunction with being slightly flattened. This type of post-burial alteration is rampant across much of MOR 623, and with a process as thin as the scapular spine, we would expect it to easily be altered in this manner. There is no medial tuberosity on any *Orodromeus* scapulae in opposition to the thescelosaurine condition exemplified by *Fona*, *Oryctodromeus*, and *Thescelosaurus neglectus* (Avrahami et al., 2024). Conversely, a sharp posterior scapular flange projects prominently in larger *Orodromeus* individuals [PU 23442 and 23443], which is a feature shared with the presumed adult specimens of *Pikunidromeus* [MOR 473 and ROM 64600], one *Oryctodromeus* specimen [MOR 1642], and *Hypsilophodon* (Galton, 1975; Hulke, 1882). The lack of this feature in immature *Orodromeus* specimens advocates some degree of ontogenetic control influencing its expression, a shared trajectory manifested in *Hypsilophodon* [R5830 and R196].

Coracoid—Three *Orodromeus* specimens [MOR 294, 623, and PU 23442] provide a holistic picture of this element's overall morphology. Here, we preface this description with the acknowledgment that the right coracoid recovered in MOR 623 is mediolateral compressed evidenced by its complete lack of curvature, which makes the coracoid appear exceptionally thin. The coracoids of *Orodromeus* are rather conservative in their morphology and do not demonstrate the distinctive hatched-shaped profile (Chapter 3) observed in the coracoids of thescelosaurines, some thescelosaurids, hypsilophodontids, rhabdodontomorphs, and neoceratopsians (Chapter 3). *Orodromeus*, and other orodromines (Chapter 3; Boyd, 2012; Kutter, 2003), instead present a sternal process acutely angled away from the glenoid, a feature

they share with *Changchunsaurus* (Butler et al., 2011), *Changmiania* (Yang et al., 2020), and *Convolosaurus* (Andrzejewski et al., 2019). The glenoid process is robust in *Orodromeus* like *Pikunidromeus* (Chapter 3). Just posterior to the glenoid lies the coracoid foramen completely enclosed within the coracoid, and ventral to the glenoid is a continuous ventral fossa incising the ventral border of the coracoid. Only the juvenile holotype *Orodromeus* specimen presents a fused scapulocoracoid [MOR 294], but only in the right scapula and coracoid. The nueonces of scapulocoracoid fusion through ontogeny in ornithischians has not be explored. In thescelosaurids, the timing of scapulocoracoid fusion can be intraspecifically variable in taxa like *Fona* (Avrahami et al., 2024), *Oryctodromeus* [MOR 1636a, 1642, and IMNH 44939], *Haya* (Barta and Norell, 2021), and *Pikunidromeus* (Chapter 3). *Orodromeus* specimens described here seem to reenforce this interpretation as only the juvenile holotype [MOR 294] demonstrates fusion of the scapulocoracoid, which is lacking in specimens of more advanced ontogenetic stages [MOR 623, PU 23442 and 23443].

Humerus—The humerus of *Orodromeus* is an elongate bone, that is shorter than the scapula [MOR 294 and 623] and is represented best by six complete humeri [MOR 248, 294, 404, and 1136]. The humerus is sigmoidal in lateral profile and presents a humeral head deflected from the shaft at angles of 148° [MOR 248], 153° [right humerus, MOR 294], 147° [MOR 404], and 158° [MOR 1136] across these specimens. This range (147°-158°) is more obtuse than *Pikunidromeus* (115°-144°), but steeper than *Fona* (165°-180°) and *Haya* (166°) [IGM 100/2015]. Two specimens of *Hypsilophodon* [R5830 & R196] demonstrate a range (138°-152°) overlapping with those of *Pikunidromeus* and *Orodromeus*. The humeral head is robust and flanked by a diminutive lateral tuberosity and a moderately developed medial tuberosity.

Orodromines and thescelosaurids broadly present humeri that stand in stark contrast to the long and gracile morphology exemplified by the distinctive humeri of Gondwanan elasmerians such as *Notohypsilophodon* (Ibiricu et al., 2014), *Talenkauen* (Rozadilla et al., 2019), *Anabisetia* (Coria and Calvo, 2002), *Mahuidacursor* (Cruzado-Caballero et al., 2018), *Trinisaura* (Coria et al., 2013) and *Chakisaurus* (Nogueira et al., 2024). The anterior face of the proximal humeral head is concave (=bicipital sulcus) in *Orodromeus*. The deltopectoral crest emerges proximal to the mid-point of the humerus and is well-developed in *Orodromeus*; more so than the aforementioned elasmerians. Distally, the humerus subdivides into the medial ulnar condyle and lateral radial condyle.

Ulna—The ulna of *Orodromeus* is represented by a handful of incomplete ulnae [MOR 623 and PU 23246] and only a singular complete specimen, the holotype [MOR 294]. When it comes to arguments of proportional robustness, or lack thereof, it is difficult to make comparisons with other thescelosaurid taxa due to the juvenile stage of the *Orodromeus* holotype [MOR 294]; however, it clearly does not resemble the elasmerian condition where the ulna, along with the radius and humerus, are very elongate and slender (Coria and Calvo, 2002; Cruzado-Caballero et al., 2019). MOR 294 demonstrates a slight lateral bend in the ulna in anterior profile. The proximal epiphysis is well developed in *Orodromeus*. The olecranon process is bulbous and rises above the coronary process, both contribute to a strongly curved trochlear notch. This evident curvature differs from the weak curvature seen in *Pikunidromeus* (Chapter 3), the “Kaiparowits Orodromine” (Boyd, 2012), *Fona* (Avrahami et al., 2024), and *Haya* (Barta and Norell., 2021). The ulna shaft narrows distally from the proximal epiphysis in MOR 294 and

demonstrates a rough D-shaped cross-section. Distally the ulna swells into a rounded articular surface.

Radius—Like the ulna, only the juvenile holotype specimen retains a complete radius [MOR 294]; however, there are fragments of a radius also retained in MOR 623. The radius is bowed both anteriorly and laterally. The proximal epiphysis is mediolaterally flattened where it tightly presses against the lateral surface of the coronary process of the ulna. A faint ridge runs the long axis of the radius along the lateral surface which is a feature shared with *Akanthodromeus* (Chapter 2), *Pikunidromeus* (Chapter 3), *Haya* (Barta and Norell, 2021), and *Fona* (Avrahami et al., 2024). The cross-section of the radius is sub-ovular. The distal epiphysis is rounded and bulbous.

Manus—Three specimens provide key insights into the manus of *Orodromeus makelai* [PU 23442, MOR 294, and MOR 623]. Chapter 3 discusses at length the discrepancies of the manus presented and figured in Scheetz (1999) as *Orodromeus*. In summary, the manus portrayed in Figure 23 (Scheetz, 1999) is a composite of *Orodromeus* specimen PU 23442 and the *Pikunidromeus* holotype MOR 473. Consequently, the manus of *Orodromeus* is only partially accounted for. PU 23442 is a likely adult specimen presenting a good portion of the left manus. PU 23442 encompasses four carpals, along with metatarsals I through IV. Unfortunately, these delicate manual elements exhibit some corrosive damage from the acid preparation methods employed which affect some morphological inferences. Furthermore, PU 23442 is thickly coated in an unknown consolident that obscures large swaths of each bone. Still, general insights can be gained from PU 23442. The carpus of *Orodromeus* is unfused, as in *Pikunidromeus* (Chapter 3) and the “Kaiparowits Orodromine” (Boyd, 2012). PU23442 retains the cuboid radiale,

intermedium, ulnare, and the oblong distal carpal in relative articulation. Again, their specific features are somewhat blurred by acid preparation damage and consolident. What is better understood is the first three metatarsals whose morphology is corroborated by MOR 294 and 623. When comparing PU 23442 to the manus of another similarly sized *Pikunidromeus* specimen [MOR 473], *Pikunidromeus* demonstrates a more robust metacarpal morphology. The metacarpi of *Orodromeus* are more gracile (anteroposteriorly narrowed) especially at the proximal epiphyses in contrast to *Pikunidromeus* (Chapter 3), and *Fona* (Avrahami et al., 2024). Metacarpal I in *Orodromeus* presents an obliquely angled distal articular face with asymmetrically distal condyles, a morphology shared with *Pikunidromeus* and a potential synapomorphy of Orodrominae. Overall, the incomplete manus of PU23442 appears to show *Orodromeus* a similar morphology to *Pikunidromeus*, reflecting the apparent thescelosaurid manus blueprint outlined in (Chapter 3), where the metacarpals are relatively "uniform" in length, which is perhaps convergently seen in elasmerians like *Mahuidacursor* (Cruzado-Caballero et al., 2019) and *Anabisetia* (Coria and Calvo, 2002). This "uniform" metacarpal condition diverges from the widespread SBEDO blueprint where an elongate second- and third-digit contrasts with shortened digits I, IV, and V, as exemplified by the manus of *Minimocursor* (Manitkoon et al., 2023), *Heterodontosaurus* (Santa Luca, 1980), *Hypsilophodon* (Galton, 1975), *Convolosaurus* (Andrzejewski et al., 2019), *Lesothosaurus* (Baron et al., 2017), and *Hexinlusaurus* (He and Chai, 1984).

Ilium—The morphology of the ilium for *Orodromeus* is well represented by multiple specimens [MOR 294, 331, 623, F#06.26.95, and PU 23257]; however, only the left ilium of MOR 623 retains a complete preacetabular process. Scheetz (1999) states the preacetabular

process of *Orodromeus* is variable in shape and its degree of curvature, and has been cited as thus (Brown et al., 2013); however, this is inconsistent with our observations here. There are only two complete orodromine ilia from the Two Medicine Formation; (1) MOR 623 preserves a complete left ilia for *Orodromeus*, and (2) an indeterminant orodromine ilia collected from locality TM-088. The rest exhibit broken preacetabular processes just dorsal to the pubic peduncle [MOR 294, 331, right ilium MOR 623, and F# 06.26.95], making it difficult to quantify the variability and degree of curvature in *Orodromeus*. In *Orodromeus* specimen MOR 623, the preacetabular process demonstrates a process length to total ilium length ratio of 0.35, showing that although this process is elongate, it is still proportionally shorter compared to other thescelosaurids (Avrahami et al., 2024), notably when gauged to two indeterminate orodromine specimens. The first, TMP 2008.045.0002 comes from the lower Oldman Formation and exhibits a preacetabular process ratio of 0.43, while the other is the TM-088 indeterminate left ilium which closely pairs at 0.42. Other thescelosaurids hover around 40% (Avrahami et al., 2024).

The dorsal margin of the ilia in *Orodromeus* is convex in lateral view which is a shared condition with other orodromines like the indeterminate specimens TMP 2008.045.0002 (Brown et al., 2013) and the TM-088 ilium, *Zephyrosaurus* [OMNH V1051], and *Pikunidromeus* (Chapter 3), but also with *Jeholosaurus* (Han et al., 2012), *Haya* (Barta and Norell, 2021), *Parksosaurus* (Sues et al., 2023), *Changmiania* (Yang et al., 2020), and *Hypsilophodon* (Galton, 1975). This contrasts with the sigmoidal dorsal border of the ilia seen in *Talenkauen* (Agnolín et al., 2024; Rozadilla et al., 2019), *Macrogryphosaurus* (Rozadilla et al., 2020), *Kulindadromeus* (Godefroit et al., 2014), *Gasparinisaura* (Coria and Salgado, 1996), *Fona* (Avrahami et al., 2024), *Thescelosaurus neglectus* [MOR 979, 1125, 1185, and NCSM 15728], and the flat dorsal

margin observed in *Trinisaura* (Coria et al., 2013), *Gideonmantellia* (Ruiz-Omeñaca et al., 2012), *Anabisetia* (Coria and Calvo, 2002), *Lesothosaurus* (Baron et al., 2017), *Convolosaurus* (Andrzejewski et al., 2019), and *Nanosaurus* (Galton and Jensen, 1973; Carpenter and Galton, 2018). In dorsal view the lateral face of *Orodromeus* ilia are concave. The postacetabular process ends in a squarish terminus in contrast to the pointed terminus of *Changmiania* (Yang et al., 2020), TMP 2008.045.0002 (Brown et al., 2013), and the indeterminate TM-088 ilium, nor is it like the rounded/bulbous termini seen in *Nanosaurus* (Carpender and Galton, 2018), *Thescelosaurus neglectus* [NSCM 15728, MOR 979], and *Talenkauen* (Agnolín et al., 2024; Rozadilla et al., 2019). The brevis shelf projects medially from the ventral border of the postacetabular process at a near right angle, traveling anteriorly, it slopes ventrally to meet the ischiac peduncle and can be seen laterally in some *Orodromeus* specimens [MOR 294, F#06.26.95, and PU 23257]. The ischiac peduncle frames the posterodorsal corner of the acetabulum and is bulbous in *Orodromeus* [MOR 294, 623, and PU 23257]. Scheetz (1999) describes the ischiac peduncle as “strap-like” in *Orodromeus* which we recognize in-part. The juveniles and the potential subadults in the same offer anteroposteriorly narrow, but still bulbous ischiac peduncles [MOR 294, 331, 623, F#06.26.95], when compared to the largest individual in the *Orodromeus* sample [PU 23257]. PU 23257 consists of the posteroventral half of a large *Orodromeus* ilia and is ~ 22% larger than the next largest specimen [MOR 623]. The ischiac peduncle is extremely large and bulbous in PU 23257 and not anteroposteriorly narrowed. This may demonstrate an ontogenetic trend from theses “strap-like” ischiac peduncles to robust bulbous peduncles in adults.

Pubis—Four specimens retain pubes for *Orodromeus* [MOR 294, MOR 623, and PU23442]. The pubis is an elongate and delicate bone. A complete right pubis is accounted for in MOR 623 (Figure 26, Scheetz, 1999). At some point in the past 25 years the postpubic process of the right pubis was broken, with a small chip of shaft near the break being lost; however, the shaft still connects seamlessly on one side and therefore the total length of the pubis does not appear to be affected by the break in its newly repaired state. The left and right pubes recovered for MOR 623 are remarkably complete, but as explained in Chapter 3, the morphologies of these two bones are heavily altered by post-burial compression, which was not readily apparent during the write-up of Scheetz (1999). This unfortunately has led to a persisting mischaracterization of the true morphology of the orodromine prepubic processes (Chapter 3). Chapter 3 reveals a trio of features characteristic of orodromine prepubic processes, two of which are apparent in the *Orodromeus* sample. The prepubic process incorrectly was described as mediolaterally compressed and rod-like (Avrahami et al., 2024; Brown et al., 2013; Scheetz, 1999), largely because of MOR 623. *Pikunidromeus* specimens MOR 473 and ROM 64600 instead reveal the prepubic process presents a prominent lateral inflection midway along the shaft (Chapter 3). This mid-lateral inflection is also seen in the indeterminate orodromine specimen TMP 2008.045.0002, while the thescelosaurine *Fona* exhibits a lateral inflection, or swelling, proximal to the main body of the pubis shared with at least one specimen of *Oryctodromeus* [MOR 1636b] and potentially *Nanosaurus* (Carpender and Galton, 2018). This lateral inflection is not obvious in any *Orodromeus* specimens, but in *Pikunidromeus* this lateral inflection arises to a narrow apex, which downturns ventrally as it nears the pubic body. This narrow ridge is visible in the pubes of MOR 623, and we surmise it would have also exhibited this lateral inflect if not for

post-burial compression flattening the prepubic shaft mediolaterally. The distal terminus of the prepubic in *Orodromeus* swells dorsoventrally into a pad and presents anteroposteriorly trending striations [MOR 623], the two characteristics are also shared by *Pikunidromeus* (Chapter 3), TMP 2008.045.0002, but also convergently in *Minimocursor* (Manitkoon et al., 2023).

The main body of the pubis is cuboid and emerges from the medial face of the shaft to frame the anteroventral corner of the acetabulum. In *Orodromeus*, the pubis articulates with the axial column through a triple junction articulation that includes the sacrum, sacral ribs, and pubic peduncle of the ilium in MOR 623. This triple junction articulation is a proposed autapomorphy for *Thescelosaurus neglectus* but now is found in *Fona* (Avrahami et al., 2024), potentially *Pikunidromeus* (Chapter 3), *Oryctodromeus* [MOR 1636a, 1642], and now here in *Orodromeus* [MOR 623] and thus may be instead a thescelosaurid synapomorphy. As noted in the discussion of the sacrum, the intercentral sockets migrate dorsally through ontogeny and are more laterally place in more skeletally mature *Orodromeus* specimens. At present, it is uncertain how this would affect the development of this triple junction, or even if it is a feature of juveniles. The main body of the pubis showcases a prominent obturator foramen (=notch) which is open in PU 23442 and completely closed in both pubes of MOR 623. Inside the open obturator notch [PU 23442], an anteriorly placed fossa is clearly seen and is pierced centrally by a foramen. This fossa/foramen is not seen in either pubis of MOR 623, nor in *Pikunidromeus* [MOR 473] and is not reported in any other thescelosaurid. The post pubic process is long and slender in MOR 623. Distally, the shaft concludes in a bulbous terminus.

Ischium—Three *Orodromeus* specimens retain ischia [MOR 294, PU 23246 and 23431]. The ischium is elongated and straight in lateral view in *Orodromeus*, as in other thescelosaurids

(Chapter 3; Avrahami et al., 2024; Krumenacker et al., 2024). Anteriorly, the ischium bifurcates into subequal processes, the dorsally inclined iliac peduncle and ventrally inclined pubic peduncle. The processes are not as robust when compared to the ischia of *Pikunidromeus* (Chapter 3). *Orodromeus* instead follows the narrow profile of other thescelosaurids (Avrahami et al., 2024; Han et al., 2012). No medial protrusion is obvious on the pubic peduncle of any *Orodromeus* ischia. Some specimens of *Pikunidromeus* and *Fona* both display such a protuberance (Chapter 3; Avrahami et al., 2024). The obturator process emerges from the medial margin of the ischia shaft in the proximal third, contrary to the reconstructions presented in both ischia of MOR 294. Both the left and right ischia of MOR 294 are incomplete and were originally reconstructed with some synthetic puddy substituting missing portions. This reconstruction presented two ischia with the obturator process incorrectly placed midpoint along the shaft, only recently rectified. Though the obturator process appears tab-like in its morphology none of these processes in the *Orodromeus* sample are complete. The ischia shaft in *Orodromeus* is straight in lateral view like in most thescelosaurids (Avrahami et al., 2024; Barta and Norell, 2021; Krumenacker et al., 2024) and does not exhibit any twisting of the shaft in the distal third unlike in *Pikunidromeus* which demonstrates some slight twisting (Chapter 3). This contrasts with the distal twist observed in *Fona* (Avrahami et al., 2024), *Haya* (Barta and Norell, 2021), and *Thescelosaurus neglectus* [NCSM 15728 and MOR 979]. The cross-section of the ischial shaft in *Orodromeus* shifts from sub-oval anteriorly to a flattened triangular cross-section distally. The change is facilitated by the emergence of a flattened ventromedial faceted edge along the ischial shaft posterior to the obturator process which the postpubic shafts pressed against. There is no rugose sutural surface medially nor a shallow lateral groove as in

Pikunidromeus (Chapter 3). Distally, the ischia tapers but does not terminate into the bulbous boot presented by *Oryctodromeus* (Krumenacker et al., 2024), *Fona* (Avrahami et al., 2024), *Thescelosaurus neglectus* [NCSM 15728 and MOR 979], *Convolosaurus* (Andrzejewski et al., 2019), *Talenkauen* (Agnolín et al., 2024), *Trinisaura* (Coria et al., 2013), and *Anabisetia* (Coria and Calvo, 2002). Notably, none of the *Orodromeus* ischia exhibit the blade-like lateral protrusion which extends from the distal third of the shaft seen in most other thescelosaurids like *Nanosaurus* [BYU ESM 163R], *Pikunidromeus* (Chapter 3), *Fona* (Avrahami et al., 2024), *Jeholosaurus* (Fig. 6, Han et al., 2012), *Haya* [IGM 100/2015], *Oryctodromeus* (Krumenacker et al., 2024), *Zephyrosaurus* [OMNH V1051], but also in some other SBEDOs like *Convolosaurus* (Andrzejewski et al., 2019), *Hexinlusaurus* (He and Cai, 1984), and *Hypsilophodon* (Galton, 1975).

Femur—Roughly 80 femora are known for *Orodromeus* spanning the full ontogenetic spectrum and includes an exceptionally small specimen [MOR 248], which would be the smallest reported thescelosaurid specimen if not for a second indeterminate orodromine perinate from younger strata in the Two Medicine Formation (Horner et al., 2009). On the flipside, a distal portion of an isolated right femur collected from TM-160 is the largest orodromine femur discovered to date with an estimated complete femur length of 22.8 cm, and comparable in length to the largest *Oryctodromeus* [MOR 1642 and IMNH 50877] and *Fona* [NCSM 33548, 36522, and 33546] specimens. This suggests an entire unsampled size class of *Orodromeus* and potentially orodromines broadly. Overall, femora are easily the most frequently recovered appendicular element for this taxon with the largest sampling coming from the field locality called Egg Mountain (TM-006).

This large femur sample showcases the extensive taphonomic deformation afflicting *Orodromeus* specimens with most specimens demonstrating some degree of post-burial crushing. The is best exemplified by the mid-shaft diaphysis which are often collapsed on themselves which likely facilitates the significant variation in the degree of anterior bowing [MOR 248, 294, 623, PU 22412, 23443, F# 7.16.15.14, and F#0709.096]. This post-burial deformation also significantly impacts the angle of deflection pertaining to the femur heads projection from the femur shaft, with a wide range exhibited in the sample. This variation in femur head projection is also a shared trend in the *Fona* sample but no such taphonomic inferences were conjured to explain the variation there; however, Avrahami et al. (2024) does acknowledge significant taphonomic alterations to the distal femur was attributed to similar taphonomic. Similarly, *Oryctodromeus* femora, especially from the Blackleaf locality are significantly altered from tectonic process [MOR 1642] and demonstrate quite a range in this deflection (pers. observ.) and loosely referenced (Krumenacker et al., 2024). As these three thescelosaurids present some of most sizeable assemblages for the group with wide ranges demonstrated for this character, in conjunction with taphonomic overprints facilitating its post-burial expressions, we caution its application in character matrixes. However, it may not be ubiquitously fallible character as *Pikunidromeus* presents a sizeable femora sample (n=11) and the angle of femur head deflection is rather restricted in its range of variation (Chapter 3). Likely, the tectonic history and burial depth of the host formation/localities provide an important context in evaluating this character.

The proximal femur is robust in *Orodromeus* with a globular femur head presented on a constricted neck, framed laterally by the trochanteric region. The trochanteric region is subdivided between the well-developed greater trochanter and a finger-like lesser trochanter

closely pressed against the greater trochanter anteriorly. There is no intertrochanteric cleft (=notch) separating the trochanters, some specimens like MOR 623 and F#07.09.096 show erosions divisions which we do not regard as authentic intertrochanteric clefts. The full ontogenetic spectrum in the *Orodromeus* sample confirms the assertions made by Chapter 3 that the development of the lesser trochanter in orodromines is under some ontogenetic control. In juvenile *Orodromeus* specimens [MOR 294 and F7.16.15.14] the lesser trochanter is poorly developed, laterally flattened, and does not meet the dorsal margins of the greater trochanter. Through ontogeny the lesser trochanter rounds slightly and extends dorsally until it is subequal with the dorsal margin of the greater trochanter [MOR 2726 and PU 23443]. This developmental trend is mirrored in the *Pikunidromeus* sample (Chapter 3), but notably is not in the *Fona* sample where the dorsal expressions of the trochanters are intraspecifically variable regardless of ontogenetic stage (Avrahami et al., 2024). This illuminates some of the uncertainties surrounding the problematic holotype specimen of *Laosaurus minimus*, a taxon largely erected because of the small size of the holotype specimen (Gilmore, 1924). This taxonomic affinity of *Laosaurus minimus* will be explored further in the discussion, but here we note this specimen does demonstrate at least orodromine synapomorphy making it one of the earliest orodromine specimens in the Two Medicine-Judith River-Belly River clastic wedge. This specimen also clearly demonstrates a lesser trochanter that does not extend dorsally to be subequal with the greater trochanter, as demonstrated by adult specimens of *Orodromeus* and *Pikunidromeus*, indicates this specimen is probably a juvenile.

The pendent-shaped, mediolaterally thin, and terminally tapered fourth trochanter emerges from the posteromedial potion of the femur shaft, in the proximal upper half of the

femur. A shallow rugose elliptical fossa marks the femur diaphysis medially below just anterior to the base of the fourth trochanter likely making the insertion sites for the *M. caudofemoralis longus* and *M. puboischiofemoralis internus* muscles (Chapter 3; Maidment and Barrett, 2011). A small circular nutrient is centrally placed on the diaphysis [PU 22412] just lateral to the base of the fourth trochanter, a shared feature with other orodromines (Chapters 2 & 3; Brown et al., 2013), *Fona* (Avrahami et al., 2024), and other SBEDOs (Barta and Norrell, 2021; Cooper, 1985; Galton and Jensen, 1973; Galton, 1975; Forester et al., 2022). The femur shaft is D-shaped in cross-section at mid-shaft [MOR 623].

The distal epiphysis is subdivided into lateral (=fibular) and medial (=tibial) condyles, separated only by a posterior intercondylar sulcus (=groove). There is no anterior intercondylar sulcus in *Orodromeus*, nor in any other orodromines (Chapter 3; Brown et al., 2013; Kutter, 2004). The medial condyle does not inflate into the posterior intercondylar groove in most *Orodromeus* specimens as it does in *Pikunidromeus* (Chapter 3). *Orodromeus* specimens MOR 2726 and F#07.09.96 present the three total femora with intrusive medial condyles. In Chapter 3, this medial inflation is presented as an autapomorphic character linking specimens in the Two Medicine Formation and the Upper Oldman Formation, and justified by the overwhelming absence of this medial inflation in orodromine specimens across the board (Brown et al., 2013; Hudgins, 2021; Kutter, 2004) This may mean MOR 2726 and F#07.09.96 represent the earliest occurrences of *Pikunidromeus*, extending its temporal range into the lacustrine interval of the Flag Butte Member of the Two Medicine Formation, or alternatively, this demonstrates this medial inflation is more variable in orodromines than Chapter 3 considered. However, we are hesitant to suggest these specimens are representative of *Pikunidromeus* with no other supporting

characters in these specimens to lend credence, especially when these specimens are so clearly taphonomically altered (i.e. crushed); furthermore, the entirety of the orodromine assemblage in the lacustrine interval of the Flag Butte Member demonstrates a morphological consensus that *Orodromeus* lacks this medial inflection of the posterior intercondylar sulcus. Therefore, we assert these three specimens are likely just taphonomic outliers, assignable to *Orodromeus makelai* until a well-preserved specimen with a femur exhibiting a clearly inflated medial condyle is produced in the lacustrine interval of the Flagg Butte Member.

Tibia—Nearly 45 tibiae are recovered for *Orodromeus*. They are exceptionally fragmentary, with only two complete tibiae in the entire sample [MOR 623, "Jacket A"]. The tibia of Orodromeus is longer than the femur [MOR 623, "Jacket A"], and exhibits an averaged tibia to femur length ratio of 1.18. This ratio falls within the narrow range exhibited by most SBEDOS [1.18-1.22] (Chapter 3). The proximal epiphysis is moderately anteroposteriorly expanded in *Orodromeus* like in *Pikunidromeus* (Chapter 3) *Albertadromeus* (Brown et al., 2013), and *Micropachycephalosaurus* (Butler and Zhao, 2009). This moderate expansion pales in comparison to the significant proximal expansions seen in thescelosaurines like *Fona* (Avrahami et al., 2024), *Thescelosaurus assiniboiensis* (Brown et al., 2011), and some specimens of *Oryctodromeus* (pers. observ.). The proximal epiphysis of the tibia is separated into a trifecta of condyles in *Orodromeus*: the cnemial crest, lateral condyle (=outer), and inner condyle (=medial). The cnemial crest frames the anterior portion of the proximal tibia, is rounded and robust like other orodromines (Chapter 3; Brown et al., 2013), and curves laterally. There is no fossa medial to the cnemial crest in *Orodromeus*, unlike in *Haya* (Barta and Norell, 2021) and perhaps *Fona* (Avrahami et al., 2024) and *Oryctodromeus* [MOR 8660]. The lateral condyle

bifurcates into a larger fibular and smaller accessory condyle which is the condition shared with the thescelosaurids *Pikunidromeus* (Chapter 3), *Fona* (Avrahami et al., 2024) *Oryctodromeus* (Krumenacker et al., 2024), *Changchunsaurus* (Jin et al., 2010), *Haya* (Barta and Norell, 2021), but also in *Gideonmantellia* and *Hypsilophodon* (Galton, 1975; Ruiz-Omeñaca et al., 2012). In other SBEOs the accessory condyle is not developed (Baron et al., 2017; Coria and Salgado 2010; Han et al., 2012; Ibiricu et al., 2014; Li et al., 2021). The inner condyle tapers to a subtriangular slighly downturned apex posteriorly. The inner condyle is not strongly hooked like in some *Oryctodromeus* specimens [MOR 1636a, 1642, 8660; IMNH 44604, 44939].

The tibia shaft twists proceeding distally and exhibits a sub-triangular cross-section at midshaft. Just below midshaft in MOR 623, the shaft buldges laterally in a structed denoted the fibular eminence. Distally the tibia expands mediolaterally into two robust malleoli, the medial (=inner) and lateral (=outer) malleoli. Of the two, the lateral malleolus is larger and descends past the articular face of the medial malleolus, a condition observed in most SBEDOs (Andrzejewski et al., 2019; Baron et al., 2017; Herne et al., 2018; Krumenacker et al., 2024). The lateral malleolus presents a sharp flange where the distal fibula tightly pressed. Posteriorly, a pronounced ridge separates the two malleoli.

Fibula—The fibula of *Orodromeus* is best represented by the complete right fibula retained in MOR 623. The proximal epiphysis is anteroposteriorly expanded, but mediolaterally compressed, with an obliquely angled dorsal margin. This obliquely angled dorsal margin is shared with thescelosaurids broadly (Chapter 3; Avrahami et al., 2024; Brown et al., 2013; Butler et al., 2011; Han et al., 2012; Krumenacker et al., 2024) and differs from the more horizontal inclination of some other SBEDOs like *Hypsilophodon* (Galton, 1975), *Gasparinisaura* (Coria

and Salgado, 1996), *Parksosaurus* (Sues et al., 2023), and *Heterodontosaurus* (Santa Luca, 1980). The fibula of *Orodromeus* tapers distally, twisting medially on its long axis mirroring the rotation of the tibia, and terminates in a bulbous distal epiphysis. A prominent flange emerges at mid-shaft and projects medially along the distal half of the element. In MOR 623, this flange is obvious, though much of its medial edge is fractured. This flange is documented in other orodromines (Chapter 3; Brown et al., 2013) but is widest in the holotype specimen of *Albertadromeus* (Brown et al., 2013) and an indeterminate orodromine fibula from the Upper Oldman Formation [TMP 1995.12.127]. In Orodromeus, juvenile specimens [PU 23246 and F# 08.05.95] demonstrate a reduced medial flange on their fibula. This paints a picture of ontogenetic change in *Orodromeus* where the medial flange on the fibula widens progressively with maturation. *Pikunidromeus* demonstrates an opposing neotenous trend, where the adult specimens [MOR 473 and ROM 64600] retain the juvenile condition (=reduced flange) into adulthood. The *Laosaurus minimus* holotype specimen presents a reduced flange also on the medial edge of its fibula [CMN 9483], further reinforcing its juvenile orodromine interpretation.

Astragalus—The astragalus is not fused to the calcaneum in MOR 623 but they appear to be at least partially fused in the juvenile *Orodromeus* specimen PU 23246 (both feet). The fused astragalus-calcaneum [PU 23246] are not fused to the tibia in a tibiotarsus as in *Changmiania* (Yang et al., 2020). The astragalus is crescentic in lateral profile, with a smoothly concave dorsal surface which cups the medial malleolus of the distal tibia. A forked ascending process arises anteromedially into the flexor groove on the anterior face of the distal tibia [MOR 623 and PU 23246] as in *Pikunidromeus* (Chapter 3), *Fona* (Avrahami et al., 2024), *Oryctodromeus* (Krumenacker et al., 2024), and *Jeholosaurus* (Han et al., 2012). A large foramen pierces the

concave dorsal surface of the astragalus just ventral to the ascending process, just as in *Fona* and *Jeholosaurus* (Avrahami et al., 2024; Han et al., 2012).

Calcaneum—The calcaneum is crescentic in lateral profile with two distinct facets for articulation with the distal fibula and lateral malleolus of the tibia. The angle separating these two facets covers a range from 120° to 133° in *Orodromeus*. This angled division is similar to *Fona* and *Oryctodromeus* (Avrahami et al., 2024), which are more obtuse then *Pikunidromeus* (Chapter 3). A small depression marks the anteromedial corner at the apex of the fibula facet which accommodates the medial fork of the ascending process of the astragalus [MOR 623]. There is no foramen piercing the medial wall of the calcaneum like in *Fona* (Avrahami et al., 2024) and *Oryctodromeus* [MOR 1642].

Distal tarsals—The *Orodromeus* specimens MOR 623 and PU 23246 both retain distal tarsals and though the medial distal tarsal remains in articulation in PU 23246, it is not fused to the metatarsals like in *Akanthodromeus* (Chapter 2) and are clearly cemented together by matrix instead. In thescelosaurids, the medial distal tarsal is surprisingly diverse between taxa. *Orodromeus* presents a dorsoventrally thin medial distal tarsal, which is squarish in dorsal view, with an elongate triangular medial projecting process. This morphology is most similar to *Pikunidromeus* [MOR 473] and an indeterminate orodromine medial distal tarsal from the Two Medicine locality TM-088. These three differ greatly from the short triangular medial processes of *Akanthodromeus* (Chapter 2) and *Fona* (Avrahami et al., 2024) and the elongate rectangular medial process exhibited by *Oryctodromeus* [MOR 1642]. A proximal ridge crosses catacorner across the medial distal tarsal in thescelosaurids, but in *Oryctodromeus* this ridge is sharp and extends the length of the medial process [MOR 1642]. Ventrally a sharply defined ridge

emanates from the medial distal tarsal trending anteroposteriorly. This ridge marks the outline of the proximal epiphyses of metatarsal two and three, which the medial distal tarsal caps in *Orodromeus*. A large foramen pierces the lateral face of the medial distal tarsal in MOR 623, and perhaps in PU 23246, which is distinct from *Pikunidromeus* which lacks this foramen [MOR 473].

The lateral distal tarsal is roughly cuboid in shape. The dorsal surface is gently concave where the rounded margin of the calcaneum slid, while the lateral face can be strongly [MOR 623] to weekly concave [PU 23246]. In MOR 623, the lateral, medial, anterior, and posterior faces present very irregular surfaces, with deeply incising rugose fossae. A circular foramen pierces the medial face of the lateral distal tarsal in rough opposition to the foramen piercing the lateral face of the medial distal tarsal [MOR 623]. Another foramen pierces the anterior face of the lateral distal in *Orodromeus* as in *Zephyrosaurus* [YPM 56695] and *Heterodontosaurus* (Sereno, 2012), but only a circular depression marks the posterior face in roughly the same position as the posterior foramen in *Fona*, *Jeholosaurus*, *and Heterodontosaurus* (Avrahami et al., 2024; Han et al., 2012; Santa Luca, 1980). The lateral distal tarsal caps the proximal epiphysis of metatarsal IV.

Pes—A complete account of the pes blueprint of *Orodromeus* is accounted for based on four specimens [MOR 331, 623, 994, and PU 23246]. As highlighted in Chapter 3, the left pes figured in Scheetz (1999) is MOR 623 and not MOR 530; furthermore, the overall interpretation portrayed therein was inaccurate facilitated by an incorrect reconstruction of both pes in MOR 623. Here we rectify and present a new interpretation of the pes layout for MOR 623 corroborated by new thescelosaurid discoveries unavailable at the time of Scheetz (1999)

(Chapters 2 & 3; Avrahami et al., 2024; Barta and Norell, 2021; Butler et al., 2011; Han et al., 2012; Krumenacker et al., 2024). We also note pathologies in MOR 623 on the metatarsal I, II, and phalange PII-I which may have hindered the original interpretation. In conjunction, we document an exceptionally well preserved small juvenile *Orodromeus* specimen that retains a complete left pes, the smallest documented for a thescelosaurid yet [MOR 331].

Five metatarsi are described here for *Orodromeus*. There is no complete metatarsal I recovered for *Orodromeus*. When complete metatarsal I was likely splint-like as evidence by close relatives (Chapter 3; Boyd, 2012), which is hinted at in the right metatarsal I of MOR 623 which retains some of the shaft. The cross-section of the shaft of metatarsal I is sub-oval in *Orodromeus* [MOR 623, 994, PU 23246] like in *Pikunidromeus* (Chapter 3), both in contrast with the D-shaped cross-section of *Fona* (Avrahami et al., 2024) and the triangular cross-sections of some other SBEDOs (Chapter 2; Andrzejewski et al., 2019; Butler et al., 2011; Galton, 1975; Manitkoon et al., 2023; Sues et al., 2023). The distal epiphysis of metatarsal I in *Orodromeus* subdivides into two weakly developed articular condyles separated by a shallow U-shaped intercondylar groove.

Metatarsal II through IV serves as the main weight bearing elements of the foot. All three are mediolaterally compressed proximally and together configure into a stairstep articular surface to accommodate the medial and lateral distal tarsals [PU 23246]. Shafts narrow moving distally before mediolaterally expanding into lateral and medial articular condyles. Collateral ligament pits mark each distal epiphysis., and overall, these three metatarsi do not deviate much from the orodromine pes morphology (Chapters 2 & 3; Boyd, 2012).

The morphology of metatarsal V is noteworthy and distinct from other thescelosaurids. Here we figure metatarsal V for the first time [MOR 623], and though its presence is noted in Scheetz (1999), Gates et al. (2013), and Avrahami et al. (2024), only the later identified the specimen retaining the digit. Scheetz (1999) describes metatarsal V as splint-like and rounded terminally. In a modern context, this terminology is no longer accurate as the morphology of metatarsal V is quite diverse across different SBEDO groups (Chapter 3). Splint-like instead applies best to the morphologies of the fifth metatarsi in *Jeholosaurus* [IVPP V12529], *Haya* [IGM 100/2013], and *Nanosaurus* [BYU ESM-163R]. Alternatively, *Orodromeus* [MOR 623], *Pikunidromeus*, and the "Kaiparowits Orodromine" exhibit a "mailbox flag" hinged morphology distinct from other thescelosaurids (Chapter 3; Boyd, 2012). This mailbox flag morphology is discrete from the three *Thescelosaurus* species which present an hourglass profile [RSM P 1225.1, USNM 7757, LACM 33542], nor is it like the elongate metatarsi V of *Oryctodromeus* [MOR 1642], *Fona* [NCSM 36276], *Diluvicursor* [NMV P221080], and *Zephyrosaurus* [YPM 56695, formally MOR 759]. *Orodromeus* further distinguishes itself from *Pikunidromeus* and the "Kaiparowits Orodromine" in its diminutive size.

The phalangeal formula for *Orodromeus* is 2-3-4-5-0 [MOR 331, 623 and PU 23246]. Phalange PI-I is perhaps the most distinctive phalange in the pes of orodromines. In *Orodromeus*, phalange PI-I exhibits an average length/midshaft width ratio of 3.83 which falls within the ~ 3.0 and 4.0 range Avrahami et al. (2024) notes most SBEDOs fall within, excluding *Pikunidromeus* (Chapter 3); specifically, *Orodromeus* specimens demonstrate ratios of 3.43 [left pes, PU 23246], 3.82 [right pes, PU 23246], 4.07 [MOR 331], and 4.01 [MOR 623]. In *Orodromeus* specimens PU 23246 and MOR 623, a deeply incising ventromedial pit penetrates the shaft of PI-I just

posterior to the distal articular condyles. This ventromedial pit is the synapomorphic condition of Orodrominae (Chapter 3) and also is manifested in the holotype specimen of *Laosaurus minimus* (pers. observ.).

Discussion

The original description for *Orodromeus makelai* (Weishampel and Horner, 1988) diagnoses *Orodromeus* based on the following characters: (1) palpebral anchored to the postorbital part of the posterior margin of orbit; lateral boss on the jugal; (2) maxillary and dentary teeth broadly triangular in lateral view, often as wide as they are high; (3) rounded apical (primary) ridge sub-equally dividing anterior and posterior region of the crown; (4) anterior and posterior edges of the crown bear five to six uniformly-sized denticles in adult; and (5) the radiale, intermedium, and ulnare, plus one distal carpal form unfused wrist. We now recognize that many of these characters are not *Orodromeus*, or even orodromine, specific. The proposed first character is difficult to interpret at face value as this verbiage we understand to reference a posterior supraorbital, which were not recognized in any SBEDOs of the time; furthermore, the holotype specimen [MOR 294] does not preserve a posterior supraorbital, only an anterior supraorbital. Therefore, we surmise the authors likely were referencing a probable cartilaginous extension connecting the anterior supraorbital to the posterior supraorbital which articulates with the anterior protuberance of the postorbital [MOR 1141]. This postorbital protuberance is shared broadly across thescelosaurids (Chapter 3; Avrahami et al., 2024; Barta and Norell, 2021; Bertozzo et al., 2024; Krumenacker et al., 2024; Sues, 1980), but also convergently arose in some other SBEDOS (Barrett et al., 2010; Porro et al., 2015). The lateral boss (=horn) on the jugal is a valid character now recognized to be the synapomorphic condition of Orodrominae

(Chapters 2 and 3; Boyd, 2012; Scheetz, 1999; Sues, 1980). The dental morphology will be assessed in detail in a future cranial description (Hannebaum et al., in prep), but we note that the dental characters here are muddied in their interpretation due to the inclusion of troodontid embryonic material (Weishampel and Horner, 1996). Lastly, in a modern context, an unfused wrist is documented broadly in SBEDOs (Chapter 3; Cruzado-Caballero et al., 2019; Manitkoon et al., 2023). Therefore, if most of the only published diagnosis for *Orodromeus makelai* is not diagnostic, what characters do distinguish this taxon?

The skull of *Orodromeus* presents prominent collateral supraorbital ridges composited from the nasal, lacrimal, prefrontal, and supraorbitals. The prominence of this ridge, and its more middling placement along the anterior margin of the orbit, appears unique to *Orodromeus,* but we do acknowledge most orodromines lack comparable skull material. Two supraorbitals are present in *Orodromeus*, the first documentation for an orodromine and confirming its hypothesized presence (Barta and Norell, 2021) and demonstrating two supraorbital to be likely a synapomorphy of Thescelosauridae (Avrahami et al., 2024). All orodromines preserving a jugal also exhibit jugal horns, which demonstrate a wide range of morphologies (Chapters 2 and 3; Boyd, 2012; Sues, 1980). *Orodromeus* differs from other orodromines in its horn manifestation by presenting a large, dorsolaterally upturned, subconical horn encircled by prominent ridging [MOR 1141]. Medial to this horn, are two nutrient foramina, which is a configuration shared with other orodromines (Chapters 2 and 3; Boyd, 2012). *Orodromeus* exhibits an ovoid foramen which mediolaterally pierces the pterygoid wing of the quadrate, a feature shared only with *Zephyrosaurus*. In many thescelosaurids a pronounced medial process protrudes ventrally from the dentary symphysis (Chapter 3; Barta and Norell, 2021; Boyd, 2014; Morris, 1976), in

Orodromeus, this medial process is exceptionally pronounced as in other orodromines (Chapter 3; Brown et al., 2013). Unique to *Orodromeus*, a lateral fossa straddles the angular-surangular contact [MOR 294 and 1141]. *Orodromeus* demonstrates a prominent transverse dorsal groove on atlantal intercentrum present in other thescelosaurids, but notably absent in *Pikunidromeus* (Chapter 3). This lack of ubiquity in its manifestation in thescelosaurids, and the lack of descriptions of the atlantal intercentrum in other taxa preclude any definitive stance on whether it is a synapomorphy. *Orodromeus* is distinct from other thescelosaurids in exhibiting subequal capitulate processes on the anterior cervical ribs, which transition posteriorly to an elongate capitulum in the cervical series. *Orodromeus* also shows a vertical to horizontal transition of dorsal rib articulation occurs between dorsal vertebrae five and six. This differs from *Pikunidromeus* which shows this transition between dorsal vertebrae fix and eight. A clear sub-oval distal cross-section in anterior dorsal ribs clearly links *Orodromeus* with other orodromines (Chapter 3). *Orodromeus* demonstrates a caudal vertebrae transverse process to centrum length ratio of 0.72. There may be an intercentrum cavity between sacral vertebrae two and three in specimen MOR 623, which would be a feature shared with *Pikunidromeus* and *Fona*, and perhaps *Oryctodromeus* [MOR 1636a]. *Orodromeus* retains epaxial tendons but no hypaxial tendons, which is a pattern prevalent in orodromines (Chapter 3; Avrahami et al., 2024; Brown et al., 2013) and distinguishes the group from thescelosaurines. Mature *Orodromeus* specimens [PU 23442 and 23443] display a scapular flange on the posterior margin of the scapula. This flange is also shared with mature specimens of *Pikunidromeus* [MOR 473 and ROM 64600], a specimen of *Oryctodromeus* [MOR 1642], and *Hypsilophodon* (Galton, 1975; Hulke, 1882). A singular continuous ventral fossa on coracoid is observed in *Orodromeus*, and other orodromines

(Chapter 3), and not the two ventral fossae seen in *Oryctodromeus* and *Fona* (Avrahami et al., 2024). In *Orodromeus*, the preacetabular process length to total ilium length ratio is 0.35, which differs from an indeterminate orodromine specimen 0.43 [TMP 2008.045.0002]; Thescelosaurids present a rounded dorsal margin of the ilium, which is present here in *Orodromeus*. Orodromines exhibit a striated prepubic process on its anterior terminus, which is dorsoventrally expanded into a pad, characteristics observed in *Orodromeus*. *Orodromeus* lacks an ischial shaft with a lateral blade-like protrusion in its distal third, which all other thescelosaurids do. Orodromines lack an intertrochanteric cleft on femur. *Orodromeus* also lacks this cleft, though as discussed above, superficial clefts are manifest in some specimens but likely are taphonomically altered. There is no medial inflection of distal femur medial condyle into the posterior intercondylar groove like there is in *Pikunidromeus* (Chapter 3). Prominently in orodromines like *Albertadromeus*, *Orodromeus*, and an indeterminate specimen [TMP 1995.12.127] a sizeable flange emerges medially from the distal half of fibula. *Orodromeus* exhibits a forked ascending process of astragalus. A large foramen pierces the lateral face of the medial distal tarsal in *Orodromeus*. Orodromines present a unique morphology for metatarsal V. This morphology is best described as “mailbox flag” shaped. The metatarsal V of *Orodromeus* is distinct from other orodromines in its shortened length. Lastly, *Orodromeus* presents a deeply incising ventromedial pit penetrating shaft of PI-I, shared with other orodromines (Chapter 3).

Orodromine systematics overview

Orodrominae suffers from an unfortunate prevalence of informal, fragmentary, indeterminate, and potentially dubius orodromine taxa/specimens. This lack of systemic bracketing has allowed for the proliferation of multiple informal osteologies to persist in

character matrixes. The above re-diagnosis of *Orodromeus makelai*, in conjunction with the recent descriptions of *Pikunidromeus* (Chapter 3), and *Akanthodromeus* (Chapter 2), create clear taxonomic distinctions within Orodrominae and present new opportunities to review the systematics of problematic taxa/specimens; namely *Albertadromeus*, *Laosaurus minimus*, the "BV Orodromine", the "Kaiparowits Orodromine", TMP 1995.12.127 (fibula), and TMP 2008.045.0002 (postcranial skeleton).

Albertadromeus syntarsus

The phosphatized holotype skeleton of *Albertadromeus syntarsus* is an extremely fragmentary specimen [TMP 2009.037.0044]. A certain amount of phylogenetic uncertainties has surrounded this specimen because of this, likely exasperated by the lack of orodromine synapomorphies presented in its original diagnosis (Brown et al., 2013). The new synapomorphies proposed in Chapter 3 of this thesis allow definitive placement of *Albertadromeus* within Thescelosauridae, and combined with other anatomical observations lend more support for an orodromine designation. Also, recent updates to the chronostratigraphy of the Oldman and Dinosaur Park Formations now places *Albertadromeus* in the Upper Oldman Formation, and now time equivalent with *Pikunidromeus*, the "BV Orodromine", and multiple indeterminate specimens (ca. 76.2 Ma) (Chapter 3; Brown et al., 2013; Eberth et al., 2023), warranting revisiting its diagnosis.

Albertadromeus presents a well-developed bifurcated lateral condyle of the proximal tibia. The fibular condyle is larger than the accessory condyle in *Albertadromeus* and unites this taxon with other thescelosaurids like *Pikunidromeus* (Chapter 3), *Haya* (Barta and Norell, 2021), *Oryctodromeus* (Krumenacker et al., 2024), *Fona* (Avrahami et al., 2024), *Koreanosaurus* (Huh

et al., 2010), *Changchunsaurus* (Butler et al., 2011), and *Jeholosaurus* (Han et al., 2012). The most distinctive feature of the *Albertadromeus* holotype is a prominent medially projecting flange on distal half of the fibula which is fused to the anterior face of the tibia. This fibular flange is demonstrated by multiple thescelosaurids (Chapter 3; Avrahami et al., 2024; Barta and Norell, 2021; Han et al., 2012; Herne et al., 2018; Krumenacker et al., 2024). *Orodromeus* [MOR 623] and *Albertadromeus* share a wide fibula flange, much wider than other thescelosaurids. In the *Albertadromeus* holotype [TMP 2009.037.0044] this flange is distinctive from *Orodromeus* [MOR 623], as it is wider and fused to the anterior face of the tibia (Brown et al., 2013). Another isolated fibula from temporally equivalent strata in the Upper Oldman Formation mirrors the *Albertadromeus* morphology and is similarly sized [TMP 1995.12.127] and likely represents a second specimen; however, TMP 1995.12.127 shows no signs of fusion to any tibia. This may indicate the timing of its fusion to the tibia is variable in *Albertadromeus*. *Pikunidromeus* presents a reduced fibula flange, and the fibula is not fused to the tibia.

"*Laosaurus minimus*"

"*Laosaurus minimus*" is a dubious taxon erected in Gilmore (1924) based on a partial thescelosaurid postcranial skeleton [CMN 9483]. Initially, this specimen was noted to originate from the Lower Cretaceous Blairmore Formation in southern Alberta (Gilmore, 1924), but follow-up research instead suggested the *Laosaurus minimus* holotype specimen [CMN 9483] originated in the lower portion of the Upper Cretaceous Allison Formation (Russel, 1949). It wasn't for another 45 years until a detailed survey was published for this stratigraphic section, revealing these beds instead represented the proximal deposition of the Belly River Group and were subdivided into five new formations (Jerzykiewicz and Norris, 1994). CMN 9483 likely

originates somewhere along the boundary of the Connelly Creek and Lundbreck Formations ca. 78.0 Ma (pers. conv. Caleb Brown). This revelation about its potential age shows that the *Laosaurus minimus* holotype represents one of the oldest orodromine occurrences in the Two Medicine-Judith River-Belly River clastic wedge, only surpassed by *Akanthodromeus* (Chapter 2) and an indeterminate orodromine specimen MOR 554.

The original diagnosis for *Laosaurus minimus* is not valid, and centers on the small size of the specimen as the main distinguishing characteristic. CMN 9483 exhibits a handful of orodromine synapomorphies: (1) lack of an intertrochanteric notch, (2) medially projecting flange on distal half of fibula, and (3) deep pit just posterior to the distal articular condyles on the ventral surface of PI-I. The calcaneum the most distinctive bone retained in CMN 9483, as the angle separating the fibula and tibia facets is rather square unlike *Orodromeus*, *Albertadromeus*, *Zephyrosaurus*, and the "Kaiparowits Orodromine", but still this squared condition is shared with one other orodromine, *Pikunidromeus* (Chapter 3). Furthermore, the relationship of the lesser trochanter to the greater trochanter in CMN 9483 suggests this specimen is a juvenile, as the lesser trochanter does not extend to meet the dorsal margin of the greater trochanter. As discussed in Chapter 3, and verified in the above *Orodromeus* description, there is an ontogenetic trajectory in orodromines where the lesser trochanter rises through ontogeny until the trochanteric region is subequal in its dorsal marginations between the trochanters. With these revelations, we argue this specimen should be considered indeterminate in its taxonomic placement until further orodromine discoveries in its type area illuminate distinct characters.

<u>"BV Orodromine"</u>

The informal orodromine taxon the “BV Orodromine” is represented by two isolated partial left jugal horns collected from the Two Medicine Formation fossil locality TM-088. This is the only site in the Two Medicine-Judith River-Belly River clastic wedge with documented overlap between orodromines; at least two, the “BV Orodromine” and *Pikunidromeus* (Chapter 3). These two jugals are distinct from *Pikunidromeus* and their morphotype does not appear anywhere else in the wedge; and therefore, making it unlikely to represent another jugal morph of *Pikunidromeus*. The BV jugals are partially intact. Neither preserves much of the maxillary ramus, with both presenting breaks just anterior to the jugal horn. The larger jugal, comparable in size to the adult specimen of *Orodromeus* [MOR 1141], exhibits a complete posterolaterally deflected jugal horn, as in *Pikunidromeus* (Chapter 3), *Zephyrosaurus* (Sues, 1980), and the “Kaiparowits Orodromine” (Boyd, 2012) but differs from these other orodromines as the horn is distally upturned trend. The faces of the jugal horns in the “BV Orodromine” are ringed by numerus fine ridges, which trend its long axis while also radiating outward from the base across the lateral face of the jugal. The jugals are circular in cross-section at the base but narrow distally into a sub-oval cross-section. The two features in combination (ridges + cross-section) are distinct from *Orodromeus*, which shows also demonstrates ridging, but these are fewer and much larger [MOR 1141]; furthermore, the horn cross-section of *Orodromeus* is roughly circular. *Pikunidromeus* offers a diminutive triangular horn in contrast (Chapter 3).

TM-088 presents at least one other orodromine, *Pikunidromeus*, in cooccurrence with the “BV Orodromine”. Other postcranial material at the TM-088 gives us pause in erecting a new taxon based on these jugal horns, namely a single left ilia which demonstrates a preacetabular process to total ilia length of 0.42. This ratio closely links with another indeterminate orodromine

specimen from the Oldman Formation, TMP 2008.045.0002, which presents a ratio of 0.43. TMP 2008.045.0002 is still extensively encased within matrix which preludes further analyses outside of its initial description (Brown et al., 2013) until this specimen is explored further though non-invasive CT imaging. As *Pikunidromeus* lacks any complete ilia, there remains the possibility TMP 2008.045.0002 and the left ilia from TM-088 are examples of that taxon. Furthermore, the lack of skeletal material in association with the jugals of the "BV Orodromine" and the abundance of isolated indeterminate orodromine material precluded erecting a new taxon without anatomic clarification from TMP 2008.045.0002.

"Kaiparowits Orodromine"

The "Kaiparowits Orodromine" is largely comprised of juvenile specimens with occurrences constrained to the middle and lower units of the Kaiparowits Formation (Gates et al., 2013; Boyd et al., 2015). Boyd (2012) provides a detailed description, published in part (Gates et al., 2013), which provides systematics for this taxon and erected a new species based on this material, *Skaladromeus goldenii*; however, *Skaladromeus goldenii* has not been used in literary sources since when referencing the "Kaiparowits Orodromine". The juvenile status of much of the material has hindered a published diagnosis, but with the new morphological constraints presented above for *Orodromeus*, and elsewhere for *Pikunidromeus* (Chapter 3), clear ontogenetic trends emerge in orodromines which facilitate new opportunities for comparison with the Kaiparowits Formation material.

Boyd (2012) offers a handful of potential autapomorphies in the diagnosis for *Skaladromeus*, which are not valid in the updated orodromine systematic context: (1) the ventral ramus of the postorbital inserts into a socket in the anterolateral margin of the dorsal ramus of the

jugal; (2) the presence of an ovoid foramen on the ventral margin of the sternal process of the coracoid; and (3) a reduction of manual digit IV from three to two phalanges, including the ungual. These three characters are not distinct from other orodromines. The first character, a lateral articulation of the ventral ramus of the postorbital with the ascending postorbital ramus of the jugal is a condition shared with other orodromines like *Pikunidromeus* (Chapter 3), *Zephyrosaurus* (Sues et al., 1980), and *Orodromeus* [MOR 1141]. The second proposed autapomorphy is difficult to interpret, as the ventral "foramen" is in like placement to a ventral fossa documented widely in thescelosaurids (Chapter 3; Avrahami et al., 2024; Krumenacker et al., 2024) but described to occur within a ventral groove which may also allude to the fossa too. This structure is figured in Figure 3.8 (Boyd, 2012) and unfortunately the pictures do not illuminate on the validity of these foramen. Lastly, the assertion Boyd (2012) makes that digit IV exhibits a reduction of the number of phalanges in the manus is incorrect, and instead specimen UMNH VP 12667 likely presents an incomplete digit IV. This is corroborated by the exceptionally complete manus of the *Pikunidromeus* specimen MOR 473 and the *Thescelosaurus neglectus* ROM cast 80129 which demonstrate three phalanges in manual digit IV.

The main compounding factor precluding a reanalysis of the Kaiparowits Formation material is the immaturity of the specimens. In the interest of brevity, we will focus on the jugal horn of a juvenile specimen [UMNH VP 16773] to assess the validity of this taxon. Orodromines demonstrate a wide range of horn morphologies in the adult jugals (Chapters 2 & 3; Sues, 1980), and their ontogenetic trajectories were not well understood at the time of Boyd (2012). Both *Orodromeus* and *Pikunidromeus* offer sizeable samples of juvenile and adult jugal horns. *Pikunidromeus* shows that its adult morphology is established relatively early in ontogeny [MOR

613]. This early onset in the horn morphology is corroborated by both *Zephyrosaurus* [MCZ 4392, YPM 56695, and OMNH V1048], and the "BV Orodromine"; however, *Orodromeus* exhibits a change in the orientation of the jugal horn through ontogeny from a lateral deflection [MOR 294 and 1136] to one that upturns dorsolaterally [MOR 1141]. The "Kaiparowits Orodromine", though a juvenile [UMNH VP 16773], presents an apparent distinct jugal horn morphology. The horn is sub-oval in cross-section like the "BV Orodromine", but demonstrates a singular prominent ventral ridge not observed in other orodromines (Boyd, 2012). The tip of the horn is rounded, while the horn demonstrates a plethora of vascular channels crossing its surface. The horn posterolaterally deflects from the lateral surface of the jugal and slightly upturns as in the "BV Orodromine". UMNH VP 16773 differs as it is very flat backed posteriorly, where the "BV Orodromine" is more rounded. To conclude, these observations warrant a new survey of the Kaiparowits orodromine assemblage.

TMP 2008.045.0002 (Oldman Formation)

TMP 2008.045.0002 is an indeterminate partial articulated postcranial orodromine skeleton described by Brown et al. (2013). Brown et al. (2013) precluded a specific taxonomic assignment for TMP 2008.045.0002, a judgement we support as the specimen is still mostly encased in matrix obscuring key morphological features. Still, we note new observations which further cement TMP 2008.045.0002 is an orodromine. First we note TMP 2008.045.0002 presents a couple thescelosaurid synapomorphies: (1) rounded dorsal margin of the ilium, a condition TMP 2008.045.0002 shared with *Orodromeus* [MOR 331, 294, and 623], *Pikunidromeus* (Chapter 3), *Jeholosaurus* (Han et al., 2012), *Haya* (Barta and Norell, 2021), and *Zephyrosaurus* [OMNH V1051], and (2) a lateral inflection of the prepubic process is displayed

by the left pubis of TMP 2008.045.002, which is manifested also in *Fona* (Avrahami et al., 2024), *Pikunidromeus* (Chapter 3). TMP 2008.045.0002 specifically offers three orodromine synapomorphies: (1) a prepubic process terminally striated, which unites this specimen with *Orodromeus* [MOR 623] and *Pikunidromeus* (Chapter 3); (2) the left pubis of TMP 2008.045.0002 also enlarges terminally into a dorsoventral oriented pad, a condition also demonstrated by *Orodromeus* [MOR 623] and *Pikunidromeus* (Chapter 3); (3) lateral of infection of the prepubic process is medially placed along the shaft, unites this specimen with *Pikunidromeus*.

Brown et al. (2013) observed the proportionally elongate preacetabular process of both ilia in TMP 2008.045.0002. We specifically note the ilia of TMP 2008.045.0002 presents a preacetabular process to total ilia length of 0.43. This ratio closely links with another indeterminate orodromine specimen from younger strata in the Two Medicine Formation at the locality TM-088, which presents a ratio of 0.42. Both specimens differ from *Orodromeus*, which offers a shorter preacetabular process demonstrate by a ratio of 0.35 [MOR 623]. This may indicate the validity of this character distinction between TMP 2008.045.002, the BV ilium, and *Orodromeus*; however, the BV ilium overlaps temporally with another orodromine, *Pikunidromeus*, which does not offer any complete ilia. Therefore, until TMP 2008.045.0002 is prepared further, or CT imaged, its taxonomic affinity must remain indeterminate, as it may be representative of *Orodromeus makelai*, *Pikunidromeus*, or an as yet unrecognized orodromine.

Conclusion

Orodromeus makelai is a pivotal taxon with wide reaching influence over ornithischian systematics and phylogenetic relationships. However, endeavors to explore either have suffered

from the lack of a valid published description. Here we present an updated diagnosis clarifying the morphology of *Orodromeus makelai* and confirming its restriction to the lacustrine interval of the Flagg Butte Member of the Two Medicine Formation. This bracketing produces a significantly large sample in the lacustrine interval, producing obvious ontogenetic trends, trends confirmed in the temporally younger *Pikunidromeus* (Chapter 3), and utilized to show the proposed holotype of the dubius "*Laosaurus minimus*" is a juvenile. Furthermore, this new understanding of *Orodromeus makelai* systematics builds on the precedents assessed in Chapter 3 and brings clarity to any validities in informal and fragmentary taxa/specimens.

Acknowledgments

This research was conducted as partial fulfillment of Z. J. H.'s Master's degree at Montana State University in Bozeman, MT. Special thanks to all the past MOR field crews, and to the past MSU Field Paleo students who amassed the sizable orodromine sample reposited at the MOR. Specimen access was granted by J. Scannella and E. Metz at the MOR, C. Brown and B. Strilisky at the TMP. Thanks to J. Horner for his patience and willingness to answer the never-ending emails sent by Z. J. H, and for sharing a photograph of the late Robert Makela. Research was supported by the generous funding of the Jurassic Foundation and by the Geological Society of America through a Graduate Student Geoscience Grant. Discussions with L. J. Krumenacker and J. Scannella greatly enhanced the quality of this paper. Thanks to S. Hannebaum for reviewing drafts of this manuscript. Special thanks to the editors for their feedback and corrections which greatly improved the scholarship of this research.

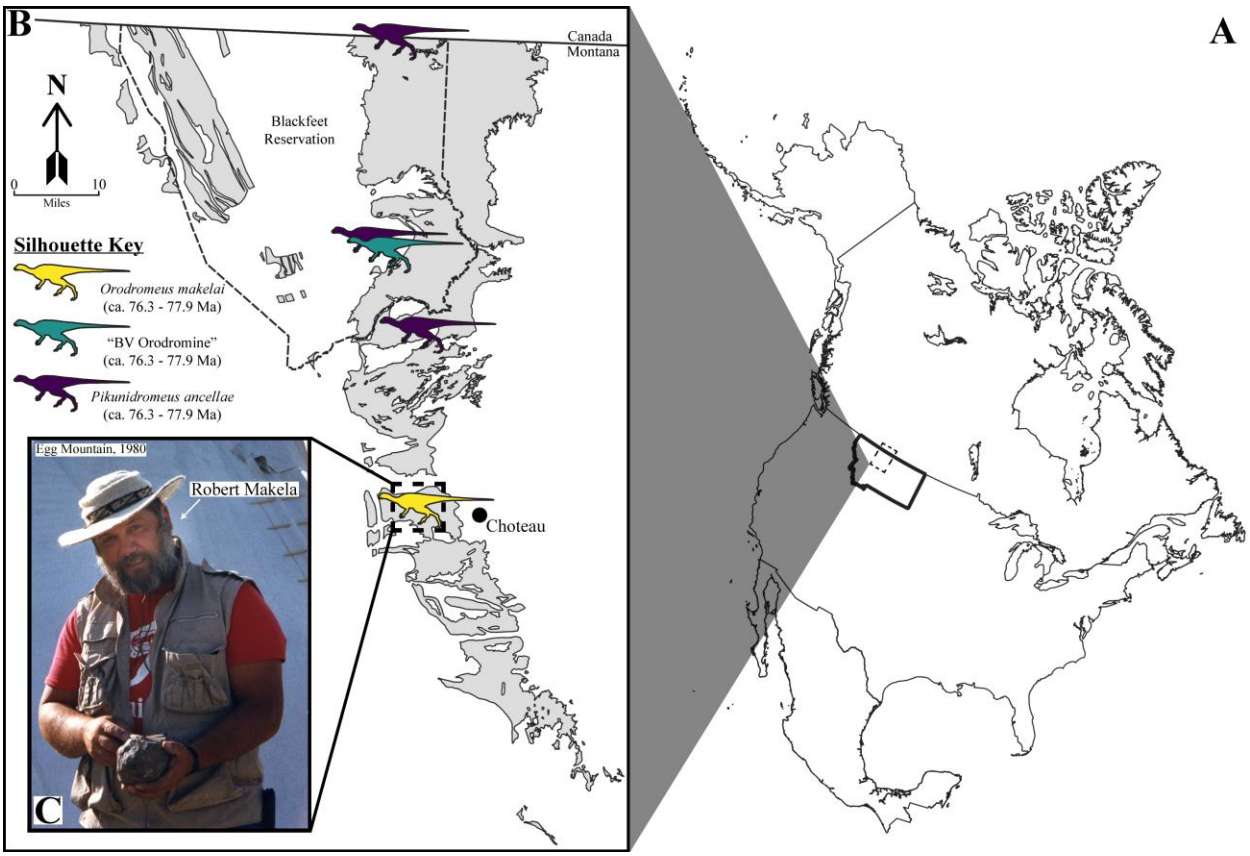


FIGURE 1. Geographic map of Two Medicine Formation with orodromine taxa occurrences denoted by colored silhouettes. (A) North America; (B) Two Medicine Formation; and (C) the late Robert Makela, photo taken in front of his tipi at Egg Mountain in 1980. Photo of Robert Makela courtesy of John Horner. Blackfeet Reservation is outlined with a dashed border, and the Two Medicine Formation is shaded gray. [Planned for page width]

Table 1.1 Measurements for figured *Orodromeus* vertebrae (cm.)

Specimen	Vertebra type	# in series	Le(A/P)	Wc(M/L)	Hc(D/V)
MOR 294	Odontoid process	1	-	0.6	0.36
	Axis	2	1.54	1.24	1.02
	Cervical	3	1.39	0.92	1.03
		4	1.53	1.24	1.07
		5	1.37	1.23	1.17
		6	1.41	1.24	1.11
		7	1.32	1.32	1.02
		8	1.36	1.39	1.25
		9	1.37	1.44	1.42
	Dorsal	1	1.32	0.96	1.52
		2	1.26	0.93	1.09
		3	1.2	0.93	1.06
		4	1.28	1.04	1.08
		5	1.16	0.99	1.1
		6	1.18	1.03	1.01
		?	1.44	1.09	1.05
		12	1.47	1.2	1.22
		13	1.4	1.22	1.36
		14	1.39	1.32	1.34
	Sacral	1	1.43	1.42	1.11
		2	1.53	1.96	1.24
		3	1.29	1.27	-
		4	1.23	1.5	-
		5	1.2	1.12	-
		6	1.33	1.06	-
		7	1.38	1.14	1.23
	Caudal	1	1.27	1.17	1.2
		2	1.27	1.12	1.2

Table 1.1 Continued

Specimen	Vertebra type	# in series	Le(A/P)	Wc(M/L)	Hc(D/V)
MOR 623	Atlantal intercentrum	1	1.06	1.91	0.81
	Odontoid process	2	1.31	1.22	0.95
	Cervical	3	1.98	1.58	1.38
		4	1.34	1.04	1.16
		?	2.31	1.67	0.96
		6			
		7	1.85	1.07	1.22
		8	1.9	0.97	1.24
		9	1.42	2.15	1.23
	Dorsal	?	2.01	1.3	1.38
		?	1.62	1.25	1.31
		?	1.74	1.57	1.45
		?	1.89	1.43	1.05
		11	1.76	1.6	1.58
		12	1.91	1.54	1.24
		13	2.05	1.62	1.48
		14	1.87	1.68	1.76
	Sacral	1	2.2	1.59	1.68
		2	2.13	2.07	1.84
		3	1.65	2.18	1.65
		4	1.73	1.36	1.34
		5	1.79	1.59	1.45
		6	1.9	1.4	1.46
		7	1.8	1.42	1.46
	Caudal	1	1.89	1.52	1.59
		2	1.9	1.42	1.72
		3	1.53	1.43	1.64
		4	2.02	1.23	1.65
		5	1.86	1.27	1.57
		?	1.92	1.06	1.46
		?	1.79	1.06	1.15
MOR1136	Caudal	?	1.52	1.34	1.25
		?	1.56	1.21	1.26
MOR 1141	Atlantal intercentrum	1	1.16	1.9	1.02
	Cervical	3	2.42	1.36	1.41
		4	2.58	1.57	1.65
		?	2.24	1.65	1.63
	Sacral	7	2.18	1.36	1.23
PU 23409	Sacral	3	1.78	2.99	1.75

Table 1.2: *Orodromeus* forelimb measurements (cm.)

Specimen	Element	L/R	Le(D/P)	Wp(M/L)	Wp(A/P)	Wd(M/L)	Wd(A/P)
MOR 248	Humerus	R	6.28	1.09	1.87	0.99	1.22
MOR 294	Humerus	L	**4.63**	0.96	1.84	-	-
	Scapula	L	7.04	0.9	2.8	0.16	2.16
	Coracoid	L	2.77	0.94	2.51	0.24	
	Humerus	R	6.36	0.9	1.86	0.97	1.21
	Scapula	R	7.51	0.94	2.9	0.29	2.58
	Coracoid	R	-	0.92	-	-	-
	Ulna	R	5.2	0.69	1.2	0.47	0.79
	Radius	R	4.91	0.53	0.84	0.6	0.8
	Metacarpal I	R	0.93	0.31	0.49	0.31	0.33
	Metacarpal II	R	1.03	0.39	0.51	0.27	0.36
MOR 404	Humerus	L	7.06	1.16	2.12	1.18	1.43
MOR 623	Coracoid	L	4.88	0.9	5.18	0.25	-
	Scapula	R	10.72	1.33	4.35	0.29	-
	Humerus	R	9.29	1.17	1.15	0.96	2.32
	Ulna	?	**4.97**	1.02	1.2	-	-
	Radius	?	**3.64+2.59**	0.49	1.06	0.54	1.07
	Metacarpal II	L	1.44	0.45	0.7	0.38	0.52
	Metacarpal III	L	1.4	0.37	0.61	0.37	0.51
MOR 1136	Humerus	L	**4.68+2.54**	1.05	2.04	-	-
PU 23246	Scapula	R	**5.47**	-	-	-	-
PU 23442	Scapula	L	**6.74**	1.3	**4.78**	-	-
	Coracoid	L	4.85	1.34	-	0.32	5.95
	Radiale	L	0.43	0.63	0.81	-	-
	Intermedium	L	0.62	0.69	0.83	-	-
	Ulnare	L	0.59	0.52	0.63	-	-
	Metacarpal I	L	1.41	0.52	0.69	0.54	0.5
	Metacarpal II	L	1.59	0.48	0.97	0.31	0.64
	Metacarpal III	L	1.25	-	-	-	-
	Phalange I	L	-	0.37	0.58	-	-
PU 23443	Scapula	L	**5.16**	-	-	-	-

Table 1.3: *Orodromeus* pelvic measurements (cm.)

Specimen	Element	L/R	Le(A/P)	Wp(M/L)	Wp(D/V)	Wd(M/L)	Wd(D/V)
MOR 294	Ilium	L	**8.45**	-	-	-	-
	Ilium	R	**7.51**	-	-	-	-
	Pubis	R	**2.26**	-	-	-	-
MOR 331	Ilium	L	**3.58**	-	-	-	-
MOR 623	Ilium	L	11.73	-	-	-	-
	Pubis	L	**8.13+4.83**	0.19	0.72	-	-
	Ilium	R	**10.48**	-	-	-	-
	Pubis	R	21.84	0.18	0.64	0.5	0.41
F#06.26.95	Ilium	R	**7.37**	-	-	-	-
PU 23246	Ischium	L	12.4	0.75	2.71	0.34	0.75
	Ischium	R	**9.77**	-	-	-	-
PU 23257	Ilia	R	**7.66**	-	-	-	-
PU23431	Ischium	L	14.62	3.39	0.88	0.76	0.33
	Ischium	R	**4.55+3.39**	-	-	-	-
PU 23442	Pubis	R	**6.09**	-	-	-	-

Table 1.4: *Orodromeus* hindlimb measurements (cm.)

Specimen	Element	L/R	Le(D/V)	Wp(M/L)	Wp(A/P)	Wd(M/L)	Wd(A/P)
MOR 248	Femur	L	**1.23+1.12**	0.55	0.64	0.43	0.61
	Femur	R	**1.24**	-	-	0.58	0.55
	Tibia	L	**1.57**	0.59	0.61	-	-
MOR 294	Femur	L	10.07	-	-	-	-
	Tibia	L	**10.46**	-	-	2.57	1.12
	Femur	R	10.74	-	-	-	-
MOR 623	Femur	L	14.05	-	-	-	-
	Fibula	L	15.64	0.84	1.95	0.92	0.66
	Femur	R	14.11	-	-	-	-
	Tibia	R	16.57	-	-	-	-
	Metatarsal I	L	**1.71**	-	-	0.87	0.82
	Phalange I	L	2.31	1.08	0.89	0.78	0.67
	Phalange II	L	1.51	0.66	0.65	-	-
	Metatarsal II	L	7.26	0.94	1.51	1.26	1.06
	Phalange I	L	2.63	1.45	1.18	1.05	0.93
	Phalange II	L	1.9	1.02	1.04	0.85	0.76
	Phalange III	L	2.26	0.8	0.78	-	-
	Metatarsal III	L	8.02	1.43	1.05	1.14	1.08
	Phalange I	L	2.54	1.46	1.15	1.2	0.92
	Phalange II	L	**1.37**	1.18	1.09	-	-
	Phalange IV	L	2.6	0.85	0.73	-	-
	Metatarsal IV	L	7.19	1.13	1.16	0.91	1.19
	Phalange I	L	1.65	1.23	1.11	0.96	0.92
	Phalange II	L	**1.12**	1.07	0.95		
	Phalange III	L	1.46	0.95	1.03	0.91	0.84
	Phalange IV	L	1.27	0.88	0.97	0.87	0.71
	Phalange V	L	2.06	0.69	0.66	-	-

Table 1.4 Continued

Specimen	Element	L/R	Le(D/V)	Wp(M/L)	Wp(A/P)	Wd(M/L)	Wd(A/P)
MOR 623	Metatarsal I	R	**2.52**	-	-	0.77	0.81
	Phalange II	R	**1.57**	0.78	0.73	-	-
	Metatarsal II	R	7.32	0.69	2.39	1.19	1.07
	Phalange I	R	2.65	1.15	1.1	0.96	0.9
	Phalange II	R	1.93	1.03	1.06	0.84	0.72
	Phalange III	R	2.51	0.83	0.75	-	-
	Metatarsal III	R	8.24	1.01	1.82	1.42	1.12
	Phalange I	R	2.5	1.47	1.16	-	0.97
	Digit IV Phalange I	R	1.7	1.19	1.11	1.02	0.93
	Phalange V	R	1.88	0.69	0.65	-	-
	Metatarsal V	R	2.25	0.59	0.3	0.64	0.13
MOR 1003	Femur	L	-	1.89	2.01	2.26	1.45
	Tibia	L	-	1.27	2.47	1.26	2.1
	Tibia	R	-	-	-	1.17	1.84
MOR 1136	Femur	L	11.5	2.28	2.5	2.88	1.94
MOR 2726	Femur	L	-	3.46	3.4	4.19	2.12
F#7.9.96	Femur	L	**6.86**	2.06	2.7	-	-
	Femur	L	-	-	-	3.45	1.38
	Femur	R	-	-	-	0.28	2.4
	Femur	R	7.61	1.57	-	1.7	0.71
F#7.16.15.14	Femur	L	12.7	2.99	2.58	3.09	2.4
TM-006.Float	Tibia	L	**5.26**	1.47	2.1	-	-

Table 1.4 Continued

Specimen	Element	L/R	Le(D/V)	Wp(M/L)	Wp(A/P)	Wd(M/L)	Wd(A/P)
PU 23246	Tibia	L	-	-	-	2.53	1.06
	Metatarsal I	L	**1.7**	-	-	0.66	0.6
	Phalange I	L	1.77	0.82	0.65	0.67	0.54
	Metatarsal II	L	5.79	0.74	1.88	0.83	0.81
	Metatarsal III	L	6.42	0.58	1.42	1.15	0.83
	Phalange I	L	1.98	1.09	0.92	0.96	0.72
	Metatarsal IV	L	5.7	1.06	0.97	0.84	0.9
	Phalange I	L	1.42	0.95	0.85	0.81	0.71
	Phalange II	L	1.16	0.79	-	0.73	0.64
	Metatarsal I	R	**1.16**	-	-	0.61	0.65
	Phalange I	R	1.76	0.82	0.74	0.66	0.52
	Phalange II	R	**1.22**	0.57	0.55	-	-
	Metatarsal II	R	5.87	0.91	1.51	0.93	0.83
	Phalange I	R	2.05	0.93	0.94	0.79	0.68
	Phalange II	R	1.45	0.83	0.85	0.78	0.58
	Metatarsal III	R	5.88	1.09	1.16	1.2	0.81
	Phalange I	R	1.95	1.15	0.93	1.01	0.73
	Phalange II	R	1.54	0.99	0.87	0.91	0.66
	Metatarsal IV	R	**4.37**	-	-	0.67	0.92
	Phalange II	R	1.09	0.84	0.84	0.76	0.64
	Phalange IV	R	0.82	0.58	0.65	0.54	0.51
PU 23443	Femur	L	15.64	3.29	3.44	3.81	2.44

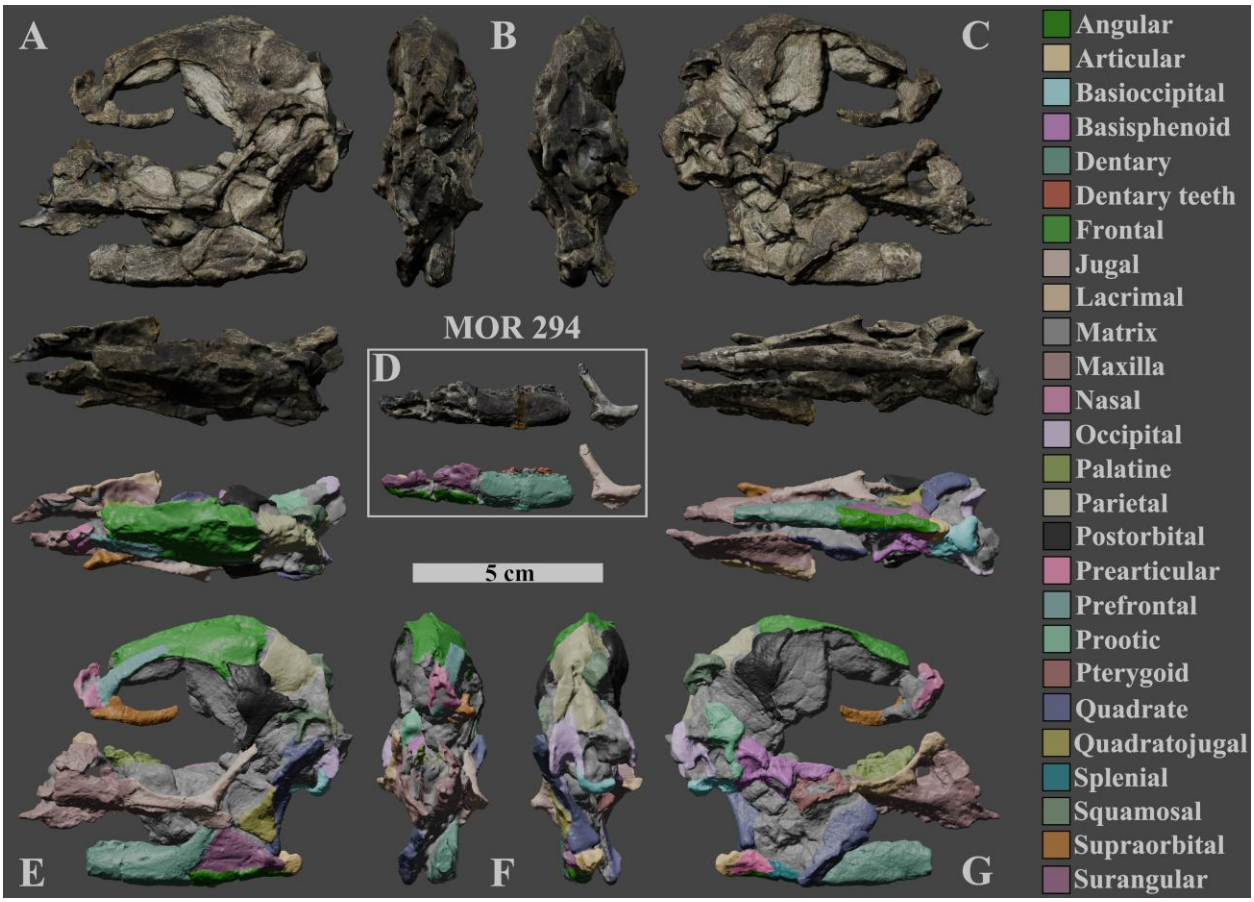


FIGURE 2. *Orodromeus makelai* holotype [MOR 294] skull rendered with and without texture. (**A**) MOR 294 in left lateral and dorsal views; (B) anterior and posterior views; (**C**) right lateral and ventral views; (D) disarticulated right mandible and jugal; (E) MOR 294 in left lateral and dorsal views with colored element interpretation; (F) anterior and posterior views; and (G) right lateral and ventral views. [planned for page width]

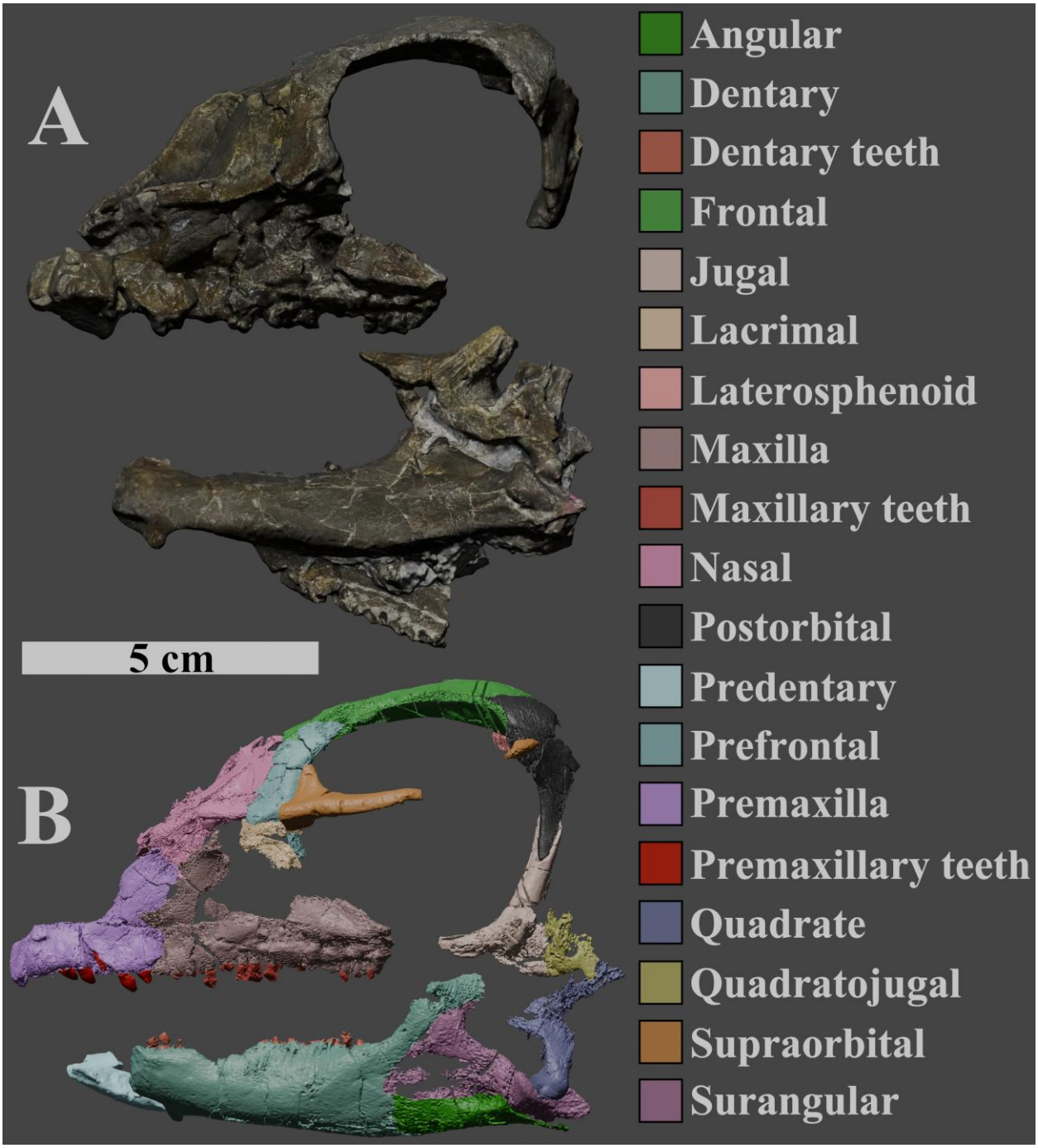


FIGURE 3. *Orodromeus makelai* paratype [MOR 1141] skull rendered with and without texture. (**A**) Textured model in left lateral view and (B) Reconstruction of MOR 1141 in left lateral view. [planned for page width]

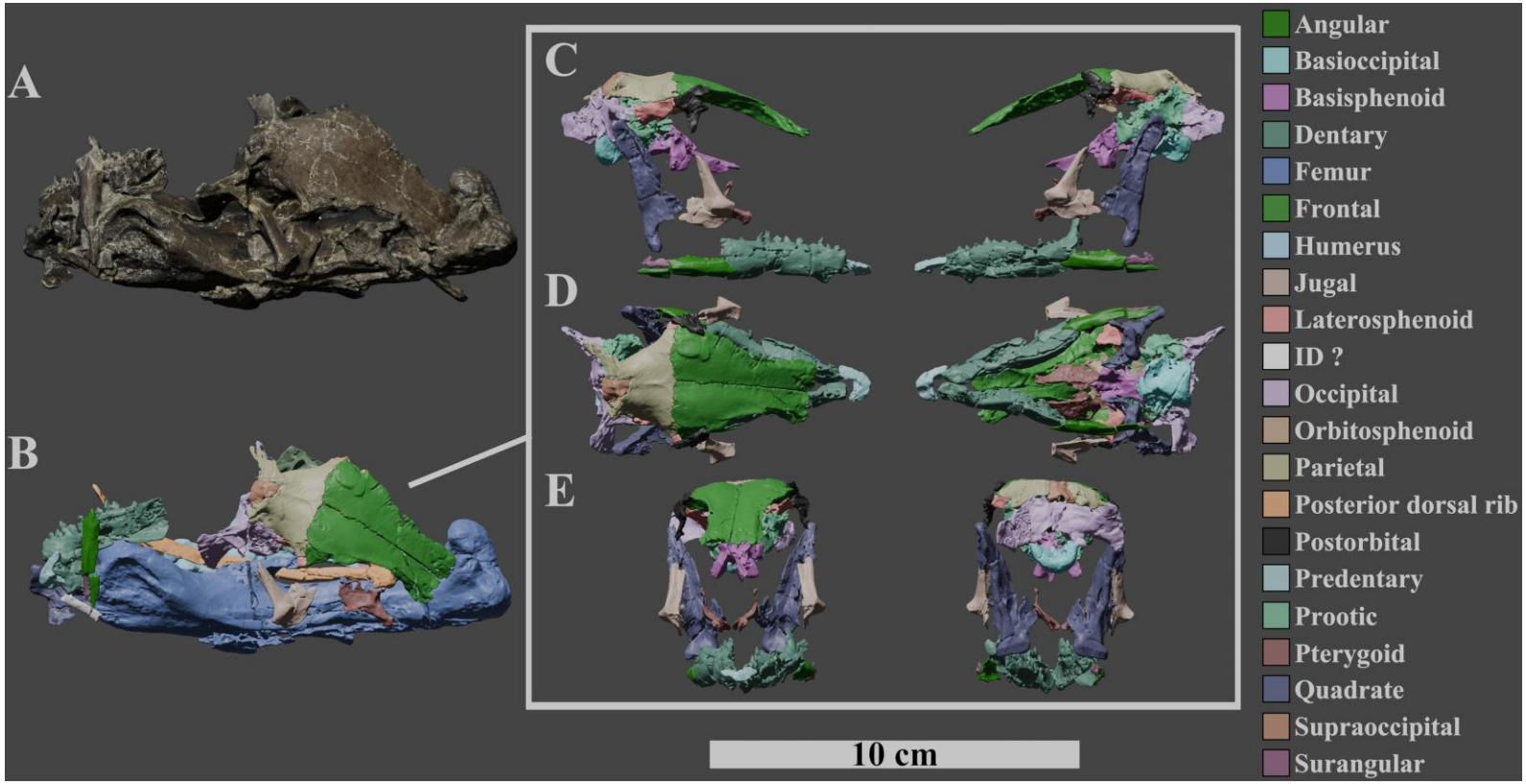


FIGURE 4. *Orodromeus makelai* juvenile skull [MOR 1136] skull rendered with and without texture. (**A**) Textured model with in-situ elements; (B) Untextured model with colored interpretation of skeletal elements in-situ; (C) MOR 1136 reconstructed in left and right lateral views; (D) dorsal and ventral views; and (E) anterior and posterior views. [planned for page width]

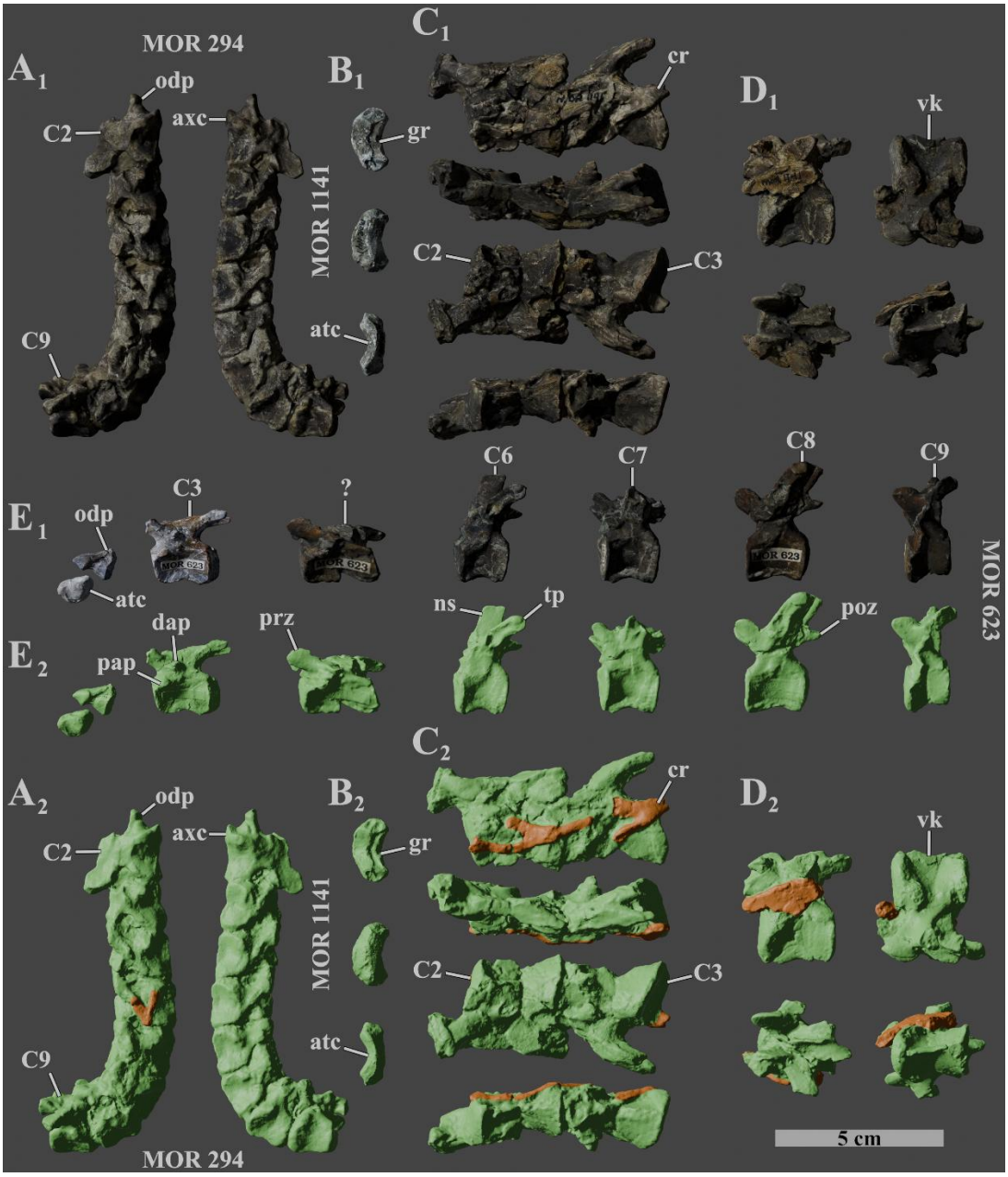


FIGURE 5. *Orodromeus makelai* cervical series rendered with and without texture. (A1 & A2) Holotype specimen [MOR 294] cervical series C2 through C9 in right and left lateral view; (B1 & B2) paratype specimen [MOR 1141] atlantal intercentrum in dorsal, ventral, and anterior views; (C1 & C2) MOR 1141 cervical vertebrae two and three in left lateral, dorsal, right lateral, and ventral views; (D1 & D2) MOR 1141 posterior cervical vertebra of uncertain placement in (left to right) left lateral, right lateral, dorsal, and ventral views; and (E1 & E2) . Abbreviations: atc, atlantal intercentrum; axc, axis intercentrum; cr, cervical rib; dap, diapophysis; gr, groove; ns, neural spine; odp, odontoid process; pap, parapophysis; poz, postzygapophysis; prz, prezygapophysis; tp, transvers process; vk, ventral keel. [planned for page width]

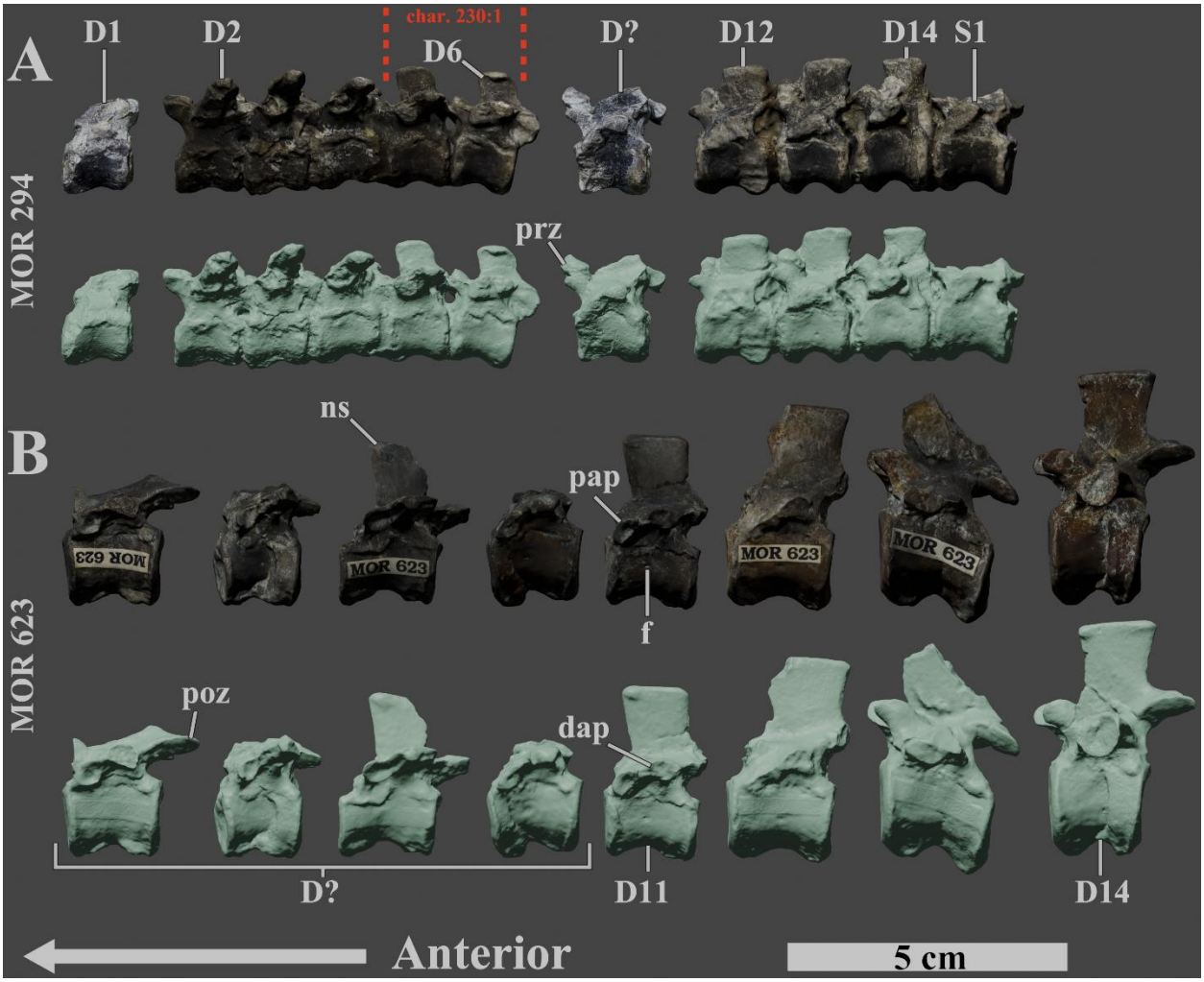


FIGURE 6. *Orodromeus makelai* dorsal series rendered with and without texture. (A) Holotype specimen [MOR 294] incomplete dorsal series in left lateral view, and (B) MOR 623 incomplete dorsal series in left lateral view. **Abbreviations**: **dap**, diapophysis; **f**, foramen; **ns**, neural spine; **pap**, parapophysis; **poz**, postzygapophysis; **prz**, prezygapophysis. [planned for page width]

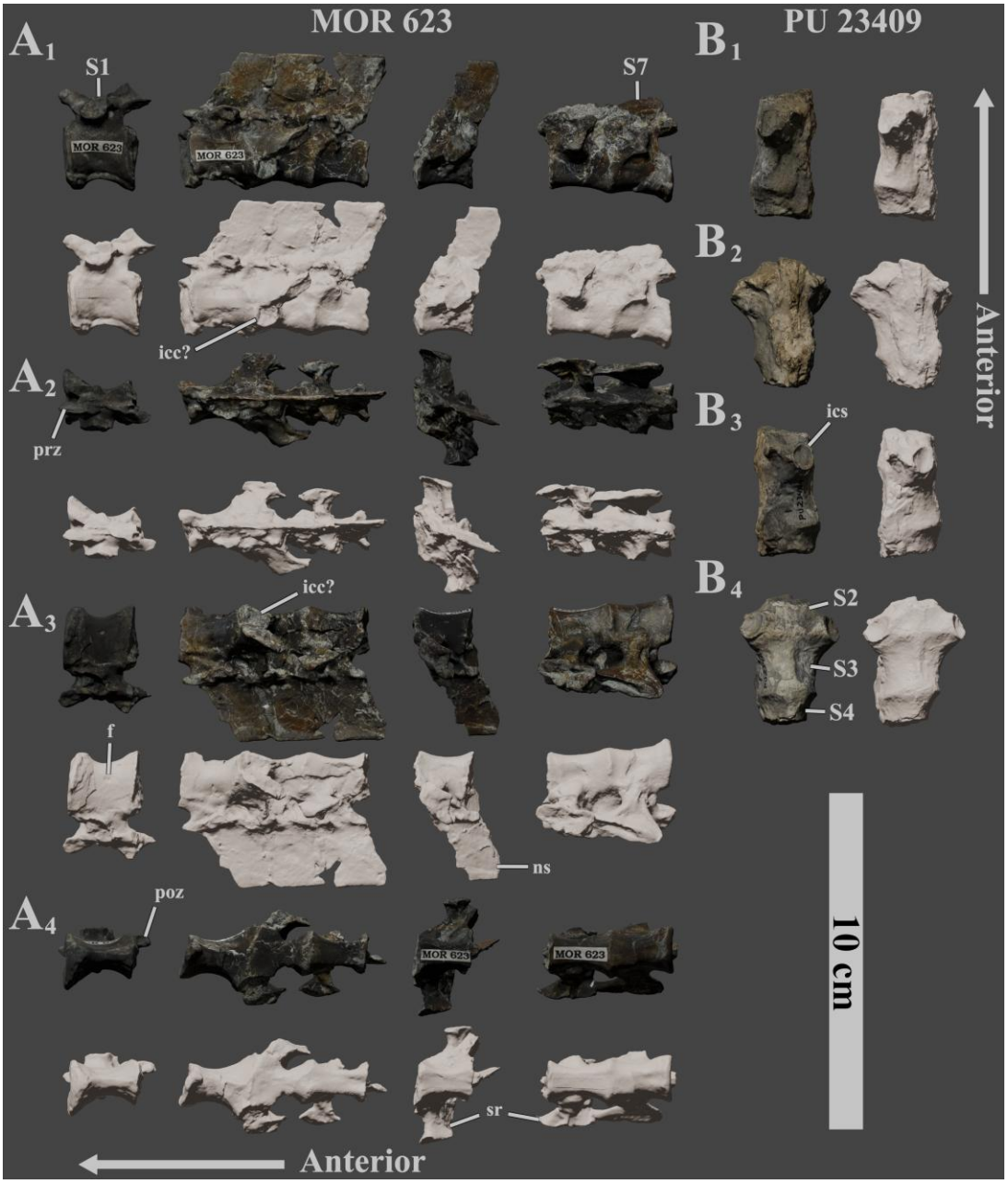


FIGURE 7. *Orodromeus makelai* sacral series [MOR 623 and PU 23409] rendered with and without texture. (A_1) MOR 623 in left lateral view; (A_2) MOR 623 in dorsal view; (A_3) MOR 623 in right lateral view; (A_4) MOR 623 in ventral view; (B_1) PU 23409 in left lateral view; (B_2) PU 23409 in dorsal view; (B_3) PU 23409 in right lateral view; and (B_4) PU 23409 in ventral view. **Abbreviations**: **f**, foramen; **icc**, intercentral cavity; **ics**, intercentral socket; **ns**, neural spine; **prz**, prezygapophysis; **poz**, postzygapophysis; **sr**, sacral rib. [planned for page width]

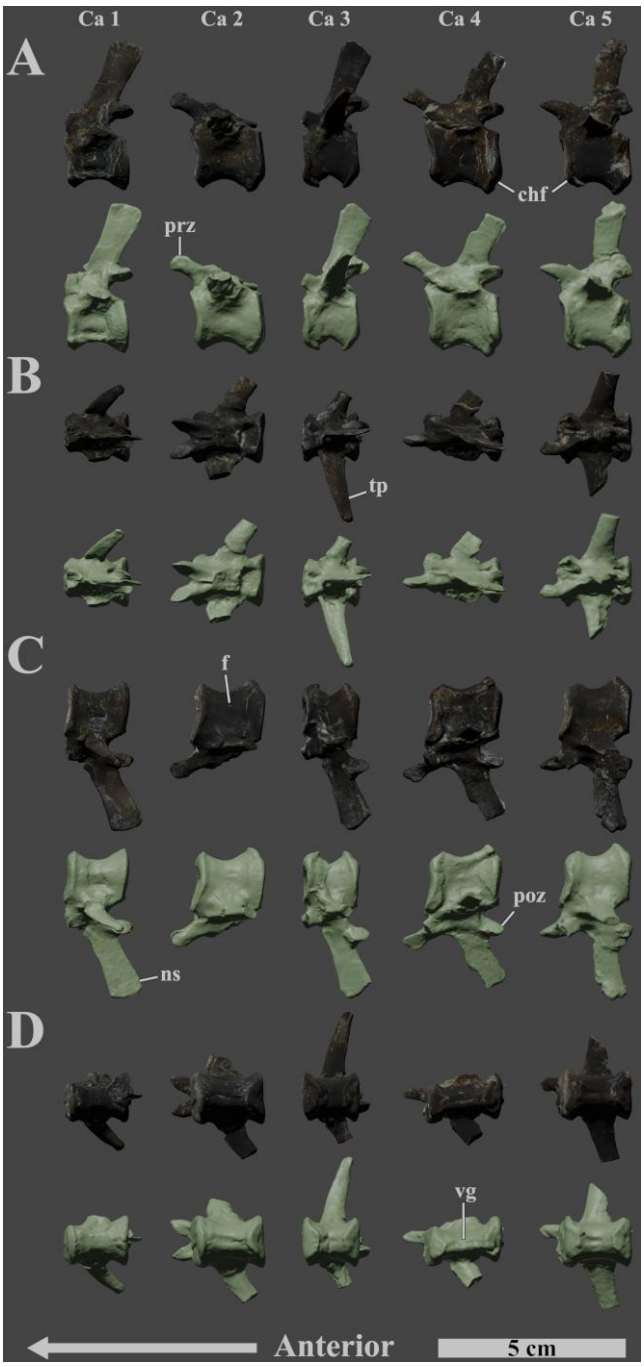


FIGURE 8. *Orodromeus makelai* caudal series 1-5 [MOR 623] rendered with and without texture. (A) MOR 623 left lateral view; (B) MOR 623 dorsal view; (C) MOR 623 right lateral view; and (D) MOR 623 ventral view. **Abbreviations**: **chf**, chevron facet; **f**, foramen; **ns**, neural spine; **prz**, prezygapophysis; **poz**, postzygapophysis; **tp**, transverse process; **vg**, ventral groove. [planned for column width]

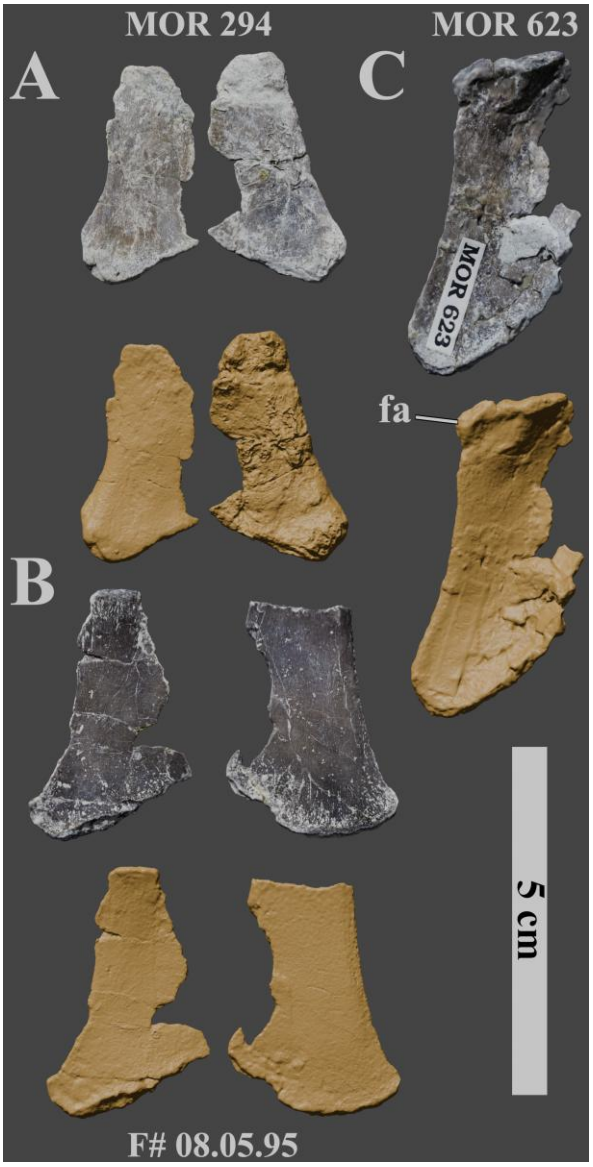


FIGURE 9. *Orodromeus makelai* sternal plates rendered with and without texture. (A) Holotype specimen [MOR 294] sternal plates; (B) F# 08.05.95 ("Frankies *Orodromeus*") sternal plates; and (C) MOR 623 sternal plate. **Abbreviations**: **fa**, facet. [planned for column width]

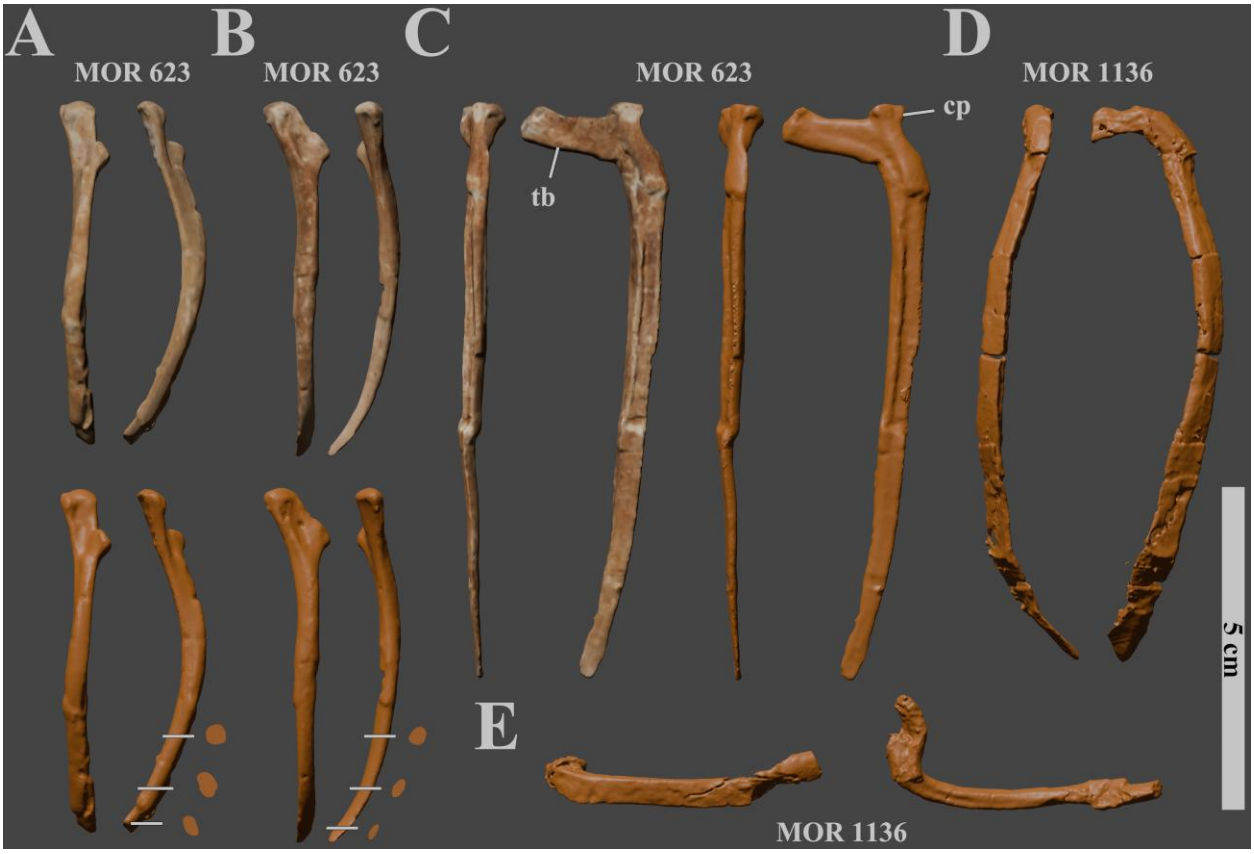


FIGURE 10. *Orodromeus makelai* dorsal ribs rendered with and without texture. (A-C) MOR 623 dorsal ribs in lateral and anterior views. **Abbreviations**: **cp**, capitulum; and **tp**, tuberculum. [planned for page width]

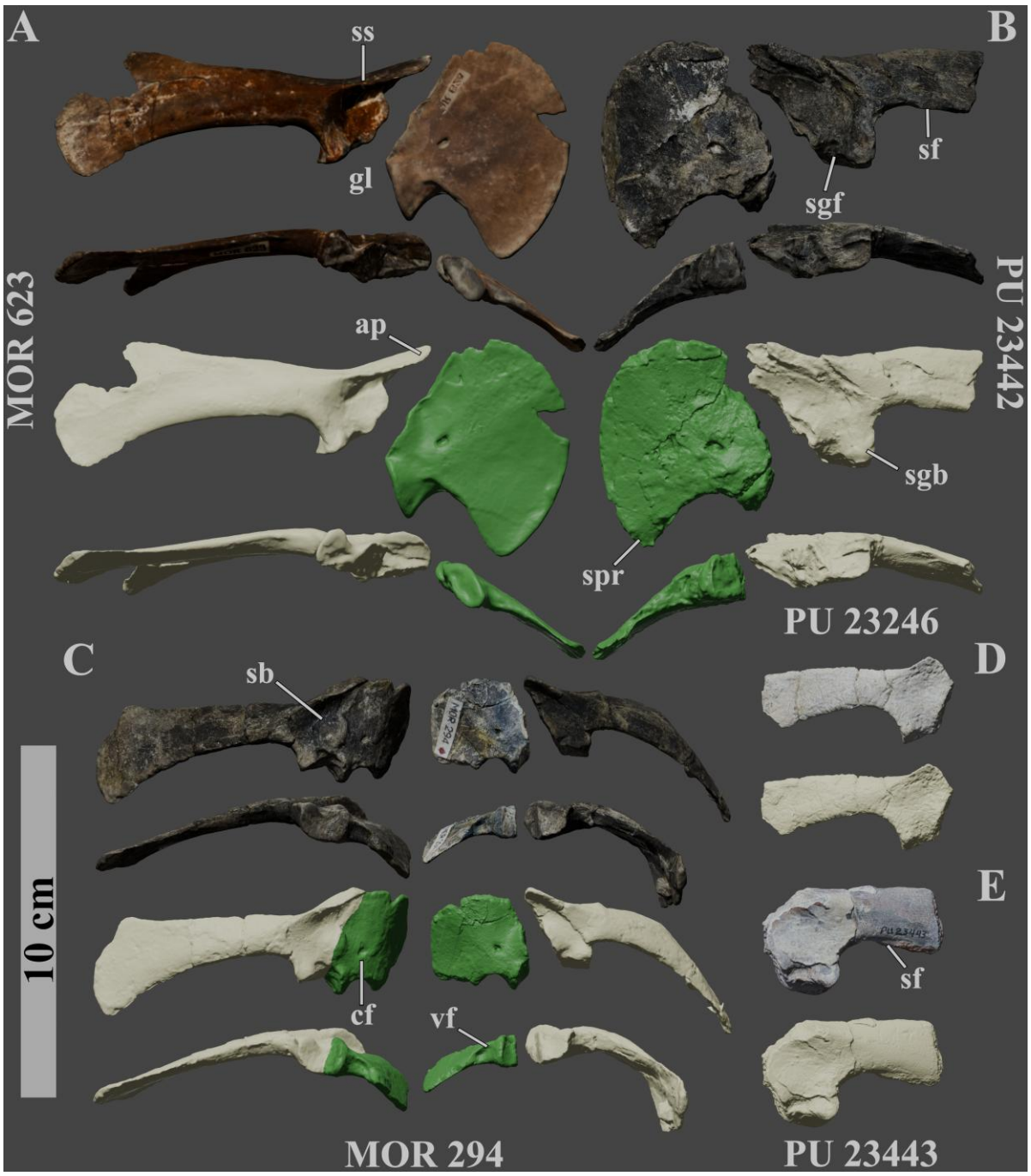


FIGURE 11. *Orodromeus makelai* scapulocoracoid rendered with and without texture. (A) MOR 623 left scapula and coracoid in lateral and ventral view; (B) PU 23443 left scapula and coracoid in lateral and ventral views; (C) holotype specimen [MOR 294] left and right scapulocoracoid in lateral and ventral views; (D) PU 23246 right scapula in lateral view; and (D) PU 23443 lefft scapula in lateral view. **Abbreviations**: **ap**, acromion process; **cf**, coracoid foramen; **gl**, glenoid fossa; **sb**, supraglenoid boss; **sf**, scapular flange; **sgb**, supraglenoidal buttress; **sgf**, supraglenoid fossa; **spr**, sternal process; **ss**, scapular spine; **vf**, ventral fossa. [planned for page width]

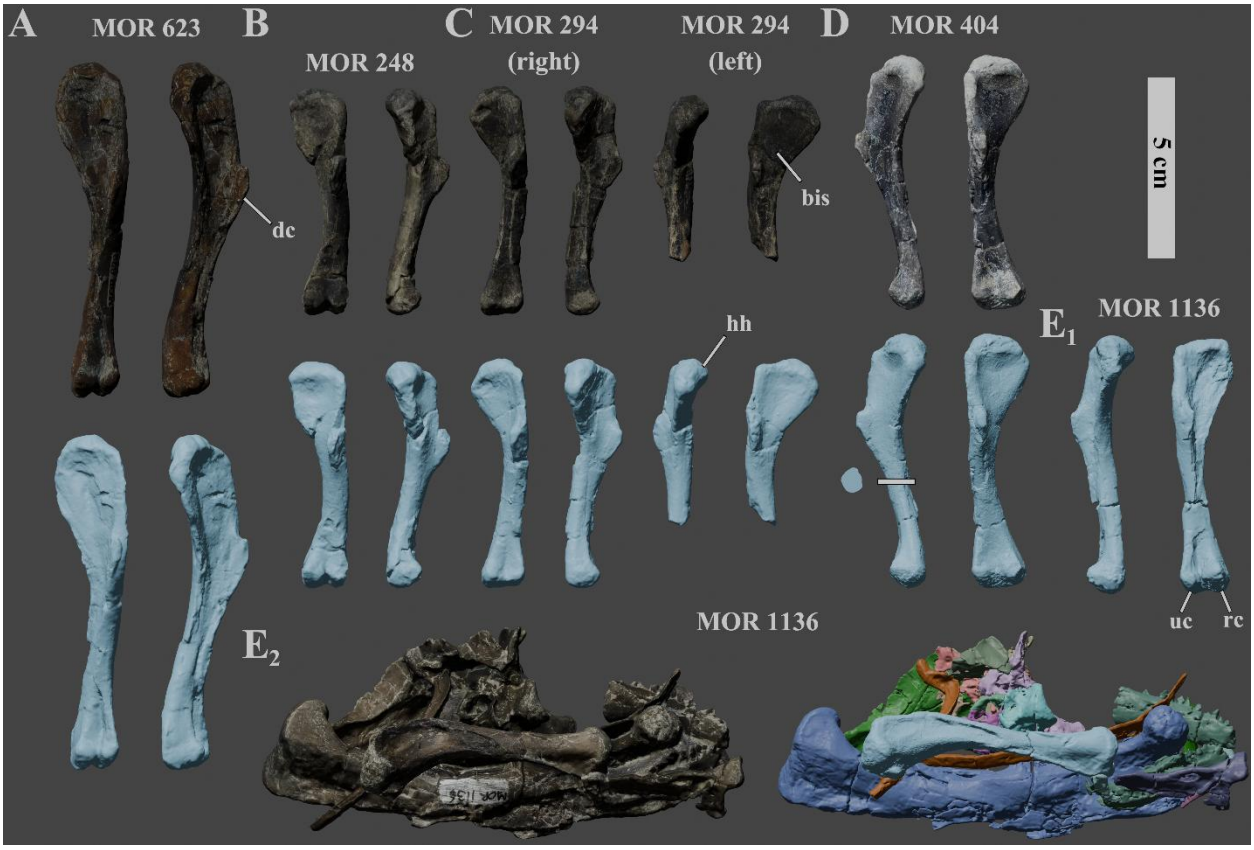


FIGURE 12. *Orodromeus makelai* humeri rendered with and without texture. (A) MOR 623 left humerus in anterior, and lateral views; (B) MOR 248 left humerus in anterior and lateral views; (C) both humeri holotype specimen [MOR 294] in anterior and lateral views; (D) MOR 404 right humerus in lateral and anterior views; (E_1) MOR 1136 right humerus in lateral and anterior views; and (E_2) MOR 1136 right humerus in-situ placement. **Abbreviations: bis,** bicipital sulcus**; dc**, deltopectoral crest; **hh**, humeral head olecranon process; **rc**, radial condyle; **uc**, ulnar condyle. [planned for page width]

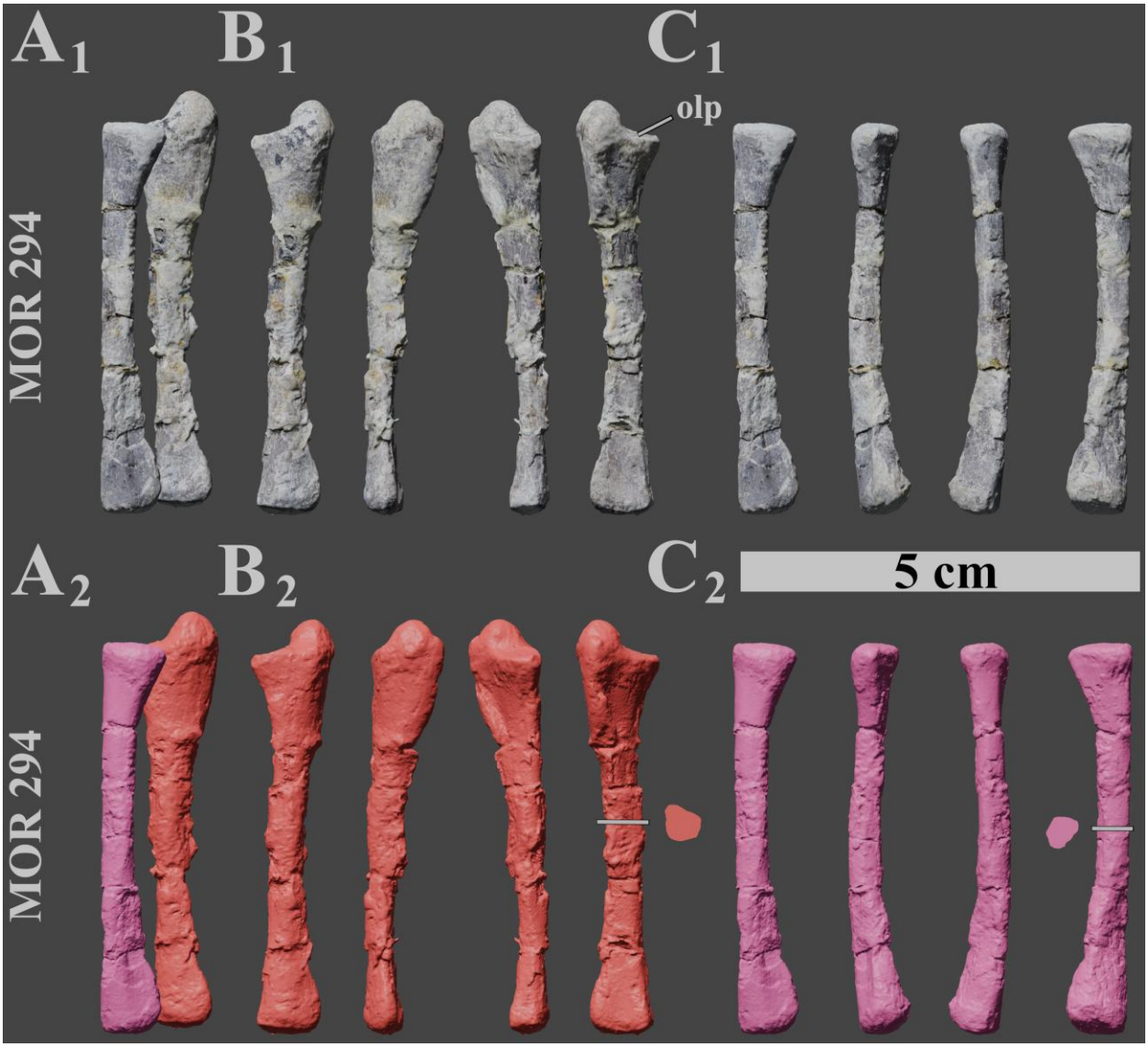


FIGURE 13. *Orodromeus makelai* holotype specimens forearm rendered with texture and without. (A_1 & A_2) MOR 294 left radius and ulna in articulation; (B_1 & B_2) MOR 294 ulna in lateral, posterior, anterior, and medial views; and (C_1 & C_2) MOR 294 radius in lateral, posterior, anterior, and medial views. **Abbreviations**: **olp**, olecranon process. [planned for page width]

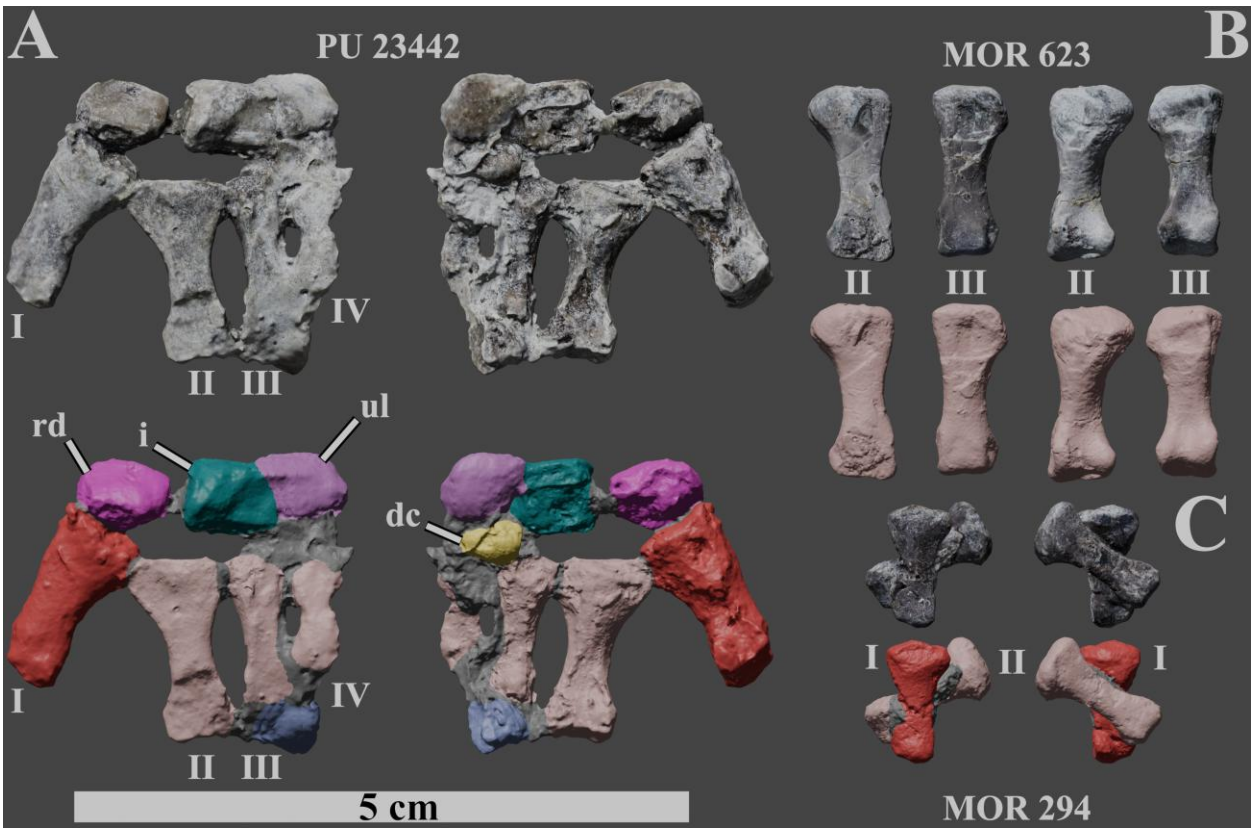


FIGURE 14. *Orodromeus makelai* manus rendered with and without texture. (A) PU 23442 in antipalmar and palmar views; (B) MOR 623 metacarpi in antipalmar and palmar views; (C) holotype specimen [MOR 294] metacarpi in two views. **Abbreviations**: **dc**, distal carpal; **i**, intermedium; **rd**, radiale; **ul**; ulnare. [planned for column width]

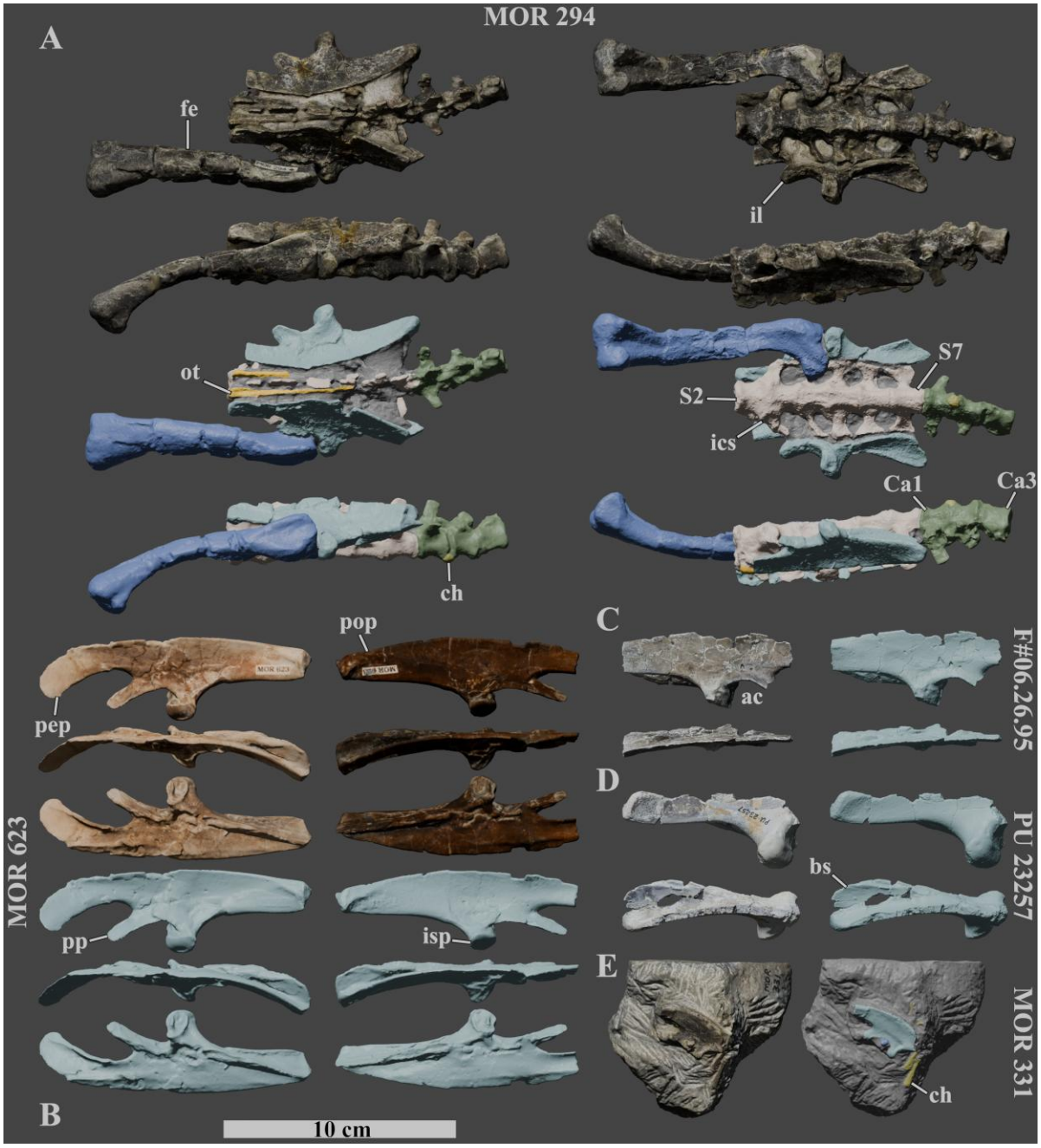


FIGURE 15. *Orodromeus makelai* ilia rendered with and without texture. (A) Holotype specimen [MOR 294] articulated ilia, ossified tendon, left femur, sacral vertebrae two through seven, and caudal vertebrae one through three in (left to right) dorsal, ventral, left lateral, and right lateral views; (B) MOR 623 left and right ilia in lateral, dorsal, and medial; (C) F#06.29.95 right ilia in lateral and dorsal views; (D) PU 23257 right partial ilia in lateral and dorsal views; and (E) MOR 331 left ilia in lateral view. **Abbreviations**: **bs**, brevis shelf; **ch**, chevron; **fe**, femur; **ics**, intercentrum socket; **il**, ilium; **isp**, ischiac peduncle; **ot**, ossified tendon; **pep**, preacetabular process; **pop**, postacetabular process; **pp**, pubic peduncle; [planned for page width]



FIGURE 16. *Orodromeus makelai* ischia rendered with and without texture. (A) PU 23431 and PU 23246 left and right ischia in dorsal view; and (B) PU 23431 and PU 23246 in ventral view. **Abbreviations**: **ip**, iliac peduncle; **obp**, obturator process; **pup**, pubic peduncle; **st**, sutural surface. [planned for page width]

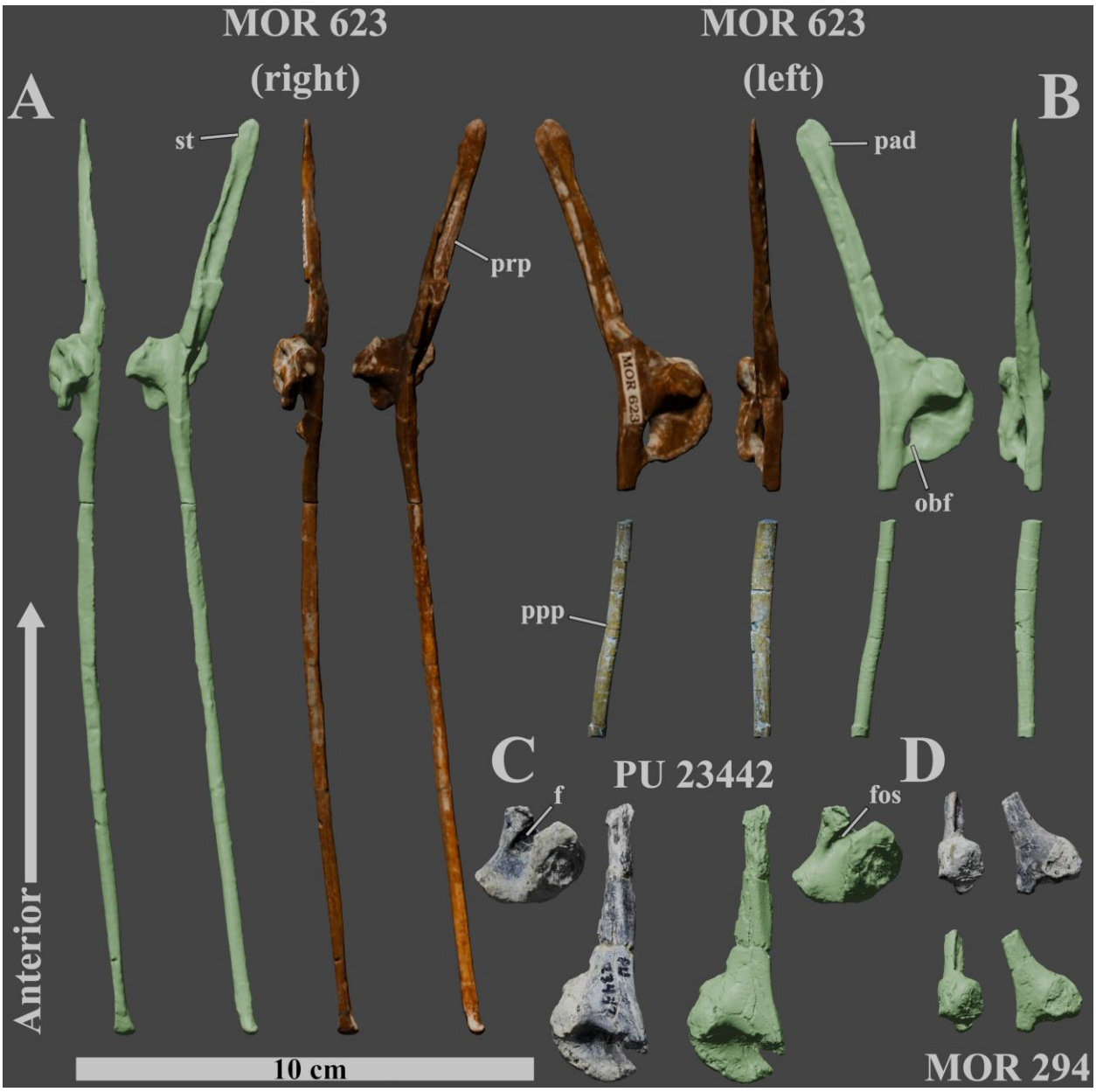


FIGURE 17. *Orodromeus makelai* pubis rendered with and without texture. (A) MOR 623 right pubis in dorsal and lateral views; (B) MOR 623 left pubis in dorsal and lateral views; (C) PU 23442 right pubis in posterior and lateral views; (D) holotype specimen MOR 294 left pubis in dorsal and lateral views. **Abbreviations**: **f**, foramen; **fos**, fossa; **obf**, obturator foramen; **pad**, prepubic pad; **ppp**, postpubic process; **prep**, prepubic process; **st**, striations. [planned for column width]

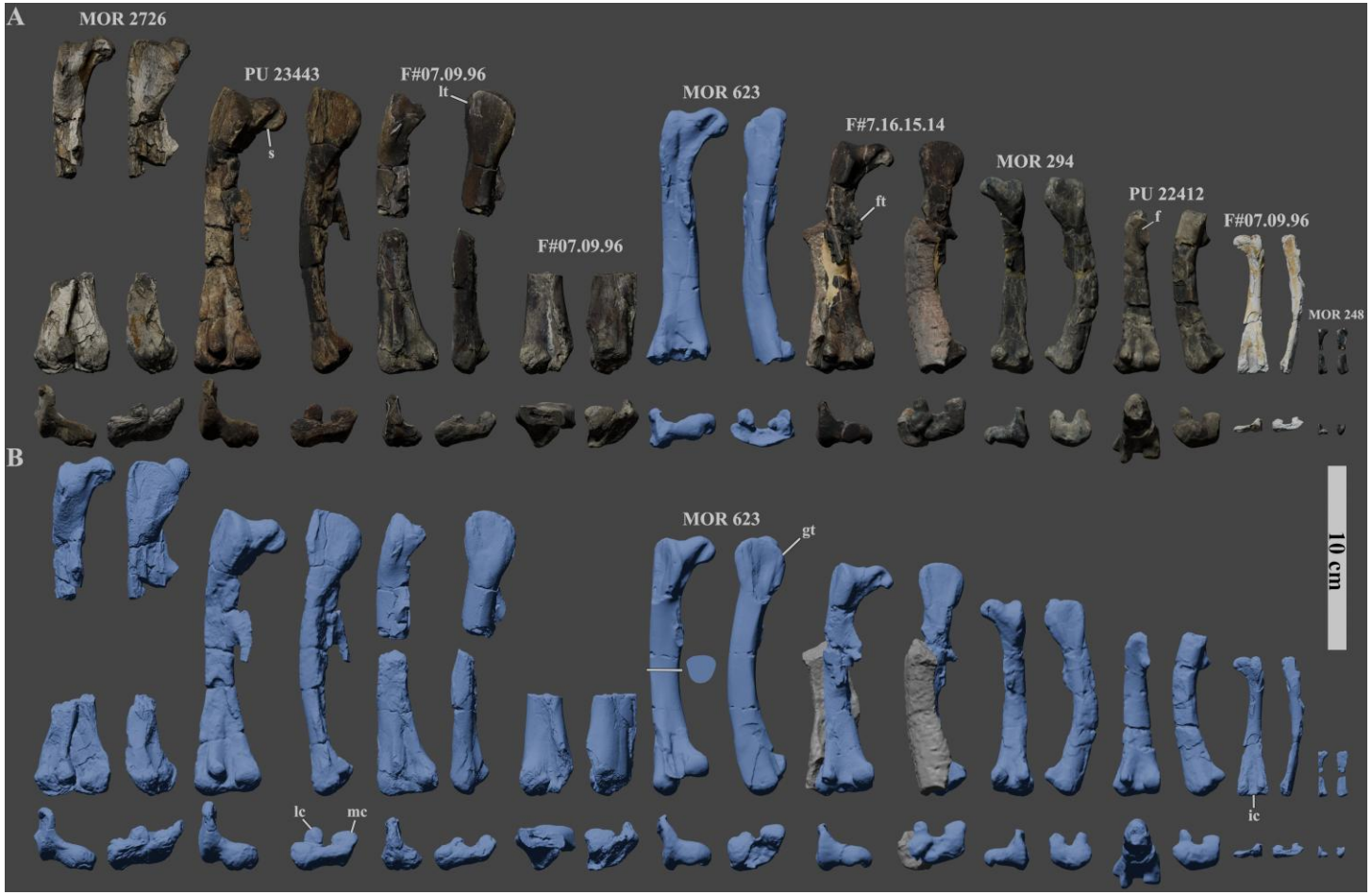


FIGURE 18. *Orodromeus makelai* femora in posterior and lateral views. (A) Nine femora rendered with texture. MOR 623 is the exception as the texture file was not retained in error when the mesh was created. Both left femora are currently undergoing histological sampling and are unavailable to rescan; (B) Nine femora rendered without texture. **Abbreviations**: **ic**, posterior intercondylar groove; **f**, foramen; **ft**, forth trochanter; **gt**, greater trochanter; **lc**, lateral condyle; **lt**, lesser trochanter; **mc**, medial condyle; **s**, sulcus. [planned for age width]

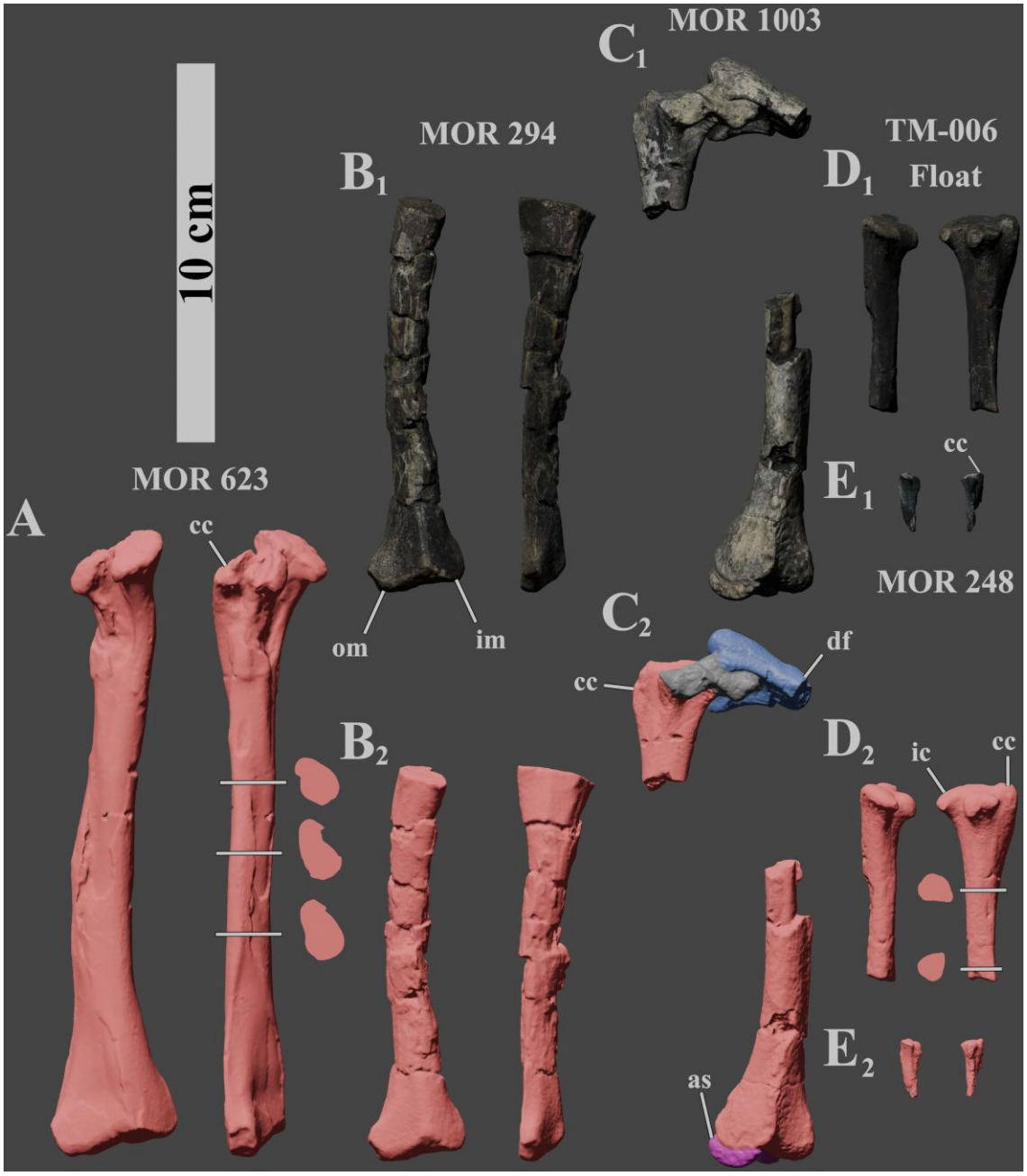


FIGURE 19. *Orodromeus makelai* tibiae rendered with and without texture. (A) MOR 623 left tibia in posterior and lateral views, no textured scan available and tibia is currently unavailable due to histological sampling; (B_1 & B_2) holotype specimen left tibia [MOR 294] in posterior and lateral views; (C_1 & C_2) MOR 1003 distal epiphysis and proximal head in articulation with the right femur, also distal half of left tibia with articulated astragalus; (D_1 & D_2) TM-006 proximal half of a right tibia in posterior and lateral views; and (E_1 & E_2) MOR 248 proximal half of the right tibia. **Abbreviations**: **as**, astragals; **cc**, cnemial crest; **df**, distal femur; **ic**, inner condyle; **im**, inner malleolus; **om**, outer malleolus. [planned for page width]

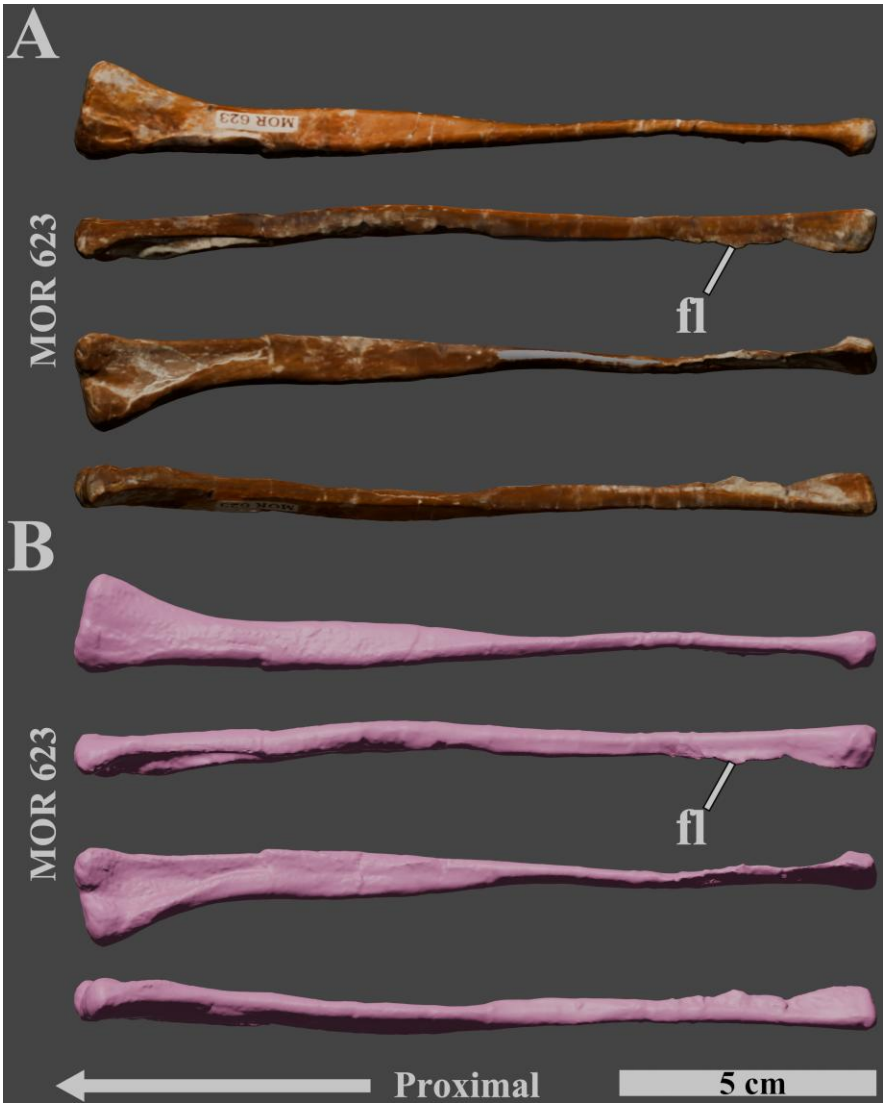


FIGURE 20. *Orodromeus makelai* fibula [MOR 623]. (A) MOR 623 right fibula rendered with texture, and (B) MOR 623 right fibula rendered without texture. **Abbreviations**: **fl**, flange. [planned for column width]

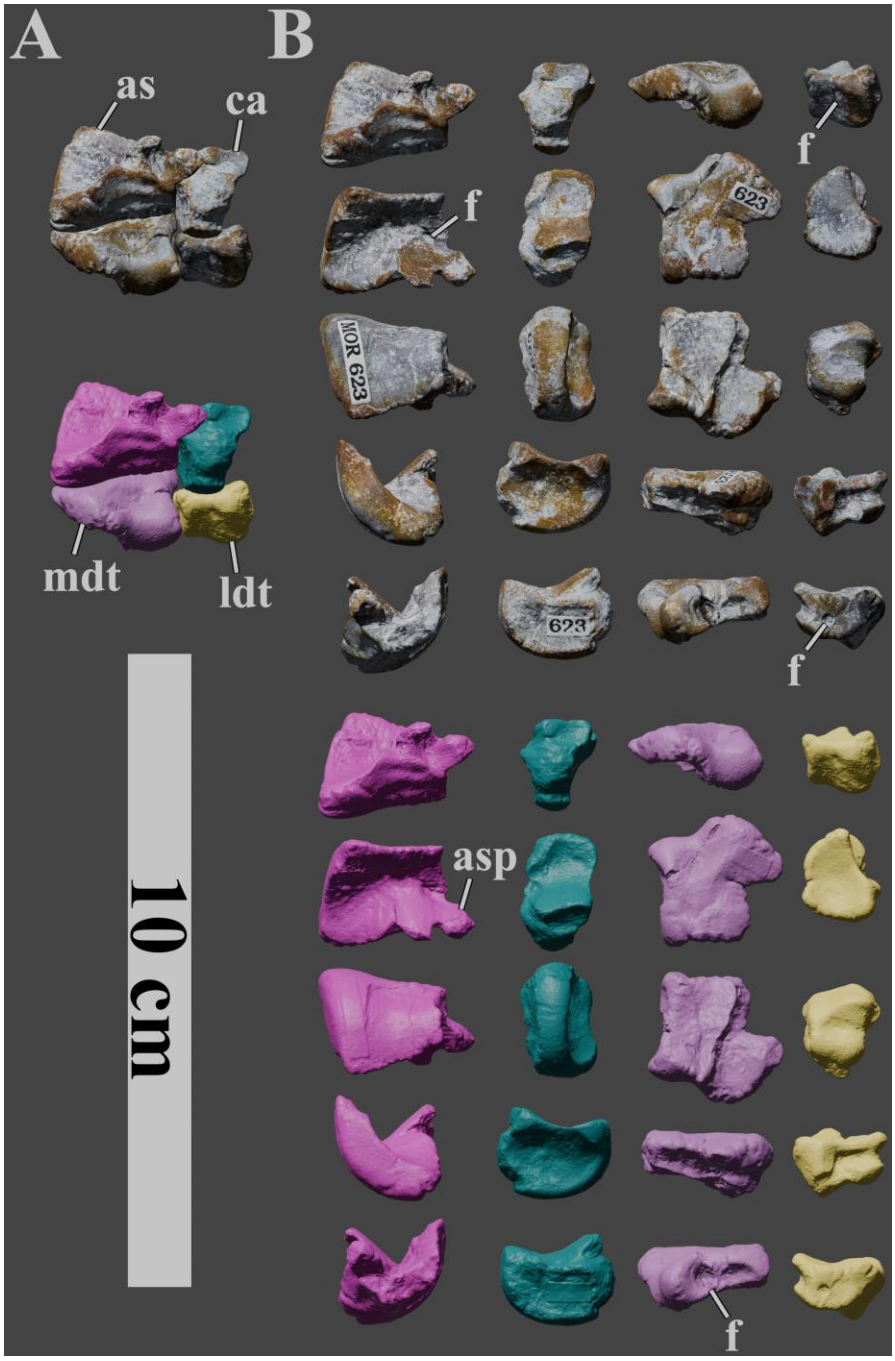


FIGURE 21. *Orodromeus makelai* tarsals rendered with and without texture. (A) Interpreted articulation of disarticulated tarsals of right hindlimb [MOR 623], and (B) tarsals in (descending order) anterior, dorsal, ventral, lateral, and medial views. **Abbreviations**: **as**; astragalus; **asp**: ascending process; **ca**, calcaneum; **f**, foramen; **ldt**, lateral distal tarsal; **mdt**, medial distal tarsal. [planned for column width]

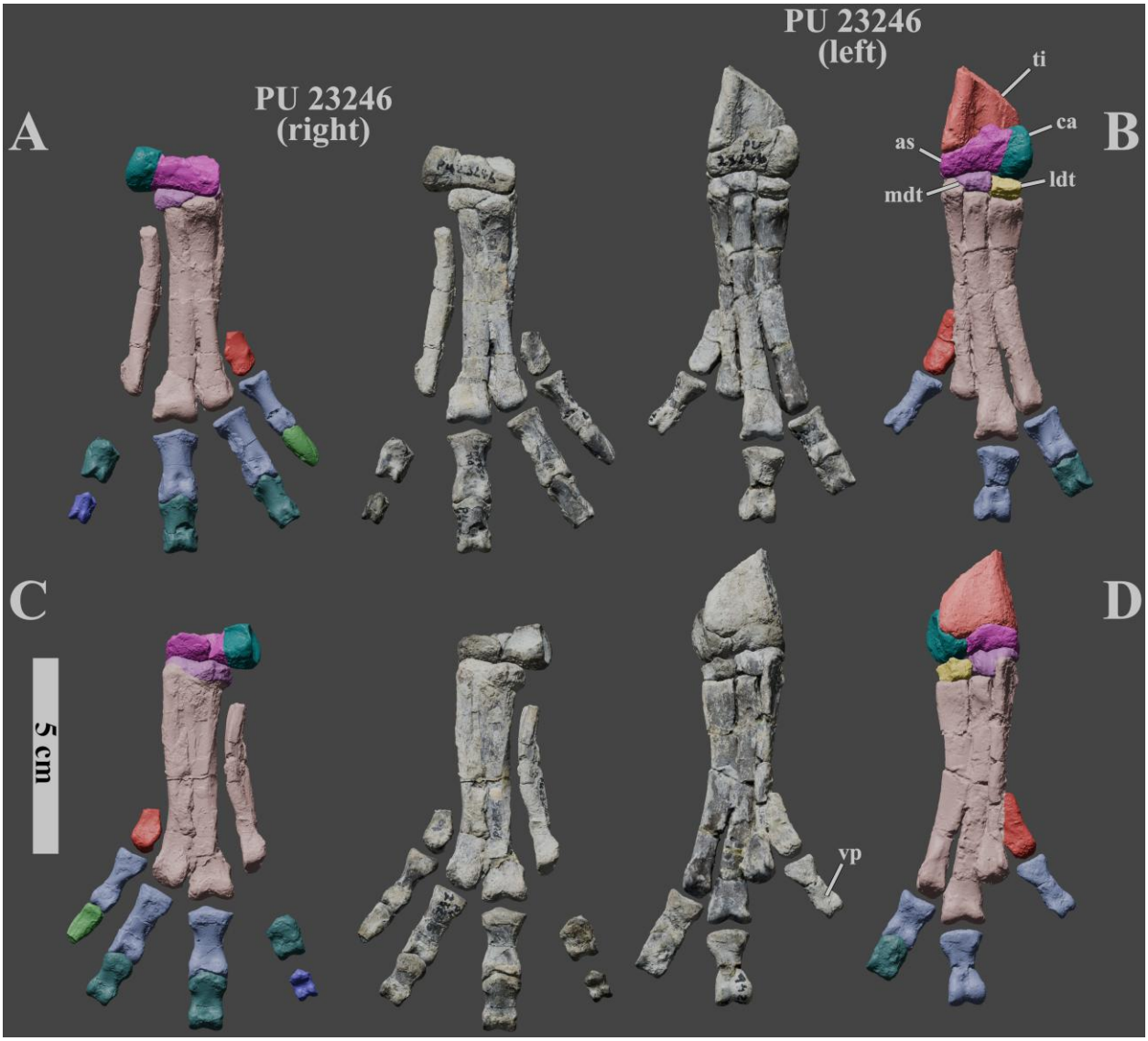


FIGURE 22. *Orodromeus makelai* juvenile pes [PU 23246] rendered with and without texture. (A) PU 23246 right pes with tarsals in anterior view; (B) PU 23246 left pes, tarsals, and tibia in anterior view; (C) PU 23246 right pes and tarsal in posterior view; and (D) PU 23246 left pes, tarsals, and tibia in posterior view. **Abbreviations**: **as**, astragalus; **ca**, calcaneum; **ldt**, lateral distal tarsal; **mdt**, medial distal tarsal; **ti**, tibia; **vp**, ventral pit. [planned for page width]



FIGURE 23. *Orodromeus makelai* subadult pes [MOR 623] rendered with and without texture. (A) MOR 623 right pes in anterior view; (B) MOR 623 left pes in anterior view; (C) MOR 623 right pes in posterior view; and (D) MOR 623 left pes in posterior view. **Abbreviations**: **vp**, ventral pit. [planned for page width]

Literature Cited

Agnolín, F. L., Herrera, G. Á., Rolando, M. A., Motta, M., Rozadilla, S., Verdiquio, L., D'Angelo, J. S., Mayano-Paz, D., Verela, A. N., Sterli, J., Bogan, S., Miner, S., Rodríguez, A. M., Muñoz, G., Isasi, M. P., & Novas, F. E. (2024). Fossil vertebrates from the Cerro Fortaleza Formation (Upper Cretaceous), Santa Cruz Province, Argentina. *Cretaceous Research*, *154*, 105735.

Andrzejewski, K. A., Winkler, D. A., & Jacobs, L. L. (2019). A new basal ornithopod (Dinosauria, Ornithischia) from the Early Cretaceous of Texas. *PloS one*, 2019(3), e0207935-e0207935. https://doi.org/10.1371/journal.pone.0207935

Avrahami, H. M., Makovicky, P. J., Tucker, R. T., & Zanno, L. E. (2024). A new semi-fossorial thescelosaurine dinosaur from the Cenomanian-age Mussentuchit Member of the Cedar Mountain Formation, Utah. *The Anatomical Record*.

Averianov, A. O., Voronkevich, A. V., Leshchinskiy, S. V., & Fayngertz, A. V. (2006). A ceratopsian dinosaur *Psittacosaurus sibiricus* from the Early Cretaceous of West Siberia, Russia and its phylogenetic relationships. *Journal of Systematic Palaeontology*, *4*(4), 359-395.

Baron, M. G., Norman, D. B., & Barrett, P. M. (2017). Postcranial anatomy of *Lesothosaurus diagnosticus* (Dinosauria: Ornithischia) from the Lower Jurassic of southern Africa: implications for basal ornithischian taxonomy and systematics. *Zoological Journal of the Linnean Society*, *179*(1), 125-168.

Barrett, P. M., Butler, R. J., & Knoll, F. (2005). Small-bodied ornithischian dinosaurs from the Middle Jurassic of Sichuan, China. *Journal of Vertebrate Paleontology*, *25*(4), 823-834.

Barrett, P. M. & Han, F. -L. (2009) Cranial anatomy of *Jeholosaurus shangyuanensis* (Dinosauria: Ornithischia) from the Early Cretaceous of China. Zootaxa, 2072, 31-55.

Barta, D. E., & Norell, M. A. (2021). The osteology of *Haya griva* (Dinosauria, Ornithischia) from the Late Cretaceous of Mongolia. *Bulletin of the American Museum of Natural History*, 445 (1), 1-112. https://doi.org/10.1206/0003-0090.445.1.1

Becerra, M. G., Pol, D., Porro, L. B., Paulina-Carabajal, A., & Rauhut, O. W. (2022). Craniomandibular osteology of *Manidens condorensis* (Ornithischia: Heterodontosauridae) from the upper Lower Jurassic of Argentina. *Journal of Vertebrate Paleontology*, *42*(3), e2181087.

Bertozzo, F., Kecheng, N., Gillette, N. V., & Godefroit, P. (2025). Anatomical description and digital reconstruction of the skull of *Jeholosaurus shangyuanensis* (Dinosauria, Ornithopoda) from China. *PloS one*, *20*(1), e0312519.

Boyd, C. A. (2012). *Taxonomic revision of latest Cretaceous North american basal neonithischian taxa and a phylogenetic analysis of basal ornithischian relationships* University of Texas - Austin.

Boyd, C. A., Drumheller, S. K., & Gates, T. A. (2013). Crocodyliform feeding traces on juvenile ornithischian dinosaurs from the Upper Cretaceous (Campanian) Kaiparowits Formation, Utah. *PloS one*, *8*(2), e57605.

Brochu, C. A. (1996). Closure of neurocentral sutures during crocodilian ontogeny; implications for maturity assessment in fossil archosaurs. *Journal of Vertebrate Paleontology*, 16(1), 49-62. https://doi.org/10.1080/02724634.1996.10011283

Brown, C. M., Boyd, C. A., & Russell, A. P. (2011). A new basal ornithopod dinosaur

(Frenchman Formation, Saskatchewan, Canada), and implications for late Maastrichtian ornithischian diversity in North America. *Zoological Journal of the Linnean Society*, 163(4), 1157-1198.

Brown, C. M., Evans, D. C., Ryan, M. J., & Russell, A. P. (2013). New data on the diversity and abundance of small-bodied ornithopods (Dinosauria, Ornithischia) from the Belly, River Group (Campanian) of Alberta. *Journal of vertebrate paleontology*, 33(3), 495-520. https://doi.org/10.1080/02724634.2013.746229.

Butler, R. J., & Zhao, Q. (2009). The small-bodied ornithischian dinosaurs *Micropachycephalosaurus hongtuyanensis* and *Wannanosaurus yansiensis* from the Late Cretaceous of China. *Cretaceous Research*, *30*(1), 63-77.

Butler, R. J., Jin, L., Chen, J., & Godefroit, P. (2011). The postcranial osteology and phylogenetic position of the small ornithischian dinosaur *Changchunsaurus parvus* from the Quantou Formation (Cretaceous, Aptian-Cenomanian) of Jilin Provine, north-eastern China. *Palaeontology*, 54(3), 667-683. https://doi.org/10.1111/j.1475-4983.2011.01046.x

Carpenter, K., & Galton, P. (2018). A photo documentation of bipedal ornithischian dinosaurs from the Upper Jurassic Morrison Formation, USA. *Geology of the Intermountain West*, 5, 167-207.

Chin, K. (2007). The paleobiological implications of herbivorous dinosaur coprolites from the Upper Cretaceous Two Medicine Formation of Montana: why eat wood?. *Palaios*, 22(5), 554-566.

Cooper, M. R. 1985. A revisoin of the ornithischian dinosaur *Kangnasaurus coetzeei* Haughton, with classification of the Ornithischia. *Annals of the South African Museum*. 95, 281-317.

Coria, R. A., & Salgado, L. (1996). A basal iguanodontian (Ornithischia: Ornithopoda) from the Late Cretaceous of south America. *Journal of Vertebrate Paleontology*, 16(3), 445-457.

Coria, R. A., & Calvo, J. O. (2002). A new iguanodontian ornithopod from Neuquén Basin, Patagonia, Argentina. *Journal of Vertebrate Paleontology*, *22*(3), 503-509.

Coria, R. A., Moly, J. J., Reguero, M., Santillana, S., & Marenssi, S. (2013). A new ornithopod (Dinosauria; Ornithischia) from Antarctica. *Cretaceous Research*, *41*, 186-193.

Coria, R. A., Moly, J. J., Reguero, M., Santillana, S., & Marenssi, S. (2013). A new ornithopod (Dinosauria; Ornithischia) from Antarctica. *Cretaceous Research*, *41*, 186-193.

Cruzado-Caballero, P., Gasca, J. M., Filippi, L. S., Cerda, I. A., & Garrido, A. C. (2019). A new ornithopod dinosaur from the Santonian of Northern Patagonia (Rincón de los Sauces, Argentina). *Cretaceous Research*, *98*, 211-229.

Eberth, D. A., Evans, D. C., Ramezani, J., Kamo, S. L., Brown, C. M., Currie, P. J., & Braman, D. R. (2023). Calibrating geologic strata, dinosaurs, and other fossils at Dinosaur Provincial Park (Alberta, Canada) using a new CA-ID-TIMS U–Pb geochronology. *Canadian Journal of Earth Sciences*, *60*(12), 1627-1646.

Erickson, G. M., Lappin, A. K., & Larson, P. (2005). Androgynous rex–the utility of chevrons for determining the sex of crocodilians and non-avian dinosaurs. *Zoology*, *108*(4), 277-286.

Ferigolo, J., & Langer, M. C. (2007). A Late Triassic dinosauriform from south Brazil and the origin of the ornithischian predentary bone. *Historical Biology*, *19*(1), 23-33.

Forster, C. A., de Klerk, W. J., Poole, K. E., Chinsamy-Turan, A., Roberts, E. M., & Ross, C. F. (2023). *Iyuku raathi*, a new iguanodontian dinosaur from the Early Cretaceous Kirkwood

Formation, South Africa. *The Anatomical Record*, 306(7), 1762-1803.

Freimuth, W. J., & Varricchio, D. J. (2019). Insect trace fossils elucidate depositional environments and sedimentation at a dinosaur nesting site from the Cretaceous (Campanian) Two Medicine Formation of Montana. *Palaeogeography, Palaeoclimatology, Palaeoecology,* 534, 109262.

Freimuth, W. J., Varricchio, D. J., & Chin, K. (2021). Paleoenvironmental implications of invertebrate fecal pellets (Edaphichnium isp.) at an ichnofossil-rich dinosaur nesting locality, Upper Cretaceous Two Medicine Formation, Montana, USA. *Palaios*, 36(9), 283-300.

Fricke, H. C., Foreman, B. Z., & Sewall, J. O. (2010). Integrated climate model-oxygen isotope evidence for a North American monsoon during the Late Cretaceous. *Earth and Planetary Science Letters*, 289(1-2), 11-21.

Fuentes, F., DeCelles, P. G., & Constenius, K. N. (2012). Regional structure and kinematic history of the Cordilleran fold-thrust belt in northwestern Montana, USA. *Geosphere*, 8(5), 1104-1128.

Galton, P. M., & Jensen, J. A. (1973). Skeleton of a hypsilophodontid dinosaur (*Nanosaurus* (?) *rex*) from the Upper Jurassic of Utah. *Brigham Young University Geology Studies*, 20(4), 137-157.

Galton, P. M. (1975). The ornithischian dinosaur *Hypsilophodon* from the Wealden of th Isle of Wight. Bulletin of the British Museum (Natural History) Geology, 25(1), 1-152.

Galton, P. M. (1978). Fabrosauridae, the basal family of ornithischian dinosaurs (Reptilia: Ornithopoda). *Paläontologische Zeitschrift*, 52(1), 138-159.

Gates, T. A., Lund, E. A., Boyd, C. A., DeBlieux, D. D., Titus, A. L., Evans, D. C., Getty, M. A., Kirkland, J. I., & Eaton, J. G. (2013). Ornithopod Dinosaurs from the Grand Staircase-Escalante National Monument Region, Utah, and Their Role in Paleobiogeographic and Macroevolutionary Studies. In (pp. 463). Indiana University Press.

Gilmore, C. W. (1924). A new species of *Laosaurus*, an ornithischian dinosaur from the Cretaceous of Alberta. Royal Society of Canada.

Godefroit, P., Sinitsa, S. M., Dhouailly, D., Bolotsky, Y. L., Sizov, A. V., McNamara, M. E., Benton, M. J., & Spagna, P. (2014). A Jurassic ornithischian dinosaur from Siberia with both feathers and scales. *Science*, 345(6195), 451-455.

Han, F., Barrett, P. M., Butler, R. J., & Xu, X. (2012). Postcranial anatomy of *Jeholosaurus shangyuanensis* (Dinosauria, Ornithischia) from the Lower Cretaceous Yixian Formation of China. *Journal of Vertebrate Paleontology*, 32(6), 1370-1395.

He, X. L., & Cai, K. (1984). The Middle Jurassic Dinosaurian Fauna from Dashanpu, Zigong, Sichuan. Vol 1, The Ornithopod Dinosaurs. *Chengdu: Sichuan Scientific and Technological Publishing House*, 71, 1-66.

Herne, M. C., Tait, A. M., Weisbecker, V., Hall, M., Nair, J. P., Cleeland, M., & Salisbury, S. W. (2018). A new small-bodied ornithopod (Dinosauria, Ornithischia) from a deep, high-energy Early Cretaceous river of the Australian–Antarctic rift system. *PeerJ*, *5*, e4113.

Horner, J. R. & Weishampel, D. B. (1988). A comparative embryological study of two ornithischian dinosaurs. *Nature(London)*. 332(6161), 256-257. https://doi.org/10.1038/332256a0.

Horner, J. R., Schmitt, J. G., Jackson, F. D., & Hanna, R. (2001). Bones and rocks of the Upper

Cretaceous Two Medicine-Judith River clastic wedge complex. *In Guidebook for the Field Trips, Society of Vertebrate Paleontology 61st Annual Meeting, Montana*. Museum of the Rockies Occasional Paper (No. 3, pp. 1-14).

Horner, J. R., De Ricqlès, A., Padian, K., & Scheetz, R. D. (2009). Comparative long bone histology and growth of the "hypsilophodontid" dinosaurs *Orodromeus makelai*, *Dryosaurus altus*, and *Tenontosaurus tillettii* (Ornithischia: Euornithopoda). *Journal of Vertebrate Paleontology*, *29*(3), 734-747.

Hulke, J. W. (1882). XXIV. An attempt at a complete osteology of *Hypsilophodon foxii*; a British Wealden dinosaur. *Philosophical Transactions of the Royal Society of London*, (173), 1035-1062.

Hudgins, M. N. (2021*). The Paleobiology, Paleoecology, and Evolution of Thescelosauridae (Ornithischia) from Alberta, Canada*. University of Alberta.

Huh, M. (2010). A new basal ornithopod dinosaur from the Upper Cretaceous of South Korea. *Neues Jahrbuch für Geologie und Paläontologie. Abhandlungen*, *259*(1), 1-24.

Ibiricu, L. M., Martínez, R. D., Luna, M., & Casal, G. A. (2014). A reappraisal of *Notohypshilophodon comodorensis* (Ornithischia: Ornithopoda) from the Late Cretaceous of Patagonia, Argentina. *Zootaxa*, 3786 (4), 401-422.

Jin, L., Chen, J., Zan, S., Butler, R. J., & Godefroit, P. (2010). Cranial anatomy of the small ornithischian dinosaur *Changchunsaurus parvus* from the Quantou Formation (Cretaceous, Aptian-Cenomanian) of Jilin Province, northeastern China. Journal of vertebrate paleontology, 30(1), 196-214. https://doi.org/10.1080/02724630903412372

Kauffman, E. G. (1977). Geological and biological overview: Western Interior Cretaceous basin.

The Mountain Geologist.

Krumenacker, L. J., Varricchio, D., J., Organ, C., Gardner, J. D., Britt, B. B., & Boyd, C. (2024). Osteology and phylogenetic relationships of the mid-Cretaceous neornithischian dinosaur *Oryctodromeus cubicularis* Varricchio, 2007. Journal of Vertebrate Paleontology. https://doi.org/10.1080/027724634.2024.2330581

Kutter, M. M. (2004). *New material of Zephyrosaurus schaffi (Dinosauria; Ornithischia) from the Cloverly Formation (Aptian-Albian) of Montana and the phylogeny of Hypsilophodontidae*. College of the Pacific – Stockton, Department of Biological Scienece.

Lageson, D. R., Schmitt, J. G., Horton, B. K., Kalakay, T. J., & Burton, B. R. (2001). Influence of Late Cretaceous magmatism on the Sevier orogenic wedge, western Montana. *Geology*, 29(8), 723-726.

Li, N., Dai, H., Tan, C., Hu, X., Wei, Z., Lin, Y., Wei, G., Li, D., Meng, L., Hao, B., You, H., & Peng, G. (2021). A neornithischian dinosaur from the Middle Jurassic Xintiangou Formation of Yunyang, Chongquing, China: the earliest record in Asia. *Historical Biology*, 33(7), 1089-1102. https://doi.org/10.1080/08912963.2019.1679129

Lorenz, J. & Gavin, W. (1984). *Geology of the Two Medicine Formation and the sedimentology of a dinosaur nesting ground*. Montana Geological Society Field Conference Northwestern Montana.

Madzia, D., Arbour, V. M., Boyd, C. A., Farke, A. A., Cruzado-Caballero, P., & Evans. D. C. (2021). The phylogenetic nomenclature of ornithischian dinosaurs. PeerJ (San Francisco, CA), 9, e122362-e12362. https://doi.org/10.7717/peerj.12362.

Makovicky, P. J., Kilbourne, B. M., Sadleir, R. W., & Norell, M. A. (2011). A new basal ornithopod (Dinosauria, Ornithischia) from the Late Cretaceous of Mongolia. *Journal of Vertebrate Paleontology*, 31(3), 626-640. https://doi.org/10.1080/02724634.2011.557114

Manitkoon, S., Deesri, U., Khalloufi, B., Nonsrirach, T., Suteethorn, V., Chanthasit, P., Boonla, W., & Buffetaut, E. (2023). A New Basal Neornithischian Dinosaur from the Phu Kradung Formation (Upper Jurassic) of Northeastern Thailand. *Diversity*, 15(7), 851.

Marsh, O. C. (1878). Notice of new dinosaurian reptiles. *American Journal of Science*, *3*(87), 241-244.

Morschhauser, E. M., Li, D., You, H., & Dodson, P. (2018). Cranial Anatomy of the Basal Neoceratopsian Auroraceratops rugosus (Ornithischia: Ceratopsia) from the Yujingzi Basin, Gansu Province, China. *Journal of Vertebrate Paleontology*, *38*(sup1), 36-68.

Nabavizadeh, A., & Weishampel, D. B. (2016). The predentary bone and its significance in the evolution of feeding mechanisms in ornithischian dinosaurs. *The Anatomical Record*, *299*(10), 1358-1388.

Nogueira, R. A., Rozadilla, S., Agnolín, F. L., Marsà, J. A. G., Motta, M. J., & Novas, F. E. (2024). A new ornithopod from the Upper Cretaceous (Huincul Formation) of northwestern Patagonia, Argentina: Implications on elasmarian postcranial anatomy. *Cretaceous Research*, *159*, 105874.

Norman, D. B., Sues, H. -D., Witmer, L. M., & Coria, R. A. (2004). Basal Ornithopoda. In D. B. Weishampel, P. Dodson, and H. Osmólska (editors), The Dinosauria: 413-437. Berkeley: Unversity of California Press.

Norman, D. B., Crompton, A. W., Butler, R. J., Porro, L. B., & Charig, A. J. (2011). The Lower Jurassic ornithischian dinosaur Heterodontosaurus tucki Crompton & Charig, 1962: cranial anatomy, funtional morphology, taxonomy, and relationships. *Zoological journal of the Linnean Soceity*, https://doi.org/10.1111/j.1096-3642.2011.00697.x

Owens, R. 1842. Report on British fossil reptiles. Part II. *Report for the British Association for the Advancement of Science*, 11, 60-204.

Porro, L. B., Witmer, L. M., & Barrett, P. M. (2015). Digital preparation and osteology of the skull of *Lesothosaurus diagnosticus* (Ornithischia: Dinosauria). *PeerJ*, 3, e1494.

Rogers, R. R. (1990). Taphonomy of three dinosaur bone beds in the Upper Cretaceous Two Medicine Formation of northwestern Montana: evidence for drought-related mortality. *Palaios*, 394-413.

Rogers, R. R., Swisher, C. C. III, & Horner, J. R. (1993). $^{40}Ar/^{39}Ar$ ad correlation of the nonmarine Two Medicine Formation (Upper Cretaceous), northwestern Montana, U.S.A. *Canadian journal of earth sciences*, 30(5), 1066-1075.

Rogers, R., Horner, J., Ramezani, J., Roberts, E., and Varricchio. D. (2024). Updating the Upper Cretaceous (Campanian) Two Medicine Formation of Montana: Lithostratigraphic revisions, new CA-ID-TIMS U-Pb ages, and a calibrated framework of dinosaur occurances. *The Geologial Society of America Bulletin*.

Rozadilla, S., Agnolín, F. L., & Novas, F. E. (2019). Osteology of the Patagonian ornithopod *Talenkauen santacrucensis* (Dinosauria, Ornithischia). *Journal of Systematic Palaeontology*, *17*(24), 2043-2089.

Rozadilla, S., Cruzado-Caballero, P., & Calvo, J. O. (2020), Osteology of Ornithopod

Macrogryphosaurus gondwanicus (Dinosauris, Ornithischia) from the Upper Cretaceous of Patagonia, Argentina. *Cretacesous research*, 108, 104311.

Ruiz-Omeñaca, J. I., Canudo, J. I., Cuenca-Bescós, G., Cruzado-Caballero, P., Gasca, J. M., & Moreno-Azanza, M. (2012). A new basal ornithopod dinosaur from the Barremian of Galve, Spain. *Comptes Rendus Palevol*, 11(6), 435-444.

Salgado, L., Coria, R. A., & Heredia, S. E. (1997). New materials of *Gasparinisaura cincosaltensis* (Ornithischia, Ornithopoda) from the Upper Cretaceous of Argentina. *Journal of Paleontology*, 71(5), 933-940.

Salgado, L., Canudo, J. I., Garrido, A. C., Moreno-Azanza, M., Martínez, L. C., Coria, R. A., & Gasca, J. M. (2017). A new primitive Neornithischian dinosaur from the Jurassic of Patagonia with gut contents. *Scientific Reports*, 7(1), 1-10.

Santa Luca, A. P. (1980). The postcranial skeleton of *Heterodontosaurus tucki* (Reptilia, Ornithischia) from the Stormberg of South Africa. Annals of the South African Museum. 79: 159-211.

Scheetz, R. D. (1999). *Osteology of Orodromeus makelai and the phylogeny of basal ornithopod dinosaurs*. Montana State University-Bozeman.

Seeley H. G. 1887. On the classification of the fossil animals commonly named Dinosauria. *Proceedings of the Royal Society of London*, 43, 481-494.

Sereno, P. C. (2012). Taxonomy, morphology, masticatory function and phylogeny of heterodontosaurid dinosaurs. *ZooKeys*, (226), 1.

Sternberg, C. M. 1937. A classification of *Thescelosaurus*, with a description of a new species. *Geological Society of America, Proceedings and Abstracts*, 1936-375.

Sues, H.-D. (1980). Anatomy and relationships of a new hypsilophodontid dinosaur from the Lower Cretaceous of North America. *Palaeontographica. Abt. A., Palaeozoologie-Stratigraphie*, 169, 51-72.

Sues, H. D., Evans, D. C., Galton, P. M., & Brown, C. M. (2023). Anatomy of the neornithischian dinosaur *Parksosaurus warreni* (Parks, 1926) from the Upper Cretaceous (lower Maastrichtian) Horseshoe Canyon Formation of Alberta, Canada. *Cretaceous Research*, 141, 105369.

Weishampel, D. B., & Heinrich, R. E. (1992). Systematics of hypsilophodontidae and basal Iguanodontia (Dinosauria: Ornithopoda). *Historical Biology*, 6(3), 159-184.

Weishampel, D. B., Jianu, C. M., Csiki, Z., & Norman, D. B. (2003). Osteology and phylogeny of *Zalmoxes* (n.g.), an unusual euornithopod dinosaur from the latest Cretaceous of Romania. *Journal of Systematic Palaeontology*, *1*(2), 65-123.

Wilson, J. A. (2006). Anatomical nomenclature of fossil vertebrates: standardized terms or 'lingua franca'?. *Journal of Vertebrate Paleontology*, 26(3), 511-518.

Xu, X., Forster, C. A., Clark, J. M., & Mo, J. (2006). A basal ceratopsian with transitional features from the Late Jurassic of northwestern China. *Proceedings of the Royal Society B: Biological Sciences*, 273(1598), 2135-2140.

Yang, Y., Wu, W., Dieudonné P.-E., & Godefroit, P. (2020). A new basal ornithopod dinosaur from the Lower Cretaceous of China. *PeerJ* (San Francisco, CA), 8, e9832-e9832. https://doi.org/10.7717/peerj.9832

Zanno, L. E., Gates, T. A., Avrahami, H. M., Tucker, R. T., & Makovicky, P. J. (2023). An early-diverging iguanodontian (Dinosauria: Rhabdodontomorpha) from the Late Cretaceous of

North America. *Plos one*, 18(6), e0286042.

Zheng, W., Jin, X., Shibata, M., Azuma, Y., & Yu, F. (2012). A new ornithischian dinosaur from the cretaceous Liangtoutang formation of Tiantai, Zhejiang Province, China. *Cretaceous Research*, *34*, 208-219.

CHAPTER FIVE

CONCLUSION TO THESIS

This thesis explored variation in orodromines from the Campanian Two Medicine-Juidth River-Belly River clastic wedge in northwestern North America, under the purview of detecting evidence of sexually dimorphic characters in the cranial anatomy. Little support was found for any sexually dimorphic cranial features in orodromines, and instead, new systematic divisions were erected. Two new orodromine taxa are established here, *Akanthodromeus judithi* (Chapter 2) and *Pikunidromeus ancellae* (Chapter 3), and an updated osteological description for *Orodromeus makelai* is provided (Chapter 4). This new osteological bracketing highlights a previously unrecognized diversity within Orodrominae, and demonstrates a rapid diversification, and subsequently swift disappearance of the group, during a specific transgressive-regressive phase of the Western Interior Seaway.

The argument for systematic distinctions, and not dimorphism, is evidenced by the lack of documented temporal overlaps between *Pikunidromeus*, *Orodromeus*, and *Akanthodromeus*, making it unlikely any of these three taxa represent a dimorphic form of another. Only one fossil locality [TM-088] in the entire clastic wedge offers multiple orodromines in cooccurrence; *Pikunidromeus* and the mysterious informal taxon called denoted the “BV Orodromine”. These two taxa exhibit distinct jugal horn morphologies from each other, as *Pikunidromeus* manifests a diminutive triangular jugal horn in contrast to the large sub-oval jugal horn of the “BV Orodromine”. The absence of more “BV Orodromine” specimens at other fossil localities likely precludes it as a divergent horn trajectory in *Pikunidromeus*. This argument is further supported by the ontogenetic trajectories documented here for orodromine jugal horns (Chapter 3 and 4), as

Pikunidromeus, *Orodromeus*, and the "BV Orodromine" offer multiple small juvenile specimens retaining horns that establish each separate horn morphology relatively early in ontogeny.

Orodromines are a dynamic group of small-bodied ornithischians that buck taphonomic size biases, and present often large assemblages. This provides an unprecedented opportunity to assess the understudied dinosaur representatives that were foundational to the ecosystems of Campanian Laramidia. Here, this thesis demonstrated the diversity of Orodrominae has been greatly underestimated in the past and provides a new systematic framework that can be applied to the remaining informal taxa, and indeterminate specimens.

CUMULATIVE REFERENCES CITED

Agnolin, F. L., & Varricchio, D. (2012). Systematic reinterpretation of *Piksi barbarulna* Varricchio, 2002 from the Two Medicine Formation (Upper Cretaceous) of Western USA (Montana) as a pterosaur rather than a bird. *Geodiversitas*, 34(4), 883-894.

Agnolín, F. L., Herrera, G. Á., Rolando, M. A., Motta, M., Rozadilla, S., Verdiquio, L., D'Angelo, J. S., Mayano-Paz, D., Verela, A. N., Sterli, J., Bogan, S., Miner, S., Rodríguez, A. M., Muñoz, G., Isasi, M. P., & Novas, F. E. (2024). Fossil vertebrates from the Cerro Fortaleza Formation (Upper Cretaceous), Santa Cruz Province, Argentina. *Cretaceous Research*, *154*, 105735.

Alcober, O. A. & Martinez R. N. (2010). A new herrerasaurid (Dinosauria, Saurischia) from the Upper Triassic Ischigualasto Formation of northwestern Argentina. *ZooKeys*, 63(2), 55-87. https://doi.org/10.3897/zookeys.63.550

Andrzejewski, K. A., Winkler, D. A., & Jacobs, L. L. (2019). A new basal ornithopod (Dinosauria, Ornithischia) from the Early Cretaceous of Texas. *PloS one*, 2019(3), e0207935-e0207935. https://doi.org/10.1371/journal.pone.0207935

Arbour, V. M., & Evans, D. C. (2017). A new ankylosaurine dinosaur from the Judith River Formation of Montana, USA, based on an exceptional skeleton with soft tissue preservation. *Royal Society Open Science*, 4(5), 161086–161086.

Arbour, V. M., & Evans, D. C. (2019). A new leptoceratopsid dinosaur from Maastrichtian-aged deposits of the Sustut Basin, northern British Columbia, Canada. *PeerJ*, *7*, e7926.

Arbour, V. M., Evans, D. C., Simon, D. J., Cullen, T. M., & Braman, D. (2020). Cretaceous flora and fauna of the Sustut Group near the Sustut River, northern British Columbia, Canada. *Canadian Journal of Earth Sciences*, *57*(6), 671-680.

Averianov, A. O., Voronkevich, A. V., Leshchinskiy, S. V., & Fayngertz, A. V. (2006). A ceratopsian dinosaur *Psittacosaurus sibiricus* from the Early Cretaceous of West Siberia, Russia and its phylogenetic relationships. *Journal of Systematic Palaeontology*, 4(4), 359-395.

Averianov, A. O., Voronkevich, A. V., Leshchinskiy, S. V., & Fayngertz, A. V. (2006). A ceratopsian dinosaur *Psittacosaurus sibiricus* from the Early Cretaceous of West Siberia, Russia and its phylogenetic relationships. *Journal of Systematic Palaeontology*, *4*(4), 359-395.

Avrahami, H. M., Lindsey, K. P., & Herzog, L. (2023). Advances in 3D surface scanning: Mobile device applications set a new standard for digitization of fossils and museum artifacts. *Journal of Vertebrate Paleontology* Program Abstract 83:77.

Avrahami, H. M., Makovicky, P. J., Tucker, R. T., & Zanno, L. E. (2024). A new semi-fossorial thescelosaurine dinosaur from the Cenomanian-age Mussentuchit Member of the Cedar Mountain Formation, Utah. *Anatomical record (Hoboken, N.J.: 2007)*. doi:10.1002/ar.25505

Baron, M. G., Norman, D. B., & Barrett, P. M. (2017). Postcranial anatomy of *Lesothosaurus diagnosticus* (Dinosauria: Ornithischia) from the Lower Jurassic of southern Africa: implications for basal ornithischian taxonomy and systematics. *Zoological Journal of the Linnean Society*, 179(1), 125-168.

Barrett, P. M., Butler, R. J., & Knoll, F. (2005). Small-bodied ornithischian dinosaurs from the Middle Jurassic of Sichuan, China. *Journal of Vertebrate Paleontology*, 25(4), 823-834.

Barrett, P. M. & Han, F. -L. (2009) Cranial anatomy of *Jeholosaurus shangyuanensis* (Dinosauria: Ornithischia) from the Early Cretaceous of China. Zootaxa, 2072, 31-55.

Barrett, P. M. (2016). A new specimen of *'Valdosaurus canaliculatus'* (Ornithopoda: Dryosauridae) from the Lower Cretaceous of the Isle of Wight, England. *Memoirs of Museum Victoria*, *74*, 29-48.

Barta, D. E., & Norell, M. A. (2021). The osteology of *Haya griva* (Dinosauria, Ornithischia) from the Late Cretaceous of Mongolia. *Bulletin of the American Museum of Natural History*, 445 (1), 1-112. https://doi.org/10.1206/0003-0090.445.1.1

Becerra, M. G., Pol, D., Porro, L. B., Paulina-Carabajal, A., & Rauhut, O. W. (2022). Craniomandibular osteology of *Manidens condorensis* (Ornithischia: Heterodontosauridae) from the upper Lower Jurassic of Argentina. *Journal of Vertebrate Paleontology*, *42*(3), e2181087.

Bertozzo, F., Kecheng, N., Gillette, N. V., & Godefroit, P. (2025). Anatomical description and digital reconstruction of the skull of *Jeholosaurus shangyuanensis* (Dinosauria, Ornithopoda) from China. *PloS one*, *20*(1), e0312519.

Bonde, J. W., Hall, R. L., Krumenacker, L. J., & Varricchio, D. J. (2022). *Nevadadromeus schmitti* (gen. et sp. nov.), a New Basal Neornithischian with Affinities to the Thescelosaurinae, from the Upper Cretaceous (Cenomanian) Willow Tank Formation of Southern Nevada. *Journal of the Arizona-Nevada Academy of Science*, 50(1), 1-8.

Boulenger GA. 1881. *Iguanodon bernissartensis*. p. 606. In: Beneden P-J, ed. *Sur l'arc pelvien chex les dinosauriens de Bernissart. Bulletin de l'Académie royal de Belgique 3 Sér. 1*. Brussels, Belgium: Académie royal de Belgique, 600–608.

Boyd, C. A. (2012). *Taxonomic revision of latest Cretaceous North american basal neonithischian taxa and a phylogenetic analysis of basal ornithischian relationships* University of Texas - Austin.

Boyd, C. A. (2014). The cranial anatomy of the neornithischian dinosaur *Thescelosaurus neglectus*. *PeerJ*, 2, e669.

Boyd, C. A. (2015). The systematic relationships and biogeographic history of ornithischian dinosaurs. *PeerJ*, 3, e1523.

Boyd, C. A., Brown, C. A., Scheetz, R. D., & Clarke, J. A. (2009). Taxonomic revision of the basal Neornithischian taxa *Thescelosaurus* and *Bugenasaura*. *Journal of Vertebrate Paleontology*, 29, 758-770.

Boyd, C. A., Drumheller, S. K., & Gates, T. A. (2013). Crocodyliform feeding traces on juvenile ornithischian dinosaurs from the Upper Cretaceous (Campanian) Kaiparowits Formation, Utah. *PloS one*, *8*(2), e57605.

Brochu, C. A. (1996). Closure of neurocentral sutures during crocodilian ontogeny; implications for maturity assessment in fossil archosaurs. *Journal of Vertebrate Paleontology*, 16(1), 49-62. https://doi.org/10.1080/02724634.1996.10011283

Brown, B. (1914). *Leptoceratops*, a new genus of Ceratopsia from the Edmonton Cretaceous of Alberta. Bulletin of the AMNH; v. 33, article 36.

Brown, C. M., & Druckenmiller, P. (2011). Basal ornithopod (Dinosauria: Ornithischia) teeth from the Prince Creek formation (early Maastrichtian) of Alaska. *Canadian Journal of Earth Sciences*, *48*(9), 1342-1354.

Brown, C. M., Boyd, C. A., & Russell, A. P. (2011). A new basal ornithopod dinosaur (Frenchman Formation, Saskatchewan, Canada), and implications for late Maastrichtian ornithischian diversity in North America. *Zoological Journal of the Linnean Society*, 163(4), 1157-1198.

Brown, C. M., Evans, D. C., Campione, N. E., O'Brien, L. J., & Eberth, D. A. (2013). Evidence for taphonomic size bias in the Dinosaur Park Formation (Campanian, Alberta), a model Mesozoic terrestrail alluvial-paralic system. *Palaeogeography, palaeoclimatology, palaeoecology*, 372 (S1), 180-122. https://doi.org/10.1016/j.palaeo.2012.06.027

Brown, C. M., Evans, D. C., Ryan, M. J., & Russell, A. P. (2013). New data on the diversity and abundance of small-bodied ornithopods (Dinosauria, Ornithischia) from the Belly, River Group (Campanian) of Alberta. *Journal of vertebrate paleontology*, 33(3), 495-520. https://doi.org/10.1080/02724634.2013.746229.

Butler, R. J., & Zhao, Q. (2009). The small-bodied ornithischian dinosaurs *Micropachycephalosaurus hongtuyanensis* and *Wannanosaurus yansiensis* from the Late Cretaceous of China. *Cretaceous Research*, 30(1), 63-77.

Butler, R. J., Jin, L., Chen, J., & Godefroit, P. (2011). The postcranial osteology and phylogenetic position of the small ornithischian dinosaur *Changchunsaurus parvus* from

the Quantou Formation (Cretaceous, Aptian-Cenomanian) of Jilin Provine, north-eastern China. *Palaeontology*, 54(3), 667-683. https://doi.org/10.1111/j.1475-4983.2011.01046.x

Button, D. J. & Zanno, L. E. (2023). Neuroanatomy of the late Cretaceous *Thescelosaurus neglectus* (Neornithischia: Thescelosauridae) reveals novel ecological specialisations within Dinosauria. Scientific Reports, 13(1), 19224-19224. https://doi.org/10.1038/s41598-023-45658-3

Carpenter, K., & Galton, P. (2018). A photo documentation of bipedal ornithischian dinosaurs from the Upper Jurassic Morrison Formation, USA. *Geology of the Intermountain West*, 5, 167-207.

Carpenter, K., & Wilson, Y. (2008). A new species of *Camptosaurus* (Ornithopoda: Dinosauria) from the Morrison Formation (Upper Jurassic) of Dinosaur National Monument, Utah, and a biomechanical analysis of its forelimb. *Annals of Carnegie Museum*, 76(4), 227-263.

Chanthasit, P. (2010). *The ornithopod dinosaur Rhabdodon from the Late Cretaceous of France: anatomy, systematics and paleobiology* (Doctoral dissertation, Université Claude Bernard-Lyon I).

Chiba, K., Ryan, M. J., Fanti, F., Loewen, M. A., & Evans, D. C. (2018). New material and systematic re-evaluation of *Medusaceratops lokii* (Dinosauria, Ceratopsidae) from the Judith River Formation (Campanian, Montana). *Journal of Paleontology*, 92(2), 272–288.

Chin, K. (2007). The paleobiological implications of herbivorous dinosaur coprolites from the Upper Cretaceous Two Medicine Formation of Montana: why eat wood?. *Palaios*, 22(5), 554-566.

Chinnery, B. (2004). Description of *Prenoceratops pieganensis* gen. et sp. nov. (Dinosauria: Neoceratopsia) from the Two Medicine Formation of Montana. *Journal of Vertebrate Paleontology*, 24(3), 572-590.

Cooper, M. R. (1985). A revisoin of the ornithischian dinosaur *Kangnasaurus coetzeei* Haughton, with classification of the Ornithischia. *Annals of the South African Museum*. 95, 281-317.

Coria, R. A., & Calvo, J. O. (2002). A new iguanodontian ornithopod from Neuquén Basin, Patagonia, Argentina. *Journal of Vertebrate Paleontology*, *22*(3), 503-509.

Coria, R. A., & Salgado, L. (1996). A basal iguanodontian (Ornithischia: Ornithopoda) from the Late Cretaceous of south America. *Journal of Vertebrate Paleontology*, 16(3), 445-457.

Coria, R. A., Moly, J. J., Reguero, M., Santillana, S., & Marenssi, S. (2013). A new ornithopod (Dinosauria; Ornithischia) from Antarctica. *Cretaceous Research*, *41*, 186-193.

Cruzado-Caballero, P., Gasca, J. M., Filippi, L. S., Cerda, I. A., & Garrido, A. C. (2019). A new ornithopod dinosaur from the Santonian of Northern Patagonia (Rincón de los Sauces, Argentina). *Cretaceous Research*, *98*, 211-229.

Cullen, T. M., Fanti, F., Capobianco, C., Ryan, M. J., & Evans, D. C. (2016). A vertebrate microsite from a marine-terrestrial transition in the Foremost Formation (Campanian) of Alberta, Canada, and the use of faunal assemblage data as a paleoenvironmental indicator. *Palaeogeography, Palaeoclimatology, Palaeoecology*, 444, 101-114.

Dalman, S. G., & Lucas, S. G. (2015). New data on the tyrannosaurid theropods from the middle Campanian lower Judith River Formation of north-central Montana. *New Mexico Museum of Natural History and Science*, 67, 77-89.

Dodson, P. (1986). *Avaceratops lammersi*: a new ceratopsid from the Judith River Formation of Montana. *Proceedings of the Academy of Natural Sciences of Philadelphia*, 305-317.

Druckenmiller, P. S., Erickson, G. M., Brinkman, D., Brown, C. M., & Eberle, J. J. (2021). Nesting at extreme polar latitudes by non-avian dinosaurs. *Current Biology*, 31(16), 3469-3478.

Dyer, A., Powers, M., & Currie, P. (2022). Problematic putative pachycephalosaurids: Synchrotron μCT imaging shines new light on the anatomy and taxonomic validity of *Gravitholus albertae* from the Belly River Group (Campanian) of Alberta, Canada. *Vertebrate Anatomy Morphology Palaeontology*, *10*(1).

Dzik, J. (2003). A beaked herbivorous archosaur with dinosaur affinities from the early Late Triassic of Poland. *Journal of Vertebrate Paleontology*, *23*(3), 556-574.

Eberth, D. A. (2015). Origins of dinosaur bonebeds in the Cretaceous of Alberta, Canada. *Canadian Journal of Earth Sciences*, 52(8), 655-681.

Eberth, D. A. (2024). Stratigraphic architecture of the Belly River Group (Campanian, Cretaceous) in the plains of southern Alberta: Revisions and updates to an existing model and implications for correlating dinosaur-rich strata. *Plos one*, 19(1), e0292318.

Eberth, D. A., Currie, P. J., & Koppelhus, E. B. (2005). The geology. *Dinosaur Provincial Park: a spectacular ancient ecosystem revealed*, Indiana University Press, Bloomington, 54-82.

Eberth, D. A., Evans, D. C., Ramezani, J., Kamo, S. L., Brown, C. M., Currie, P. J., & Braman, D. R. (2023). Calibrating geologic strata, dinosaurs, and other fossils at Dinosaur Provincial Park (Alberta, Canada) using a new CA-ID-TIMS U–Pb geochronology. *Canadian Journal of Earth Sciences*, *60*(12), 1627-1646.

Erickson, G. M., & Tumanova, T. A. (2000). Growth curve of *Psittacosaurus mongoliensis* Osborn (Ceratopsia: Psittacosauridae) inferred from long bone histology. *Zoological Journal of the Linnean Society*, *130*(4), 551-566.

Erickson, G. M., Lappin, A. K., & Larson, P. (2005). Androgynous rex–the utility of chevrons for determining the sex of crocodilians and non-avian dinosaurs. *Zoology*, *108*(4), 277-286.

Evans, D. C., Vavrek, M. J., & Larsson, H. C. (2015). Pachycephalosaurid (Dinosauria: Ornithischia) cranial remains from the latest Cretaceous (Maastrichtian) Scollard Formation of Alberta, Canada. *Palaeobiodiversity and Palaeoenvironments*, *95*, 579-585.

Evans, D. C., Williamson, T., Loewen, M. A., & Kirkland, J. I. (2013). Review of pachycephalosaurian dinosaurs from Grand Staircase-Escalante National Monument, southern Utah. *At the Top of Grant Staircase: The Late Cretaceous of Southern Utah*, 482-487.

Ferigolo, J., & Langer, M. C. (2007). A Late Triassic dinosauriform from south Brazil and the origin of the ornithischian predentary bone. *Historical Biology*, *19*(1), 23-33.

Fiorillo, A. R., & Currie, P. J. (1994). Theropod teeth from the Judith River Formation (Upper Cretaceous) of south-central Montana. *Journal of Vertebrate Paleontology*, 14(1), 74–80.

Forster, C. A., de Klerk, W. J., Poole, K. E., Chinsamy-Turan, A., Roberts, E. M., & Ross, C. F. (2023). *Iyuku raathi*, a new iguanodontian dinosaur from the Early Cretaceous Kirkwood Formation, South Africa. *The Anatomical Record*, 306(7), 1762-1803.

Fowler, D. W. (2017). Revised geochronology, correlation, and dinosaur stratigraphic ranges of the Santonian-Maastrichtian (Late Cretaceous) formations of the Western Interior of North America. *PloS one*, *12*(11), e0188426.

Freedman Fowler, E. A., & Horner, J. R. (2015). A new brachylophosaurin hadrosaur (Dinosauria: Ornithischia) with an intermediate nasal crest from the Campanian Judith River Formation of northcentral Montana. *PloS one*, *10*(11), e0141304.

Freedman, E. A. (2015). *Evolution and ontogeny of Hadrosaurs (Dinosauria: Ornithischia) in the Judith River Formation (late Cretaceous: Campanian) of northcentral Montana*. Montana State University – Bozeman, College of Letters & Science.

Freimuth, W. J., & Varricchio, D. J. (2019). Insect trace fossils elucidate depositional environments and sedimentation at a dinosaur nesting site from the Cretaceous (Campanian) Two Medicine Formation of Montana. *Palaeogeography, Palaeoclimatology, Palaeoecology,* 534, 109262.

Freimuth, W. J., Varricchio, D. J., & Chin, K. (2021). Paleoenvironmental implications of invertebrate fecal pellets (Edaphichnium isp.) at an ichnofossil-rich dinosaur nesting locality, Upper Cretaceous Two Medicine Formation, Montana, USA. *Palaios*, 36(9), 283-300.

Fricke, H. C., Foreman, B. Z., & Sewall, J. O. (2010). Integrated climate model-oxygen isotope

evidence for a North American monsoon during the Late Cretaceous. *Earth and Planetary Science Letters*, 289(1-2), 11-21.

Fuentes, F., DeCelles, P. G., & Constenius, K. N. (2012). Regional structure and kinematic history of the Cordilleran fold-thrust belt in northwestern Montana, USA. *Geosphere*, 8(5), 1104-1128.

Galton, P. M. (1975). The ornithischian dinosaur *Hypsilophodon* from the Wealden of th Isle of Wight. Bulletin of the British Museum (Natural History) Geology, 25(1), 1-152.

Galton, P. M. (1978). Fabrosauridae, the basal family of ornithischian dinosaurs (Reptilia: Ornithopoda). *Paläontologische Zeitschrift*, 52(1), 138-159.

Galton, P. M. (1981). *Dryosaurus*, a hypsilophodontid dinosaur from the Upper Jurassic of North America and Africa postcranial skeleton. *Paläontologische Zeitschrift*, 55(3), 271-312.

Galton, P. M. (1995). The species of the basal hypsilophodontid dinosaur *Thescelosaurus* Gilmore (Ornithischia: Ornithopoda) from the Late Cretaceous of North America. *Neues Jahrbuch für Geologie und Paläontologie-Abhandlungen*, 198(3), 297-311.

Galton, P. M., & Jensen, J. A. (1973). Skeleton of a hypsilophodontid dinosaur (*Nanosaurus* (?) *rex*) from the Upper Jurassic of Utah. *Brigham Young University Geology Studies*, 20(4), 137-157.

Galton, P. M., & Taquet, P. (1982). *Valdosaurus*, a hypsilophodontid dinosaur from the Lower Cretaceous of Europe and Africa. *Geobios*, 15(2), 147-159.

Gates, T. A., Lund, E. A., Boyd, C. A., DeBlieux, D. D., Titus, A. L., Evans, D. C., Getty, M. A., Kirkland, J. I., & Eaton, J. G. (2013). Ornithopod Dinosaurs from the Grand Staircase-Escalante National Monument Region, Utah, and Their Role in Paleobiogeographic and Macroevolutionary Studies. In (pp. 463). Indiana University Press.

Gilmore, C. W. (1913). A new dinosaur from the Lance Formation of Wyoming: Smithson. *Misc. Coll*, 61, 1-5.

Gilmore, C. W. (1915). Osteology of *Thescelosaurus*, an orthopodous dinosaur from the Lance Formation of Wyoming. *Proceedings of the United States National Museum*.

Gilmore, C. W. (1924). A new species of *Laosaurus*, an ornithischian dinosaur from the Cretaceous of Alberta. Royal Society of Canada.

Godefroit, P., Sinitsa, S. M., Dhouailly, D., Bolotsky, Y. L., Sizov, A. V., McNamara, M. E., Benton, M. J., & Spagna, P. (2014). A Jurassic ornithischian dinosaur from Siberia with both feathers and scales. *Science*, 345(6195), 451-455.

Han, F., Barrett, P. M., Butler, R. J., & Xu, X. (2012). Postcranial anatomy of *Jeholosaurus*

shangyuanensis (Dinosauria, Ornithischia) from the Lower Cretaceous Yixian Formation of China. *Journal of Vertebrate Paleontology*, 32(6), 1370-1395.

Hannebaum, Z. J., Varricchio, D. J., and Krumenacker, L. J. (2023). Beneath the feet of giants: a case study of the population dynamics of *Oryctodromeus cubicularis* and *Orodromeus makelai*, two potential burrowing dinosaurs. 83rd Annual Meeting – Society of Vertebrate Paleontology, Cincinnati, Ohio.

Hannebaum, Z. J., Varricchio, D. J., Scheetz, R., Brown, C. M., and Avrahami, H. (2024). The three species problem: a revised look at the systematics and phylogenetic relationships of neornthischian dinosaurs in the Upper Cretaceous Two Medicine Formation of northcentral Montana. *Journal of Vertebrate Paleontology Program Abstracts*, (2024).

He, X. L., & Cai, K. (1984). The Middle Jurassic Dinosaurian Fauna from Dashanpu, Zigong, Sichuan. Vol 1, The Ornithopod Dinosaurs. *Chengdu: Sichuan Scientific and Technological Publishing House*, 71, 1-66.

He, Y., Makovicky, P. J., Wang, K., Chen, S., Sullivan, C., Han, F., & Xu, X. (2015). A new leptoceratopsid (Ornithischia, Ceratopsia) with a unique ischium from the Upper Cretaceous of Shandong Province, China. *PLoS One*, *10*(12), e0144148.

Hedrick, B. P., & Dodson, P. (2013). Lujiatun Psittacosaurids: Understanding Individual and Taphonomic Variation Using 3D Geometric Morphometrics. *PloS one, 8*(8), e69265. doi:10.1371/journal.pone.0069265

Herne, M. C., Tait, A. M., Weisbecker, V., Hall, M., Nair, J. P., Cleeland, M., & Salisbury, S. W. (2018). A new small-bodied ornithopod (Dinosauria, Ornithischia) from a deep, high-energy Early Cretaceous river of the Australian–Antarctic rift system. *PeerJ*, *5*, e4113.

Hone, D. W. E., & Mallon, J. C. (2017). Protracted growth impedes the detection of sexual dimorphism in non-avian dinosaurs. *Palaeontology, 60*(4), 535-545. doi:10.1111/pala.12298

Horner, J. R., & Goodwin, M. B. (2009). Extreme cranial ontogeny in the Upper Cretaceous dinosaur *Pachycephalosaurus*. *PLoS One*, *4*(10), e7626.

Horner, J. R., & Weishampel, D. B. (1988). A comparative embryological study of two ornithischian dinosaurs. *Nature*, 332(6161), 256-257.

Horner, J. R., De Ricqlès, A., Padian, K., & Scheetz, R. D. (2009). Comparative long bone histology and growth of the "hypsilophodontid" dinosaurs *Orodromeus makelai*, *Dryosaurus altus*, and *Tenontosaurus tillettii* (Ornithischia: Euornithopoda). *Journal of Vertebrate Paleontology*, *29*(3), 734-747.

Horner, J. R., Goodwin, M. B., & Evans, D. C. (2022). A new pachycephalosaurid from the Hell Creek Formation, Garfield County, Montana, USA. *Journal of Vertebrate*

Paleontology, *42*(4), e2190369.

Horner, J. R., Goodwin, M. B., & Myhrvold, N. (2011). Dinosaur census reveals abundant *Tyrannosaurus* and rare ontogenetic stages in the Upper Cretaceous Hell Creek Formation (Maastrichtian), Montana, USA. *PLoS One*, *6*(2), e16574.

Horner, J. R., Schmitt, J. G., Jackson, F., & Hanna, R. (2001). Bones and rocks of the Upper Cretaceous Two Medicine-Judith River clastic wedge complex, Montana. In *Society of Vertebrate Pa− leontology 61th Annual Meeting: Mesozoic and Cenozoic Paleontol− ogy in the Western Plains and Rocky Mountains. Museum of the Rockies Occasional Paper* (Vol. 3, pp. 1-14).

Hudgins, M. N. (2021). *The Paleobiology, Paleoecology, and Evolution of Thescelosauridae (Ornithischia) from Alberta, Canada*. Univeristy of Alberta.

Hudgins, M. N., Currie, P. J., & Sullivan, C. (2022). Dental assessment of *Stegoceras validum* (Ornithischia: Pachycephalosauridae) and *Thescelosaurus neglectus* (Ornithischia: Thescelosauridae): paleoecological inferences. *Cretaceous Research*, *130*, 105058.

Huh, M., Lee, D.-G., Kim, J.-K., Gwangju, Lim, J.-D., Daejeon, & Godefroit, P. (2010). A new basal ornithopod dinosaur from the Upper Cretaceous of South Korea. *Neues Jahrbuch für Geologie und Paläontologie. Abhandlungen, 259(1), 1-24.*, *259*, 1-24. https://doi.org/10.1127/0077-7749/2010/0102

Hulke, J. W. (1882). XXIV. An attempt at a complete osteology of *Hypsilophodon foxii*; a British Wealden dinosaur. *Philosophical Transactions of the Royal Society of London*, (173), 1035-1062.

Huxley, T. H. (1870). On *Hypsilophodon foxii*, a new dinosaurian from the Wealden of the Isle of Wight. *Quarterly Journal of the Geological Society*, 26(1-2), 3-12.

Ibiricu, L. M., Martínez, R. D., Luna, M., & Casal, G. A. (2014). A reappraisal of *Notohypshilophodon comodorensis* (Ornithischia: Ornithopoda) from the Late Cretaceous of Patagonia, Argentina. *Zootaxa*, 3786 (4), 401-422.

Ishikawa, H., Tsuihiji, T., & Manabe, M. (2023). *Furcatoceratops elucidans*, a new centrosaurine (Ornithischia: Ceratopsidae) from the upper Campanian Judith River Formation, Montana, USA. *Cretaceous Research*, *151*, 105660.

Jackson, F. D., Horner, J. R., & Varricchio, D. J. (2010). A study of a *Troodon* egg containing embryonic remains using epifluorescence microscopy and other techniques. *Cretaceous Research*, 31(2), 255-262.

Jerzykiewicz, T., & Norris, D. K. (1994). Stratigraphy, structure and syntectonic sedimentation of the Campanian'Belly River'clastic wedge in the southern Canadian Cordillera. *Cretaceous Research*, *15*(4), 367-399.

Jin, L., Jun, C., Zan, S., Butler, R. J., & Godefroit, P. (2010). Cranial anatomy of the small ornithischian dinosaur *Changchunsaurus parvus* from the Quantou Formation (Cretaceous, Aptian-Cenomanian) of Jilin Province, northeastern China. Journal of vertebrate paleontology, 30(1), 196-214. https://doi.org/10.1080/02724630903412372

Kauffman, E. G. (1977). Geological and biological overview: Western Interior Cretaceous basin. *The Mountain Geologist*.

Kim, Y. K., Koyabu, D., Lee, H., & Kimura, J. (2013). Sexual Dimorphism of Craniomandibular Size in the Korean Water Deer, Hydropotes inermis argyropus. *Journal of Veterinary Medical Science, 75*(9), 1153-1159. doi:10.1292/jvms.13-0125

Krumenacker, L. J. (2017). *Osteology, phyloheny, taphonomy, and ontogenetic histology of Oryctodromeus cubicularis, from the middle Cretaceous (Albian-Cenomanian) of Montana and Idaho*. Montana State Univerisity – Bozeman, College of Letters and Science.

Krumenacker, L. J., Varricchio, D., J., Organ, C., Gardner, J. D., Britt, B. B., & Boyd, C. (2024). Osteology and phylogenetic relationships of the mid-Cretaceous neornithischian dinosaur *Oryctodromeus cubicularis* Varricchio, 2007. Journal of Vertebrate Paleontology. https://doi.org/10.1080/027724634.2024.2330581

Kutter, M. M. (2004). *New material of Zephyrosaurus schaffi (Dinosauria; Ornithischia) from the Cloverly Formation (Aptian-Albian) of Montana and the phylogeny of Hypsilophodontidae*. College of the Pacific – Stockton, Department of Biological Scienece.

Lageson, D. R., Schmitt, J. G., Horton, B. K., Kalakay, T. J., & Burton, B. R. (2001). Influence of Late Cretaceous magmatism on the Sevier orogenic wedge, western Montana. *Geology*, 29(8), 723-726.

LaRock, J. W. (2000). *Sedimentology and taphonomy of a dinosaur bonebed from the Upper Cretaceous (Campanian) Judith River Formation of north central Montana*. Montana State University – Bozeman, College of Letters & Science.

Lee, Y. N., Ryan, M. J., & Kobayashi, Y. (2011). The first ceratopsian dinosaur from South Korea. *Naturwissenschaften*, *98*, 39-49.

Leidy, J. (1856). Notices of remains of extinct reptiles and fishes, discovered by Dr. F. V. Hayden in the badlands of the Judith River, Nebraska Terr. *Proceedings of the Academy of Natural Sciences of Philadelphia*, 72–73.

Li, N., Dai, H., Tan, C., Hu, X., Wei, Z., Lin, Y., Wei, G., Li, D., Meng, L., Hao, B., You, H., & Peng, G. (2021). A neornithischian dinosaur from the Middle Jurassic Xintiangou Formation of Yunyang, Chongquing, China: the earliest record in Asia. *Historical Biology*, 33(7), 1089-1102. https://doi.org/10.1080/08912963.2019.1679129

Loewen, M. A., Sertich, J. J. W., Sampson, S., O'Connor, J. K., Carpenter, S., Sisson, B., Øhlenschlaeger, A., Farke, A. A., Makovicky, P. J., Longrich, N., and Evans, D. C. (2024). *Lokiceratops rangiformis* gen. et sp. nov. (Ceratopsidae: Centrosaurinae) from the Campanian Judith River Formation of Montana reveals rapid regional radiations and extreme endemism within centrosaurine dinosaurs. *PeerJ*, 12:e17224.

Longrich, N. R. (2013). *Judiceratops tigris*, a new horned dinosaur from the middle Campanian Judith River Formation of Montana. *Bulletin of the Peabody Museum of Natural History*, 54(1), 51-65.

Lorenz, J. & Gavin, W. (1984). *Geology of the Two Medicine Formation and the sedimentology of a dinosaur nesting ground*. Montana Geological Society Field Conference Northwestern Montana.

Madzia, D., Arbour, V. M., Boyd, C. A., Farke, A. A., Cruzado-Caballero, P., & Evans. D. C. (2021). The phylogenetic nomenclature of ornithischian dinosaurs. *PeerJ* (San Francisco, CA), 9, e122362-e12362.

Madzia, D., Arbour, V. M., Boyd, C. A., Farke, A. A., Cruzado-Caballero, P., & Evans. D. C. (2021). The phylogenetic nomenclature of ornithischian dinosaurs. PeerJ (San Francisco, CA), 9, e122362-e12362. https://doi.org/10.7717/peerj.12362.

Maidment, S. C., & Barrett, P. M. (2011). The locomotor musculature of basal ornithischian dinosaurs. *Journal of Vertebrate Paleontology*, 31(6), 1265-1291.

Makovicky, P. J. (2010). A redescription of the *Montanoceratops cerorhynchus* holotype, with a review of referred material. *New perspectives on horned dinosaurs*, 68-82.

Makovicky, P. J., Kilbourne, B. M., Sadleir, R. W., & Norell, M. A. (2011). A new basal ornithopod (Dinosauria, Ornithischia) from the Late Cretaceous of Mongolia. *Journal of Vertebrate Paleontology*, 31(3), 626-640.

Mallon, J. C. (2017). Recognizing sexual dimorphism in the fossil record; lessons from nonavian dinosaurs. *Paleobiology, 43*(3), 495-507. doi:10.1017/pab.2016.51

Mallon, J. C., Evans, D. C., Tokaryk, T. T., & Currie, M. L. (2015). First pachycephalosaurid (Dinosauria: Ornithischia) from the Frenchman Formation (upper Maastrichtian) of Saskatchewan, Canada. *Cretaceous Research*, *56*, 426-431.

Mallon, J. C., Ott, C. J., Larson, P. L., Iuliano, E. M., & Evans, D. C. (2016). *Spiclypeus shipporum* gen. et sp. nov., a boldly audacious new chasmosaurine ceratopsid (Dinosauria: Ornithischia) from the Judith River Formation (Upper Cretaceous: Campanian) of Montana, USA. *PloS one*, *11*(5), e0154218.

Manitkoon, S., Deesri, U., Khalloufi, B., Nonsrirach, T., Suteethorn, V., Chanthasit, P., Boonla, W., & Buffetaut, E. (2023). A New Basal Neornithischian Dinosaur from the Phu Kradung Formation (Upper Jurassic) of Northeastern Thailand. *Diversity*, 15(7), 851.

Marsh, O. C. (1878). Notice of new dinosaurian reptiles. *American Journal of Science*, *3*(87), 241-244.

Maryanska, T. E. R. E. S. A., & Osmólska, H. (1974). Pachycephalosauria, a new suborder of ornithischian dinosaurs. *Palaeontologia Polonica*, 30, 45-102.

Matheron P. 1869. Notice sur les reptiles fossiles des dépôts fluvio-lacustres crétacés du bassin à lignite de Fuveau. In: *Mémoires de l'Académie des Sciences, Belles-Lettres, et Arts de Marseille 1868–1869*. 345–379.

Matson, C. C. (2010). *Paleoenvironments of the Upper Cretaceous Dinosaur Park Formation in southern Alberta, Canada* (Doctoral dissertation, University of Calgary, Department of Geoscience).

Mayo, K., Silva, R. L., & Durkin, P. R. (2023). Paleoenvironmental reconstruction of Late Cretaceous rivers, Dinosaur Park Formation, Alberta, Canada. *Sedimentary Geology*, 457, 106499.

Moore, B. R. S. (2021). *The postcranial anatomy of pachycephalosaurs (Ornithischia: Pachycephalosauria) and its phylogenetic and myological implications* (Doctoral dissertation, Carleton University).

Morris, W. J. (1976). Hypsilophodont dinosaurs: a new species and comments on their systematics. *Athlon: essays on Palaeontology in Honour of Loris Shano Russell. Toronto: Royal Ontario Museum*, 93-113.

Morschhauser, E. M., Li, D., You, H., & Dodson, P. (2018). Cranial Anatomy of the Basal Neoceratopsian *Auroraceratops* rugosus (Ornithischia: Ceratopsia) from the Yujingzi Basin, Gansu Province, China. *Journal of Vertebrate Paleontology*, 38(sup1), 36-68.

Nabavizadeh, A., & Weishampel, D. B. (2016). The predentary bone and its significance in the evolution of feeding mechanisms in ornithischian dinosaurs. *The Anatomical Record*, *299*(10), 1358-1388.

Nogueira, R. A., Rozadilla, S., Agnolín, F. L., Marsà, J. A. G., Motta, M. J., & Novas, F. E. (2024). A new ornithopod from the Upper Cretaceous (Huincul Formation) of northwestern Patagonia, Argentina: Implications on elasmarian postcranial anatomy. *Cretaceous Research*, *159*, 105874.

Norman, D. B., Crompton, A. W., Butler, R. J., Porro, L. B., & Charig, A. J. (2011). The Lower Jurassic ornithischian dinosaur *Heterodontosaurus tucki* Crompton & Charig, 1962:

cranial anatomy, functional morphology, taxonomy, and relationships. *Zoological Journal of the Linnean Society*, 163(1), 182-276.

Norman, D. B., Sues, H. -D., Witmer, L. M., & Coria, R. A. (2004). Basal Ornithopoda. In D. B. Weishampel, P. Dodson, and H. Osmólska (editors), The Dinosauria: 413-437. Berkeley: Unversity of California Press.

Novas, F. E. (1994). New information on the systematics and postcranial skeleton of *Herrerasaurus ischigualastensis* (Theropoda: Herrerasauridae) from the Ischigualasto Formation (Upper Triassic) of Argentina. *Journal of Vertebrate Paleontology*, 13(4), 400-423.

Osmólska, H. (1981). Coossified tarsometatarsi in theropod dinosaurs and their bearing on the problem of bird origins. *Palaeontologia Polonica*, 42, 79-95.

Owens, R. 1842. Report on British fossil reptiles. Part II. *Report for the British Association for the Advancement of Science*, 11, 60-204.

Pol, D., Rauhut, O. W., & Becerra, M. (2011). A Middle Jurassic heterodontosaurid dinosaur from Patagonia and the evolution of heterodontosaurids. *Naturwissenschaften*, 98, 369-379.

Porro, L. B., Witmer, L. M., & Barrett, P. M. (2015). Digital preparation and osteology of the skull of *Lesothosaurus diagnosticus* (Ornithischia: Dinosauria). *PeerJ*, 3, e1494.

QGIS.org (2023). QGIS Geographic Information System. Open Source Geospatial Foundation Project. http://qgis.org

Ramezani, J., Beveridge, T. L., Rogers, R. R., Eberth, D. A., & Roberts, E. M. (2022). Calibrating the zenith of dinosaur diversity in the Campanian of the Western Interior Basin by CA-ID-TIMS U-Pb geochronology. *Scientific Reports*, 12(1). 16026-16026. https://doi.org/10.1038/s41598-022-19896-w.

Rich, T. H., Galton, P. M., & Vickers-rich, P. (2010). The holotype individual of the ornithopod dinosaur *Leaellynasaura amicagraphica* Rich & Rich, 1989 (late Early Cretaceous, Victoria, Australia). *Alcheringa: An Australasian Journal of Palaeontology*, 34(3), 385-396.

Rinehart, L. F., Lucas, S. G., Heckert, A. B., Spielmann, J. A., & Celesky, M. D. (2009). The Paleobiology of Coelophysis bauri (Cope) from the Upper Triassic (Apachean) Whitaker quarry, New Mexico, with detailed analysis of a single quarry block. *New Mexico Museum of Natural History and Science Bulletin* (45), 1-260.

Rogers, R. R. (1990). Taphonomy of three dinosaur bone beds in the Upper Cretaceous Two Medicine Formation of northwestern Montana: evidence for drought-related mortality. *Palaios*, 394-413.

Rogers, R. R., Eberth, D. A., & Ramezani, J. (2023). The “Judith River-Belly River problem” revisited (Montana-Alberta-Saskatchewan); new perspectives on the correlation of Campanian dinosaur-bearing strata based on revised stratigraphic model updated with CA-ID-TIMS U-Pb geochronology. Geological Society of America bulletin, 136(3/4), 1221.

Rogers, R. R., Eberth, D. A., & Ramezani, J. (2024). The “Judith River–Belly River problem” revisited (Montana-Alberta-Saskatchewan): New perspectives on the correlation of Campanian dinosaur-bearing strata based on a revised stratigraphic model updated with CA-ID-TIMS U-Pb geochronology. *Bulletin*, *136*(3-4), 1221-1237.

Rogers, R. R., Kidwell, S. M., Deino, A. L., Mitchell, J. P., Nelson, K., & Thole, J. T. (2016). Age, correlation, and lithostratigraphic revision of the Upper Cretaceous (Campanian) Judith River Formation in its type area (north-central Montana), with a comparison of low-and high-accommodation alluvial records. *The Journal of Geology*, 124(1), 99-135.

Rogers, R. R., Swisher, C. C. III, & Horner, J. R. (1993). $^{40}Ar/^{39}Ar$ ad correlation of the nonmarine Two Medicine Formation (Upper Cretaceous), northwestern Montana, U.S.A. *Canadian journal of earth sciences*, 30(5), 1066-1075.

Rogers, R., Horner, J., Ramezani, J., Roberts, E., and Varricchio. D. (2024). Updating the Upper Cretaceous (Campanian) Two Medicine Formation of Montana: Lithostratigraphic revisions, new CA-ID-TIMS U-Pb ages, and a calibrated framework of dinosaur occurances. *The Geologial Society of America Bulletin*.

Ronquist, F., Teslenko, M., van der Mark, P., Ayres, D., Darling, A., Höhna, S., Larget, B., Liu, L., Suchard, M. A., & Huelsenbeck, J. P. (2012). MrBayes 3.2: Efficient Bayesian phylogenetic inference and model choice across a large model space. Systematic Biology, 61(3), 539–542.

Rozadilla, S., Agnolín, F. L., & Novas, F. E. (2019). Osteology of the Patagonian ornithopod *Talenkauen santacrucensis* (Dinosauria, Ornithischia). *Journal of Systematic Palaeontology*, 17(24), 2043-2089.

Rozadilla, S., Agnolin, F. L., Novas, F. E., Rolando, A. M. A., Motta, M. J., Lirio, J. M., & Isasi, M. P. (2016). A new ornithopod (Dinosauria, Ornithischia) from the Upper Cretaceous of Antarctica and its palaeobiogeographical implications. *Cretaceous Research*, *57*, 311-324.

Rozadilla, S., Cruzado-Caballero, P., & Calvo, J. O. (2020), Osteology of Ornithopod *Macrogryphosaurus gondwanicus* (Dinosauris, Ornithischia) from the Upper Cretaceous of Patagonia, Argentina. *Cretacesous research*, 108, 104311.

Ruiz-Omeñaca, J. I., Canudo, J. I., Cuenca-Bescós, G., Cruzado-Caballero, P., Gasca, J. M., & Moreno-Azanza, M. (2012). A new basal ornithopod dinosaur from the Barremian of Galve, Spain. *Comptes Rendus Palevol*, 11(6), 435-444.

Russell, L. S. (1949). The relationships of the Alberta Cretaceous dinosaur" *Laosaurus*" *minimus* Gilmore. *Journal of Paleontology*, 518-520.

Ryan, M. J., Russell, A. P., & Hartman, S. (2010). A new chasmosaurine ceratopsid from the Judith River Formation, Montana. *New perspectives on horned dinosaurs*, 181-188.

Ryan, M. J., Evans, D. C., Currie, P. J., Brown, C. M., & Brinkman, D. (2012). New leptoceratopsids from the upper Cretaceous of Alberta, Canada. *Cretaceous Research*, *35*, 69-80.

Ryan, M. J., Evans, D. C., Currie, P. J., & Loewen, M. A. (2014). A new chasmosaurine from northern Laramidia expands frill disparity in ceratopsid dinosaurs. *Naturwissenschaften*, *101*, 505-512.

Ryan, M.J. L. Micucci, H. Rizo, C. Sullivan, Y.-N. Lee, and D. C. Evans. 2023. A new Late Cretaceous leptoceratopsid (Dinosauria: Ceratopsia) from the Oldman Formation (Campanian) of Alberta, Canada. In Y.-N. Lee, Ed., Windows into Sauropsid and Synapsid Evolution: Essays in Honor of Prof. Louis L. Jacobs, pp. 151-165. Dinosaur Science Center Press: Hwaseong City, South Korea.

Sahni, A. (1972). The vertebrate fauna of the Judith River Formation, Montana. Bulletin of the AMNH; v. 147, article 6.

Saitta, E. T. (2015). Evidence for sexual dimorphism in the plated dinosaur Stegosaurus mjosi (Ornithischia, Stegosauria) from the Morrison Formation (Upper Jurassic) of western USA. *PloS one, 2015*(4), e0123503-e0123503. doi:10.1371/journal.pone.0123503

Salgado, L., Canudo, J. I., Garrido, A. C., Moreno-Azanza, M., Martínez, L. C., Coria, R. A., & Gasca, J. M. (2017). A new primitive Neornithischian dinosaur from the Jurassic of Patagonia with gut contents. *Scientific Reports*, 7(1), 1-10.

Salgado, L., Coria, R. A., & Heredia, S. E. (1997). New materials of *Gasparinisaura cincosaltensis* (Ornithischia, Ornithopoda) from the Upper Cretaceous of Argentina. *Journal of Paleontology*, 71(5), 933-940.

Salgado, L., Coria, R. A., & Heredia, S. E. (1997). New materials of *Gasparinisaura cincosaltensis* (Ornithischia, Ornithopoda) from the Upper Cretaceous of Argentina. *Journal of Paleontology*, 71(5), 933-940.

Sampson, S. D. (1995). Two new horned dinosaurs from the Upper Cretaceous Two Medicine Formation of Montana; with a phylogenetic analysis of the Centrosaurinae (Ornithischia: Ceratopsidae). *Journal of vertebrate paleontology*, 15(4), 743-760.

Santa Luca, A. P. (1980). The postcranial skeleton of *Heterodontosaurus tucki* (Reptilia, Ornithischia) from the Stormberg of South Africa. Annals of the South African Museum. 79: 159-211.

Scheetz, R. D. (1999). *Osteology of Orodromeus makelai and the phylogeny of basal ornithopod dinosaurs*. Montana State University-Bozeman.

Schott, R. K., & Evans, D. C. (2017). Cranial variation and systematics of *Foraminacephale brevis* gen. nov. and the diversity of pachycephalosaurid dinosaurs (Ornithischia: Cerapoda) in the Belly River Group of Alberta, Canada. *Zoological Journal of the Linnean Society*, *179*(4), 865-906.

Schott, R. K., Evans, D. C., Williamson, T. E., Carr, T. D., & Goodwin, M. B. (2009). The anatomy and systematics of *Colepiocephale lambei* (Dinosauria: Pachycephalosauridae). *Journal of Vertebrate Paleontology*, 29(3), 771-786.

Schweitzer, M. H., Zheng, W., Zanno, L., Werning, S., & Sugiyama, T. (2016). Chemistry supports the identification of gender-specific reproductive tissue in *Tyrannosaurus rex*. *Scientific Reports, 6*(1), 23099-23099. doi:10.1038/srep23099

Seeley H. G. 1887. On the classification of the fossil animals commonly named Dinosauria. *Proceedings of the Royal Society of London*, 43, 481-494.

Sereno, P. C. (2012). Taxonomy, morphology, masticatory function and phylogeny of heterodontosaurid dinosaurs. *ZooKeys*, (226), 1.

Sereno, P. C., & Novas, F. E. (1994). The skull and neck of the basal theropod *Herrerasaurus ischigualastensis*. *Journal of Vertebrate Paleontology*, 13(4), 451-476.

Sharp, A. C., Siu, K., & Rich, T. H. (2017). Revealing the skeleton of the polar dinosaur *Leaellynasaura amicagraphica* using synchrotron computed tomography. In *Society of Vertebrate Paleontology 77th Annual Meeting, Meeting Program and Abstracts* (Vol. 193).

Shine, R., Reed, R., Shetty, S., & Cogger, H. (2002). Relationships between sexual dimorphism and niche partitioning within a clade of sea-snakes (Laticaudinae). *Oecologia, 133*(1), 45-53. doi:10.1007/s00442-002-1012-7

Sternberg, C. M. 1937. A classification of *Thescelosaurus*, with a description of a new species. *Geological Society of America, Proceedings and Abstracts*, 1936-375.

Sues, H. D., Evans, D. C., Galton, P. M., & Brown, C. M. (2023). Anatomy of the neornithischian dinosaur *Parksosaurus warreni* (Parks, 1926) from the Upper Cretaceous (lower Maastrichtian) Horseshoe Canyon Formation of Alberta, Canada. *Cretaceous Research*, 141, 105369.

Sues, H.-D. (1980). Anatomy and relationships of a new hypsilophodontid dinosaur from the Lower Cretaceous of North America. *Palaeontographica. Abt. A., Palaeozoologie-Stratigraphie*, 169, 51-72.

Sullivan, R. M. (2006). A taxonomic review of the Pachycephalosauridae (Dinosauria: Ornithischia). *New Mexico Museum of Natural History and Science Bulletin*, *35*(47), 347-365.

Takasaki, R., Chiba, K., Fiorillo, A. R., Brink, K. S., Evans, D. C., Fanti, F., Saneyoshi. M., Maltese, A. & Ishigaki, S. (2023). Description of the first definitive *Corythosaurus* (Dinosauria, Hadrosauridae) specimens from the Judith River Formation in Montana, USA and their paleobiogeographical significance. *The Anatomical Record*, 306(7), 1918-1938.

Tarnawski, B. A., Cassini, G. H., & Flores, D. A. (2014). Skull allometry and sexual dimorphism in the ontogeny of the southern elephant seal (Mirounga leonina). *Canadian journal of zoology, 92*(1), 19-31. doi:10.1139/cjz-2013-0106

Thulborn, R. A. (1974). A new heterodontosaurid dinosaur (Reptilia; Ornithischia) from the Upper Triassic red beds of Lesotho. *Zoological journal of the Linnean Society, 55*(2), 151-175. doi:10.1111/j.1096-3642.1974.tb01591.x

Umeno, A., & Tanoue, K. (2016). Description of Dinosaur Teeth from the Upper Cretaceous Judith River Formation in Montana, USA. *福岡大学理学集報*, 46(2), 77-84.

Varricchio, D. J. (2002). A new bird from the Upper Cretaceous Two Medicine Formation of Montana. *Canadian Journal of Earth Sciences*, 39(1), 19-26.

Varricchio, D. J., Martin, A. J., & Katsura, Y. (2007). First trace and body fossil evidence of a burrowing, denning dinosaur. *Proceedings of the Royal Society. B, Biological sciences*, 274(1616), 1361-1368. https://doi.org/10.1098/rspb.2006.0443.

Verdú, F. J., Royo-Torres, R., Cobos, A., & Alcalá, L. (2018). New systematic and phylogenetic data about the early Barremian *Iguanodon galvensis* (Ornithopoda: Iguanodontoidea) from Spain. *Historical Biology*, 30(4), 437-474.

Warshaw, E. A., & Fowler, D. W. (2022). A transitional species of *Daspletosaurus* Russell, 1970 from the Judith River Formation of eastern Montana. *PeerJ* (San Francisco, CA), 10, e14461–e14461.

Weishampel, D. B., & Heinrich, R. E. (1992). Systematics of hypsilophodontidae and basal Iguanodontia (Dinosauria: Ornithopoda). *Historical Biology*, 6(3), 159-184.

Weishampel, D. B., Jianu, C. M., Csiki, Z., & Norman, D. B. (2003). Osteology and phylogeny of *Zalmoxes* (ng), an unusual euornithopod dinosaur from the latest Cretaceous of Romania. *Journal of Systematic Palaeontology*, 1(2), 65-123.

Wilson, J. A. (2006). Anatomical nomenclature of fossil vertebrates: standardized terms or 'lingua franca'?. *Journal of Vertebrate Paleontology*, *26*(3), 511-518.

Wilson, J. P., & Fowler, D. W. (2021). The easternmost occurrence of *Saurornitholestes* from the Judith River Formation, Montana, indicates broad biogeographic distribution of *Saurornitholestes* in the Western Interior of North America. *Historical Biology*, 33(12), 3302–3306.

Wolff, E., & Horner, J. R. (2003). The first occurrence of *Orodromeus makelai* postcrania from the Late-Campanian Judith River Formation of eastern Montana. *Journal of Vertebrate Paleontology*, 23(3), 122.

Woodruff, D. C. (2022). *New insights into pachycephalosaurian (Dinosauria: Ornithischia) anatomy, functional morphology, and evolution* (Doctoral dissertation, University of Toronto (Canada)).

Woodruff, D. C., Schott, R. K., & Evans, D. C. (2023). Two new species of small-bodied pachycephalosaurine (Dinosauria, Marginocephalia) from the uppermost Cretaceous of North America suggest hidden diversity in well-sampled formations. *Papers in Palaeontology*, *9*(6), e1535.

Woodward, H. N., Fowler, E. A. F., Farlow, J. O., & Horner, J. R. (2015). *Maiasaura*, a model organism for extinct vertebrate population biology: a large sample statistical assessment of growth dynamics and survivorship. *Paleobiology*, 41(4), 503-527.

Xu, X., Forster, C. A., Clark, J. M., & Mo, J. (2006). A basal ceratopsian with transitional features from the Late Jurassic of northwestern China. *Proceedings of the Royal Society B: Biological Sciences*, 273(1598), 2135-2140.

Yang, Y., Wu, W., Dieudonné P.-E., & Godefroit, P. (2020). A new basal ornithopod dinosaur from the Lower Cretaceous of China. PeerJ (San Francisco, CA), 8, e9832-e9832. https://doi.org/10.7717/peerj.9832

Zanno, L. E., Gates, T. A., Avrahami, H. M., Tucker, R. T., & Makovicky, P. J. (2023). An early-diverging iguanodontian (Dinosauria: Rhabdodontomorpha) from the Late Cretaceous of North America. *Plos one*, 18(6), e0286042.

Zheng, W., Jin, X., Shibata, M., Azuma, Y., & Yu, F. (2012). A new ornithischian dinosaur from the cretaceous Liangtoutang formation of Tiantai, Zhejiang Province, China. *Cretaceous Research*, *34*, 208-219.